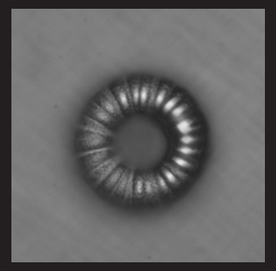

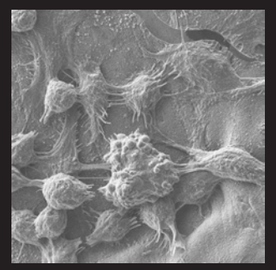

IMEM

APPLICATION OF CONDUCTING POLYMERS IN NANOBIOTECHNOLOGY

UPC

2011

# APPLICATION OF CONDUCTING POLYMERS IN NANOBIOTECHNOLOGY

BRUNO JOSÉ DA CRUZ TEIXEIRA DIAS

UPC UNIVERSITAT POLITÈCNICA DE CATALUNYA IMEM

**BRUNO JOSÉ DA CRUZ TEIXEIRA DIAS**

**UNIVERSITAT POLITÈCNICA DE CATALUNYA**

**2011**

# APPLICATION OF CONDUCTING POLYMERS IN NANOBIOTECHNOLOGY

Presented by:

M.Sc. Bruno José da Cruz Teixeira Dias

Under direction of:

Dr. Carlos Alemán Llansó

Dr. Francesc Estrany Coda

Dr. Luis Javier del Valle Mendonza

Realized at Departament d'Enginyeria Química (DEQ) of Escola Tècnica Superior d'Enginyeria Industrial de Barcelona (ETSEIB) of Universitat Politècnica de Catalunya (UPC)

**Barcelona, July 2011**

## Abstract

This Thesis reports different nanobiotechnological applications of electrochemically and electrically conducting polymers. The central, and also common, focus of all the studies and experiments described in Chapters 4 to 6 is the interaction between synthetic conducting polymers and bioentities (DNA, proteins, polysaccharides, small peptides, drugs and cells).

One of the major challenges of this Thesis consisted on the characterization of the interactions between conducting polymers and DNA. The studies described in Chapter 4 evidenced that specific hydrogen bonding interactions, in addition to conventional electrostatic interactions, are formed between conducting polymers bearing polar groups and plasmid DNA. In order to get more information about such interactions, studies were essentially focused on poly(3,4-ethylenedioxythiophene), a conducting polymer with excellent technological properties. On the basis of both the structural changes undergone by the DNA upon the formation of specific interactions with the conducting polymer and the preferences of the latter towards well-defined nucleotide sequences and bases, a mechanism has been proposed to explain the interaction between the two macromolecules. This mechanism, which is supported by theoretical calculations, is consistent with all the experimental data reported in this Thesis.

Chapter 5 is devoted to examine the interaction between morphine molecules and conducting polymers. Within this general context, this block of results is essentially focused on the optimization of the conditions necessary for the detection of this drug using poly(*N*-methylpyrrole) and poly(3,4-ethylenedioxythiophene). Studies have been performed considering the effect of: the polymer morphology (*i.e.* both flat films and films containing hollow microstructures with doughnut-like morphologies have been examined), the time of incubation with morphine, and the pH of the environment. In all cases detection was carried out using electrochemical techniques, which include electrochemical impedance spectroscopy and cyclic voltammetry. Results reflect that, under controlled conditions, the investigated conducting polymers exhibit a high ability to capture morphine molecules, retaining them for a long period of time. In addition, the fabrication of a portable drug detector device based on conducting polymers has been proposed.

Finally, Chapter 6 is devoted to the preparation and characterization of new hybrid conducting biocomposites for nanobiotechnological and biomedical purposes. More specifically, this block of the work presents the electropolymerization of poly(3,4-ethylenedioxythiophene) with different biomolecules (*i.e.* an enzyme, poly- and oligosaccharides, and a small peptide) and the interaction of these new hybrid materials with cells. It was found that, in general, the prepared biocomposites retain the electrical and electrochemical properties of the individual conducting polymer and, in addition, show a prominent cellular activity. Lysozyme-containing biocomposites, which form compact and stable films, exhibit a high bactericidal activity against Gram (+) bacteria, which is promoted by a controlled release of the enzyme. The remarkable cellular activity of dextrins-containing materials suggests that they are potential candidates for the fabrication of cellular scaffolds. Finally, the incorporation of a low concentration of CREKA peptide into the polymer matrix resulted in a very positive effect on the electrochemical properties of the conducting polymer, which were considerably enhanced.

**Keywords:** conducting polymers; nanobiotechnology; electrochemistry; biological entities; especific interactions; drug detection; hybrid conducting biocomposites; biocompatibility.

## Resumen

La presente tesis describe diferentes aplicaciones en el ámbito de la nanobiotecnología de los polímeros conductores generados electroquímicamente. El objetivo principal de la Tesis, que además es el nexo común de los diferentes estudios que se presentan en los Capítulos 4 al 6, es el análisis de las interacciones entre los polímeros conductores sintéticos y diversas entidades biológicas (ADN, proteínas, polisacáridos, pequeños péptidos, drogas, y células).

Uno de los retos más importantes de esta Tesis ha sido la caracterización de las interacciones entre los polímeros conductores y el ADN. Los estudios descritos a lo largo del Capítulo 4 ponen en evidencia la existencia de interacciones específicas por puentes de hidrógeno entre plásmidos de ADN y polímeros conductores con sustituyentes polares. Estas interacciones específicas actúan reforzando las interacciones electrostáticas convencionales intrínsecas a la naturaleza cargada de ambos sistemas. Con la intención de obtener la máxima información acerca de estas interacciones, los estudios se han centrado esencialmente en el poli(3,4-etilendioxitiofeno), un polímero conductor con excelentes propiedades y un amplio número de aplicaciones tecnológicas. Los cambios estructurales que se producen en el ADN como consecuencia de la formación de interacciones específicas, las preferencias del polímero conductor por secuencias nucleotídicas bien definidas, así como por con algunas bases nitrogenadas, han permitido proponer un mecanismo que explica la interacción entre las dos sistemas. Este mecanismo, que también se apoya en cálculos teóricos, es totalmente consistente con todos los datos experimentales descritos en esta Tesis.

El Capítulo 5 está dedicado al análisis de la interacción entre las moléculas de morfina y los polímeros conductores. Dentro de este contexto general, este el proposito general de este bloque de resultados ha sido optimizar las condiciones necesarias para la detección de esta droga con poli(*N*-metilpirrol) y con poli(3,4-etilendioxitiofeno). Los estudios se han realizado teniendo en cuenta el efecto de: la morfología del polímero (es decir, se han examinado las tanto películas planas como películas formadas por microestructuras huecas con morfología tipo rosquilla), el tiempo de incubación con la morfina, y el pH del entono. En todos los casos la detección se ha realizado mediante técnicas electroquímicas, que incluyen tanto la espectroscopia de impedancia

electroquímica, como la voltametría cíclica. Los resultados reflejan que, en condiciones controladas, los polímeros estudiados muestran no solo una elevada capacidad para capturar las moléculas de morfina, sino también para retenerlas por un período de tiempo largo. Se ha propuesto la fabricación de un dispositivo portátil para la detección de drogas basado en polímeros conductores.

Finalmente, el Capítulo 6 está dedicado a la preparación y caracterización de nuevos biocomposites conductores híbridos para aplicaciones en nanobiotecnología y biomedicina. Concretamente, este bloque de resultados presenta la electropolimerización del poli(3,4-etilendioxitiofeno) con diferentes biomoléculas (es decir, un enzima, poli- y oligosacáridos, y un péptido) y la interacción de estos nuevos materiales híbridos con células. Se ha descubierto que, en general, estos biocomposites conservan las propiedades electroquímicas del polímero conductor y que, además, muestran una prominente actividad celular. Los biocomposites que contienen lisozima, forman películas compactas y estables, muestran una elevada actividad bactericida contra las bacterias Gram (+), la cual es debida a que el enzima se libera de forma controlada. La notable actividad celular observada en los materiales que contienen dextrinas, sugiere que estos biocomposites son candidatos potenciales para la fabricación de soportes celulares. Por ultimo, la incorporación de una baja concentración del CREKA en la matriz polimérica, tiene un efecto muy positivo en las propiedades electroquímicas del polímero conductor, las cuales mejoran considerablemente.

**Palabras-clave:** Polímeros conductores; Nanobiotecnología; Electroquímica; Entidades biológicas; Interacciones específicas; detección de drogas; biocomposites conductores híbridos; biocompatibilidad.

## Acknowledgments

Throughout the journey of life, I have being surrounded by exceptional people. Without their guidance and friendship, the completion of this stage would not have been possible. Firstly, I would like to express my deep gratitude towards Professor Dr. Carlos Alemán (Thesis Director), for giving me the opportunity to do the Ph.D. studies in his group (IMEM), for his valuable guidance and direction, for his knowledge and scientific vision, professionalism, patience, encouragement, friendship, and for being an excellent and sensible person. I also, would like to express my gratitude to the thesis co-directors. Without them, this thesis would be incredibly incomplete. To Dr. Francesc Estrany, by his wide knowledge in electrochemistry, for being an excellent teacher, for his availability to guide me and help in my first steps in electrochemistry fields, and at last for his commitment and friendship during these 4 years. To Dr. Luis J. del Valle (Lucho), for his friendship and endless commitment, dedication, constant support, and for sharing with me a little bit of his vast knowledge and experience in biology and biotechnology.

I am very thanked to MICINN by a FPI grant that made possible my Ph.D. work, as well as my stay in Barcelona, during the last 48 months, and by the financial support for the three months stay at the 3B's Research Group (Portugal).

A note of gratitude is also addressed here to all co-authors who participated not only in the papers that were published but also in those that will be published in a near future. I must note Dra. Elaine Armelin, Dr. David Zanuy, Dr. Ramón Oliver, Dr. Francisco Liesa, Dr. Jordi Poater, Prof. Miquel Solá, Prof. Denise Azambuja, Dr. Julien Preat, Dr. Eric Perpète, Dra. Catherine Michaux, Prof. Rui Reis and Dr. João Mano.

Past and present members of IMEM Research Group have contributed immensely to my personal and professional time in Barcelona. The group has been a source of friendship as well as of good advices and collaborations. I am especially grateful to: Elaine Armelin (for the collaboration and great help in some works, and for the friendship), Cintia Ocampo (thanks for some work with DNA, which was the starting point of my research), Francisco Rodríguez-Ropero (thanks for being a good friend, a Metal brother, for the integration help and precious advices since the first days at Barcelona till today and, of course, for the Voll Damm initiation), Guillem Revilla (for your fellowship and friendship, for clarify and solve some biologic/biochemical doubts, principally about CREKA, and for the advices in the

thesis writing part), David Zanuy (for your great work in MD calculations and graphical TOCs, for the politics/football/religious jokes and friendship), David Aradilla, Georgina Fabregat (for being a sensible and extremely good person and a good friend, for the comments, opinions and advices, for the hours that we work together in which we exchange some biotechnological knowledge), Daniel, Mar and Esther (for you that recently began this journey, I wish you much luck, and just tell you that with work, dedication, patience and persistence, all is possible).

It is absolutely necessary to thank some people from other research groups/institutions that I had the pleasure of knowing throughout this time, and that also contribute to this thesis. I would like to emphasize here: Koji, Anaïs, Abdel, Antxon, Ainhoa, Cristina Lavilla, Nathalie, Romina, Elsa, Alejandra Rodriguez, and Alex Linardi.

I express gratitude to Prof. Rui Reis and Dr. João Mano from 3B's Research Group (Portugal) for hosting me during my stay in their group. I also want to thank to some individual persons that in some way helped me during this stay in 3B's Research Group: Tiago Silva, Nuno Oliveira, Constancio González, Ana Frias, and Miguel Oliveira.

I am also grateful to the secretary members of the Chemical Engineering Department. They provided me invaluable help since my arrival till the end of the Ph.D. Also thanks to the past and present technicians of the CRNE for the helpfulness with equipments: Néstor, Montse and Trifon.

The next paragraphs will be devoted to the family and closely friends, who directly and/or indirectly contributed and helped me during these last four years. Firstly, I must address a deep gratitude to José and Maria de Jesus (my parents), for their valuable advices, for helping me to fight for a better future, for the constant support and love that they always gave me in the good and less good moments, for all support and comprehension when I decided that dreams for something better required a change of country, for the patience they have had throughout all life and for their sacrifices that allowed me to be what I am today. I thank to Nuno Dias (my brother) for the deep friendship and support (thanks a lot for all work that you had with the cover of this thesis), to Joana for all support, friendship, and also for the entertaining football discussions (one day you will converted to F.C. Porto!!), thanks to Gabriel (the very new family member, nephew) who with his "Gabrialês" (baby imperceptible language), put everybody happy and in a good mood.

I would like to thank to Mónica (my girlfriend) for the love, encouragement, support and patience (at tons!!) during this almost 3 years that she shared with me. I also want to thank to her family too, whose greatly contribute with support, friendship, and also by the gastronomic delicacies. This is for you too: Marisa Ogando, Eduardo and Élida Cifuentes, Vicente Cifuentes and Carmen.

I offer here a special note of appreatiation to Dra. Ligia Martins (ITQB, Oeiras – Portugal), who was the first that opened to me the door to the vast world of scientific research. Certainly, without your invitation my scientific feel would not be possible and I would not be here today writing these words. Thank you so much!

Also like to express my gratitude to Dr. Celso Cunha (IHMT, Lisbon – Portugal) by the enriching period in which you welcomed me in your unit of molecular biology, and also to Dr. Isabel Cordeiro (HSM, Lisbon – Portugal) and all her team of Human Genetics Unit, who welcomed and allowed me to make the university final course project. They allowed me to obtain a better knowledge about the human genetic chromosomal. Thank you all for the motivation.

Finally, the last words of gratitude are here dedicated to the friends who were always by my side during this journey. Thank you for all advices, words of encouragement, for that "big hug" at the right time, and of course for being friends not only for the happy moments, but also for the least happy moments. A would like to mention with special love: Dora Rolo and Nuno Mendes (and baby Sebastião), Nuno Lavado and Catarina, Luís Possante and Isabel Cavaco (and Insaniae music!), Claúdio Almeida, Guilherme Cardoso, Hugo Guerreiro and Marta, Sofia Mendes, Christine Alexandra and Anders Jacobsson (thanks for Draconian music too!), Jordi Chalmeta, Emilio Sanchez and Montse, Cris and Dani.

"*The value of things is not in the time they last, but in the intensity which they occur. That is why they are unforgettable moments, inexplicable things, and unique people." Fernando Pessoa (Portuguese poet, 1888-1935)*

Barcelona, 31 of May, 2011

*"Success consists in being successful, not in having potential for success. Any wide piece of ground is the potential side of a palace, but there is no palace till it is built."*

*Fernando Pessoa (Portuguese poet, 1888-1935)*

*"A scientist is happy, not in resting on his attainments but in the steady acquisition of fresh knowledge."*

*Max Planck (German physicist, 1858-1947)*

## TABLE OF CONTENTS

## LIST OF STANDARD ABBREVIATIONS

| Abbreviation | Meaning |
|---|---|
| 5'-G/AATTC-3' | 5'-Guanine/Adenine.Adenine.Thymine.Thymine.Cytosine-3' |
| 5'-G/GATCC-3' | 5'-Guanine/Guanine.Adenine.Thymine.Cytosine.Cytosine-3' |
| AFM | Atomic force microscopy |
| A | Adenine |
| ADF | Amsterdam Density Functional |
| Ag\|AgCl | Silver\|Silver chloride |
| Ala | Alanine |
| Arg | Arginine |
| Asp | Aspartic acid |
| ATR | Attenuated total reflectance |
| $\beta$-NSA | $\beta$-naphthalenesulfonic acid |
| BRB | Britton-Robinson Buffer |
| BS | Basis set |
| BSSE | Basis-set superposition error |
| C | Cytosine |
| CA | Chronoamperometry |
| CD | Circular dichroism; (in sub-chapter 6.2, means Cyclodextrin) |
| CDPCYIGSR | Cys-Asp-Pro-Cys-Tyr-Ile-Glu-Ser-Arg |
| CE | Counter electrode |
| CFU | Colony forming units |
| CHL | Chloroform |
| $Cl^-$ | Chloride ion |
| $ClO_4^-$ | Perchlorate |
| CM | Counterpoise method |
| COS-7 | Line derived of *Cercopithecus aethiops* - African green monkey-kidney and immortalized by transformation with SV40 |
| CP or CPs | Conducting polymer(s) |

| | |
|---|---|
| CREKA | Cys-Arg-Glu-Lys-Ala |
| CSA | (±)-camphorsulfonic acid |
| CT | Charge transfer |
| CV | Cyclovoltammetry |
| CVC | Cyclic voltammetry control |
| Cys | Cysteine |
| DFT | Density functional theory |
| DMEM | Dubelco's Modified Eagle's Medium |
| DMP | Dimethylphosphate |
| DMSO | Dimethyl sulfoxide |
| DNA | Deoxyribonucleic acid |
| DTE | Dithioerythritol |
| DU145 | Human line derived from a prostate carcinoma |
| EC | Equivalent circuit |
| EDA | Energy decomposition analyses |
| EDOT | 3,4-ethylenedioxythiophene |
| EDTA | Ethylenediaminetetraacetic acid |
| EDX | Energy dispersive X-ray spectroscopy |
| EG | Ethylene glycol |
| EIS | Electrochemical impedance spectroscopy |
| FA | Formaldehyde |
| FBS | Fetal bovine serum |
| $FeCl_3$ | Iron chloride |
| FRA | Frequency response analyzer |
| FTIR | Fourier transform infrared |
| FWHM | Full-Width Half-Maximum |
| G | Guanine |
| GGA | Generalized gradient approximation |
| Glu | Glutamic acid |
| Gly | Glycine |

| | |
|---|---|
| GPC | Gel permeation chromatography |
| GPES | General purpose electrochemical system |
| $H_2$ | Hydrogen |
| $H_2O_2$ | Hydrogen peroxide |
| $H_2SO_4$ | Sulfuric acid |
| He/Ne | Helium/Neon |
| HEp-2 | Human line derived from an epidermoid carcinoma of larynx |
| HOMO | Highest occupied molecular orbital |
| HPLC | High-performance liquid chromatography |
| Ile | Isoleucine |
| IR | Infrared |
| ITO | Indium-tin oxide |
| KCl | Potassium chloride |
| $KH_2PO_4$ | Potassium dihydrogen phosphate |
| LD or LDs | Linear dextrin(s) |
| $LiClO_4$ | Lithium Perchlorate |
| LUMO | Lowest unoccupied molecular orbital |
| Lys | Lysine |
| LZ | Lysozyme |
| mA | 9-methyladenine |
| mC | 1-methylcytosine |
| MD | Molecular dynamics |
| mG | 9-methylguanine |
| $MgCl_2$ | Magnesium chloride |
| mNA | Methylated nucleic acids |
| MO or MOs | Molecular orbital(s); (in sub-chapter 5.2, MO means Morphine) |
| mT | 1-methylthymine |
| MTT | 3-(4,5-dimethylthiazol-2-yl)-2,5-diphenyltetrazolium |
| $Na_2HPO_4$ | Disodium hydrogen phosphate |
| NaCl | Sodium chloride |

| | |
|---|---|
| NaOH | Sodium hydroxide |
| NMPy | *N*-methylpyrrole |
| NMR | Nuclear magnetic resonance |
| PA | Polyacetylene |
| PAni | Polyaniline |
| PBE | PerdewBurke-Ernzerhof |
| PBS | Phosphate buffer saline |
| PCM | Polarizable continuum model |
| PEDOT | Poly(3,4-ethylenedioxythiophene) |
| PME | Particle-Mesh Ewald |
| PNMPy | Poly(*N*-methylpyrrole) |
| PPy | Polypyrrole |
| Pro | Proline |
| $PSS^-$ | Poly(styrene sulfonate) |
| PSSA | Poly(styrenesulfonic acid) |
| Pt | Platinum |
| PT3AME | Poly(3-thiophen-3-yl-acrylic acid methyl ester) |
| PT3M or P3MT | Poly(3-methylthiophene) |
| PT3MDE | Poly(2-thiophen-3-yl-malonic acid dimethyl ester) |
| PTh | Polythiophene |
| Py | Pyrrole |
| RAHB | Resonance assisted hydrogen bonds |
| RE | Reference electrode |
| RGD | Arg-Gly-Asp |
| RGDS | Arg-Gly-Asp-Cys |
| RMS | Root mean square |
| RNA | Ribonucleic acid |
| SCRF | Self-consistent Reaction-Field |
| SDS | Sodium dodecyl sulfate |
| SEM | Scanning electron microscopy |

| | |
|---|---|
| Ser | Serine |
| $SO_3^-$ | Sulfur trioxide |
| ss-hn | Single-stranted homo-nucleotides |
| STOs | Slater type orbitals |
| T | Thymine |
| T3M | 3-methylthiophene |
| TAE | Tris-acetate-EDTA |
| TBE | Tris-borate-EDTA buffer |
| TCPS | Tissue culture polystyrene |
| TDDFT | Time-dependent density functional theory |
| Th | Thiophene |
| TRIS | Tris(hydroxymethyl)aminomethane |
| Tyr | Tyrosine |
| UV-Vis | Ultraviolet visible |
| WAT | Aqueous solution |
| WE | Working electrode |

## LIST OF GENERAL SYMBOLS

| Symbol | Meaning | Usual Units |
|---|---|---|
| *A* | Absorbance | nm |
| $C_{dl}$ | Double layer capacitance | µF |
| CPE | Constant phase element | $F.cm^{-2}$ |
| $CPE_c$ | Capacitance of the polymer film | $F.cm^{-2}$ |
| $CPE_{dl}$ | Capacitance of the double layer | $F.cm^{-2}$ |
| Δ | Energy gap | eV |
| $\Delta E_b$ | Binding energies | kcal/mol |

| | | |
|---|---|---|
| $\Delta E_{b,,sol}$ | Binding energy of the complexes in solution | Kcal/mol |
| $\Delta E_{b,g}$ | Binding energy without counterpoise correction | kcal/mol |
| $\Delta E_{disp}$ | Dispersion energy | kcal/mol |
| $\Delta E_{int}$ | Interaction energy | kcal/mol |
| $\Delta E_{Pauli}$ | Pauli repulsion energy | kcal/mol |
| $\Delta E_{prep}$ | Preparation energy | kcal/mol |
| $\Delta E_{oi}$ | Orbital interaction energy | kcal/mol |
| $\Delta E_{b,g}^{CP}$ | Binding energy with counterpoise correction | kcal/mol |
| $\Delta E_{r,g}$ | Relative energy | kcal/mol |
| $\Delta E_{b,CHL}^{CP}$ | Binding energy with counterpoise correction in chloroform | kcal/mol |
| $\Delta E_{b,WAT}^{CP}$ | Binding energy with counterpoise correction in aqueous solution | kcal/mol |
| $\Delta G$ | Complexation driving force | kcal/mol |
| $\Delta G_{sol}$ | Free energy of solvation | kcal/mol |
| $\Delta G_{r,g}$ | Relative free energy | kcal/mol |
| $\Delta G_{r,CHL}$ | Relative free energy in chloroform | kcal/mol |
| $\Delta G_{r,WAT}$ | Relative free energy in aqueous solution | kcal/mol |
| $\Delta Q$ | Electroactivity | mC |
| $\Delta R_p$ | Polymer resistance variation | $\Omega.cm^{-2}$ |
| $\Delta V_{elstat}$ | Electrostatic interaction energy | kcal/mol |
| $E^\circ$ | Standard Potential of an electrode or couple | V |
| $\varepsilon$ | Dielectric constant | - |
| $\varepsilon_g$ | Transition energy | - |
| $j_{max}$ | Anodic current maximum density | $mA.cm^{-2}$ |
| $n_{ox\text{-}red}$ | Number of oxidation-reduction cycles | - |
| pH | Hydrogen potential | - |
| pKa | Acid dissociation constant | - |
| Q | Frequency-independent constant | - |

| | | |
|---|---|---|
| $r$ | Average RMS roughness | nm |
| $r^2$ | Correlation coefficient | - |
| $R_{ct}$ | Charge transfer resistance | $\Omega.cm^2$ |
| $R_p$ | Polymer resistance | $\Omega.cm^{-2}$ |
| $R_{po}$ | Pore resistance | $\Omega.cm^2$ |
| $R_s$ | Resistance between WE and RE | $\Omega.cm^2$ |
| $\sigma$ | Conductivity | S/cm |
| $t$ | Time | min |
| $\tau$ | Residence time | ps |
| $\vartheta$ | Polimerization time | s |
| Z | Impedance | $\Omega.cm^{-2}$ |
| $Z_{re}$ | Impedance: real component | $\Omega.cm^{-2}$ |
| $Z_{im}$ | Impedance: imaginary component | $\Omega.cm^{-2}$ |
| $\omega$ | Angular frequency | rad/s |

# Chapter 1

# Introduction

# 1. – Introduction

## 1.1 – Brief historical introduction

The conducting polymers (CPs) history is a sequence of discovery and rediscovery. Many CPs were known before any evidence about their electrical properties. The first reference describing the synthesis of a CP dates from 1862 when Letheby reported the anodic oxidation of aniline in dilute sulphuric acid, which yielded an insoluble deep-blue shiny powdered deposit on a platinum electrode.[1] At the end of 19$^{th}$ century, Goppelsroeder established that oligomers were formed by the oxidation of aniline, and were named "aniline black".[1,2]

In 1958, Natta synthesized polyacetylene (PA) by bubbling acetylene gas through a titanium/trialkyl-aluminum catalyst solution, resulting in an insoluble and unstable black crystalline powder. PA was the first organic polymer to be shown as conductive.[3] While organic conductors were intermittently discussed, the field was particularly energized by the prediction of superconductivity.[4]

In 1963, Bolto reported the presence of high electric conductivity in oxidized iodine-doped polypyrrol (PPy).[5,6] In 1967, Hideki Shirakawa prepared a thin silvery PA film using a Zieglar-Natta catalyst. He found found that the treatment of PA with halogens promotes a drastic increase of its electrical conductivity. Thus, semiconducting PA transforms into an organic "pseudometal" by changing the dopant nature and/or concentration.[7] In 1968, Dall'Ollio synthesized the first electronically CP bearing conjugated double bonds. He re-discovered PPy, which until such moment was known as "pyrrole black".[8,9] High conducting polyaniline (PAni) was reported by De Surville in the same year.[10]

In 1974, McGinness and co-workers described an electronic device made of organic polymers.[1,11] In 1977, Alan J. Heeger, Alan MacDiarmid and Hideki Shirakawa reported that the partial oxidation of PA films with iodine vapors or other similar reagents enhances the conductivity of the films by $10^9$ times.[6,12] Their research was distinguished in 2000 with the Nobel Prize in Chemistry "*For the discovery and development of conductive polymers*".[1]

In 1979 Heeger reported that CPs submitted to chemical and electrochemical redox processes yield materials with relatively high electronic conductivities.[13] At the same time Diaz and co-workers, reported that PPy prepared under controlled electrochemical conditions is a high conducting material with strong adhesion to metal surfaces and good

stability.[14] After the Heeger and Diaz studies, many CPs including PPy, polythiophene (PTh), poly(3,4-ethylenedioxythiophene) (PEDOT), polyfuran, polyflurene, PAni, poly(*p*-phenylene vinylene), and poly(*p*-phenylene), have been developed and extensively investigated.[3,8,15]

## 1.2 – Introduction to the conducting mechanism

Conductivity ($\sigma$ ) has units of Siemens per centimetre (S/cm). Usually materials are deemed as insulators when their conductivities are below $10^{-8}$ S/cm, semiconductors when their conductivities are between $10^{-7}$ and 1 S/cm and conductors when they have conductivities higher than 100 S/cm. Most CPs in their neutral states are insulators or weak semiconductors. They only achieve high conductivity after being "doped" by either an oxidizing or a reducing dopant.[16,17] It is generally believed that the so-called "soliton" or "polaron" and "bipolaron" structure is/are formed as a result of a redox reaction. PA will be used here to demonstrate the concept of solitons and PTh will be used to explain the concept of polaron and bipolaron.

Neutral *cis* PA is an insulator ($\sigma$= 1.7 x $10^{-9}$ S/cm), while its neutral *trans* isomer is a weak semiconductor ($\sigma$= 4.4 x $10^{-5}$ S/cm). Upon doping, either cationic radicals or anionic radicals are formed, depending on the dopant used. These redox processes generate charge transfer complexes on the polymer backbone called soliton (Figure 1), which is responsible for the intramolecular conductivity. Further, it seems that doping rearranges the *cis* isomer to the *trans* configuration as well.

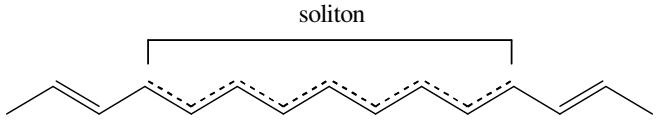


**Figure 1 –** Proposed conducting unit of PA. Soliton may be neutral (radical), positive (carbocation), or negative (carbanion).

However, when the soliton extends along the polymer backbone, energy accumulates due to double bond stretching and single bond constriction. This build-up of energy will eventually outweigh the stabilisation energy that arises from delocalisation. Therefore, solitons can only be elongated to a certain extent. Conductivity of the bulk PA though, depends not only on the solitons length and intramolecular conductivity. Electrons

moving intermolecularly across solitons also contribute to conductivity. The conduction thus generated is highly dependent on the polymer's crystalline structure. For example, the conductivity of PA film can be increased to $10^5$ S/cm level by properly orienting the polymer chains.[18]

Upon doping PTh, polarons and bipolarons are formed.[19] A polaron is a radical cation that stabilises itself by polarising the medium around it. Each polymer segment containing polaron can be further oxidised to form two polarons or a bipolaron. Figure 2 illustrates the formation of polaron and bipolaron. A bipolaron usually stretches from 1 to 6 carbon atoms and has a structural deformation associated with it. For example, the rearrangement of the arylene rings form aromatic to quinoidal configuration, thus maintaining planarity along this chain and moving in tandem as a pair. Movement of a polaron or a bipolaron via rearrangement of the double and single bonds in the conjugated polymer backbone accounts for conductivity at the intra-molecular level.

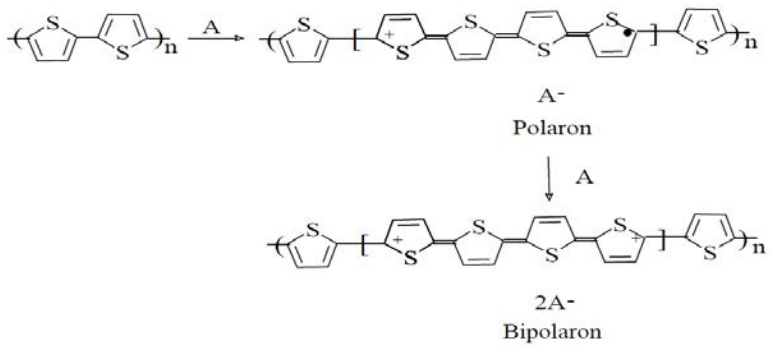


**Figure 2 –** Formation of polaron and bipolaron in PTh.

Quantum-chemical calculations revealed that the removal of an electron out of a polyarylene system like PPy or PTh leads to the formation of polaron and associated quinoid-like geometry (Figure 2) over four to five rings.[20] The quinoid structure has a lower ionisation potential and a larger electron affinity than the benzenoid structure. This lowering of the ionisation energy compensates the increase in total electronic energy due to lattice deformation around the polaron, thus energetically favouring the formation of polaron.[21,22]

Further oxidation results in the formation of bi-polaron as shown in Figure 2 above. At high doping levels, electrical transport is affected by bipolaron hopping (tunneling). Interchain hopping is believed to be the rate-determining step for the observed

macroscopic conductivity. Figure 3 illustrates interchain hopping of bipolaron according to Bredas *et al.*[23,24]

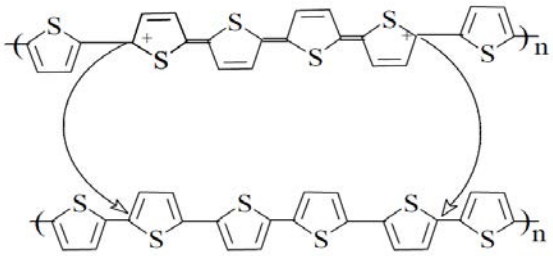

**Figure 3 –** Interchain hopping of bipolaron according to Bredas *et al*.

Almost all polymers are heterogeneous in terms of morphology, usually exhibiting two or more of the following characters: amorphous, quasi-amorphous, microcrystalline or fibrilar. However, it is generally agreed that the following criteria are necessary to obtain highly conducting systems: (i) extended-electron configuration; (ii) conjugated system over a planar polymer backbone; (iii) low ionisation potential (< 6.5 eV) for p-doping; (iv) low degree of structural defects, e.g., $sp^3$ defects and cross-linkages along conduction backbone; (v) high degree of macrostructural order, for example, a face-to-face arrangement of monomeric units from neighbouring chains and highly oriented fibres obtained via poling or mechanical stretching. Such orders are believed to facilitate inter-chain transport.

## 1.3 – Classification of conducting polymers

A number of conjugated polymer chains consisting of only unsaturated carbon atoms in the backbone or carbon atoms with electron rich heteroatoms or even totally non-carbon atom backbones have been synthesized in the last three decades (Figure 4).[1,25]

Polyvinylenes, polyarylenes and polyheterocycles are the major classes of CPs (Figure 4). Polyvinylenes are well known polymers, which possess good thermal stabilities and appreciably high electrical conductivities. Poly(*p*-phenylene) and poly(phenylene vinylene) belong to the class of polyarylenes or polyaromatics. Poly(*p*-phenylene) was the first non-acetylenic hydrocarbon polymer that showed high conductivity on doping.[26] PTh, PPy,

polyfuran and their derivatives having a five membered ring structure with one heteroatom like sulphur or nitrogen or oxygen, constitute the heterocyclic family of the CPs.[27-31]

Firstly, PPy and their derivatives received greater attention because of their ease of preparation, good chemical and thermal stabilities, and high condutivity.[14] However, in the last two decades some PTh derivatives with excellent electrical and electrochemical properties, as well as very high environmental stability, have been reported.[1,25,32] Among them, PEDOT (Figure 4), is the most important due to its high conductivity (up to 400-600 S/cm), good thermal and chemical stability, fast redox processes and excellent biocompatibility.[33] Consequently, this material has attracted considerable interest and many applications based on these properties have been rapidly developed, *e.g.* anti-static coatings, electrode material in supercapacitors, hole injection layer in organic light-emitting diodes, and solar cells.[34-36] Finally, PAni an electroactive conjugated polymer shows very good environmental stability and became an important subject of investigations since 1980 because of its significant potential for technological applications.[37]

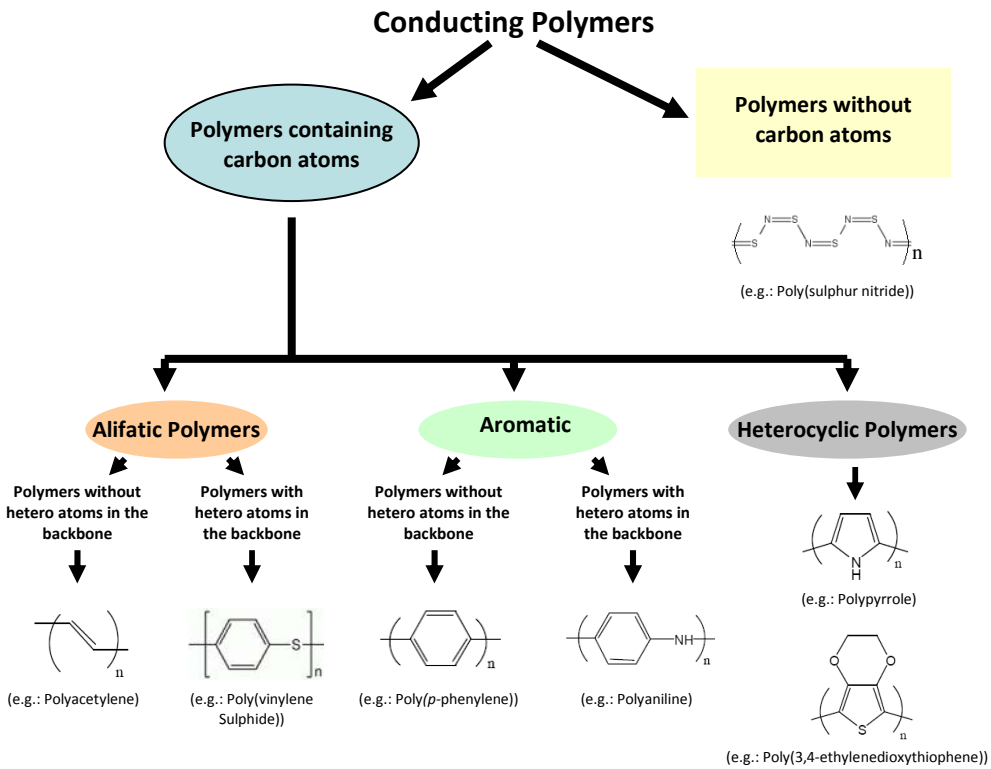


**Figure 4 –** Classification of Conducting Polymers.

## 1.4 – Synthesis of conducting polymers

Synthesized conjugated CPs can be classified into two major categories: chemically and electrochemically polymerized materials. In chemical polymerization, conjugated monomers react with an excess amount of an oxidant in a suitable solvent. The polymerization takes place spontaneously and requires constant stirring. The second method is the electrochemical polymerization, which involves placing working, counter and reference electrodes into a solution containing diluted monomer and electrolyte (dopant agent). After applying a suitable voltage, the polymer film immediately starts to form on the working electrode.

A major advantage of chemical polymerization concerns the possibility of mass-production at a reasonable cost. This is often difficult with electrochemical methods. On the other hand, an important feature of the electropolymerization technique is the direct formation of CP films that are highly conductive.

**1.4.1 – Chemical polymerization.** Chemical synthesis offers two advantages compared with electrochemical synthesis: a greater selection of monomers, and, using the proper catalysts, the ability to synthesize perfectly regioregular substituted polyheterocycles. The procedure involves a solution mixture of monomers and oxidizing agents (*e.g.* $FeCl_3$, $H_2O_2$, $H_2SO_4$ and some Lewis acids), the latter transforming the monomers into chemically active cation radicals.[9,38,39] These reactive species interact with other monomers yielding the polymer.[40]

Catalyzed chemical polymerization is particularly important for PTh, which like many other linear polyaromatic compounds is insoluble in organic solvents (rigid backbone) and substitution in the 3 and/or 4 position is necessary to render the polymer soluble (*i.e.* with the introduction of substituents, a number of different regioisomers is possible). Although substituted PTh derivatives were chemically synthesized by accident more than a century ago, the first planed chemical syntheses using metal-catalysts were reported by two independent groups in 1980.[41-43] Yamamoto *et al.* used Mg in tetrahydrofuran and nickel(bipyridine) dichloride, while Lin and Dudek also used Mg in tetrahydrofuran but with a series of acetyacetonate catalysts (*i.e.* $Pd^{+2}$, $Ni^{+2}$, $Co^{+2}$ and $Fe^{+3}$ complexes). The first synthesis of perfectly regioregular alkylated PThs was described by McCullough *et al.* in

1992.[44] As shown in Figure 5, selective bromination produces 2-bromo-3-alkylthiophene, which is followed by transmetallation and then Kumada cross-coupling in the presence of a Ni catalyst. This method produces approximately 100% of head-to-tail couplings, according to NMR spectroscopy analysis of the diads. While the McCullough method produces structurally homogeneous alkylated PThs, it requires low temperatures, the careful exclusion of water and oxygen, and brominated monomers. Currently, the most popular method is the oxidative polymerization of thiophenes using ferric chloride described by Sugimoto in 1986, which can be performed at room temperature under less demanding conditions.[45]

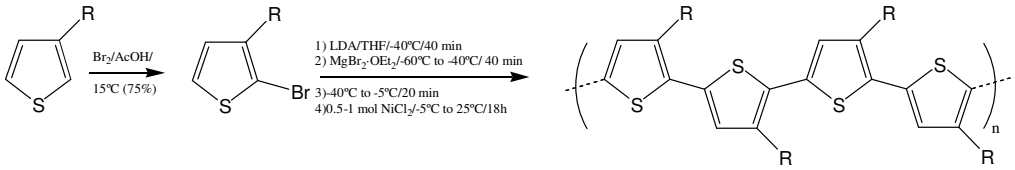


**Figure 5 –** Method for the production of head-to-tail coupling in PThs.

The use of very strong oxidizing agents may result in an overoxidation and other eventual degradation processes, as for example the decomposition and/or even the loss of the polymer, which lead to materials of poor quality.[46] Another disadvantage typically associated with the chemical polymerization occurs when the oxidized polymer precipitates in the polymerization medium reducing drastically the polymerization degree.[47]

**1.4.2 – Electrochemical polymerization.** In electrochemical polymerization, the monomer, dissolved in an appropriate solvent containing the desired anionic doping salt, is oxidized at the surface of the working electrode by application of an anodic potential (oxidation). The choice of the solvent and electrolyte is of particular importance in electrochemistry since both solvent and electrolyte should be stable at the oxidation potential of the monomer and provide an ionically conductive medium. Organic solvents like acetonitrile or propylene carbonate have very large potential windows, and high relative permittivities, which allow a good dissociation of the electrolyte and thus a good ionic conductivity.[41] For monomers with relatively low oxidation potentials, electropolymerization can be carried out in aqueous electrolytes. As a result of the initial oxidation, the radical cation of the monomer is formed and reacts with other monomers

present in solution to form oligomeric products and then the polymer. The extended conjugation in the polymer results in a lowering of the oxidation potential compared to the monomer. Therefore, the synthesis and doping of the polymer are generally done simultaneously. The anion is incorporated into the polymer to ensure the electrical neutrality and, at the end of the reaction, a polymeric film of controllable thickness is formed at the anode. The anode can be made of a variety of materials including steel, platinum, gold, glassy carbon, and tin or indium–tin oxide (ITO) coated glass.[48] The electropolymerization is generally achieved by potentiostatic (constant potential) or galvanostatic (constant current) methods. These techniques are easier to describe quantitatively and have been therefore commonly utilized to investigate the nucleation mechanism and the macroscopic growth. Potentiodynamic techniques such as cyclic voltammetry correspond to a repetitive triangular potential waveform applied at the surface of the electrode. The latter method is mainly used to obtain qualitative information about the redox processes involved in the early stages of the polymerization reaction, and to examine the electrochemical behaviour of the polymer film after electrodeposition.[49]

## 1.5 – A nanobiotechnological approach

Nanobiotechnology is defined as a discipline that applies the nanoscale principles to understand and transform biosystems, and using biological principles and materials to create new devices and systems integrated from the nanoscale. Nanotecnology provides the tools and technological platforms for the investigation of biological systems, while biotechnology inspires models and offers bio-assembled components to nanotechnology.[50] The combination of these two disciplines, as well as infotechnology and cognitive science, is expected to accelerate the development of new nanobiotechnological materials.[51,52]

The study of nanostructured materials involves manipulation, creation and use of materials, devices and systems, with dimensions smaller than 100 nm. Nanometer-scale materials provide important physical properties which are different from those of their bulk counterparts. Therefore, these are the keys features of nanomaterials which play an important role in the development of nanotechnology for human healthcare.[53,54] The progress in nanobiotechnology fields promotes the demand of methods to observe, characterize and control material and biological phenomena at the nanometer-scale.[55]

Nanostructured CPs are relatively inexpensive and can be functionalized using methods to achieve required optical, electronic or mechanical properties, and they also demonstrate biocompatibility, non-toxicity, specific surface area, high chemical and thermal stability, electro-catalytic activity and fast electron communication features, which make them suitable materials as immobilization platform or labels for the sensitive recognition events.[53] These unique features of conducting materials have led them to a variety of applications in analytical sciences. Such conducting nanostructured-based analytical tools are expected to have a major impact upon clinical diagnostics, environmental monitoring, security surveillance, and for ensuring food safety.[54,56] However, this area is still in development. In order to fully exploit the potential application of conducting nanomaterials in clinical chemistry for construction of biomedical devices, more perfect nanoparticles with well-defined geometry and properties, and long-term stability in various environments have to be designed and synthesized.[55]

## 1.6 – Nanobiotechnological applications

CPs have been used for a large variety of applications in microelectronics industry (battery technology, photovoltaic devices, light emitting diodes, and electronic displays). More recently, the use of these materials has been extended to the biotechnological and biomedical fields.[57] Thus, CPs have been shown to modulate cellular activities, including cell adhesion, migration, DNA synthesis, and protein secretion, upon electrical stimulation.[58] Many CPs present a number of important advantages for this kind of applications, which include biocompatibility, ability to entrap and control the release of biological molecules, ability to transfer charge from a biochemical reaction, etc. These unique characteristics make them useful for many specific applications, such as biosensors, tissue-engineering, scaffolds, neural probes, drug-delivery devices, and bio-actuators.[59]

**1.6.1 – Biosensors.** A biosensor is defined as a device that combines a bioreceptor, the biological component, and a transducer, which converts the recognition events into an analytical signal (preferably an electric signal). In the last decades, a wide variety of biosensors based on CPs have been developed for the detection of ions, small molecules, proteins, DNA, cells, and drugs. Biosensors have found extensive applications in medical

diagnostics, food quality assurance, environmental monitoring (air and water pollutants), industrial process control (e.g. fermentation processes) and to biological warfare agent detection.[60-63]

Commonly the transduction principles employed in biosensors derived from CPs are based on electrochemistry or reflectance/absorption techniques, due to their small size and simple instrumentation. The majority of biosensors used for the detection of biological entities are from electrochemical/electrical type, such their applied for glucose, proteins and DNA detection. They present great advantages, attributed to their good analytical performance associated with easy instrument maintenance.[63]

**1.6.2 – Tissue engineering.** Among biomedical applications of CPs, those based on their use as substrates for different cell types and functions are particularly important. Early *in vitro* and *in vivo* studies showed that cells such fibroblasts, neurons, and osteoblasts respond to electrical fields.[64-67] The general CP properties desired for tissue engineering applications include conductivity, reversible oxidation, redox stability, biocompatibility, hydrophobicity (40-70˚ water contact angle promotes cell adhesion), three-dimensional geometry, and surface topography. Different studies have demonstrated cell and tissue compatibility not only of PPy but also of PTh derivatives.[59,68,69] The advantage of CPs in tissue-engineering applications is based on the response of cells to the electrical field induced when a current or voltage is applied to the polymer.[70,71] For example, the ability to support mammalian cell growth on CP surfaces is enhanced by the application of electrical stimuli. The majority of studies to date have focussed on nerve cells. Given the enormous benefits to be gained from effectively interfacing nerves and conducting materials for implants such as the cochlear implant or artificial retina, this is not surprising. The possibility of using such materials for nerve repair either in the peripheral nervous system or even for spinal chord regeneration underscores the need for this ongoing research.[72,73]

Two different approaches are frequently employed. The first one uses micro- or nano-patterned CP surfaces created for potential tissue engineering applications, including three dimensional honeycombs, porous CP films, microsized circles and microfluidic mimics of the vascular network.[74-77] For example, the application of PPy coated-microtubes as blood vessels connectors, which produces the expansion of the tissues on the polymer connecting the two ends together and reinforcing the vessel.[77] In the second one, metallic

surfaces coated by electrodeposited CPs are applied as biocompatible and biofunctional interfaces for medical implants.[59,78] For example, it has been demonstrated that neural glial cells grow on PPy-coated electrodes containing the nonapeptide CDPCYIGSR.[79]

**1.6.3 – Scaffolds.** Scaffolds of electrically conducting and biologically active polymers are desirable for promote adhesion and proliferation.[80] During the last years, CPs have been employed as tissue engineering scaffolds for restoring, maintaining and reconstructing the function of impaired tissues and organs. In most cases, conducting scaffolds are obtained by using a biodegradable synthetic/natural polymer as a matrix and an intrinsically CP as a conductive component. Electrically CPs such as PPy, PAni, PTh and their derivatives have been widely used as scaffolds in many areas such as cartilage formation, joint resurfacing, cell transplantation and neurite outgrowth. However, as scaffolds CPs present some weaknesses: poor biodegradability, hydrophobicity, and, depending on the material, they can liberate acidic products during their degradation.[80,81] Research in this field is expected to contribute for the attainment of more efficient scaffolds, which should also avoid infections, multiple surgeries and additional costs to the patients.[82]

The versatility of CPs synthesis enables the creation of a great variety of bioactive surfaces. For example, the incorporation of biomolecules such as proteins (enzymes and antibodies) in the synthesis medium results in the attainment of new hybrid materials, which may play and improve the intrinsic deficiencies of CPs in this field.

**1.6.4 – Neural probes.** Many of the advances made in CPs for tissue engineering applications, in particular with respect to neurons, are important for the development of optimized neural electrodes. The need to intimately interface electrodes with neural tissue and to relay efficient signals between the cells and the electrode are particularly relevant in this field. CPs are attractive candidates for interface electrodes with neurons because they can provide a large surface area, promoting effective ion exchange between the recording sites and the surrounding tissue.[59,71] Thus, the capacitance increases with surface area resulting in a reduction of the impedance and, therefore, in an improvement of the signal-to-noise ratio. Ideally, a neural probe tends to: (i) maximize the recorded neural signals; (ii) minimize the noise; (iii) maintain high capacitances; and (iv) retain the conductivity.

Although PPy is the most studied CP for coating neural probes, PEDOT has been also considered in some recent studies because of its high stability and electrical conductivity.[59]

**1.6.5 – Drug delivery.** Electroactive CP films are also ideal hosts for the controlled release of chemical substances, including therapeutic drugs. The redox state of CPs can be modulated and controlled through electrical external stimuli. Therefore, electrically-controlled drug releasing system based on CPs can be easily designed and fabricated. Chronic diseases in which dosing requirements of drugs are not constant are among the most obvious applications of such drug-delivery systems. As was mentioned above, the biosensing capabilities of CPs have been largely developed in the last decades.[83] Amperometric biosensing devices able to provoke a response when the concentration of a specific compound (*e.g.* glucose, cholesterol, lactate or urea) is larger than a threshold value, have been developed by immobilizing enzymes on CP films.[84-88] Accordingly, in a near future the same CP is expected to be used as both biosensor and drug delivery device by creating a self regulating system.[83,89]

**1.6.6 – Bioactuators.** Bioactuators consist on devices able to transform energy, especially chemical or electrochemical, into mechanical force.[72] The combination of chemical reactions and molecular energy contributes to the development of electrochemical actuator devices, as for example, artificial muscles and smart membranes.[90] Artificial muscles could be considered as electrochemo-mechanical actuators. Among the advantages of CPs to act as bioactuators, the most important are: (i) their strength at the molecular level; (ii) the ability of these materials to work at room or physiological temperatures; (iii) they can be fabricated at the micro and nanoscales; and (iii) their light-weight, which is due to their organic nature.[91]

Recent studies on PPy, PAni and some PTh derivatives showed that these materials undergo significant changes in the volume upon electrochemical oxidation-reduction processes, which can be used to produce mechanical energy. The changes of volume can be due to the diffusion and intercalation of ionic species in the polymer bulk film (mechanism I), which maintain the electro-neutrality during the oxidation process, or due to drastic conformational changes that are induced by electrical activation (mechanism II).[92-98] When the generation of work upon consumption of electromechanical energy involves mechanism I, resembles that of natural muscles.[99] Thus, the muscular motion is initiated

with an electric impulse generated on the brain towards de nervous system, promoting an increase of $Ca^{2+}$ concentration, which is subsequently released in the myofibrils of the muscles. The increase of ionic concentration in the muscles originates important conformational changes in the troponin-tropomyosin complex.[100,101] When the operating mechanism of the actuator is based on the molecular flexibility (mechanism II), the CP responds to the electrochemical stimuli with conformational changes, producing contraction-expansion movements. In both mechanisms the magnitude of the structural change can be regulated by the external electrochemical potential.

## 1.7 – References

[1] G. Inzelt, "*Conducting Polymers: A new era in electrochemistry*", Springer, Berlin (2008).

[2] J. Heinze, *Top. Curr. Chem*. 152 (1990) 1.

[3] H. S. Nalwa, "*Handbook of Advanced Electronic and Photonic Materials and Devices*", Academic Press, USA (2001) 132.

[4] W. A. Little, *Phys. Rev. A* 1416 (1964) 134.

[5] B. A. Bolto, R. McNeill, D. E. Weiss, *Aust. J. Chem.* 16 (1963) 1103.

[6] Z. P. Li, B. H. Liu, *J. Appl. Electrochem.* 40 (2010) 475.

[7] C. T. Kuo, S.-A. Chen, G.-W. Hwang, H.-H. Kuo, *Synth. Metals* 93 (1998) 155.

[8] A. Dall'Ollio, Y. Dascola, V. Varacca, V. Bocchi, *Comptes Rendus C* 267 (1968) 433.

[9] D. D. Ateh, H. A. Navsaria, P. Vadgama, *J. R. Soc. Interface* 3 (2006) 741.

[10] R. De Surville, M. Jozefowicz, L. T. Yu, J. Pepichon, R. Buvet, *Electrochim. Acta* 13 (1968) 1451.

[11] J. McGinness, P. Corry, P. Proctor, *Science* 183 (1974) 853.

[12] J. D. Stenger-Smith, *Prog. Polym. Sci.* 23 (1998) 57.

[13] A. G. McDiarmid, A. J. Heeger, "*Molecular Materials*", Plenum, New York (1979) 1.

[14] A. F. Diaz, K. K. Kanasawa, G. P. Gardini, *J. Chem. Soc. Chem. Comm.* (1979) 635.

[15] H. Peng, L. Zhang, C. Soeller, J. Travas-Sejdic, *Biomaterials* 30 (2009) 2132.

[16] U. Evans, O. Soyemi, M. S. Doescher, U. H. F. Bunz, L. Kloppenburg, M. L. Myrick, *Analyst* (Cambridge, U. K.) *126* (2001) 508.

[17] M. D. McClain, D. S. Dudis, *Synth. Metals* 116 (2001) 199.

[18] H. Shirakawa, Angew. *Chem. Int. Ed.* 40 (2001) 2575.

[19] A. Johansson, S. Stafstrom, *Physical Review B* 65: art. no. 045207 (2002).

[20] C. Casanovas, C. Alemán, *J. Phys. Chem.* C 111 (2007) 4823.

[21] J. L. Bredas, B. Thelmans, J. M. Andre, *Phys. Rev. B* 27 (1983) 7827.

[22] J. L. Bredas, F. Wudl, A. J. Heeger, *Solid State Commun.* 63 (1987) 577.

[23] J. L. Bredas, G. B. Street, *Acc. Chem. Res.* 18 (1985) 309.

[24] J. L. Bredas, B. Thelmans, J. M. Andre, *Phys. Rev.* B26 (1982) 6000.

[25] G. G. Wallace, G. M. Spinks, L. A. P. Kane-Maguire, P. R. Teasdale, "*Conducting Electroactive Polymers: Intelligent Polymer Systems*", New York: CRC Press (2008) 1.

[26] L. W. Shacklette, H. Hckhard, R. R. Chance, R. H. Baughman, *J. Chem. Soc. Chem. Commun.* (1980) 635.

[27] G. Tourillon, F. Garnier, *J. Electroanal. Chem.* 135 (1982) 173.

[28] R. J. Waltman, J. Bargon, A. F. Diaz, *J. Phys. Chem.* 87 (1983) 1459.

[29] R. Janson, H. Arwin, A. Bjorklund, I. Lunstrom, *Thin Solid Films* 125 (1980) 205.

[30] A. F. Diaz, A. Matninez, K. K. Kanazawa, M. Salmon, *J. Electroanal. Chem.* 130 (1980) 181.

[31] J. J. Ohsawa, K. Kaneto, K. Yoshino, *J. Appl. Phys.* 23 (1984) L663.

[32] C. Ocampo, E. Armelin, F. Estrany, L. J. Del Valle, R. Oliver, F. Sepulcre, C. Alemán, *Macromol. Mater. Eng.* 292 (2007) 85.

[33] N. Rozlosnik, *Anal. Bioanal. Chem.* 395 (2009) 637.

[34] C. J. Brabec, N. S. Sariciftci, J. C. Hummelen, *Adv. Funct. Mater*. 11 (2001) 15.

[35] M. Granstörm, M. Berggren, O. Inganäs, *Science* 267 (1995) 1479.

[36] L. Groenendaal, G. Zotti, P.-H. Aubert, S. M. Waybright, J. R. Reynolds, *Adv. Mater.* 15 (2003) 855.

[37] A. F. Diaz, J. A. Logan, *J. Electroanal. Chem.* 111 ( 1980) 111.

[38] N. Toshima, S. Hara, *Prog. Polym. Sci.* 20 (1995) 155.

[39] K. Jackowska, A. T. Bieguński, M. Tagowska, *J. Solid State Electrochem.* 12 (2008) 435.

[40] A. Malinauskas, *Polymer* 42 (2001) 3957.

[41] V. Meyer, *Ber. Deutsch. Chem. Ges.* 16 (1883) 1465.

[42] T. Yamamoto, K. Sanechika, A. Yamamoto, *J. Polym. Sci., Polym. Lett.* Ed. 18 (1980) 9.

[43] J. W. P. Lin, L. P. Dudek, *J. Polym. Sci., Polym. Chem. Ed.* 18 (1980) 2869.

[44] R. D. McCullough, R. D. Lowe, *J. Chem. Soc. Chem. Commun.* (1992) 70.

[45] R. Sugimoto, S. Taketa, H. B. Gu, K. Yoshino, *Chem. Express* 1 (1986**)** 635.

[46] M. Nuñez, "*Progress in Electrochemistry Research*", Nova Science Publishers, Inc., New York (2005) 93.

[47] R. H. Baughman, J. L. Brédas, R. R. Chance, R. L. Elsenbaumer, L. W. Shacklette, *Chem. Rev.* 82 (1982) 209.

[48] A. J. Bard, L. R. Faulkner, "*Electrochemical Methods, Fundamentals and Applications*", John Wiley & Sons, New York (1980).

[49] M. E. G. Lyons, "*Advances in Chemical Physics*", *Polymeric Systems*, ed. I. Prigogine and S. A. Rice, John Wiley & Sons, New York 94 (1997) 297.

[50] A. Ishijima, T. Yanagida, *Trends Biochem. Sci.* 26 (2001) 438.

[51] National Research Council: "*Implications of emerging micro and nanotechnologies*". The National Academies Press, Washington DC (2002).

[52] M. C. Roco, *Curr. Opi. Biotechnol.* 14 (2003) 337.

[53] O. V. Salata, *J. Nanobiotechnol.* 2 (2004) 3.

[54] K. M. Abuh-Salah, A. A. Ansari, S. A. Alrokayan, *J. Biom. Biotechnol.* (2010) DOI:10.1155/2010/715295.

[55] A. A. Ansari, M. Alhoshan, M. S. Alsalhi, A. S. Aldwayyan, *Sensors* 10 (2010) 6535.

[56] D. W. Hatchett, M. Josowicz, *Chem. Rev.* 108 (2008) 746.

[57] K. Gurunathan, A. V. Murugan, R. Marimuthu, U. P. Mulik, D. P. Amalnekar, *Mater. Chem. Phys.* 61 (1999) 173.

[58] J. Y. Wong, R. Langer, D. E. Ingber, *Proc. Natl. Acad. Sci.* USA 91 (1994) 3201.

[59] N. K. Guimard, N. Gomez, C. E. Schmidt, *Prog. Polym. Sci.* 32 (2007) 876.

[60] B. Adhikari, S. Majumdar, *Prog. Polym. Sci.* 29 (2004) 699.

[61] Z. Lin, L. W. Burgess, *Anal. Chem.* 66 (1994) 2544.

[62] I. Turyan, D. Mandler, *Anal. Chem.* 69 (1997) 894.

[63] T. M.-H. Lee, *Sensors* 8 (2008) 5535.

[64] P. Aebischer, R. F. Valentini, P. Dario, C. Domenici, P. M. Galleti, *Brain Res.* 436 (1987) 165.

[65] G. Fine, R. F. Valentini, R. Bellamkonda, P. Aebischer, *Biomaterials* 12 (1991) 775.

[66] L. F. Jaffe, M. M. Poo, *J. Exp. Zool.* 209 (1979) 115.

[67] J. M. Kerns, I. M. Pavkovik, A. J. Fakhouri, K. L. Wickersham, J. A. Freeman, *J. Neurosci. Methods* 19 (1987) 217.

[68] X. Wang, X. Gu, C. Yuan, S. Chen, P. Zhang, T. Zhang, J. Yao, F. Chen, G. Chen, *J. Biomed. Mat. Res. A* 68 (2003) 411.

[69] L. J. del Valle, D. Aradilla, R. Oliver, F. Sepulcre, A. Gamez, E. Armelin, C. Alemán, F. Estrany, *Eur. Polym. J.* 43 (2007) 2342.

[70] C. E. Schmidt, V. R. Shastri, J. P. Vacanti, R. Langer, *Proc. Natl. Acad. Sci.* USA 94 (1997) 8948.

[71] R. L. Williams, P. J. Doherty, *J. Mater. Sci.: Mater. Med.* 5 (1994) 429.

[72] R. Ravichandran, S. Sundarrajan, J. R. Venugopal, S. Mukherjee, S. Ramakrishna, *J. R. Soc. Interface* (2010) 1. DOI:10.1098/rsif.2010.0120.focus.

[73] R. D. Breukers, K. J. Gilmore, M. Kita, K. K. Wagner, M. J. Higgins, S. E. Moulton, G. M. Clark, D. L. Officer, R. M. I. Kapsa, G. G. Wallace, *J. Biomed. Mat. Res. A* 95 (2010) 256.

[74] P. N. Bartlett, P. R. Birkin, M. A. Ghanem, C.-S. Toh, *J. Mater. Chem.* 11 (2001) 849.

[75] T. Cassagneau, F. Caruso, *Adv. Mater.* 14 (2002) 34.

[76] D. A. LaVan, P. M. George, R. Langer, *Angew Chem. Int. Ed.* 42 (2003) 1262.

[77] E. Smela, *Adv. Mater.* 15 (2003) 481.

[78] Z. Weiss, D. Mandler, G. Shustak, A. J. Domb*, J. Polym. Sci. Part A: Polym. Chem.* 42 (2004) 1658.

[79] A. Wirsen, "*Electroactive Polymer Materials*". Technomic Publishing Co., Inc. Lancaster (1987).

[80] J. Y. Lee, J.-W. Lee, C. E. Schmidt, *J. R. Soc. Interface* 6 (2009) 801.

[81] D.-H. kim, M. Abidian, D. C. Martin, *J. Biomed. Mater. Res. A* 71(4) (2004) 577.

[82] A. Subramanian, U. M. Krishnan, S. Sethuraman, *J. Biomed. Sci.* 16 (2009) 1.

[83] S. Geetha, C. R. Rao, M. Vijayan, D. Trivedi, *Anal. Chim. Acta* 568 (2006) 119.

[84] Y.-M. Uang, T.-C. Chou, *Electroanalysis* 14(22) (2002) 1564.

[85] S. Tirkes, L. Toppare, S. Alkan, U. Bakir, A. Onen, Y. Yagci, *Int. J. Biol. Macromolecules* 30 (2002) 81.

[86] J. L. Besombes, S. Cosnier, P. Labbe, G. Reverdy, *Anal. Chim. Acta* 317 (1995) 275.

[87] S. Cosnier, M. Fontecave, C. Innocent, V. Niviere, *Electroanalysis* 9(9) (1997) 685.

[88] S. Komaba, M.Seyama, T. Osaka, *Electrochim. Acta* 42(3) (1997) 383.

[89] D. Svirskis, J. Travas-Sejdic, A. Rodgers, S. Garg, *J. Control. Rel.* 146 (2010) 6.

[90] T. F. Otero, *J. Mater. Chem.* 19 (2009) 681.

[91] E. Smela, *Adv. Mater.* 15 (2003) 481.

[92] E. W. H. Jager, E. Smela, O. Inganäs, *Science* 290 (2000) 1540.

[93] W. Lu, A. G. Fadeev, B. Qui, E. Smela, B. R. Mattes, J. Ding, G. M. Spinks, J. Mazurkiewicz, D. Zhou, G. G. Wallace, D. R. MacFarlane, S. A. Forsyth, M. Forsyth, *Science* 297 (2002) 983.

[94] T. F. Otero, M. T. Cortes, *Adv. Mater.* 15 (2003) 279.

[95] J. Casanovas, D. Zanuy, C. Aleman, *Angew. Chem.* 118 (2006) 1121; *Angew. Chem. Int. Ed.* 45 (2006) 1103.

[96] D. Zanuy, C. Alemán, *Chem. Eur. J.* 13 (2007) 2695.

[97] H.-H. Yu, B. Xu, T. M. Swager, *J. Am. Chem. Soc*. 125 (2003) 1142.

[98] D. Zanuy, J. Casanovas, C. Alemán, *J. Phys. Chem. B* 110 (2006) 9876.

[99] Y. Osada, D. E. De Rossi, "*Polymer Sensors and Actuators*", Springer, Berlin (2000) 295.

[100] B. Alberts, D. Bray, A. Johnson, J. Lewis, M. Raff, P. Walter, "*Essential Cell Biology: an introduction to the molecular biology of the cell*", Garland Publishing, Inc., New York & London (1998) 539.

[101] H. S. Nalwa, "*Handbook of Organic Conductive Molecules and Polymers: Conductive Polymers – Synthesis and electrical properties*", John Wiley & Sons Ltd., New York (1997) 517.

# Chapter 2

# Objectives

# 2. – Objectives

**2.1 – The principal objective of the first block of this Thesis (Chapter 4) consists on the understanding of the more important characteristics of the specific non-electrostatic interactions formed between selected CPs and DNA bases. In order to ascertain such characteristics, different secondary well-defined objectives have been explicitly studied in the five sections (from 4.1 – to 4.5) involved in this block. These secondary objectives can be summarized as follows:**

(a) The formation of stable adducts involving plasmid DNA and CPs has been examined. Special attention has been given to detect the possible existence of specific interactions will well-defined nucleotide sequences. Investigations of both the chemical requirements necessary for the formation of such specific interactions and the structural alterations induced in the DNA have analyzed with some detail. Studies have been developed considering a relatively wide number of PTh derivatives, even though the work has been mainly focussed on PEDOT because of its technological interest.

(b) The influence of the doping level on CP···DNA interactions has been investigated considering PEDOT with three different doping levels, which include a reduced state with about +0.1 charges per repeating unit and a completely oxidized state with more than +1.0 charges per repeating unit. This will allow us to evaluate the importance of non-specific electrostatic interactions against specific weak interactions.

(c) The interaction between PEDOT and the four DNA bases have been explicitly investigated using short single-stranded homo-nucleotides (ss-hn). The possible existence of hydrogen bonding and/or $\pi$-$\pi$ stacking interactions in adducts involving such CP and different ss-hn have been studied using UV-Vis spectroscopy and circular dichroism (CD). In addition, a top-down hierarchical modelling approach has allowed us to provide a comprehensive picture of the experimental observations obtained for all the studied complexes.

(d) The chemical nature of the complexes involving the building block of PEDOT (*i.e.* a monomeric unit) and guanine, which is the DNA base preferred by this CP, has been investigated not only at the molecular level but also at the electronic one.

**2.2 – The second block of the Thesis (Chapter 5) is devoted to investigate the possible use of conventional CPs for the detection of morphine, a drug with well-known anaesthetic properties. For this purpose, the interaction of different CPs and morphine molecules has been examined through electrochemical techniques considering two different strategies, which correspond to the two sections (from 5.1 – to 5.2) of this block. The secondary objectives of this chapter are:**

(a) In order to improve the electrochemical properties of conventional PNMPy films, which are known to be poor, and promote the interaction of this material with morphine molecules, the synthesis of PNMPy hollow microstructures have been investigated. More specifically, anodic polymerization in aqueous solution assisted by gas templates was used for this purpose, three organic surfactants, which differ in their chemical nature and molecular weight, being considered.

(b) The ability of PNMPy hollow microstructures to detect electrochemically morphine has been investigated using EIS measurements.

(c) As the intrinsic electrochemical properties of PEDOT are known to be very good, films of this material have been used for the electrochemical detection of morphine molecules. The performance of both CV and EIS techniques have been examined and compared, different experimental conditions (i.e. incubation times and pHs) being considered for this purpose.

**2.3 – The last block of results (Chapter 6) presents three new biocomposites, which have been prepared by combining PEDOT with a protein (lysozyme), oligo- and poly-saccharides (α-cyclodextrin and linear dextrin, respectively), and a peptide (CREKA). It should be remarked the main objective of this Chapter was to initiate a new research line in IMEM's group devoted to the formulation of electroactive**

**biocomposites. PEDOT was selected for these preliminary studies not only because of its excellent electrochemical and electrical properties but also because previous studies of the own group showed that it is a biocompatible material. Currently, other researchers of the group are extending these investigations. More specifically, they are developing deeper studies on some of the systems reported in this work and preparing new biocomposites based on other CPs and/or biomolecules. The secondary objectives of this chapter can be summarized as follows:**

(a) A new biocomposite to protect PEDOT films from infection of bacterial microorganisms have been prepared and characterized. PEDOT has been reported to be an efficient electroactive substrate for the adhesion and growing of eukaryotic cells. Two different strategies have been used to prepare the biocomposite: adsorption of a bactericidal protein on the surface of PEDOT substrates and electropolymerization of the CP but introducing such protein in the generation medium with the monomer.

(b) Bioactive platforms with good electrical properties have been fabricated by combining PEDOT with linear and cyclic dextrines. The electrochemical and electrical properties, morphology and structure, and hydrophobicity of the surface of the new biocomposites have been characterized. Furthermore, the behaviour of these hybrid materials as cellular matrix has been examined by cell adhesion and proliferation assays considering different epithelial- and fibroblast-like lines.

(c) PEDOT has been modified with CREKA, a positively charged peptide that recognizes clotted plasma proteins. The effectiveness of conventional electropolymerization techniques to entrap this peptide in the polymer matrix has been evaluated. Furthermore, the influence of the peptide in the electrochemical, structural and bioactive properties of the CP has been examined.

# Chapter 3

# Methodology

# 3. – Methodology

## 3.1 – Electrochemistry

All CPs used in the present work were produced by electrochemical synthesis, with exception to poly(3-thiophen-3-yl-acrylic acid methyl ester) (PT3AME) and poly(2-thyophen-3-yl-malonic acid dimethyl ester) (PT3MDE), that were produced by chemical synthesis. The anodic polymerizations and electrochemical studies were performed using a VersaStat II potenciostat-galvanostat connected to a computer controlled through a Power Suite Princenton Applied Research Program. CPs were prepared using the chronoamperometry (CA) technique, in which a fast-rising potential pulse is enforced on the working electrode of an electrochemical cell and the current flowing through this electrode is measured as a function of time. Doping and dedoping processes were studied using the chronopotenciometry technique, in which the potential at the working electrode is measured against a reference electrode as a function of time after apply a fast-rising current pulse on the former electrode. Finally, oxidation-reduction processes have been examined by potentiodynamic electrochemical measurements through the cyclic voltammetry (CV) technique. In CV experiments the working electrode potential is ramped linearly versus time like linear sweep voltammetry. When the set potential is reached, the working electrode's potential ramp is inverted. This inversion can happen multiple times during a single experiment. The current at the working electrode is plotted versus the applied voltage to give the cyclic voltammogram trace. CV is generally is used to study not only the potential of oxidation-reduction processes but also the potential range in which the solvent is stable, the reversibility grade and efficiency of the reaction, the ability of the material to storage charge, etc.[1]

## 3.2 – Electrochemical impedance spectroscopy

Electrochemical impedance spectroscopy (EIS) studies were performed in an Autolab PGSTAT 302N potentiostat/galvanostat equipped with a frequency response analyzer (FRA) software program. This technique measures the impedance of a system over a range of frequencies, and therefore the frequency response of the system, including the energy storage and dissipation properties, is revealed. Typically, data obtained by EIS are

represented graphically to show the system's frequency (Bode plot) and/or stability (Nyquist plot) responses.

The impedance of a system at a given frequency is defined by reason between the amplitude of alternate current signal and the phase angle. All these parameters at different frequencies constitute the impedance spectrum.[1] EIS has been found to be a powerful tool to study charge-transfer parameters, ion diffusion, capacitance of CP-modified electrodes and corrosion.

## 3.3 – Ultraviolet visible spectrophotometry

Ultraviolet visible (UV-Vis) spectrophotometry studies were performed in a Nicolet Evolution 300 (Thermo Electron Co.) spectrophotometer controlled by the VisionPro software, and in a UV-3600 (Shimadzu) UV-Vis-NIR spectrophotometer controlled by the UVProbe 2.31 software. UV-Vis absorption spectroscopy was used to examine the between DNA (both plasmid and oligonucleotides) with PEDOT and the dextrins delivery from biocomposites used as cellular scaffolds.

UV-Vis spectroscopy is used to obtain the absorbance spectrum of a material in solution or as a solid. What is actually being observed spectroscopically is the absorbance of light energy or electromagnetic radiation, which excites electrons from the ground state to the first singlet excited state of the material. The UV-Vis region of energy for the electromagnetic spectrum covers 1.5-6.2 eV which relates to a wavelength range of 800-200 nm. The Beer-Lambert law ($A=\varepsilon \cdot b \cdot c$) is the principle behind the absorbance spectroscopy. For a single wavelength, $A$ is absorbance (unitless, usually seen as arbitrary units), $\varepsilon$ is the molar absorptivity of the compound or material in solution ($M^{-1} \cdot cm^{-1}$), $b$ is the path length of the cuvette or sample holder (usually 1 cm), and $c$ is the concentration of the solution (M).

The absorption of UV-Vis radiation corresponds to the excitation of outer electrons. There are three types of electronic transition which can be considered: 1) Transitions involving $\pi$, $\sigma$ and $n$ electrons (those of functional groups of organic molecules, typically named chromophores, that contain valence electrons of low excitation energy); 2) Transitions involving charge-transfer electrons (those of complexes made of a component with electron donating properties and the other able to accept electrons, absorption of

radiation involving the transfer of an electron from the donor to an orbital associated with the acceptor); and 3) Transitions involving *d* and *f* electrons (not frequent in organic materials).[2] When an atom or molecule absorbs energy, electrons are promoted from their ground state to an excited state. In a molecule, the atoms can rotate and vibrate with respect to each other. These vibrations and rotations also have discrete energy levels, which can be considered as being packed on top of each electronic level.

## 3.4 – Circular dichroism spectroscopy

Circular Dichroism (CD) spectroscopy measurements were carried out in a Jasco J-810 spectropolarimeter. CD spectroscopy technique was used to detect structural alterations undergone by DNA oligonucleotides and plasmidic DNA upon interaction with CPs.

CD spectroscopy measures the difference in the absorption of left-handed circularly polarised light and right-handed polarised light, which occurs in molecules containing one or more chiral chromophores:

$$\Delta A(\lambda) = A_L(\lambda) - A_R(\lambda)$$

where L and R refers to left- and right-handed, respectively, and $\lambda$ is the wavelength

CD is used extensively to study chiral molecules of all types and sizes, but it is in the study of large biological molecules where it finds its most important applications. A primary use is in analysing the secondary structure or conformation of macromolecules, particularly proteins and DNA, and because secondary structure is sensitive to its environment, e.g. temperature or pH, circular dichroism can be used to observe how molecular structure changes with environmental conditions or on interaction with other molecules. Structural, kinetic and thermodynamic information about macromolecules can be derived from CD spectroscopy.[3]

Measurements carried out in the visible and ultra-violet region of the electro-magnetic spectrum monitor electronic transitions, and, if the molecule under study contains chiral chromophores then one circularly polarised light state will be absorbed to a greater extent than the other and the CD signal over the corresponding wavelengths will be non-zero. A circular dichroism signal can be positive or negative, depending on whether

left-handed circularly polarised light is absorbed to a greater extent than right-handed circularly polarised light (CD signal positive) or to a lesser extent (CD signal negative).

## 3.5 – Fourier transform infrared spectroscopy

Fourier Transform Infrared (FTIR) spectroscopy studies were performed in a FT/IR-4100 Jasco spectrometer equipped with an attenuated total reflectance (ATR) ATR-MKII Golden Gate Heated Single Reflection Diamond Specac model.

FTIR spectroscopy is a technique that provides information about the chemical bonding or molecular structure of materials. It is essentially used to identify the materials present in a specimen and is usually complemented with energy dispersive X-ray spectroscopy (EDX) analyses. The technique works on the fact that bonds and groups of bonds vibrate at characteristic frequencies. A molecule that is exposed to infrared radiation absorbs infrared energy at frequencies which are characteristic to that molecule. During FTIR analysis, a sample is subjected to a modulated IR beam. The sample's transmittance and reflectance of the infrared radiation at the different frequencies is translated into an IR absorption plot consisting in reverse peaks. The resulting FTIR spectral pattern is the analyzed and matched with known signatures of identified materials in the FTIR library.[4,5]

## 3.6 – Atomic force microscopy

Atomic force microscopy (AFM) measurements for topographical and morphological characterization of CP films were carried out in tapping-mode AFM with Molecular Imaging PicoSPM using a NanoScope IIIa controlled in ambient conditions.

AFM is a very high-resolution type of scanning probe microscopy. The precursor to the AFM, the scanning tunnelling microscope, was developed by Gerd Binning and Heinrich Rohrer in the early 1980s, a development that earned them the Nobel Prize for Physics in 1986. The first commercially available atomic force microscope was introduced in 1989. The AFM is one of the foremost tools for imaging, measuring, and manipulating matter at the nanoscale. The information is gathered by "feeling" the surface with a mechanical probe. The AFM consists of a cantilever with a sharp tip (probe) at its end that is used to scan the specimen surface. The cantilever is typically silicon or silicon nitride with a tip radius of

curvature on the order of nanometers. When the tip is brought into proximity of a sample surface, forces between the tip and the sample lead to a deflection of the cantilever according to Hooke's law. Depending on the situation, forces that are measured in AFM include mechanical contact force, van der Waals forces, capillary forces, chemical bonding, electrostatic forces, magnetic forces (see magnetic force microscope, MFM), Casimir forces, solvation forces, etc. Along with force, additional quantities may simultaneously be measured through the use of specialized types of probe. Typically, the deflection is measured using a laser spot reflected from the top surface of the cantilever into an array of photodiodes. Other methods that are used include optical interferometry, capacitive sensing or piezoresistive AFM cantilevers. These cantilevers are fabricated with piezoresistive elements that act as a strain gauge. The AFM can be operated in a number of modes, depending on the application. In general, possible imaging modes are divided into static (also called contact) modes and a variety of dynamic (non-contact and tapping) modes where the cantilever is vibrated.[6]

In the static mode operation, the static tip deflection is used as a feedback signal. Because the measurement of a static signal is prone to noise and drift, low stiffness cantilevers are used to boost the deflection signal. However, close to the surface of the sample, attractive forces can be quite strong, causing the tip to "snap-in" to the surface. Thus, static mode AFM is almost always done in contact where the overall force is repulsive. In the dynamic mode, the tip of the cantilever does not contact the sample surface. The cantilever is instead oscillated at a frequency slightly above its resonant frequency where the amplitude of oscillation is typically a few nanometers (<10 nm). In ambient conditions, most samples develop a liquid meniscus layer. Because of this, keeping the probe tip close enough to the sample for short-range forces to become detectable while preventing the tip from sticking to the surface presents a major problem for non-contact dynamic mode in ambient conditions. Dynamic contact mode (also called intermittent contact or tapping mode) was developed to bypass this problem. In tapping mode, the cantilever is driven to oscillate up and down at near its resonance frequency by a small piezoelectric element mounted in the AFM tip holder similar to non-contact mode. However, the amplitude of this oscillation is greater than 10 nm, typically 100 to 200 nm.

## 3.7 – Scanning electronic microscopy

Scanning electron microscopy (SEM) studies for the morphological characterization of the materials prepared in this work were performed using a Focussed Ion Beam Zeiss Neon 40 scanning electron microscopy equipped with an EDX system for elemental detection. Samples involving cells adhered to the surface of films made of CPs and composites were coated with an ultrathin layer of carbon by low vacuum sputter coating. Coating prevents the accumulation of static electric charge on the specimen during electron irradiation.

The scanning electron microscope uses a focused beam of high-energy electrons to generate a variety of signals at the surface of solid specimens. The signals that derive from electron-sample interactions reveal information about the sample including external morphology (texture), chemical composition, and crystalline structure and orientation of materials making up the sample. In most applications, data are collected over a selected area of the surface of the sample, and a 2-dimensional image is generated that displays spatial variations in these properties. Areas ranging from approximately 1 cm to 5 microns in width can be imaged in a scanning mode using conventional SEM techniques (magnification ranging from 20X to approximately 30,000X, spatial resolution of 50 to 100 nm).[7] The SEM is also capable of performing analyses of selected point locations on the sample; this approach is especially useful in qualitatively or semi-quantitatively determining chemical compositions (using EDX), crystalline structure, and crystal orientations.

Accelerated electrons in an SEM carry significant amounts of kinetic energy, and this energy is dissipated as a variety of signals produced by electron-sample interactions when the incident electrons are decelerated in the solid sample. These signals include secondary electrons (that produce SEM images), backscattered electrons (BSE), diffracted backscattered electrons (EBSD that are used to determine crystal structures and orientations of minerals), photons (characteristic X-rays that are used for elemental analysis and continuum X-rays), visible light (cathodoluminescence - CL), and heat. Secondary electrons and backscattered electrons are commonly used for imaging samples: secondary electrons are most valuable for showing morphology and topography on samples and backscattered electrons are most valuable for illustrating contrasts in composition in multiphase samples (i.e. for rapid phase discrimination). X-ray generation is produced by

inelastic collisions of the incident electrons with electrons in discrete ortitals (shells) of atoms in the sample. As the excited electrons return to lower energy states, they yield X-rays that are of a fixed wavelength (that is related to the difference in energy levels of electrons in different shells for a given element). Thus, characteristic X-rays are produced for each element in a mineral that is "excited" by the electron beam. SEM analysis is considered to be "non-destructive"; that is, x-rays generated by electron interactions do not lead to volume loss of the sample, so it is possible to analyze the same materials repeatedly.

## 3.8 – Energy dispersive X-ray spectroscopy

Interaction of an electron beam with a sample target produces a variety of emissions, including x-rays. An EDX detector is used to separate the characteristic X-rays of different elements into an energy spectrum, and EDX system software is used to analyze the energy spectrum in order to determine the abundance of specific elements. EDX can be used to find the chemical composition of materials down to a spot size of a few microns, and to create element composition maps over a much broader raster area. Together, these capabilities provide fundamental compositional information for a wide variety of materials.

EDX systems are typically integrated into a SEM instrument. EDX systems include a sensitive X-ray detector, a liquid nitrogen dewar for cooling, and software to collect and analyze energy spectra. The detector is mounted in the sample chamber of the main instrument at the end of a long arm, which is itself cooled by liquid nitrogen. The most common detectors are made of Si(Li) crystals that operate at low voltages to improve sensitivity, but recent advances in detector technology make availabale so-called "silicon drift detectors" that operate at higher count rates without liquid nitrogen cooling.

An EDX detector contains a crystal that absorbs the energy of incoming X-rays by ionization, yielding free electrons in the crystal that become conductive and produce an electrical charge bias. The x-ray absorption thus converts the energy of individual X-rays into electrical voltages of proportional size; the electrical pulses correspond to the characteristic x-rays of the element.

## 3.9 – Bacterial and cellular culture

Bacterial cultures were performed using two bacterial strains: *Escherichia coli* CECT 101 and *Staphylococcus epidermis* CECT 231 from the Spanish Collection of Type Culture (CECT, Valencia, Spain). These bacteria were used to study and characterize a conducting polymer-protein composite with antibacterial and electroactive properties.

Bacteria were grown in aerobic conditions till achieve the exponential phase in broth culture (5 g/L beef extract, 5 g/L NaCl, 10 g/L peptone, pH 7.2 in distilled water). The bacterial growth was determined using a UV-Vis spectrophotometer at 600 nm of absorbance. Growth experiments were carried out in culture tubes of 15 mL. $10^3$ colony forming units (CFU) were seeded in 5 mL of broth culture containing the prepared CP-protein composites, and incubated at 37 ˚C with 100 rpm agitation. After 24 and 48 h of incubation, a 100 µL sample was diluted 10 times in distilled water and the absorbance was measured at 600 nm.

Cellular cultures were performed using three different cellular lines of adherent growth cells: cells HEp-2 (human cell derived from epidermoid larynx carcinoma), cells DU145 (human cell line derived from a prostate carcinoma), and cells COS-7 (cell line derived of *Cercopithecus aethiops*, African green monkey, kidney immortalized by transformation with SV40). The cells were plated in tissue flasks (25 $cm^2$) and grown in Dubelcco's Modified Eagle's Medium (DMEM) with 10 % of fetal bovine serum (FBS), penicillin G (100 U/ml) and streptomycin (100 mg/ml). Cultures were grown in a humid ambient (95 %) at 37 ˚C containing 5 % of carbon dioxide ($CO_2$). Two culture passages were done, and confluent cells were dispersed with trypsin (0.05 %) and EDTA (0.02 %) in Hank's Balanced Salt Solution. At last, cells were harvested by centrifugation and counted in a Neubauer camera using trypan blue (0.4 %).

## 3.10 – Gel electrophoresis

Gel electrophoresis studies were employed in order to study the interaction of CPs with plasmid DNA. For this purpose, ultrasonicated polymer solutions were mixed with plasmid DNA considering different CP:DNA mass ratios. After incubation and centrifugation, electrophoretograms were carried out.

Gel electrophoresis is a technique typically used for the separation of DNA, RNA or protein molecules using an electric field applied to a gel matrix. In simple terms: electrophoresis is a procedure which enables the sorting of molecules based on size and charge. Using an electric field, molecules (such as DNA) can be made to move through a gel. The molecules being sorted are dispensed into a well in the gel material. The gel is placed in an electrophoresis chamber, which is then connected to a power source. When the electric current is applied, the larger molecules move more slowly through the gel while the smaller molecules move faster. The different sized molecules form distinct bands on the gel.[8]

The term "gel" refers to the matrix used to separate the target molecules. In most cases, the gel is a crosslinked polymer whose composition and porosity is chosen based on the specific weight and composition of the target to be analyzed. When separating proteins or small nucleic acids (DNA, RNA, or oligonucleotides) the gel is usually composed of different concentrations of acrylamide and a cross-linker, producing different sized mesh networks of polyacrylamide. After the electrophoresis is complete, the molecules in the gel can be stained to make them visible. Ethidium bromide, silver, or Coomassie Brilliant Blue dye may be used for this process.[8]

## 3.11 – References

[1] A. J. Bard, L. R. Faulkner, "*Electrochemical methods: Fundamentals and applications*", John Wiley & Sons, Inc., New York (2001).

[2] M. G. Gore, "*Spectrophotometry and Spectrofluorimetry: a practical approach*", Oxford University Press, USA (2000).

[3] C. P. M. van Mierlo, H. H. J. de Jongh, A. J. W. G. Visser, *Applied Spectroscopy Rev*. 35 (2000) 277.

[4] P. R. Griffiths, J. A. de Haseth, "*Fourier Transform Infrared Spectrometry*", 2th edition, John Wiley & Sons, Inc., New Jersey (2007).

[5] R. T. Morrison, R. N. Boyd, "*Organic Chemistry*", 13th edition, Fundação Calouste Gulbenkian, Lisboa (1996).

[6] P. Eaton, P. West, "*Atomic Force Microscopy*", Oxford University Press Inc., New York (2010).

[7] J. Goldstein, D. Newbury, D. Joy, C. Lyman, P. Eclin, E. Lishin, L. Sawyer, J. Michael, "*Scanning Electrom Microscopy and X-Ray Microanalysis*", 3th edition, Springer-Verlag, Berlin Heidelberg, New York (2003).

[8] J. Robertson, A. M. Ross, L. A. Burgoyne, "*DNA in Forensic Science – theory, techniques and applications*", Ellis Horwood Limited, West Sussex, England (1990).

# Chapter 4

# DNA···Conducting Polymers Interaction

# 4.1 – A comprehensive study of the interactions between DNA and poly(3,4-ethylenedioxythiophene)

The interaction between poly(3,4-ethylenedioxythiophene), a CP with excellent electrical and electrochemical properties, and plasmid DNA has been investigated using electrophoresis, UV-visible and CD spectroscopy, and quantum mechanical calculations. Analyses of mixtures with different DNA:polymer mass ratios indicate that, in all cases, interactions form immediately and induce structural alterations in DNA. Furthermore, the existence of interactions between poly(3,4-ethylenedioxythiophene) and specific nucleotides sequences has been evidenced by adding restriction enzymes to the mixtures. In contrast, interactions between DNA and poly(3-methylthiophene), a similar polyheterocyclic CP but without hydrogen bonding acceptors, are weak or do not exist. These results suggest that, in addition to non-specific electrostatic interactions between the charged phosphate groups of DNA and the positively charged fragments of the CPs, specific hydrogen bonding interactions play a crucial role. The ability of 3,4-ethylendioxythiophene units to form hydrogen bonds with the methylated analogues of DNA bases has been examined in different environments using MP2/6-31G(d) and MP2/6-311++G(d,p) calculations. Results indicate that, in environments with low polarity, the formed interactions are significantly stronger than those reached by unsubstituted thiophene and similar to those established by pyrrole. However, in polar environments (aqueous solution) 3,4-ethylendioxythiophene provides stronger interactions with nucleic acids than both thiophene and pyrrole. These theoretical results are fully consistent with experimental observations.*

* - Results described in this section previously appeared in *Polymer* 50 (2009) 1965. Theoretical calculations were preformed by C. Alemán and D. Zanuy.

## 4.1.1 – Introduction

The interaction of conducting electroactive polymers, such as PTh, PPy and their derivatives, with selected bioentities (*e.g.* amino acids, proteins, DNA and oligonucleotides, and living cells) is a subject f increasing interest.[1-8,18,19,23-25] The quest to interact more efficiently with biosystems, to obtain information related to system performance and to control that performance remain not only an exciting but also an essential area of research. Thus, the development of biotechnological applications based on CPs greatly depends on the control of such interactions.

Within this area of research we are particularly interested in the interaction of CPs with DNA sequences, which may have great implications in numerous medical applications ranging from diagnosis to gene therapy.[8-18,24,25] The interaction of p-doped electroactive materials with DNA has been traditionally attributed to the tendency of the latter to

interact with positively charged molecules. However, in recent studies we found that some CPs, for example PPy, are able to interact forming specific interactions with well-defined nucleotide sequences of plasmid DNA.[15-17] This selectivity suggests that polymer:DNA adducts are stabilized not only by electrostatic interactions but also by interactions that act specifically, *i.e.* interactions that depend on the chemical environment, the spatial disposition and orientation of the chemical groups, etc. In particular, the importance of specific hydrogen bonding interactions in these complexes is expected to be significantly greater than those that are of non-specific, *e.g.* stacking, van der Waals and charge-transfer interactions. Indeed, we found that all the CPs able to form specific interactions with DNA contain functional groups that are excellent donors and acceptors of hydrogen bonds, *e.g.* the N-H in PPy or the ester side groups in some PTh derivatives.[15-17] Furthermore, we recently used sophisticated theoretical calculations to show that hydrogen bonding interactions between DNA bases and PPy are significantly stronger than interactions between DNA bases and PTh, the later lacking of hydrogen bonding donors and acceptors.[18]

Within a recent study devoted to examine the potential applications of different materials, we preliminary investigated the interaction between DNA and two different PTh derivatives using qualitative electrophoretic assays.[15,16] Specifically, the CPs examined were poly(3,4-ethylenedioxythiophene), in which dioxane rings are fused onto thiophene rings, and poly(3-methylthiophene), hereafter denoted PEDOT and PT3M, respectively. Interestingly, we found that PEDOT interacts specifically with plasmid DNA forming strong and stable complexes. This feature together with its remarkable electrochemical stability and electrical properties, and notable electro-biocompatibility make this material a good candidate for different biotechnological applications that involve DNA, *e.g.* biosensor and drug-delivery system.[22,23,26-29] In contrast, PT3M, a PTh derivative without hydrogen bonding donors and acceptors, only formed stable adducts at very high DNA:polymer mass ratios, and specific interactions were significantly weaker than in DNA:PEDOT. Attracted by this field, in this work we report a comprehensive study about the microscopic details of the interactions between plasmid DNA and PEDOT using both experimental and computational methods.

Specifically, the interaction of PEDOT with plasmid DNA has been examined considering different DNA:polymer mass ratios and using electrophoresis, UV-Vis

spectroscopy and CD. The possible formation of specific interactions have been examined by the digestion of DNA:PEDOT mixtures using restriction enzymes, which cut off at specific nucleotide sequences. Furthermore, ab initio quantum mechanical calculations have been used to examine the strength of the specific interactions between PEDOT and DNA. Calculations have been performed considering the building blocks of the two interacting systems, *i.e.* 3,4-ethylenedioxythiophene (EDOT) units and methylated analogues of DNA bases [9-methyladenine (mA), 1-methylthymine (mT), 1-methylcytosine (mC) and 9-methylguanine (mG)], as well as environments with different polarity.

### 4.1.2 – Methods

*Synthesis and characterization.* EDOT, 3-methylthiophene (T3M) and acetonitrile of analytical reagent grade were purchased from Aldrich and used as received. Anhydrous lithium perchlorate ($LiClO_4$), analytical reagent grade, from Aldrich was stored in an oven at 80ºC before its use in the electrochemical trials.

PEDOT and PT3M films were generated by anodic polymerization using a VersaStat II potentiostat-galvanostat connected to a computer controlled through a Power Suite Princenton Applied Research program. Electrochemical experiments were conducted in a three-electrode two-compartment cell under nitrogen atmosphere (99.995% in purity) at 298 K. The working compartment was filled with 40 ml of a 10 mM monomer solution in acetonitrile containing 0.1 M $LiClO_4$ as supporting electrolyte. A volume of 10 ml of the same electrolyte solution was placed in the cathodic compartment. Steel AISI 316 sheets of 4 $cm^2$ area were employed as working and counter electrodes. The reference electrode was an Ag|AgCl electrode containing a KCl saturated aqueous solution ($E^\circ$ = 0.222 V at 25 ˚C), which was connected to the working compartment through a salt bridge containing the electrolyte solution. Electrogeneration of PEDOT and PT3M was carried out by CA under a constant potential of 1.40 and 1.70 V, respectively, a polymerization time $\theta$= 900 s being used in both cases. Uniform, adherent and insoluble polymeric films were obtained by this procedure, the coloration being dark-blue and black for PEDOT and PT3M, respectively. The electrical and electrochemical characterization of the materials derived from these experimental conditions was previously reported.[15,26]

Ultrafine particles of polymer were used to interact with DNA. These were obtained by applying ultrasounds to a polymer solution (5 μg polymer/μl; milliQ water), which was prepared by considering the polymer samples grinded with a mortar. The dimensions of the resulting particles were analyzed using scanning electron microscopy (SEM) with a JSM-6400 JEOL microscope.

*Formation of DNA:PEDOT complexes and electrophoretic assays.* DNA:PEDOT complexes were prepared upon aqueous solutions by mixing 4 μl of plasmid pMT4 (0.05 μg/μl) with 0.00, 0.05, 0.50, 2.50 and 5.00 μl of polymer solution (5 μg polymer/μl; milliQ water), which corresponded to the desired DNA:PEDOT mass ratios (1:0, 1:1, 1:10, 1:50, 1:100, respectively). Final volumes were raised to 13 μl with sterile milliQ water. The mixtures were incubated overnight at 37 ˚C. After this, an aliquot of 6X gel loading buffer was added, samples being centrifuged for 10 min. The supernatant was analyzed by electrophoresis with 1% of agarose gel containing ethidium bromide (0.5 μg/ml of gel) in 1X tris-acetate-EDTA buffer (TAE). To evaluate the cleavage of pMT4 with *Eco*RI and *Bam*HI in DNA:PEDOT complexes, 1 μl of restriction enzyme (10 000 U/ml) and 1.56 μl of 10X enzyme buffer was added to each incubated sample. The digestion process was carried out at 37 ˚C for 1 h, the digested products being analysed by electrophoresis.

*Spectroscopic studies.* A Nicolet Evolution 300 (Thermo Electron Co.) spectrophotometer controlled by the Vision Pro software was used to record UV-Vis spectra of DNA:PEDOT and DNA:PT3M complexes at 22 ˚C, in the 200-1000 nm range, with a bandwidth of 2 mm and a scan speed of 600 nm/min. Light scattering effects were avoided by correcting the maximum absorbance of nucleotide bases in DNA, which is 260 nm ($A_{260nm}$), with respect to the absorbance at 350 nm ($A_{350nm}$). For each sample, 36 cycles separated by an interval of 5 minutes between consecutive cycles were recorded.

Circular dichroism (CD) measurements were carried out in a Jasco J-810 spectropolarimeter at 22 ˚C using a quartz cuvette. The CD data were recorded with standard sensitivity (100 mdeg), in the 170-360 nm range, with bandwidth of 2 mm, response time of 0.5 s and scanning speed of 500 nm/min. The reported spectra correspond to the average of five scans, the raw spectra being smoothed by the Savitsky-Golay algorithm and deconvolutioned for analysis and interpretation. For each sample, the CD

spectrum of the polymer was subtracted from that of the DNA:polymer complex, and compared with the CD spectrum of the plasmid DNA.

*Quantum mechanical calculations.* Calculations were performed using the Gaussian 03 computer program.[30] The structures of the complexes were determined by full geometry optimization in the gas-phase at the MP2 level with the 6-31G(d) basis set, frequency calculations being performed to obtain the zero-point vibrational energies and both the thermal and entropic corrections.[31,32] Single point energy calculations were performed on the MP2/6-31G(d) geometries at the MP2/6-311++G(d,p) level.[33] In order to estimate the free energies in the gas-phase, the statistical corrections obtained at the MP2/6-31G(d) level were added to the electronic energies computed at the MP2/6-311++G(d,p) level.

The counterpoise (*CP*) method was applied to correct the basis set superposition error.[34] The binding energies, which were obtained with and without apply the *CP* ($\Delta E_{b,g}^{CP}$ and $\Delta E_{b,g}$, respectively), were calculated at the MP2/6-311++G(d,p) level as the difference between the total energy of the optimized complex and the energies of the isolated monomers with the geometries obtained from the optimization of the complex.

The effect of the solvent on the relative stability of the complexes was estimated using the polarizable continuum model (PCM) developed by Miertus, Scrocco and Tomasi.[35,36] This Self-Consistent Reaction-Field (SCRF) method involves the generation of a solvent cavity from spheres centered at each atom in the molecule and the calculation of virtual point charges on the cavity surface representing the polarization of the solvent. The magnitude of these charges is proportional to the derivative of the solute electrostatic potential at each point calculated from the molecular wavefunction. Then, the point charges are included in the one-electron Hamiltonian inducing polarization of the solute. An iterative calculation is carried out until the wavefunction and the surface charges are self-consistent.

PCM calculations were performed in the framework of the ab initio MP2 level with the 6-31G(d) basis set and using the standard protocol and considering the dielectric constants of chloroform (ε= 4.9) and water (ε= 78.4). Calculations were performed considering the gas-phase optimized geometries. Thus, solvent–induced changes in bond lengths and angles have been proved to have small influence on the free energy of solvation

($\Delta G_{sol}$), *i.e.* solute geometry relaxations in solution and single point calculations on the gas-phase optimized geometries provide almost identical values of $\Delta G_{sol}$.[37-39] The relative free energies and the binding energies in solution, which provide information about the relative stability of the complexes and the strength of the interactions in solution, respectively, were computed using the classical thermodynamics schemes.

### 4.1.3 – Results and Discussion

PEDOT films were prepared by chronoamperometry (CA) under a constant potential of 1.4 V. The electrogenerated films were grinded mechanically using a mortar. Scanning electron micrographs of the resulting samples (Figure 1a) showed that they are constituted by plates of large dimensions, *i.e.* larger than 50 μm, which preclude their use for the present study. In order to reduce the size of the PEDOT particles, ultrasounds were applied to a solution prepared with such grinded samples. This process led to ultrafine particles with dimensions ranging between 3 and 18 μm (Figure 1b) that are suitable to interact with biological macromolecules.

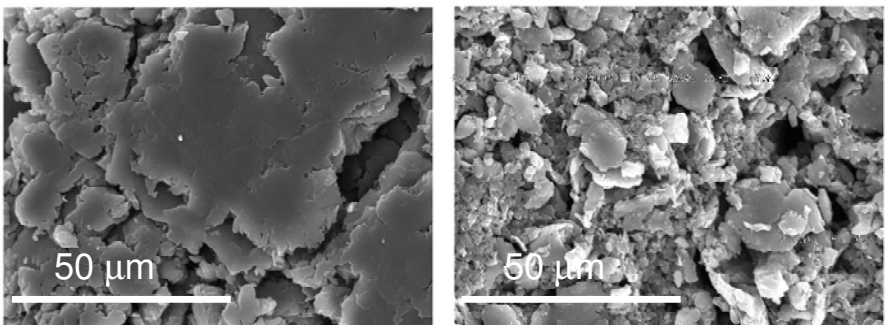


**Figure 1 –** Scanning electron micrographs of PEDOT particles obtained by grinding the electrogenerated films (a) and by submitting to ultrasounds the grinded samples (b).

The formation of DNA:PEDOT complexes was evidenced by electrophoresis (Figure 2), different DNA:polymer mass ratios (1:1, 1:10, 1:50 and 1:100) being considered for analyses. Lane 1 corresponds to the pMT4 plasmid (1:0 ratio), and shows a mixture of the supercoiled form I (bottom or band at the front) and the singly nicked form II (top or band

at the back). Lanes 2-5, which display the DNA:PEDOT series at 1:1, 1:10, 1:50 and 1:100 ratios, reflect significant alterations in the bands associated to pMT4 evidencing the formation of complexes. Specifically, DNA:polymer complexes retard the mobility of form I and increase the intensity of form II. The variation in the mobility undergone by the former band is probably due to the conformational changes induced by the CP in the plasmid DNA during the formation of the corresponding DNA:PEDOT complexes. Accordingly, hereafter form I' will refer to the altered form I. As can be seen, DNA:PEDOT complexes are formed for the four considered ratios. Specifically, interactions start at the 1:1 ratio, whereas all DNA is involved in the formation of stable adducts at the 1:100 ratio. Thus, the absence of bands in lane 5 must be attributed to the sedimentation of these adducts during the centrifugation process previous to the electrophoretic assay.

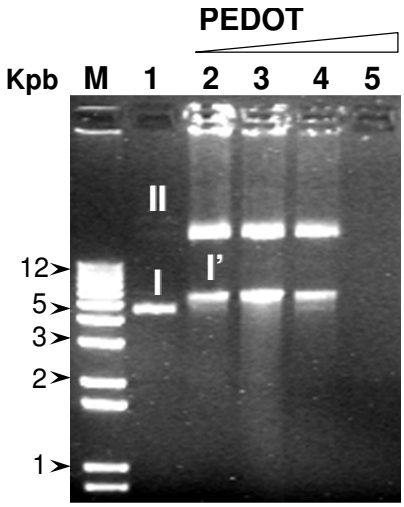


**Figure 2 –** Interaction of pMT4 plasmid DNA and increasing concentrations of PEDOT after their incubation for 3h at 37 ºC. Lane M: molecular weight marker (1 Kb Plus DNA Ladder). Lane 1: pMT4 plasmid DNA (1:0 DNA:PEDOT). Lanes 2-5: 1:1, 1:10, 1:50 and 1:100 DNA:PEDOT mass ratios. Labels I and II indicate form I and II of pMT4 plasmid DNA, respectively. Label I' refers to mobility alterations in the form I of plasmid DNA.

In order to look for specific interactions between the CP and the plasmid DNA, restriction enzymes were added to the incubated samples. These enzymes were *Eco*RI and *Bam*HI, which cut off at 5'-G/AATTC-3' and 5'-G/GATCC-3' nucleotide sequences, respectively. The pMT4 plasmid DNA contains only one restriction site for *Eco*RI converting supercoiled form I and singly nicked circular form II into linear DNA (form III). *Bam*HI has

three restriction sites producing three DNA fragments, denoted F1, F2 and F3. The molecular weights of F1 and F2 are similar, their mobility in agarose gel corresponding to a single band. Fragment F3 presents the lowest molecular weight and, therefore, shows the fastest mobility. However, *Bam*HI produces form III when it makes only one cut in the plasmid DNA.

The electrophoretograms obtained for DNA:PEDOT complexes after digestion with *Eco*RI and *Bam*HI are displayed in Figure 3. For each enzyme, lane 1 shows the untreated and undigested pMT4 plasmid DNA, lane 2 displays the digested plasmid DNA (1:0 DNA:PEDOT ratio), and lanes 3-6 correspond to the digested DNA:PEDOT complexes with increasing mass ratios. Digestion with *Eco*RI produces the band associated to the formation of linear DNA (form III) for 1:1, 1:10 and 1:50 ratios. However, as was found in the Figure 2, the formation and subsequent sedimentation of DNA:PEDOT adducts preclude the detection of bands for the 1:100 ratio. The interaction of DNA with PEDOT at the 1:1 and 1:10 ratios promotes, after digestion with *Eco*RI, the formation of new topoisomers with higher mobility than linear DNA. Regarding to the action of *Bam*HI on DNA:PEDOT complexes (Figure 3b), results are very similar to those described for *Eco*RI. Thus, the bands associated to F1, F2 and F3 are detected in lanes 3-5, whereas lane 6 reflects the formation of DNA:polymer adducts.

In order to provide details about the temporal evolution of the interaction between plasmid DNA and PEDOT, the behaviour of the nucleotide bases was investigated during the formation of the complexes by UV-Vis spectrophotometry. Figure 4 represents the evolution of $(A-A_0)/A_{max}$ against the time ($t$) for the 1:1 and 1:100 DNA:PEDOT mixtures, where $A_0$ corresponds to the absorbance of DNA in solution (1:0 DNA:PEDOT ratio) at the initial time ($t$= 0 min), $A_{max}$ is the absorbance of the bases in the DNA:polymer mixture after thermal denaturalization of DNA *i.e.* the sample is heated at 94 ºC during 15 min producing exposition of all DNA bases, and $A$ is the absorbance of nitrogen bases in the DNA:PEDOT mixture measured at different times (cycles).

As can be seen, UV-Vis results depend on the DNA:PEDOT mass ratio. The interaction between DNA and PEDOT is relatively low for the 1:1 ratio, which is reflected by the moderate exposition of the DNA nitrogen bases. In contrast, the degree of interaction found for the mixture with 1:100 mass ratio is very high. These strong interactions, which are formed immediately as revealed the fast exposition of the DNA nitrogen bases, are

consistent with the formation of adducts previously evidenced by the electrophoretic assays.

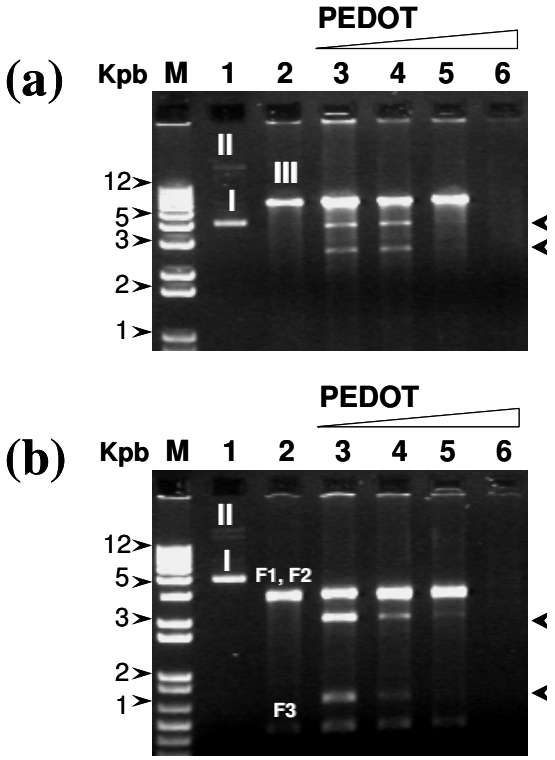


**Figure 3 –** Interaction between pMT4 plasmid DNA and increasing concentrations of PEDOT followed by *Eco*RI (a) and *Bam*HI (b) enzymatic digestion for a period of 1 h at 37 ºC. Lane M: molecular weight marker (1 Kb Plus DNA Ladder). Lane 1: undigested and untreated pMT4 plasmid DNA (1:0 ratio). Lane 2: digested pMT4 plasmid DNA (1:0 ratio). Lanes 3-6: 1:1, 1:10, 1:50, 1:100 DNA:PEDOT ratios after enzymatic digestion. Labels I, II and III refer to forms I, II and III of pMT4 plasmid DNA, respectively. F1, F2 and F3 indicate the DNA fragments obtained by digestion with *Bam*HI. The head arrow indicates new topoisomers formed during the interaction between DNA and polymers.

For the sake of comparison, UV-Vis spectra were also recorded for DNA:PT3M mixtures with 1:1 and 1:100 mass ratios (Figure 4). Ultrafine particles of this CP were prepared by applying ultrasounds to grinded samples, which were electrogenerated by CA under a constant potential of 1.7 V. The exposition of the nitrogen bases reveals the absence of interactions between the plasmid DNA and the CP for the 1:1 ratio. Similarly, no

interaction is detected during the first 50 minutes for the 1:100 ratio. After this, the exposition of the nitrogen bases increases slowly showing the formation of very stable DNA:PT3M adducts after 130 minutes. These results are fully consistent with the electrophoretograms previously reported for DNA:PT3M mixtures, which indicated that interactions between pWL102 plasmid DNA and PT3M are weak.[15] In addition, digestion with *Eco*RI and *Bam*HI showed that the protection imparted by PT3M to DNA is very small evidencing that specific interactions are weak or do not exist.

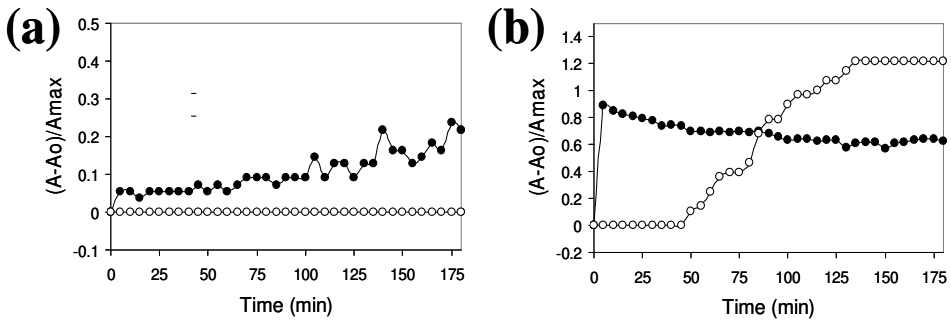


**Figure 4 –** Temporal evolution of DNA:PEDOT (-●-) and DNA:PT3M (-○-) mixtures with (a) 1:1 and (b) 1:100 DNA:polymer mass ratios followed by UV-Vis spectroscopy (see text). Spectra were recorded during the 36 cycles, two consecutive cycles being separated by a 5 minutes interval.

Structural alterations undergone by plasmid DNA when it interacts with PEDOT were examined by CD spectroscopic measurements. Figure 5 compares the CD spectra recorded for plasmid DNA (1:0 ratio) and both DNA:PEDOT and DNA:PT3M mixtures with 1:1 and 1:100 ratios. In order to detect structural changes in DNA, the CD spectrum of the polymer (0:1 ratio) was subtracted from those of the mixtures.

The plasmid used in this work is a supercoiling circular DNA and its ellipiticity is negative. The raw CD spectra recorded between 200 and 360 nm show ellipiticity changes and loss of structure for the 1:100 DNA:PT3M mixture (Figure 5b), while the two DNA:PEDOT mixtures maintain negative ellipticity but with loss of the supercoiling structure (Figure 5a). On the other hand, DNA adopts the B-form in aqueous solution, the characteristics of the CD spectrum typically found for the canonical structure being the following: positive band at 275 nm, negative band at 245 nm and crossover point near 258 nm.[40,41] Figure 5 indicates that the characteristic features of the pMT4 plasmid correspond to the B-form, even although small differences are detected with respect to the canonical

form: positive band at 280 nm, negative signal at 257 nm, and crossover point near 270 nm. The appearance of the spectrum changes in presence of the CPs. The observed differences, which include a significant reduction in the intensity of the negative and positive bands, correspond to conformational variations. Unfortunately, the DNA structure in DNA:polymer mixtures cannot be clearly defined due to the presence of the light scattering of spectral tails. Thus, the size of the complexes can contribute for the light scattering.[41

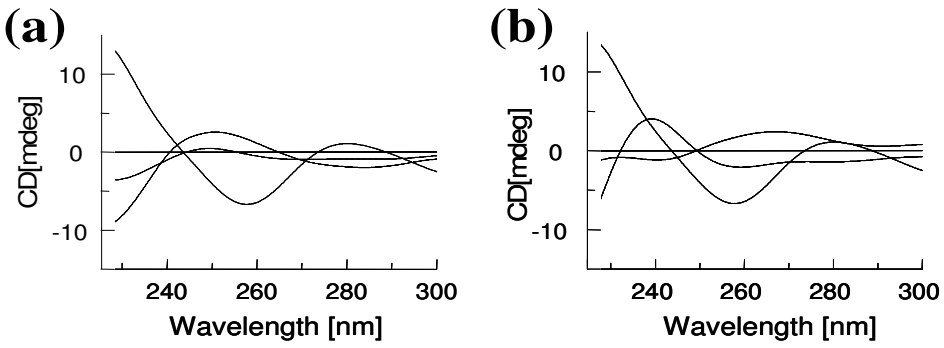


**Figure 5 –** CD spectra of DNA:polymer complexes to study the structural alterations of DNA: (a) DNA:PEDOT and (b) DNA:PT3M mixtures with 1:1 (----) and 1:100 (·····) mass ratios. In all cases the CD spectrum of the corresponding CP was subtracted from the CD spectra of the DNA:polymer mixtures. The spectrum recorded for the pMT4 plasmid DNA (—) is also included.

The CD results allow conclude that the contact between plasmid DNA and PEDOT produces changes in the secondary structure of DNA. The immediate consequence of this structural alteration is the exposition of the DNA bases, which favors the rapid formation of interactions with PEDOT. Some of such interactions are with specific nucleotide sequences, like those found for the 5'-G/AATTC-3' (target for *Eco*RI) and 5'-G/GATCC-3' (target for *Bam*HI) sequences, inducing the protective effect in the restriction cleavage. The formation of specific interactions involves not only directional preferences but also dependence on the chemical nature of the CP. These features are typically associated to hydrogen bonds. Thus, the importance of hydrogen bonds in DNA:polymer complexes with specific interactions is expected to be significantly greater than those that are of non-specific, *e.g.* stacking, van der Waals, electrostatic and charge transfer.

In order to ascertain the ability of EDOT units to form specific interactions with methylated nucleic acids (mNA), quantum mechanical calculations at the $MP2^{12}$ level were performed on EDOT···mNA complexes (where mNA= mA, mG, mC and mT). The EDOT unit

was considered in the neutral (reduced) state rather than in the doped (oxidized) one. This is because in oxidized polyconjugated polymers, as PEDOT and PTh, charges are not uniformly distributed along the whole molecular chains but are localized in small segments that involve a few number of repeating units (typically a few tenths of rings present a quinoid-like electronic structure).[42-46] These segments are separated among them by blocks of rings with a benzenoid-like electronic structure, which is characteristic of conjugated heterocyclic species in the neutral state.[42-46] Neutral EDOT units belonging to non-charged blocks are expected to participate in the formation of specific hydrogen bonding interactions with DNA bases, while charged units are probably involved in non-specific electrostatic interactions with the phosphate groups of DNA.

A total of 26 starting geometries were prepared for EDOT···mNA complexes applying the following scheme: (i) the thiophene (Th) units of the 11 Th···mNA minimum energy complexes previously characterized were transformed into EDOT units; and (ii) 15 EDOT···mNA hydrogen bonded complexes were constructed using the oxygen atoms of the dioxane ring as interaction sites.[18] Geometry optimization and frequency calculations at the MP2/6-31G(d) level provided the following distribution of minimum energy complexes: 6 EDOT···mA, 3 EDOT···mT, 7 EDOT···mC and 9 EDOT···mG, which are displayed in Figure 6, 7, 8 and 9, respectively. Single point calculations at the MP2/6-311++G(d,p) level allowed to obtain accurate estimation of the both the relative stabilities and the affinities. Table 1 lists the relative energies ( $\Delta E_{r,g}$ ), the relative free energies ( $\Delta G_{r,g}$ ), and the binding energies, which were estimated with and without correct the basis set superposition error ( $\Delta E_{b,g}^{CP}$ and $\Delta E_{b,g}$ , respectively), for all the minimum energy complexes.

The EDOT···mA minimum of lowest energy (ImA-E) is stabilized by a strong hydrogen bond between the amino group of mA and one of the oxygen atoms of the dioxane ring. The remaining minima, which show $\Delta G_{r,g} \leq 2$ kcal/mol, present N-H···O (IImA-E), N-H···π (IIImA-E and IVmA-E) or both N-H···O and C-H···N interactions (VmA-E and VImA-E). However, the most striking feature is that $\Delta E_{b,g}^{CP}$ values range from -6.9 kcal/mol (ImA-E) to -4.7 kcal/mol (IIImA-E). These results differ significantly from those obtained for the Th···mA and Py···mA minimum energy complexes previously reported.[6] Thus, the

$\Delta E_{b,g}^{CP}$ values calculated for the three Th···mA minima, which were stabilized by N-H···π interactions, were comprised between -4.5 to -3.7 kcal/mol, while those of the four N-H···N hydrogen bonded complexes found for Py···mA ranged from -9.3 to -8.3 kcal/mol. These results reflect than the affinity of EDOT by mA is higher than that of Th, even though it is lower than that of pyrrole (Py).

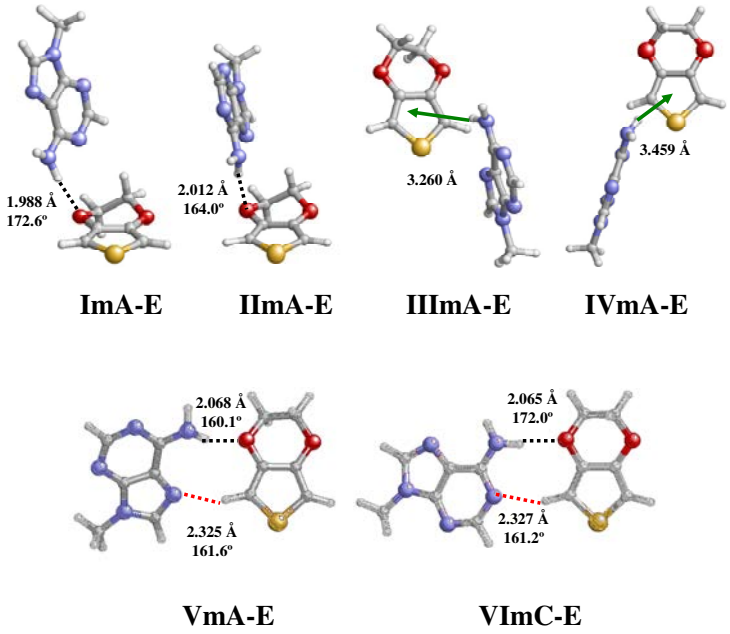


**Figure 6 –** Geometries of the six EDOT····mA minimum energy complexes calculated at the MP2/6-31G(d) level. N-H···O, C-H···O and N-H···π interactions are indicated by black dashed lines, red dashed lines and green arrows, respectively. Hydrogen bonding parameters (distances and angles) are displayed.

A completely different situation appears when the building block of PEDOT interacts with mT. In this case three minimum energy complexes, which are almost isoenergetic ($\Delta G_{r,g}$ ≤ 0.5 kcal/mol), have been characterized. The most stable one (ImT-E) presents an N-H···π interaction, while the other two (IImT-E and IIImT-E) show N-H···O hydrogen bonds. Five minimum energy complexes with $\Delta G_{r,g}$ ≤ 0.7 kcal/mol were found for Py···mT: the lowest energy one showed a π-stacked arrangement and the other four were stabilized by N-H···O hydrogen bonds.[6] In contrast, a single minimum forming a N-H···π interaction was

detected for Th···mT.[18] Interestingly, our calculations indicate that the strength of the interaction with mT is significantly higher for EDOT than for Py and Th. Thus, $\Delta E_{b,g}^{CP}$ is -10.3 kcal/mol for ImT-E and about -8 kcal/mol for IImT-E and IIImT-E, whereas it ranges from -7.7 to -6.6 in Py···mT complexes and is -3.8 kcal/mol for the Th···mT complex.

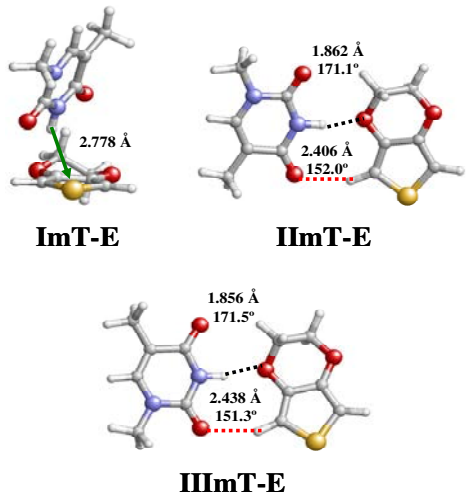


**Figure 7 –** Geometries of the three EDOT····mT minimum energy complexes calculated at the MP2/6-31G(d) level. N-H···O, C-H···O and N-H···π interactions are indicated by black dashed lines, red dashed lines and green arrows, respectively. Hydrogen bonding parameters (distances and angles) are displayed.

Inspection of the results obtained for EDOT···mC complexes suggests that the affinity of EDOT towards mC is similar to that obtained for Py. However, a detailed analysis of the structures evidences that the behavior of the two building blocks is completely different. Thus, 7 minimum energy complexes have been found for EDOT···mC, even though only 3 of them show $\Delta G_{r,g} \leq 2$ kcal/mol. The $\Delta E_{b,g}^{CP}$ values predicted for the latter structures, which are stabilized by π-stacking (ImC-E) and N-H···O hydrogen bonds (IImC-E and IIImC-E), are -9.1, -6.7 and -6.1 kcal/mol, evidencing that the strength of the former interaction is higher than that of the latter. In contrast, the three complexes characterized for Py···mC, which were close in energies ($\Delta G_{r,g} \leq$ 1.0 kcal/mol), were stabilized by N-H···O and N-H···N hydrogen bonds, and the calculated $\Delta E_{b,g}^{CP}$ values ranged from -9.7 to -8.4 kcal/mol.[18] Accordingly, hydrogen bonds with mC are stronger for Py than for EDOT, even although the

latter tends to form very stable π-stacking interactions with this mNA. Regarding to Th···mC, the $\Delta E_{b,g}^{CP}$ obtained for the three minimum energy complexes were ~ -4.5 kcal/mol, which indicate that Th provides the weakest interaction.[18]

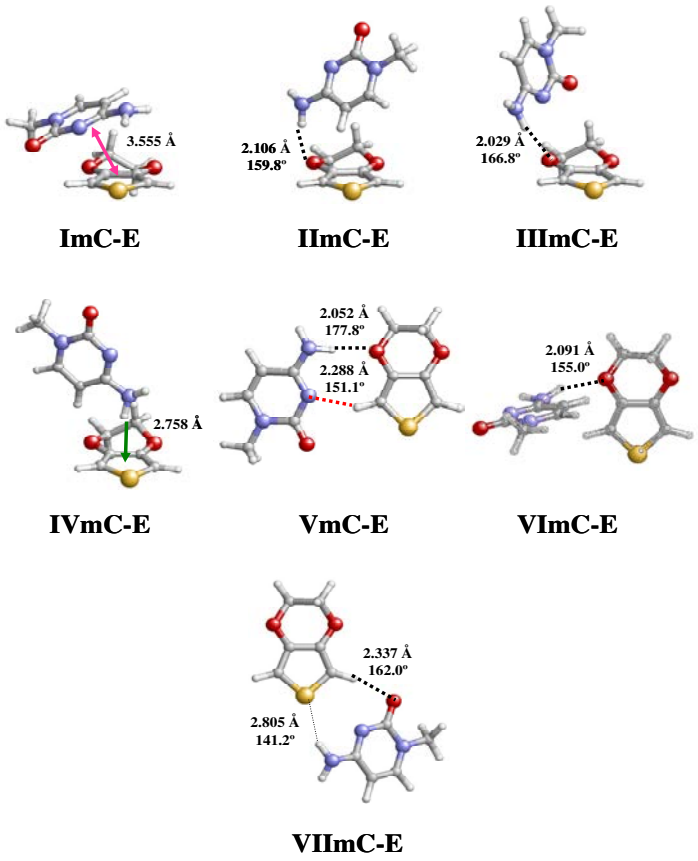


**Figure 8 –** Geometries of the seven EDOT····mC minimum energy complexes calculated at the MP2/6-31G(d) level. N-H···O, C-H···N, N-H···π and π-stacking interactions are indicated by black dashed lines, pink dashed lines, green arrows and pink arrows, respectively. Hydrogen bonding parameters (distances and angles) are displayed.

On the other hand, seven minimum energy complexes were obtained for EDOT···mG, five of them showing $\Delta G_{r,g}$ < 2 kcal/mol. The $\Delta E_{b,g}^{CP}$ of the lowest energy one (ImG-E), which is stabilized by a N-H···O hydrogen bond, is -9.8 kcal/mol. The $\Delta E_{b,g}^{CP}$ of the second complex (IImG-E) is higher by 0.6 kcal/mol, even though it involves both a N-H···O hydrogen bond and a N-H···π interaction. The next two minima, IIImG-E and IVmG-E, are stabilized by

N-H···O hydrogen bonds, and show $\Delta E_{b,g}^{CP}$ values of -7.4 and -8.6 kcal/mol, respectively. Finally, the strength of the binding produced by the N-H···O and C-H···O interactions found in VmG-E is -7.0 kcal/mol. These results differ significantly from those obtained for the four complexes obtained for Th···mG, which showed $\Delta E_{b,g}^{CP}$ values ranging between -6.8 and -4.0 kcal/mol.[6] All these structures were stabilized by N-H···π interactions rather than by intermolecular hydrogen bonds. The five minimum energy complexes calculated for Py···mG are predominantly stabilized by hydrogen bonds, even although $\Delta G_{r,g} \geq 2.8$ kcal/mol for four of them.[6] The $\Delta E_{b,g}^{CP}$ of the lowest energy one was -12.5 kcal/mol, while the strength of the interaction ranged from -8.7 to -7.5 kcal/mol for the other minima.

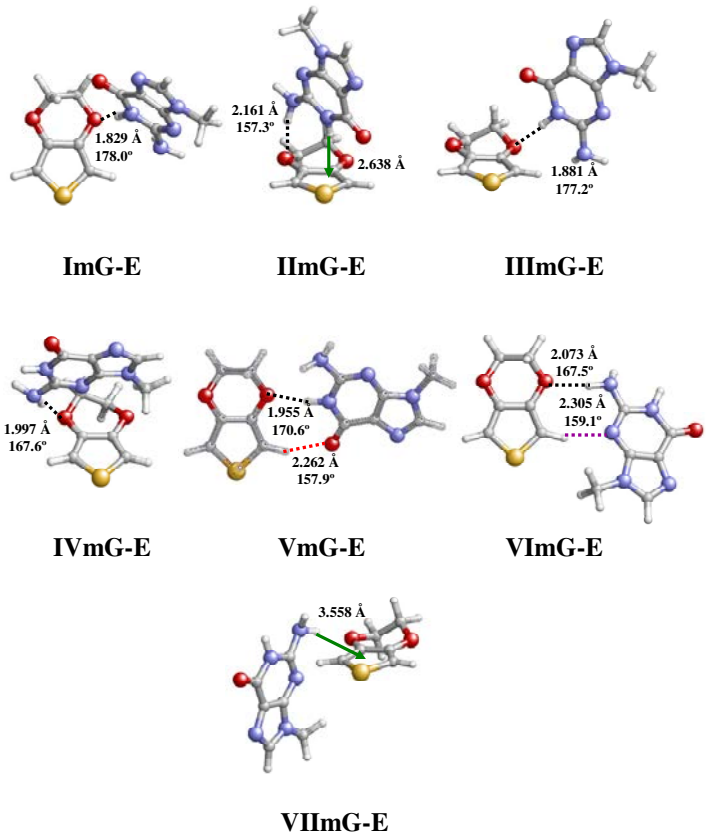


**Figure 9 –** Geometries of the seven EDOT····mG minimum energy complexes calculated at the MP2/6-31G(d) level. N-H···O, C-H···O, C-H···N and N-H···π interactions are indicated by black dashed lines, red dashed lines, purple dashed lines and green arrows, respectively. Hydrogen bonding parameters (distances and angles) are displayed.

**Table 1 –** Relative free energy[a] and energy[b] in the gas-phase ( $\Delta G_{r,g}$ and $\Delta E_{r,g}$ ; in kcal/mol), and binding energies[c] with and without correct the basis set superposition error ( $\Delta E_{b,g}^{CP}$ and $\Delta E_{b,g}$ ; in kcal/mol) for EDOT···mNA complexes.

| | $\Delta G_{r,g}$ | $\Delta E_{r,g}$ | $\Delta E_{b,g}^{CP}$ | $\Delta E_{b,g}$ |
|---|---|---|---|---|
| EDOT···mA | | | | |
| ImA-E | 0.0 | 0.5 | -6.9 | -16.2 |
| IImA-E | 0.4 | 0.0 | -6.7 | -10.4 |
| IIImA-E | 0.9 | 2.1 | -4.7 | -8.1 |
| IVmA-E | 1.5 | 2.3 | -5.6 | -8.2 |
| VmA-E | 1.7 | 1.8 | -5.6 | -8.7 |
| VImA | 2.0 | 2.4 | -5.5 | -8.1 |
| EDOT···mT | | | | |
| ImT-E | 0.0 | 0.8 | -10.3 | -5.4 |
| IImT-E | 0.3 | 0.0 | -7.9 | -11.5 |
| IIImT-E | 0.5 | 0.0 | -8.0 | -11.5 |
| EDOT···mC | | | | |
| ImC-E | 0.0 | 3.2 | -6.0 | -13.8 |
| IImC-E | 1.6 | 1.7 | -6.7 | -11.8 |
| IIImC-E | 1.7 | 1.0 | -9.1 | -12.8 |
| IVmC-E | 3.0 | 3.2 | -5.8 | -10.3 |
| VmC-E | 4.3 | 4.3 | -6.5 | -9.4 |
| VImC-E | 4.5 | 4.4 | -5.8 | -9.1 |
| VIImC-E | 5.9 | 5.9 | -4.6 | -7.6 |
| EDOT···mG | | | | |
| ImG-E | 0.0 | 0.0 | -9.8 | -14.4 |
| IImG-E | 0.4 | 0.6 | -9.2 | -13.9 |
| IIImG-E | 1.0 | 0.5 | -7.4 | -13.3 |
| IVmG-E | 1.3 | 0.9 | -8.6 | -13.1 |
| VmG-E | 1.3 | 0.5 | -7.0 | -13.3 |
| VImG-E | 2.7 | 3.1 | -7.5 | -11.0 |
| VIImG-E | 3.3 | 4.6 | -5.9 | -9.2 |
| VIIImG-E | 4.5 | 5.5 | -4.4 | -8.0 |

[a] Estimated by adding the thermodynamic corrections obtained at the MP2/6-31G(d) level to the electronic energies calculated at the MP2/6-311++G(d,p) level using the MP2/6-31G(d) geometries. [b] Derived from single point calculations at the MP2/6-311++G(d,p) level on MP2/6-31G(d) geometries.[c] Binding energies were calculated at the MP2/6-311++G(d,p) level.

The free energies of solvation for EDOT···mNA complexes were calculated using a SCRF method. Table 2 includes the relative free energy ( $\Delta G_{r,CHL}$ and $\Delta G_{r,WAT}$ ) and binding energy ( $\Delta E_{b,CHL}^{CP}$ and $\Delta E_{b,WAT}^{CP}$ ) calculated for EDOT···mNA complexes in both chloroform (CHL) and aqueous (WAT) solutions. As can be seen, the solvent produces some changes into the relative stabilities of both EDOT···mT and EDOT···mC complexes, even though they are not significant. Specifically, the lowest energy complex in the two solvents is the same that in the gas-phase, *i.e.* ImT-E and ImC-E, respectively, whereas the contribution of the other low-energy structures vary with the polarity of the environment. On the other hand, the effect of the solvent on the stability of the six EDOT···mA minimum

energy structures is small. Thus, independently of the environment all the structures are within a free energy interval smaller than 2 kcal/mol. In contrast, the influence of the solvent on the relative stabilities of the EDOT···mG complexes is very remarkable. Thus, in this case VmG-E, which was destabilized by 1.3 kcal/mol in the gas-phase, was found to be the lowest free energy structure in both chloroform and aqueous solution. Moreover, the contribution of all the other structures was negligible, *i.e.* $\Delta G_{r,CHL} \geq$ 2.6 kcal/mol and $\Delta G_{r,WAT} \geq$ 3.9 kcal/mol, even although they showed $\Delta G_{r,g}$ < 2.0 kcal/mol.

**Table 2 –** Free energies of solvation ( $\Delta G_{sol}^{CHL}$ and $\Delta G_{sol}^{WAT}$ ; in kcal/mol), relative free energies[a] ( $\Delta G_{r,CHL}$ and $\Delta G_{r,WAT}$ ; in kcal/mol) and binding energies[b] ( $\Delta E_{b,CHL}^{CP}$ and $\Delta E_{b,WAT}^{CP}$ ; in kcal/mol) in the chloroform (CHL) and aqueous (WAT) solutions for EDOT···mNA complexes.

| | $\Delta G_{sol}^{CHL}$ | $\Delta G_{sol}^{WAT}$ | $\Delta G_{r,CHL}$ | $\Delta G_{r,WAT}$ | $\Delta E_{b,CHL}^{CP}$ | $\Delta E_{b,WAT}^{CP}$ |
|---|---|---|---|---|---|---|
| EDOT···mA | | | | | | |
| ImA-E | -3.5 | -4.0 | 0.1 | 0.3 | -0.9 | 0.9 |
| IImA-E | -4.0 | -4.8 | 0.0 | 0.0 | -1.1 | 0.5 |
| IIImA-E | -4.3 | -5.1 | 0.2 | 0.2 | 0.7 | 1.8 |
| IVmA-E | -4.0 | -4.9 | 1.0 | 0.9 | -0.1 | 1.3 |
| VmA-E | -3.8 | -4.7 | 1.4 | 1.3 | 0.0 | 1.5 |
| VImA-E | -3.9 | -4.8 | 1.6 | 1.5 | -0.1 | 1.3 |
| EDOT···mT | | | | | | |
| ImT-E | -1.8 | -2.7 | 0.0 | 0.0 | -2.2 | -0.3 |
| IImT-E | -1.9 | -2.1 | 0.3 | 1.0 | 0.2 | 2.9 |
| IIImT-E | -1.7 | -1.7 | 0.6 | 1.5 | 0.3 | 3.2 |
| EDOT···mC | | | | | | |
| ImC-E | -11.5 | -17.8 | 0.0 | 0.0 | -2.1 | -2.3 |
| IImC-E | -9.6 | -13.5 | 3.4 | 5.8 | -0.8 | 1.5 |
| IIImC-E | -6.4 | -9.2 | 6.8 | 10.3 | 0.5 | 4.3 |
| IVmC-E | -7.0 | -11.1 | 4.4 | 6.6 | -0.6 | 1.4 |
| VmC-E | -9.1 | -14.1 | 8.3 | 9.6 | 1.9 | 3.3 |
| VImC-E | -8.2 | -12.8 | 7.6 | 9.2 | 0.7 | 2.3 |
| VIImC-E | -10.0 | -14.3 | 6.0 | 7.9 | -0.4 | 1.5 |
| EDOT···mG | | | | | | |
| ImG-E | -10.6 | -15.9 | 2.6 | 4.1 | -6.7 | 1.1 |
| IImG-E | -8.9 | -13.7 | 4.6 | 6.6 | 2.2 | 5.6 |
| IIImG-E | -10.0 | -14.5 | 4.2 | 6.4 | 2.3 | 5.1 |
| IVmG-E | -10.0 | -14.9 | 4.5 | 6.3 | 0.8 | 3.8 |
| VmG-E | -14.6 | -21.3 | 0.0 | 0.0 | -2.6 | -1.6 |
| VImG-E | -10.6 | -15.9 | 5.3 | 6.7 | -4.4 | 3.5 |
| VIImG-E | -13.8 | -19.3 | 3.2 | 3.9 | -0.3 | 1.3 |
| VIIImG-E | -13.3 | -20.1 | 4.0 | 4.3 | 0.6 | 2.0 |

[a] Estimated by adding the free energies of salvation to the $\Delta G_{r,g}$ values (Table 1). [b] Estimated considering the $\Delta E_{b,g}^{CP}$ values (Table 1) and the free energies of solvation calculated for the dimers and the corresponding monomers.

Analysis of the influence of the solvent on the strength of the binding reveals very remarkable features. Specifically, the interaction between mNA and EDOT has been predicted to be attractive in many cases. In chloroform solution the values of $\Delta E_{b,CHL}^{CP}$ obtained for IImA-E, ImT-E, ImC-E and VmG-E, which are the complexes with lowest $\Delta G_{r,CHL}$, are -1.1, -2.2, -2.1 and -2.6 kcal/mol, respectively. On the other hand, ImT-E, ImC-E and VmG-E are the only complexes with an attractive binding in aqueous solution, *i.e.* $\Delta E_{b,WAT}^{CP}$ is -0.3, -2.3 and -1.6 kcal/mol, respectively. It should be mentioned that repulsive interactions were predicted in aqueous solution for all the Py···mNA and Th···mNA complexes.[18] Thus, the strength of the binding with mNA undergoes a solvent-induced reduction that is more drastic for Py and Th than for EDOT. Although the local polarity in the interaction sites is not known, it is probably smaller and larger than that of water and chloroform, respectively. Therefore, the results derived from MP2 calculations on model complexes are fully consistent with experimental data.

### 4.1.4 – Conclusions

This work presents a detailed study about the interaction of plasmid DNA with PEDOT, a CP with excellent electrical, electrochemical and environmental properties. Ultrafine particles of PEDOT were obtained by applying ultrasounds to the grinded samples of polymer, which was prepared by anodic electropolymerization. Electrophoresis, UV-Vis and CD results obtained for mixtures of pMT4 plasmid DNA and PEDOT with different mass ratios indicate that interactions form immediately giving place to stable adducts. Moreover, electrophoretograms obtained after digestion with restriction enzymes show that the CP interact with specific nucleotide sequences, *i.e.* 5'-G/AATTC-3' (target for *Eco*RI) and 5'-G/GATCC-3' (target for *Bam*HI). Completely different results have been obtained for PT3M, a PTh derivative without donor and acceptors of hydrogen bonds. Thus, depending on the mass ratios, interactions between the latter material and plasmid DNA have been not detected or have been found to be weak. These features suggest that hydrogen bonds are essential to determine the specificity for selected nucleotide sequences and to define the strength and temporal evolution of the interactions between the CP and the plasmid DNA.

On the other hand, the CD spectra clearly show that the interaction with CPs provokes an alteration in the secondary structure of DNA, *i.e.* the unfolding of the double helix, which increases the exposition of the nitrogen bases. Both this result and the importance of hydrogen bonds in specific interactions lead us to propose the following hypothesis for the interaction between DNA and CPs: the latter materials produce the unfolding of the double helix promoting its intercalation between the DNA strands. This enhances the exposition of the DNA bases and, in the case of PEDOT, allows the formation of hydrogen bonding interactions between the bases and the oxygen atoms of the dioxane ring. The absence of these specific interactions explains the higher degree of exposition found in DNA:PT3M mixtures.

Ab initio quantum mechanical calculations in different environments show that the interactions with nucleic acid basis are stronger for EDOT than for Th. Indeed, EDOT usually interact through specific hydrogen bonds, while Th only forms complexes stabilized by interactions between the π-cloud of the ring and N-H groups of nucleic acid bases. These features are fully consistent with the experimental results presented for PEDOT and PT3M. On the other hand, the affinity towards the DNA bases are completely different for EDOT and Py, which should be attributed to the chemical characteristics of the oxygen atoms of EDOT (hydrogen bonding acceptors) and the N-H group of Py (hydrogen bonding donor). The strength of the binding in the gas-phase for EDOT···mNA complexes grows in the following order: mA < mC < mG ≈ mT. Furthermore, EDOT retains a significant affinity towards DNA bases when the polarity of the environment increases, whereas repulsive interactions were predicted for Py···mNA complexes in a polar solvent.

The overall of the results presented in this work indicate that PEDOT, which was found to be a biocompatible material, is a potential candidate for the development electroactive devices, *e.g.* drug-delivery systems, able to act through specific molecular recognition patterns.[22,23]

### 4.1.5 – References

[1] H. Chriswanto, G. G. Wallace, *J. Liq. Chromatogr.* 19 (1996) 2457.

[2] L. L. Miller, B. Zinger, O. X. Zhou, *J. Am. Chem. Soc.* 109 (1987) 2267.

[3] H. Guo, C. M. Knobler, R. B. Kaner, *Synt. Met.* 101 (1999) 44.

[4] P. Englebienne, *J. Mater. Chem.* 9 (1999) 1043.

[5] A. Kros, S. W. F. M van Howell, N. A. S. M. Sommerdijk, R. J. M. Nolte, *Adv. Mater.* 13 (2001) 1555.

[6] G. F. Khan, W. Wernet, *Thin Solid Films* 300 (1997) 265.

[7] A. Azioune, M. M. Chehimi, B. Miksa, T. Basinska, S. Slomkowski, *Langmuir* 18 (2002) 1150.

[8] V. Misoska, W. E. Prize, S. Ralph, G. G. Wallace, *Synth. Met.* 123 (2001) 279.

[9] J. Wang, M. Jiang, *Electroanalysis* 13 (2001) 537.

[10] H.-A. Ho, M. Boissinot, M. G. Bergeron, G. Corbeil, K. Dore, D. Boudreau, M. Leclerc, *Angew Chem. Int. Ed.* 41 (2002) 1548.

[11] D. S. Minehan, K. A. Marx, S. K. Tripathy, *Macromolecules* 27 (1994) 777.

[12] A.-H. Bae, T. Hatano, M. Numata, M. Takeuchi, S. Shinkai, *Macromolecules* 38 (2005) 1609.

[13] H. Peng, L. Zhang, J. Spires, C. Soeller, J. Travas-Sejdic, *Polymer* 48 (2007) 3413.

[14] T. Yamamoto, T. Shimizu, E. Kurokawa, *React. Funct. Polym.* 43 (2000) 79.

[15] C. Ocampo, E. Armelin, F. Estrany, L. J. del Valle, R. Oliver, F. Sepulcre, C. Alemán, *Macromol. Mat. Engin.* 292 (2007) 85.

[16] B. Teixeira-Dias, L. J. del Valle, F. Estrany, E. Armelin, R. Oliver, C. Alemán, *Eur. Polym. J.* 44 (2008) 3700.

[17] P. Pfeiffer, E. Armelin, F. Estrany, L. J. del Valle, L. Y. Cho, C. Alemán, *J. Polym. Res.* 15 (2008) 225.

[18] D. Zanuy, C. Alemán, *J. Phys. Chem. B* 112 (2008) 3222.

[19] B. Liu, G. C. Bazán, *Chem. Mater.* 16 (2004) 4467.

[20] C. E. Schmidt, V. Shastri, J. P. Vacanti, R. Langer, *Proc. Natl. Acad. Sci. USA* 94 (1997) 8948.

[21] A. Kotwal, C. E. Schmidt, *Biomaterials* 22 (2001) 1055.

[22] L. J. del Valle, D. Aradilla, R. Oliver, F. Sepulcre, A. Gamez, E. Armelin, C. Alemán, F. Estrany, *Eur. Polym. J.* 43 (2007) 2342.

[23] L. J. del Valle, F. Estrany, E. Armelin, R. Oliver, C. Alemán, *Macromol. Biosci.* (2008) *in press*.

[24] G. G. Wallace, L. A. P. Kane-Maguire, *Adv. Mat.* 14 (2002) 953.

[25] B. Adhikari, S. Majumdar, *Prog. Polym. Sci.* 29 (2004) 699.

[26] C. Ocampo, R. Oliver, E. Armelin, C. Alemán, F. Estrany, *J. Polym. Res.* 13 (2006) 193.

[27] L. B. Goenendaal, F. Jonas, D. Freitag, H. Pielartzik, J. R. Reynolds, *Adv. Mater.* 12 (2000) 481.

[28] Q. Pei, G. Zuccarello, M. Ahlskog, O. Inganäs, *Polymer* 35 (1994) 1347.

[29] F. Estrany, D. Aradilla, R. Oliver, C. Alemán, *Eur. Polym. J.* 43 (2007) 1876.

[30] M. J. Frisch, G. W. Trucks, H. B. Schlegel, G. E. Scuseria, M. A. Robb, J. R. Cheeseman, J. A. Montgomery, T. Vreven Jr., K. N. Kudin, J. C. Burant, J. M. Millam, S. S. Iyengar, J. Tomasi, V. Barone, B. Mennucci, M. Cossi, G. Scalmani, N. Rega, G. A. Petersson, H. Nakatsuji, M. Hada, M. Ehara, K. Toyota, R. Fukuda, J. Hasegawa, M. Ishida, T. Nakajima, Y. Honda, O. Kitao, H. Nakai, M. Klene, X. Li, J. E. Knox, H. P. Hratchian, J. B. Cross, C. Adamo, J. Jaramillo, R. Gomperts, R. E. Stratmann, O. Yazyev, A. J. Austin, R. Cammi, C. Pomelli, J. W. Ochterski, P. Y. Ayala, K. Morokuma, G. A. Voth, P. Salvador, J. J. Dannenberg, V. G. Zakrzewski, S. Dapprich, A. D. Daniels, M. C. Strain, O. Farkas, D. K. Malick, A. D. Rabuck, K. Raghavachari, J. B. Foresman, J. V. Ortiz, Q. Cui, A. G. Baboul, S. Clifford, J. Cioslowski, B. B. Stefanov, G. Liu, A. Liashenko, P. Piskorz, I. Komaromi, R. L. Martin, D. J. Fox, T. Keith, M. A. Al-Laham, C. Y. Peng, A. Nanayakkara, M. Challacombe, P. M. W. Gill, B. Johnson, W. Chen, M. W. Wong, C. Gonzalez, J. A. Pople, Gaussian 03, Revision B.02, Gaussian, Inc., Pittsburgh, PA, 2003.

[31] C. Møller, M. Plesset, *Phys. Rev.* 46 (1934) 618.

[32] P. C. Hariharan, J. A. Pople, *Theor. Chim. Acta* 28 (1972) 203.

[33] M. J. Frisch, J. A. Pople, J. S. Binkley, *J. Chem. Phys.* 80 (1984) 3265.

[34] S. F. Boys, F. Bernardi, *Mol. Phys.* 19 (1970) 553.

[35] M. Miertus, E. Scrocco, J. Tomasi, *Chem. Phys.* 55 (1981) 117.

[36] S. Miertus, J. Tomasi, *Chem. Phys.* 65 (1982) 239.

[37] G. D. Hawkins, C. J. Cramer, D. G. Truhlar, *J. Chem. Phys. B* 102 (1998) 3257.

[38] Y. H. Jang, W. A. Goddard III, K. T. Noyes, L. C. Sowers, S. Hwang, D. S. Chung, J. *Phys. Chem. B* 107 (2003) 344.

[39] J. I. Iribarren, J. Casanovas, D. Zanuy, C. Alemán, *Chem. Phys.* 302 (2004) 77.

[40] K. Nejedly, J. Chládková, M. Vorlícková, I. Hrabcová, J. Kypr, *Nuc. Acids Res.* 33 (2005) e5.

[41] C. S. Braun, G. S. Jas, S. Choosakoonkriang, G. S. Koe, J. G. Smith, C. R. Middaugh, *Biophys. J.* 84 (2003) 1114.

[42] J. Casanovas, C. Alemán, *J. Phys. Chem. C* 111 (2007) 4823.

[43] J. L. Brédas, *J. Chem. Phys.* 82 (1985) 3808.

[44] V. Hernandez, C. Castiglioni, M. Del Zopo, G. Zerbi, *Phys. Rev. B* 50 (1994) 9815.

[45] S. S. Zade, M. Bendikov, *J. Phys. Chem. C* 111 (2007) 10662.

[46] S. S. Zade, M. Bendikov, *J. Phys. Chem. B* 110 (2006) 15839.

## 4.2 – Influence of the doping level on the interactions between poly(3,4-ethylenedioxythiophene) and plasmid DNA

The influence of the doping level in the formation of specific interactions between plasmid DNA and poly(3,4-ethylenedioxythiophene), a CP with excellent technological properties, has been investigated using experimental assays and theoretical calculations. Electrochemical methods have been used to prepare polymer samples with oxidation degrees ranging from 0.14 to 1.05 positive charges per repeat unit. Mixtures involving different DNA:polymer mass ratios have been examined using electrophoresis, UV-Vis and CD spectroscopy. On the other hand, quantum mechanical calculations have been carried out on model complexes, different electronic and ionization states being considered for the molecules that mimic the CP. Combination of experimental and theoretical results has been used to propose a mechanism for the formation of DNA:CP complexes, which consists on the initial stabilization of the adducts through non-specific interactions followed by small structural re-arrangements that allow establish specific hydrogen bonds involving the polar groups of the CP and selected DNA bases.*

* - Results described in this section previously appeared in *Macromolecular Chemistry and Physics* 211 (2010) 1117. Theoretical calculations were preformed by D. Zanuy.

### 4.2.1 – Introduction

The interaction of CPs with bioentities, as for example living cells, proteins and DNA, to obtain information related to system performance and to control that performance, is not only an exciting but also an essential area of research.[1-7,11,12-21] Thus, the development of biotechnological applications based on CPs greatly depends on the control of such interactions. Within this topic, in the last years we have been particularly interested with the ability of CPs to form specific interactions with DNA.[15,17,19-21]

We found that CPs bearing polar functional groups able to act as hydrogen bonding donors and/or acceptors, *e.g.* N-H in PPy and ester side groups in some substituted PThs, are able to form specific interactions with well-defined nucleotide sequences of plasmid DNA.[15,17,19-21] This selectivity suggests that CP:DNA adducts are stabilized not only by electrostatic interactions, *i.e.* the existence of these complexes has been traditionally attributed to the tendency of the negatively charged DNA to interact with oxidized materials, but also by the presence of additional specific interactions, *i.e.* weak interactions that depend on the spatial disposition and orientation of the chemical groups. Among them, hydrogen bonds are expected to be significantly more important than other weak but less

specific interactions, *e.g.* π-π stacking and van der Waals. Indeed, recently reported theoretical calculations showed that hydrogen bonds between DNA bases and PPy are considerably stronger than interactions involving these biological building blocks and unsubstituted PTh.[20]

One of the most promising CPs, PEDOT (Scheme 1) shows particular abilities to interact specifically with plasmid DNA.[15,21] PEDOT is a commercial CP originally described by researchers at the Bayer company, which attracted considerable interest due to a combination of properties, *i.e.* moderate band gap, low oxidation potential, high conductivity, good optical transparency and exceptional environmental stability.[22-24] Electrophoretic and spectroscopic studies on mixtures of plasmid DNA and PEDOT showed the rapid formation of stable adducts, the formation of interactions with specific nucleotide sequences being evidenced through the protection imparted by this CP against restriction enzymes.[21] In contrast, interactions between DNA and poly(3-methylthiophene) (P3MT in Scheme 1), a PTh derivative without polar groups, were found to be non-specific, even although stable DNA:P3MT adducts were detected.[21] Thus, the specificity of PEDOT for selected nucleotide sequences as well as the temporal evolution of the DNA:PEDOT adducts, which was different from that of the DNA:P3MT ones, was attributed to the hydrogen bonds.

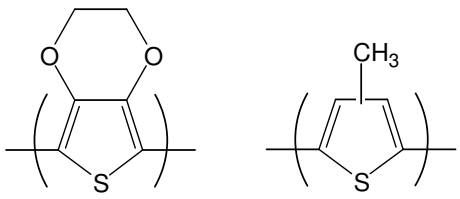


**PEDOT** **P3TM**

**Scheme 1**

In spite of these results, many aspects of the specific interactions between CPs and DNA remain unknown. Among them, the influence of the doping level on both the strength and specificity of the CP···DNA interactions is a subject that deserves consideration. Our previous studied on CP:DNA adducts were carried out using polymers yielded by anodic electropolymerization techniques, which typically produces highly oxidized (doped) CPs.[25] Thus, the unequivocal formation of strong electrostatic interactions between these doped

materials and the negatively charged DNA is essential for the formation and stability of adducts, even although specific hydrogen bonding interactions are expected to define the preferences towards selected nucleotide sequences. The importance of the doping level on CP···DNA interactions is the topic of the present study, in which we have examined experimentally and theoretically the interactions between plasmid DNA and PEDOT using samples of the latter material with three different oxidation degrees. In particular, we have performed electrophoretic assays, absorption spectroscopy, CD and quantum mechanical calculations to investigate the formation of stable adducts and specific interactions with DNA when the CP is used as prepared (0.54 charges per repeat unit), after subsequent oxidation (1.05 positive charges per repeat unit) or after subsequent reduction (0.14 charges per repeat unit).

### 4.2.2 – Methods

*Synthesis and Characterization of the CP.* EDOT monomer was purchased from Aldrich and used as received. Anhydrous $LiClO_4$, analytical reagent grade from Aldrich, was stored in an oven at 80 ºC before use in the electrochemical trials.

PEDOT was prepared by CA under a constant potential of 1.40 V using a polymerization time of 900 s. Both anodic electropolymerization and electrochemical experiments were performed on a VersaStat II potenciostat-galvanostat using a three-electrode compartment cell under nitrogen atmosphere at 25 ºC. The anodic compartment was filled with 40 ml of a 10 mM monomer solution in acetonitrile containing 0.1 M $LiClO_4$ as supporting electrolyte, while the cathodic compartment contained 10 ml of the same electrolyte solution. Steel AISI 316 sheets of 4 $cm^2$ area were employed as working and counter electrodes. The reference electrode was an Ag|AgCl electrode containing a KCl saturated aqueous solution.

The doping level of the generated PEDOT, hereafter called PEDOT-0, was altered by chronopotentiometric oxidation or reduction, respectively, using an electrochemical cell containing a 0.1 M $LiClO_4$ solution in acetonitrile, *i.e.* without monomer. Specifically, the oxidation degree of PEDOT-0 was increased and decreased by fixing the value of current density to +0.50 $mA \cdot cm^{-2}$ during 500 s and -0.50 $mA \cdot cm^{-2}$ during 300 s, respectively. Oxidized and reduced samples of PEDOT-0 are denoted PEDOT-ox and PEDOT-red, respectively. The

percentage of $ClO_4^-$ in each collected sample was obtained from reduction of approximately 2 mg of polymer with carbon, followed by determination of the amount of chloride ions released by standard ion chromatography. This analysis was performed with a Kontron 600 HPLC liquid chromatograph fitted with a Water IC-Pak anion column at 30 ºC and equipped with a Wescan conductimeter detector.

In order to facilitate the interaction with DNA, ultrafine particles of PEDOT-0, PEDOT-ox and PEDOT-red were obtained by applying ultrasounds to polymer solutions (5 µg polymer/µl; de-ionized water).

*Formation of complexes with DNA and electrophoretic assays.* The procedure employed to prepare DNA:PEDOT complexes was identical in all cases, independently of the doping level of the CP. Complexes were formed in aqueous solution by mixing 2.5 µl of plasmid pMT4 (0.1 µg/µl) with 0.00, 0.05, 0.25, 0.50, 2.50 and 5.00 µl of polymer solution (5 µg polymer/µl; de-ionized water), which corresponded to the desired DNA:PEDOT mass ratios (1:0, 1:1, 1:5, 1:10, 1:50, 1:100, respectively). Final volumes were raised to 10 µl with sterile de-ionized water. The mixtures were incubated overnight at 37 ºC. After this, an aliquot of 6X gel loading buffer was added, samples being centrifuged for 10 min. The supernatant was analyzed by electrophoresis with 1% of agarose gel containing ethidium bromide (0.5 µg/ml of gel) in 1X tris-borate-EDTA buffer (TBE). The electrophoretograms of plasmid pMT4 shows two characteristic bands, which correspond to a mixture of the supercoiled form I and the circular form II.[21]

The presence of specific interactions was examined using the *Eco*RI and *Bam*HI restriction enzymes, which cut off at 5'-G/AATTC-3' and 5'-G/GATCC-3' nucleotide sequences, respectively. The pMT4 plasmid DNA contains only one restriction site for *Eco*RI converting supercoiled form I and circular form II into linear DNA (form III). *Bam*HI has three restriction sites producing three DNA fragments, denoted F1, F2 and F3. The mobility of F1 and F2 correspond to a single band in the electrophoretogram, while F3 is the fragment of lowest molecular weight showing the fastest mobility. However, *Bam*HI produces form III when it makes only one cut in the plasmid DNA. To evaluate the cleavage of pMT4 in DNA:PEDOT complexes, 1.5 µl of restriction enzyme (10000 U/µl) and 1.28 µl of 10X enzyme buffer were added to each incubated sample. The digestion process was carried out at 37 ºC for 1 h, the digested products being analyzed by electrophoresis.

*Spectroscopic studies.* A UV-3600 (Shimadzu) UV-Vis-NIR spectrophotometer controlled by the UVProbe 2.31 software was used to record UV-Vis spectra of DNA:PEDOT at room temperature, in the 200-1000 nm range, with a bandwidth of 2 mm and a scan speed of 600 nm/min. Light scattering effects were avoided by correcting the maximum absorbance of nucleotide bases in DNA, which is 260 nm ($A_{260nm}$), with respect to the absorbance at 350 nm ($A_{350nm}$). For each sample, 36 cycles separated by an interval of 5 minutes between consecutive cycles were recorded. The interaction between the DNA and the CP was examined by following the evolution of $(A-A_0)/A_{max}$ against time ($t$) for the mixtures, where $A_0$ corresponds to the absorbance of DNA in solution (1:0 ratio) at the initial time ($t$= 0 min), $A_{max}$ is the absorbance of the bases in the mixture after thermal denaturalization of DNA *i.e.* the sample is heated at 94 ºC during 15 min producing exposition of all DNA bases, and $A$ is the absorbance of nitrogen bases in the mixture measured at different cycles.

CD measurements were carried out in a Jasco J-810 spectropolarimeter at 22 ˚C using a quartz cuvette. The CD data were recorded with standard sensitivity (100 mdeg), in the 170-400 nm range, with bandwidth of 2 mm, response time of 0.5 s and scanning speed of 200 nm/min. The reported spectra correspond to the average of five scans, the raw spectra being smoothed by the Savitsky-Golay algorithm. For each sample, the CD spectrum of the polymer was subtracted from that of the DNA:PEDOT complex, and compared with the CD spectrum of the plasmid DNA. Previous CD studies indicated that plasmid pMT4 is a supercoiling circular DNA with negative ellipticity.[19,21]

*Quantum mechanical calculations.* Calculations were performed using the Gaussian 03 computer program.[26] The structures of the complexes were determined by full geometry optimization at the MP2/6-31G(d) level.[27,28] Calculations were carried out considering the neutral, monocationic and dicationic ionization states for EDOT-oligomers, the singlet (two paired electrons) and triplet (two unpaired electrons) electronic states being considered for the dication. The restricted formalism was considered for complexes involving neutral EDOT-oligomers (closed-shell systems), while for monocationic and dicationic oligomers the unrestricted formalism of the MP2 method (UMP2) was used.

Calculated model complexes involved EDOT-oligomers, hereafter denoted $n$EDOT$^m$ (where $n$ refers to the number of EDOT units and $m$ indicates the charge and electronic

state, being *m*= 0, +1, +2S and +2T for the neutral state, monocationic state, singlet dicationic state and triplet dicationic state, respectively) and dimethylphosphate (DMP), 9-methylguanine (mG) or 1-methylthymine (mT). Previous calculations on $1EDOT^{0}$···mNA, where mNA refers to methylated nucleic acids, indicated that the interaction with mG and mT was favored with respect to that with methyladenine (mA) and methylcytosine (mC), the strength of the binding in $1EDOT^{0}$··mNA complexes growing as follows: mA < mC < mG ≈ mT.[21] Accordingly, the $n EDOT^{m}$···mNA complexes calculated for the current study are: $3EDOT^{0}$···mG, $3EDOT^{0}$···mT, $3EDOT^{+1}$···mG, $3EDOT^{+1}$···mT, $3EDOT^{+2S}$···mG, $3EDOT^{+2S}$···mT, $3EDOT^{+2T}$···mG and $3EDOT^{+2T}$···mT. On the other hand, the strength of non-specific electrostatic interactions was estimated by calculating the $1EDOT^{+1}$···DMP complex.

Binding energies ($\Delta E_b$), which were obtained by correcting the basis set superposition error with counterpoise method, were estimated as the difference between the total energy of the optimized complex and the energies of the isolated monomers with the geometries obtained from the optimization of the complex.[29] The effect of the solvent on the strength of the binding was estimated following the PCM developed by Tomasi and co-workers.[30,31] PCM calculations were performed in the framework of the ab initio (U)MP2/6-31G(d) level using the standard protocol and considering the dielectric constant of water (ε= 78.4), which is the solvent used for the experimental assays. Calculations were performed considering the gas-phase optimized geometries. Thus, solvent-induced changes in bond lengths and angles were found to have small influence on the free energy of solvation ($\Delta G_{sol}$), *i.e.*, solute geometry relaxations in solution and single point calculations on the gas-phase optimized geometries provided almost identical values of $\Delta G_{sol}$.[32-34] The binding energy of the complexes in solution ($\Delta E_{b,sol}$) was estimated by using eq. 1:

$$\Delta E_{b,sol} = \Delta E_b + \Delta\Delta G_{sol} \quad (1)$$

where $\Delta\Delta G_{sol}$ is the difference between the free energy of solvation of the complex and the separated monomers.

### 4.2.3 – Results and Discussion

*Preparation of PEDOT samples.* The electrogenerated PEDOT-0 films were dark-blue, uniform, adherent and insoluble. Although the properties of this CP are not discussed in this work because they were previously reported, it should be remarked that the number of positive charges supported by each monomeric unit of PEDOT-0 was found to be 0.54.[25] This oxidation degree was altered by chronopotentiometry, the doping level of PEDOT-ox and PEDOT-red being found to be higher and lower than that of PEDOT-0. More specifically, PEDOT-ox showed 1.05 positive charges per repeat unit, which is an extremely high value, while PEDOT-red was close to a neutral (de-doped) material with only 0.14 positive charges per repeat unit. Accordingly, the formulas of PEDOT-0, PEDOT-ox and PEDOT-red can be approximated as follows:

PEDOT-0: $[(EDOT_2)^+ ClO_4^-]_n$

PEDOT-ox: $[(EDOT)^+ ClO_4^-]_n$

PEDOT-red: $[(EDOT_7)^+ ClO_4^-]_n$

*Experimental measures on DNA:PEDOT complexes.* Previous work evidenced that PEDOT-0 forms stable complexes with specific interactions with plasmid DNA.[21] Accordingly, the current study is focused on the influence of the doping level of the CP in the strength of such interactions. Figure 1 shows the electrophoretograms obtained for DNA:PEDOT-0, DNA:PEDOT-ox and DNA:PEDOT-red mixtures considering different mass ratios. In all cases lane 1 corresponds to the 1:0 mass ratio (pMT4 plasmid without CP), while lanes 2-6 displays the series at 1:1, 1:10, 1:50 and 1:100 mass ratios. The retard in the mobility of form I and the increase in the intensity of form II evidence the formation of complexes for PEDOT-0 and PEDOT-ox when the mass ratio ranges from 1:5 to 1:100, *i.e.* they were not clearly detected for 1:1. The absence of bands in lanes 5 and 6 for the complexes with PEDOT-0 and PEDOT-ox must be attributed to the sedimentation of these adducts during the centrifugation process previous to the electrophoretic assays. In contrast, the electrophoretograms recorded for DNA:PEDOT-red mixtures do not allow a clear identification of stable complexes, a small retard in the mobility of the band of form I being the only alteration found for the 1:100 ratio. These results suggest that the formation of DNA:PEDOT complexes

are dominated by electrostatic interactions between the negative charges of the biomolecule and the positive charges of the doped CP.

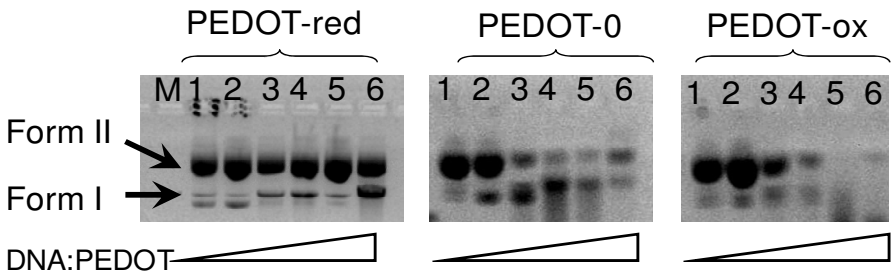


**Figure 1 –** Interaction of pMT4 plasmid DNA and increasing concentrations of CP (PEDOT-red, PEDOT-0 and PEDOT-ox) after their incubation for 3h at 37 ºC. Lane M (only for PEDOT-red): molecular weight marker (1 Kb Plus DNA Ladder). Lane 1: pMT4 plasmid DNA. Lanes 2-6: 1:1, 1:5, 1:10, 1:50 and 1:100 DNA:PEDOT mass ratios. Labels I and II indicate form I and II of pMT4 plasmid DNA, respectively.

*Eco*RI and *Bam*HI restriction enzymes were added to the DNA:PEDOT mixtures. Figure 2 displays the electrophoretograms obtained after enzymatic digestion of DNA:PEDOT-0, DNA:PEDOT-ox and DNA:PEDOT-red mixtures using 1:1, 1:10 and 1:100 mass ratios. The digestion of DNA:PEDOT-red with *Eco*RI produces the band associated to the formation of form III for all the studied ratios, while the band of linear DNA promoted by this enzyme is detected for the 1:1 and 1:10 ratios of DNA:PEDOT-0 and DNA:PEDOT-ox. Results obtained after the digestion of *Bam*HI reveal that, although fragments F1, F2 and F3 were detected for the 1:1 and 1:10 mixtures of the three systems, DNA receives some protection in the 1:100 mixtures. However, the protection imparted by PEDOT-ox was stronger than that provided by PEDOT-0 and, especially, PEDOT-red. The digestion of DNA:PEDOT-red with *Eco*RI produces the band associated to the formation of form III for all the studied ratios, while the band of linear DNA promoted by this enzyme is detected for the 1:1 and 1:10 ratios of DNA:PEDOT-0 and DNA:PEDOT-ox. Results obtained after the digestion of *Bam*HI reveal that, although fragments F1, F2 and F3 were detected for the 1:1 and 1:10 mixtures of the three systems, DNA receives some protection in the 1:100 mixtures. However, the protection imparted by PEDOT-ox was stronger than that provided by PEDOT-0 and, especially, PEDOT-red.

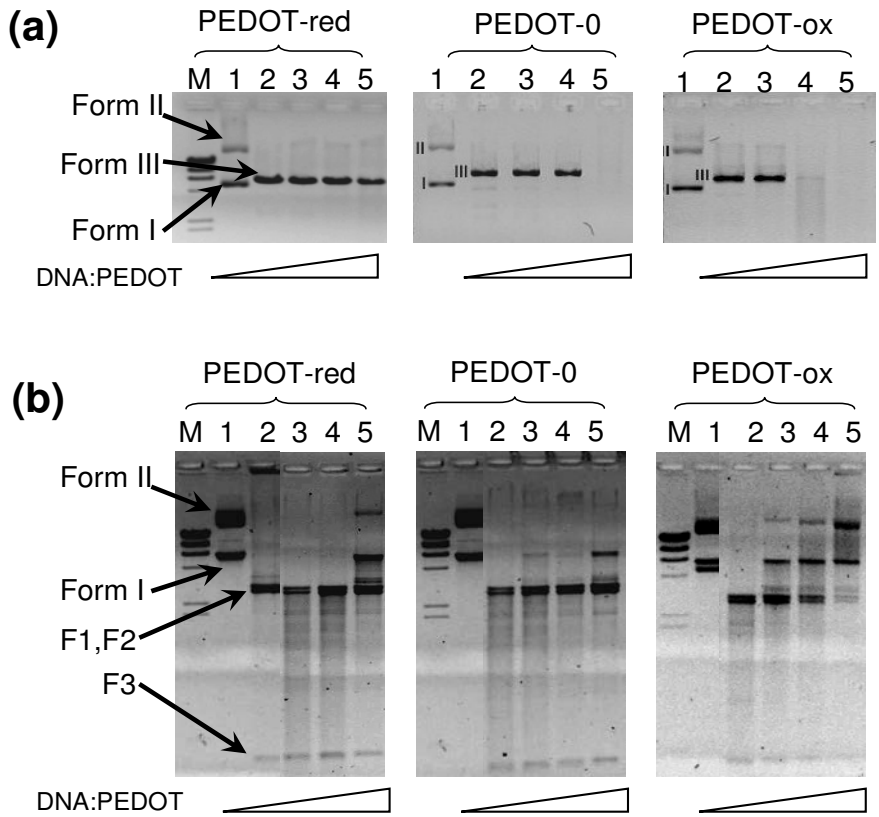


**Figure 2 –** Interaction between pMT4 plasmid DNA and increasing concentrations of CP (PEDOT-red, PEDOT-0 and PEDOT-ox) followed by *Eco*RI (a) and *Bam*HI (b) enzymatic digestion for a period of 1 h at 37 ºC. Lane M: molecular weight marker (1 Kb Plus DNA Ladder). Lane 1: undigested and untreated pMT4 plasmid DNA (1:0 ratio). Lane 2: digested pMT4 plasmid DNA (1:0 ratio). Lanes 3-5: 1:1, 1:10, 1:100 DNA:PEDOT ratios after enzymatic digestion. Forms I, II and III of pMT4 plasmid DNA, as well as fragments F1, F2 and F3 resulting from DNA digestion with *Bam*HI, have been labeled.

The temporal evolution of the mixtures formed by plasmid DNA and the different PEDOT species was examined using UV-Vis spectroscopy. Figure 3 represents the evolution of $(A-A_0)/A_{max}$ against time for the 1:1 and 1:50 mixtures.

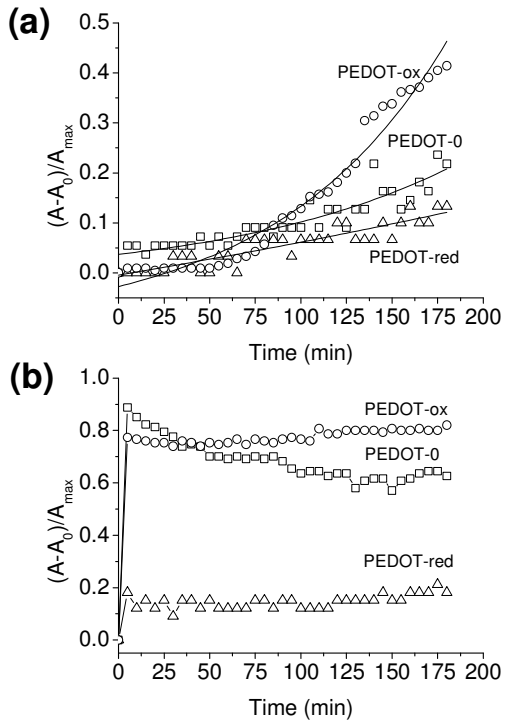


**Figure 3 –** Temporal evolution of DNA:PEDOT-red, DNA:PEDOT-0 and DNA:PEDOT-ox mixtures with (a) 1:1 and (b) 1:50 mass ratios followed by UV-Vis spectroscopy (see text). Spectra were recorded during the 36 cycles, two consecutive cycles being separated by a 5 minutes interval.

The moderate exposition of the nitrogen bases indicates that the interaction is relatively weak in the 1:1 mixture, independently of the oxidation degree of the CP. In contrast, interactions are clearly detected for the 1:50 DNA:PEDOT-0 and, especially, DNA:PEDOT-ox mixtures. These results reflect that the strength of the interactions strongly depend on the concentration of the doped CP. Moreover, the strong interactions found in the 1:50 mixtures, which are formed rapidly as revealed the fast exposition of the DNA nitrogen bases, are consistent with the formation of adducts evidenced by the electrophoretic assays. On the other hand, the interaction was found to be very weak for the 1:50 DNA:PEDOT-red mixture, which agrees with the results displayed in Figure 1 and 2.

Figure 4 shows the CD spectra recorded for DNA:PEDOT-red, DNA:PEDOT-0 and DNA:PEDOT-ox with 1:0 (isolated plasmid DNA), 1:1 and 1:100 mass ratios, which allow detect the structural changes induced by the CP in DNA.

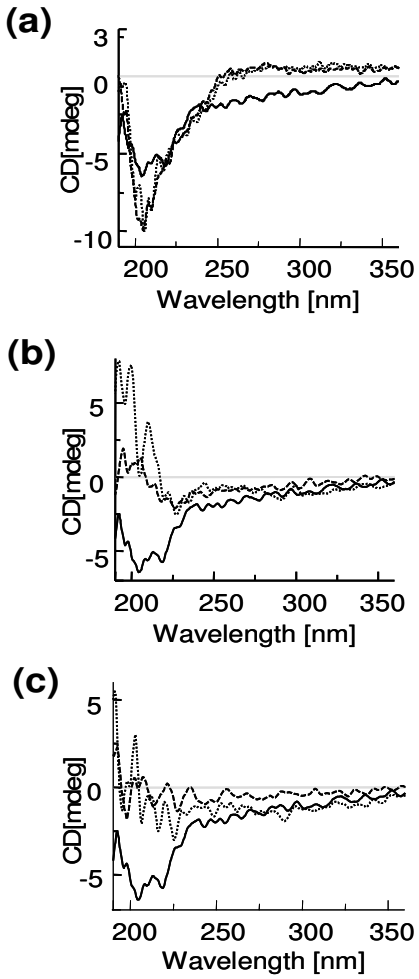


**Figure 4 –** CD spectra of DNA:PEDOT-red (a), DNA:PEDOT-0 (b) and DNA:PEDOT-ox (c) complexes to study the structural alterations of DNA. Mixtures with 1:1 (----) and 1:100 (·····) are displayed. In all cases the CD spectrum of the corresponding PEDOT specie was subtracted from the CD spectra of the mixtures. The spectrum recorded for the pMT4 plasmid DNA (—) is also included.

As it can be seen in Figure 4a, the raw spectra recorded between 200 and 260 show ellipticity changes (positive ellipticity) without loss of the supercoiling structure for the 1:1 and 1:100 DNA:PEDOT-red mixtures. Although the neutral CP is not able to alter the secondary structure of DNA, such positive ellipticity reflects a variation in the rotational movement. This feature is fully consistent with the small retard in the mobility of the band of form I displayed in Figure 1. In contrast, the spectra of DNA:PEDOT-0 and DNA-PEDOT-ox (Figure 4b and 4c, respectively) show significant structural changes, even although the

negative ellipticity is retained. The CD spectrum of the canonical B-form of DNA, which is the usually adopted in aqueous solution, typically presents a positive band at 275 nm, a negative band at 245 nm and a crossover point near 258 nm.[35,36] It worth nothing that the spectrum displayed in Figure 4 for the isolated plasmid (1:0 ratio) clearly correspond to the B-form. However, the addition of PEDOT-0 and PEDOT-ox provokes important variations in the appearance of the spectra reflecting drastic structural alterations. These changes, which increase with the doping level, produce the exposition of the DNA basis favoring favor the formation of stable complexes. Unfortunately, the DNA structure in such mixtures cannot be clearly defined due to the presence of the light scattering of spectral tails.[36]

The experimental results displayed in Figure 1-4 indicate that DNA:PEDOT-0 and DNA:PEDOT-ox complexes are formed rapidly, their strength and stability increasing with the oxidation degree of the CP. These features are consistent with the presence of non-specific electrostatic interactions between the DNA and oxidized PEDOT. Electrostatic interactions can be easily formed by all doped CPs, independently of their chemical nature, which is consistent with the stable DNA:P3MT adducts recently reported.[21] However, PEDOT is able to form interactions with specific nucleotide sequences, like those found in the 5'-G/AATTC-3' (target for *Eco*RI) and 5'-G/GATCC-3' (target for *Bam*HI) sequences, inducing protection in the restriction cleavage. These specific interactions are clearly detected for PEDOT-0 and PEDOT-ox while a high concentration of polymer is required for PEDOT-red (Figure 2). These results suggest that specific interactions are developed after the formation of stable adducts and, therefore, they should be considered as complementary reinforcement to the electrostatic ones. Structural alterations undergone by DNA are expected to facilitate the formation of specific interactions involving DNA bases once the complex has been constituted.

*Strength of the electrostatic interaction formed by the phosphate group of DNA and the oxidized PEDOT.* Figure 5 shows the most stable structure obtained for the $1EDOT^{+1}$···DMP complex. The resulting $\Delta E_b$ value, -122.9 kcal/mol, reflects the significant strength of this electrostatic interaction. Moreover, the $\Delta E_{b,sol}$ value is -41.7 kcal/mol reflecting that such interaction also remains stable in aqueous solution.

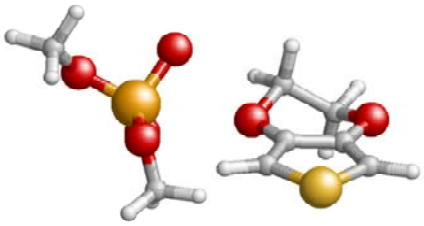

**Figure 5 –** Geometry of the most favored $1EDOT^{+1}$····DMP complex.

*Theoretical calculations on complexes formed by DNA bases and PEDOT.* Previous calculations on $1EDOT^{0}$···mNA indicated that intermolecular interactions are significantly stronger when mNA= mG and mT.[21] Accordingly, the initial structures of $3EDOT^{m}$···mG and $3EDOT^{m}$···mT were built for geometry optimization using the lowest energy arrangement reported for $1EDOT^{0}$···mG and $1EDOT^{0}$···mT, respectively.

Figure 6 shows the optimized molecular geometries of $3EDOT^{0}$···mG and $3EDOT^{0}$···mT. The former complex is stabilized by N-H···O and N-H···S hydrogen bonds, the intermolecular parameters for these interactions being [$d_{H\cdots O}$= 1.962 Å, ∠N-H···O= 167.4˚] and [$d_{H\cdots S}$= 2.862 Å, ∠N-H···S= 152.8˚], respectively. In contrast, $3EDOT^{0}$···mT presents a π-stacking stabilizing interaction, the center of masses of the central thiophene ring and the mT being separated by 3.375 Å. This represents a significant change with respect to the minimum energy structures reported for $1EDOT^{0}$···mT, which were stabilized by N-H···O and N-H···π interactions.[21] On the other hand, complexes involving $3EDOT^{+}$ (Figure 7) are completely different from those displayed in Figure 6. Specifically, the hydrogen bonding interaction pattern found for $3EDOT^{0}$···mG transforms into a π-stacked arrangement in $3EDOT^{+1}$···mG, the distance between the center of masses of the central thiophene ring and the mG being 3.367 Å. On the other hand, $3EDOT^{+1}$···mT presents a N-H···π interaction, the distance between hydrogen atom of mT and the center of the C2- C2' inter-ring bond being 2.371 Å.

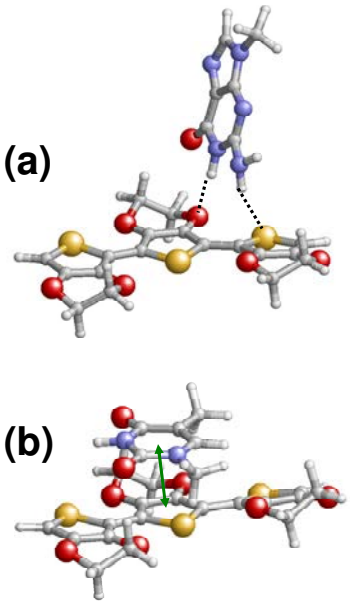


**Figure 6 –** Geometries of the (a) 3EDOT$^{0}$····mG and (b) 3EDOT$^{0}$····mT complexes calculated at the MP2/6-31G(d) level. The N-H···O and N-H···S interactions are displayed using black dashed lines, while the π-stacking interaction is indicated by a double arrow. Intermolecular parameters are given in the text.

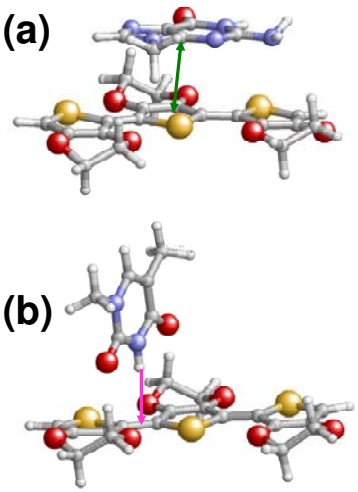


**Figure 7 –** Geometries of the (a) 3EDOT$^{+1}$····mG and (b) 3EDOT$^{+1}$····mT complexes calculated at the MP2/6-31G(d) level. The π-stacking and N-H···π interactions are indicated by double and single arrows, respectively.

Calculations on complexes containing the dicationic EDOT oligomer were performed considering both the singlet (3EDOT$^{+2S}$) and the triplet (3EDOT$^{+2T}$) electronic states. For the two nucleic acid bases the complex containing 3EDOT$^{+2S}$ was energetically stabilized with respect to that involving 3EDOT$^{+2T}$ by ~48 kcal/mol. This is an expected result since short dicationic thiophene- and EDOT-oligomers (less than ~9 repeat units) are known to prefer a bipolaronic structure (singlet state), while long oligomers form two well-defined and separated polarons (triplet state).[37-39] Figure 8 displays the optimized structures of the four complexes calculated considering the dicationic EDOT-oligomer.

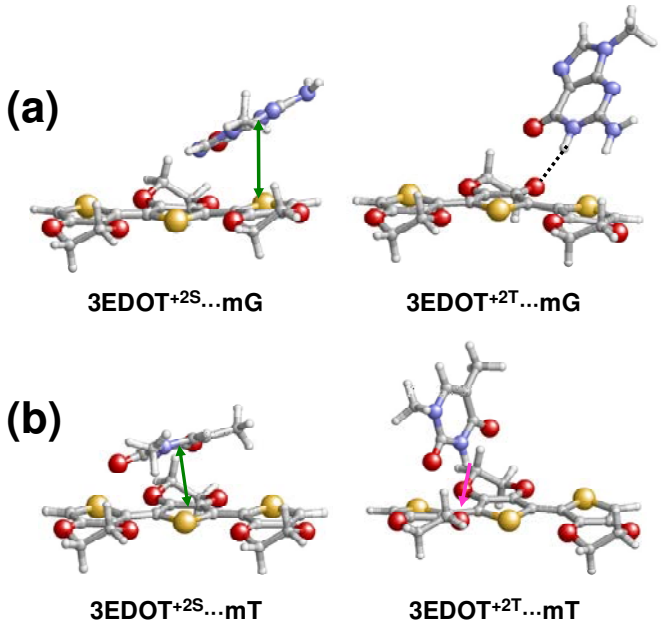


**Figure 8 –** Geometries of the (a) 3EDOT$^{+2S}$····mG and 3EDOT$^{+2T}$····mG, and (b) 3EDOT$^{+2S}$····mT and 3EDOT$^{+2T}$····mT complexes calculated at the MP2/6-31G(d) level. The π-stacking and N-H···π interactions are indicated by double and single arrows, respectively, while N-H···O interactions are displayed using black dashed lines.

As can be seen, 3EDOT$^{+2S}$···mG and 3EDOT$^{+2S}$···mT show π-stacked arrangements in which the center of masses of the nucleic acid base and the interacting thiophene ring are separated by 3.886 and 3.553 Å, respectively. In contrast, 3EDOT$^{+2T}$···mG shows a N-H···O hydrogen bond with $d_{H\cdots O}$= 2.179 Å and ∠N-H···O= 162.5°. Finally, the stability of 3EDOT$^{+2T}$···mT arises from the interaction formed by the N-H group of mT and the π-cloud of

the C2-C2' inter-ring bond, the distance between them (2.423 Å) being slightly larger than that obtained for $3EDOT^{+1}$···mT.

The values of $\Delta E_b$ for all the calculated complexes are listed in Table 1. Interactions are stronger with mG than with mT in the gas-phase, this feature being independent of the charge of the EDOT-oligomer. Indeed, the difference between the two systems increases with the oxidation degree of the oligomer. The energy gain associated to the binding increases with the charge of the EDOT-oligomer for both mG- and mT-containing complexes, even although this increment is significantly higher for the former than for the latter. Thus, $\Delta E_b$ is 44.2 kcal/mol more favorable for $3EDOT^{+2T}$···mG than for $3EDOT^{0}$···mG, whereas this difference decreases to 11.8 when $3EDOT^{+2T}$···mT and $3EDOT^{0}$···mT are compared. It should be noted that the $\Delta E_b$ values listed in Table 1 are significantly higher than that obtained for the $1EDOT^{+1}$···DMP complex, supporting the crucial role of the electrostatic interactions between the phosphate groups of DNA and the oxidized CPs in the formation of stable adducts.

**Table 1 –** Binding energies in the gas-phase and aqueous solution ($\Delta E_b$ and $\Delta E_{b,sol}$, respectively; in kcal/mol) obtained at the MP2/6-31G(d) level for the complexes calculated in this work.

| *Complex* | $\Delta E_b$ | $\Delta E_{b,sol}$ | *Complex* | $\Delta E_b$ | $\Delta E_{b,sol}$ |
|---|---|---|---|---|---|
| $3EDOT^{0}$···mG | -11.9 | 9.2 | $3EDOT^{0}$···mT | -10.9 | -2.9 |
| $3EDOT^{+1}$···mG | -12.3 | -1.1 | $3EDOT^{+1}$···mT | -10.7 | 10.1 |
| $3EDOT^{+2S}$···mG | -28.2 | 4.9 | $3EDOT^{+2S}$···mT | -18.0 | 3.5 |
| $3EDOT^{+2T}$···mG | -56.1 | -14.1 | $3EDOT^{+2T}$···mT | -22.7 | 9.0 |

A completely different situation was obtained in aqueous solution, the estimated values of $\Delta E_{b,sol}$ being included in Table 1. In this environment the relative affinities of the 3EDOT-oligomer towards mG and mT depend on both the oxidation degree and the electronic state. Specifically, $3EDOT^{0}$ and $3EDOT^{+2T}$ interact more favorably with mT than with mG, while $3EDOT^{+1}$ and $3EDOT^{+2S}$ prefer mG. However, all the $\Delta E_{b,sol}$ listed in Table 1 are significant higher than that obtained for $1EDOT^{+1}$···DMP. On the other hand, in some cases the interaction between the 3EDOT-oligomer and the base becomes repulsive in aqueous solution. The $\Delta G_{sol}$ values predicted for all the complexes and their corresponding fragments, which are listed in Table 2, indicate that the strength of the binding in aqueous solution is modulated by the hydration of both the complexes and the nucleic acid bases.

**Table 2 –** Solvation free energies in aqueous solution ($\Delta G_{sol}$; in kcal/mol) provided by the PCM method for the complexes calculated in this work as well as for the corresponding monomers.

| *Species* | *Complex* | *3EDOT*$^{m\ a}$ | *mNA* $^{b}$ |
|---|---|---|---|
| $3EDOT^{0}$···mG | -9.7 | -5.70 | -25.0 |
| $3EDOT^{+1}$···mG | -44.0 | -31.6 | -23.6 |
| $3EDOT^{+2S}$···mG | -118.8 | -127.7 | -25.3 |
| $3EDOT^{+2T}$···mG | -114.7 | -130.0 | -26.7 |
| $3EDOT^{0}$···mT | -6.9 | -5.6 | -9.4 |
| $3EDOT^{+1}$···mT | -20.1 | -31.4 | -9.6 |
| $3EDOT^{+2S}$···mT | -114.6 | -126.4 | -9.7 |
| $3EDOT^{+2T}$···mT | -105.0 | -126.9 | -9.9 |

[a] The super-index *m* refers to the charge and electronic state, being *m*= 0, +1, +2S and +2T for the neutral state, monocationic state, singlet dicationic state and triplet dicationic state, respectively. [b] mNA, which refers to methylated nucleic acid, are 9-methylguanine (mG) or 1-methythymine (mT).

Thus, the solute-solvent interaction is ~15.5 kcal/mol more favorable for mG than for mT. In spite of this, it should be emphasized that in realistic DNA:PEDOT systems the influence of the solvent is expected to be smaller. This is because in the calculated complexes the small model molecules are completely surrounded by the solvent, while in a realistic systems hydration effects are significantly smoothed by the macromolecular size of the own interacting species.

### 4.2.4 – Conclusions

Mixtures formed by pMT4 plasmid DNA and PEDOT with doping levels ranging from 0.14 to 1.05 positive charges per repeat unit were prepared considering 1:1, 1:5, 1:10 and 1:50 mass ratios. PEDOT-0 and PEDOT-ox form stable adducts and specific interactions with plasmid DNA. However, PEDOT-red interacts with DNA only when the concentration of the CP is very high. Accordingly, non-specific electrostatic interactions between the negatively charged groups of DNA and the oxidized CP are essential to form stable adducts, the stability of the complexes increasing with the doping level of the CP. Once adducts are stabilized, weak interactions that depend on the spatial disposition and orientation of the chemical

groups are formed. These specific interactions, which are the responsible of the protection imparted by PEDOT against the attack of the restriction enzymes, is possible because of the exposition of the DNA basis. Thus, the B-DNA arrangement of the plasmid DNA undergoes significant structural alterations when it interacts with PEDOT-0 and PEDOT-ox. In contrast, the formation of specific interactions in DNA:PEDOT-red mixtures is obstructed by the absence of electrostatic interactions, *i.e.* the exposition of the bases is low because structural alterations in DNA are small.

Quantum mechanical calculations on model complexes formed by $3EDOT^{m}$ and either mG or mT confirm that PEDOT is able not only to form specific interactions but also to distinguish among DNA bases. Most importantly, we found that the geometric interaction pattern and the binding energy of $3EDOT^{m}$···mNA complexes change with *m*, these features being fully consistent with experimental observations. Thus, the strength of the binding increases with the charge of the EDOT-oligomer supporting the fact that the stability of DNA:PEDOT adducts increases with the doping level. However, attractive specific interactions involving PEDOT and DNA bases, which depend on both the chemical nature of the latter and the oxidation degree of the former, are expected to play a significant role once the adducts are formed.

It should be noted that in oxidized CPs charges are not uniformly distributed along the whole molecular chains but are localized in small segments that involve a few tenths of repeating units.[40-42] Accordingly, neutral EDOT units belonging to non-charged blocks are expected to participate in the formation of specific hydrogen bonding interactions with selected DNA bases, while charged units are probably involved in non-specific electrostatic interactions with the phosphate groups of DNA. The overall of the results presented in this work are expected to be useful for the development of new CPs able to delivery drugs at specific regions of DNA.

### 4.2.5 – References

[1] B. Liu, G. C. Bazán, *Chem. Mater.* 16 (2004) 4467.

[2] R. A. Green, N. H. Lovell, L. A. Poole-Warren, *Biomaterials* 30 (2009) 3637.

[3] A. Kotwal, C. E. Schmidt, *Biomaterials* 22 (2001) 1055.

[4] L. J. del Valle, D. Aradilla, R. Oliver, F. Sepulcre, A. Gamez, E. Armelin, C. Alemán, F. Estrany, *Eur. Polym. J.* 43 (2007) 2342.

[5] J. W. Lee, F. Serna, J. Nickels, C. E. Schmidt, *Biomacromolecules* 7 (2006) 1692.

[6] L. J. del Valle, F. Estrany, E. Armelin, R. Oliver, C. Alemán, *Macromol Biosci* 8 (2008) 1144.

[7] P. Englebienne, *J. Mater. Chem.* 9 (1999) 1043.

[8] A. Kros, S. W. F. M. van Howell, N. A. S. M. Sommerdijk, R. J. M. Nolte, *Adv. Mater.* 13 (2001) 1555.

[9] A. Azioune, M. M. Chehimi, B. Miksa, T. Basinska, S. Slomkowski, *Langmuir* 18 (2002) 1150.

[10] A. B. Sanghvi, K. P. H. Miller, A. M. Belcher, C. E. Schmidt, *Nature Mat.* 4 (2005) 496.

[11] A. Azioune, M. M. Chehimi, B. Miksa, T. Basinska, S. Slomkowski, *Langmuir* 18 (2002) 1150.

[12] P. Routh, P. Mukerjee, A. Dawn, A. K. Nandi, *Biophys. Chem.* 143 (2009) 145.

[13] H. Peng, L. Zhang, J. Spires, C. Soeller, J. Travas-Sejdic, *Polymer* 48 (2007) 3413.

[14] T. Yamamoto, T. Shimizu, E. Kurokawa, *React. Funct. Polym.* 43 (2000) 79.

[15] C. Ocampo, E. Armelin, F. Estrany, L. J. del Valle R. Oliver, F. Sepulcre, C. Alemán, *Macromol. Mat. Engin.* 292 (2007) 85.

[16] Y. Fan, X. T. Chen, A. D. Trigg, C. H. Tung, J. M. Kong, Z. Q. Gao, *J. Am. Chem. Soc.* 129 (2007) 5437.

[17] P. Pfeiffer, E. Armelin, F. Estrany, L. J. del Valle, L. Y. Cho, C. Alemán, *J. Polym. Res.* 15 (2008) 225.

[18] A. Dawn, A. K. Nandi, *Macromolecules* 38 (2005) 10067.

[19] B. Teixeira-Dias, L. J. del Valle, F. Estrany, E. Armelin, R. Oliver, C. Alemán, *Eur. Polym. J.* 44 (2008) 3700.

[20] D. Zanuy, C. Alemán, *J. Phys. Chem. B* 112 (2008) 3222.

[21] C. Alemán, B. Teixeira-Dias, D. Zanuy, F. Estrany, E. Armelin, L. J. del Valle *Polymer* 50 (2009) 1965.

[22] F. Jonas, L. Shrader, *Synth. Met.* 41 (1991) 831.

[23] G. Heywang, F. Jonas, *Adv. Mater.* 4 (1992) 116.

[24] M. Dietrich, J. Heinze, G. Heywang, F. Jonas, *J. Electroanal. Chem.* 369 (1994) 87.

[25] C. Ocampo, R. Oliver, E. Armelin, C. Alemán, F. Estrany, *J. Polym. Res.* 13 (2006) 193.

[26] M. J. Frisch, G. W. Trucks, H. B. Schlegel, G. E. Scuseria, M. A. Robb, J. R. Cheeseman, J. A. Montgomery, T. Vreven Jr., K. N. Kudin, J. C. Burant, J. M. Millam, S. S. Iyengar, J. Tomasi, V. Barone, B. Mennucci, M. Cossi, G. Scalmani, N. Rega, G. A. Petersson, H. Nakatsuji, M. Hada, M. Ehara, K. Toyota, R. Fukuda, J. Hasegawa, M. Ishida, T. Nakajima, Y. Honda, O. Kitao, H. Nakai, M. Klene, X. Li, J. E. Knox, H. P. Hratchian, J. B. Cross, C. Adamo, J. Jaramillo, R. Gomperts, R. E. Stratmann, O. Yazyev, A. J. Austin, R. Cammi, C. Pomelli, J. W. Ochterski, P. Y. Ayala, K. Morokuma, G. A. Voth, P. Salvador, J. J. Dannenberg, V. G. Zakrzewski, S. Dapprich, A. D. Daniels, M. C. Strain, O. Farkas, D. K. Malick, A. D. Rabuck, K. Raghavachari, J. B. Foresman, J. V. Ortiz, Q. Cui, A. G. Baboul, S. Clifford, J. Cioslowski, B. B. Stefanov, G. Liu, A. Liashenko, P. Piskorz, I. Komaromi, R. L. Martin, D. J. Fox, T. Keith, M. A. Al-Laham, C. Y. Peng, A. Nanayakkara, M. Challacombe, P. M. W. Gill, B. Johnson, W. Chen, M. W. Wong, C. Gonzalez, J. A. Pople, Gaussian 03, Revision B.02, Gaussian, Inc., Pittsburgh, PA, 2003.

[27] C. Møller, M. Plesset, *Phys. Rev.* 46 (1934) 618.

[28] P. C. Hariharan, J. A. Pople, *Theor. Chim. Acta* 28 (1973) 213.

[29] S. F. Boys, F. Bernardi, *Mol. Phys.* 19 (1970) 553.

[30] M. Miertus, E. Scrocco, Tomasi, J. *Chem. Phys.* 55 (1981) 117.

[31] S. Miertus, J. Tomasi, *Chem. Phys.* 65 (1982) 239.

[32] G. D. Hawkins, C. J. Cramer, D. G. Truhlar, *J. Chem. Phys. B* 102 (1998) 3257.

[33] Y. H. Jang, W. A. Goddard III, K. T. Noyes, L. C. Sowers, S. Hwang, D. S. Chung, *J. Phys. Chem. B* 107 (2003) 344.

[34] J. I. Iribarren, J. Casanovas, D. Zanuy, C. Alemán, *Chem. Phys.* 302 (2004) 77.

[35] K. Nejedly, J. Chládková, M. Vorlícková, I. Hrabcová, J. Kypr, *Nuc. Acids Res.* 33 (2005) e5.

[36] C. S. Braun, G. S. Jas, S. Choosakoonkriang, G. S. Koe, J. G. Smith, C. R. Middaugh, *Biophys. J.* 84 (2003) 1114.

[37] J. Casanovas, C. Alemán, *J. Phys. Chem. C* 111 (2007) 4823.

[38] V. M. Geskin, J. L. Brédas, *Chem. Phys. Chem.* 4 (2003) 498.

[39] Y. Gao, C.-G. Liu, Y.-S. Jiang, *J. Phys. Chem. A* 106 (2002) 5380.

[40] J. Casanovas, C. Alemán, *J. Phys. Chem. C* 111 (2007) 4823.

[41] J. L. Brédas, *J. Chem. Phys.* 82 (1985) 3808.

[42] S. S. Zade, M. Bendikov, *J. Phys. Chem. C* 111 (2007) 10662.

## 4.3 – Specific interactions in complexes formed by DNA and conducting polymer building blocks: Guanine and 3,4-ethylenedioxythiophene

The present contribution presents direct experimental evidences about the existence of hydrogen bonds between PEDOT and DNA complexes as well as a deeper of the knowledge how such interactions take place in these complexes. To this end, we have employed a combination of experimental and theoretical methodologies to examine the interactions between the building blocks of such two macromolecules. Specific interactions between EDOT and doubly protonated guanine ($GH_2^{2+}$) monomers have been investigated using UV-Vis spectroscopy. Quantum mechanical calculations in the density functional theory (DFT) and time-dependent density functional theory (TDDFT) frameworks have been used to indentify the structure of the possible complexes, which differ in the interaction pattern, and to interpret the absorption spectra in terms of intermolecular interactions, respectively. Results allowed us to verify our previous hypothesis about the formation of specific N-H···O interactions between G-containing nucleotide sequences and PEDOT. Clearly, DFT calculations indicate that EDOT:$GH_2^{2+}$ complexes are stabilized by N-H···O interactions, involving an EDOT oxygen and the –NH and $–NH_2$ moieties of $GH_2^{2+}$. Furthermore, TDDFT calculations have allowed us to reproduce the absorption spectra (both energy gaps and relative oscillator strength magnitudes) of EDOT and $GH_2^{2+}$ but also of the complex. In summary, results provide evidence about the existence of specific N-H···O interaction in the systems under study, allowing us to confirm our previous hypothesis and to explain previous experimental observations.*

* - Results described in this section previously have been recently submitted for publication. Theoretical calculations were preformed by J. Preat and E. Perpète.

### 4.3.1 – Introduction

The control of the interactions between CPs and bioentities, for example living cells, proteins and DNA, is an essential research area for the development of advanced biotechnological applications.[1-4,8-13] Within this context, in the last years we have been particularly interested in the recognition of nucleotide sequences using polypyrrole and polythiophene derivatives.[14-20] Specifically, we found that CPs bearing polar functional groups are able to act as hydrogen bonding donors and/or acceptors forming specific interactions with well-defined nucleotide sequences of plasmid DNA.[14-17] In contrast, interactions between DNA and polymers without groups able to participate in hydrogen bonds, as for example poly(3-methylthiophene) and polythiophene, were found to be non-specific, even although stable adducts were detected.[5,16,18] These features evidenced that

amongst specific interactions, hydrogen bonds are more important than other weak interactions, like π-π stacking and hydrophobic.

CPs used in our investigations are usually in a highly oxidized (doped) state.[14,16-19] Spontaneous interpolymer complexation between cationic polyelectrolytes and DNA is a well-known process, which results from cooperative electrostatic forces.[21,22] Accordingly, the unequivocal formation of electrostatic interactions between positively charged CPs and negatively charged DNA is expected to essential for the formation and stability of the adducts. In a very recent study we investigated the influence of the doping level in the formation of specific interactions between DNA and CPs bearing polar functional groups.[19] Specifically, we considered a polymer in different oxidized states (1.0 and 0.5 positive charges per repeating unit) and in a reduced state (0.1 charges per repeating unit) states. Results allowed us to propose a mechanism for the formation of the adducts with DNA, which consists of an initial stabilization of the complexes through non-specific electrostatic interactions, followed by small structural re-arrangements that allow establishing specific hydrogen bonds between the polar groups of the CP and selected DNA bases. This process requires a structural alteration of the B-DNA double helix, which unfolds into two separated strands as was observed by circular dichroism and UV-Vis spectroscopy.[17,19] The proposed mechanisms was confirmed in a more recent investigation, in which the binding of an oxidized CP to a single-stranded DNA featuring the Dickerson's dodecamer sequence was examined using Molecular Dynamics (MD) simulations.[21]

Among CPs, poly(3,4-ethylenedioxythiophene), hereafter abbreviated PEDOT (Scheme 1), has attracted considerable interest due to a combination of properties: low oxidation potential, good optical transparency, high conductivity (up to 500 S/cm), exceptional thermal and chemical stabilities, fast doping-undoping processes, and excellent biocompatibility.[23-27] Electrophoretic and spectroscopic studies on mixtures of plasmid DNA and both oxidized and reduced PEDOT have shown the formation of stable adducts, the formation of interactions with specific nucleotide sequences being evidenced through the protection imparted by this material against restriction enzymes.[16,18,19] Moreover, first principle calculations using the MP2 quantum mechanical method indicated that the binding strength between the 3,4-ethylenedioxythiophene (EDOT) monomeric units and DNA bases grows in the following order: Adenine (A) < Cytosine (C) < Thymine (T) ≈ Guanine (G).[18] These preferences were confirmed in a very recent MD study, in which the interaction

between an oxidized PEDOT chain and a single DNA strand with sequence 5'-CGCGAATTCGCG-3' was investigated at the atomistic level.[20] Thus, results revealed the formation of specific O···H and S···H hydrogen bonds, π-π stacking, and N-H···π interactions, in addition to the expected electrostatic interactions. In general, O···H hydrogen bonds were found to be very abundant showing relatively large accumulated lifetimes, these specific interactions being more frequent with G and T than with A and C.

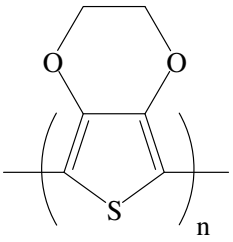


**PEDOT**

**Scheme 1**

In order to get direct experimental evidences about the existence of hydrogen bonds between PEDOT and DNA, as well as to obtain more knowledge how this interaction occurs in such complexes, in this work we use a combination of experimental and theoretical methodologies to examine the interactions between the building blocks of such two macromolecules. Specific interactions between EDOT and G monomers have been investigated using UV-Vis spectroscopy. Quantum mechanical calculations in the density functional theory (DFT) and time-dependent density functional theory (TDDFT) frameworks have been used to identify the structure of the possible EDOT:G complexes, which differ in the interaction pattern, and to interpret the absorption spectra in terms of intermolecular interactions, respectively. Results allowed us to verify our previous hypothesis about the formation of specific N-H···O interactions between G-containing nucleotide sequences and PEDOT.

### 4.3.2 – Methods

*Complexes.* EDOT and G were purchased from Aldrich and Sigma Aldrich, respectively, while HCl and dimethylsulfoxide (DMSO) of analytical reagent grade were purchased from Panreac. Trials with different solvents were performed before to find the appropriated conditions for the complete solubilisation of both EDOT and G.

Initially, the following solutions were prepared independently: (i) 1 mg of G was dissolved in 1 mL of HCl (0.5 M, pH= 0.3), to give the protonated form $GH_2^{2+}$ (see below); and (ii) 0.9 mg of EDOT was dissolved in 1 mL of DMSO. After this, a 1:1000 dilution was performed on each solution to obtain optimal concentrations for UV-Vis spectroscopy assays. Complexes were formed in aqueous solution by mixing the diluted solutions of G in HCl and EDOT in DMSO. Solutions were mixed to reach the following EDOT:$GH_2^{2+}$ mass ratios: 0:1, 1:1, 1:2, 2:1 and 1:4. Final volumes were raised to 1 mL using mixed solutions of DMSO and HCl that were explicitly prepared for each mass ratio.

*Spectroscopic studies.* An UV-3600 (Shimadzu) UV-Vis/NIR spectrophotometer controlled by the UVProbe V2.31 software was used to record UV-Vis spectra of G, EDOT and EDOT:$GH_2^{2+}$ at room temperature in the 230-400 nm range, with a bandwidth of 2 mm, a scan speed of 600 nm/min, and a sampling interval of 0.1 nm. The deconvolution of the UV-Vis spectra was performed using the PeakFit V4.0 software and applying a Gaussian deconvolution method with a width of 2 nm in Full-Width Half-Maximum (FWHM) mode and with scan amplitude of 1.5%.

*Computational details.* Calculations were performed with the Gaussian 09 computer program.[28] Geometry optimizations were performed in the solvent-phase within the density functional theory framework (DFT) at the B3LYP level of theory with the 6-311G(d,p) basis set (BS).[29,30] The counterpoise method (CM) is used to correct the basis-set superposition error (BSSE) for the evaluation of the complexation driving force ($\Delta G$) that have been obtained through the computation of the infrared spectrum for each optimized structures. The binding energies (B), which were obtained without applying the CM, are calculated as the difference between the total internal energy of the optimized complex and the isolated monomers' internal energies associated to the complex equilibrium geometry. The vertical

electronic excitations have been obtained by using the time-dependent density functional theory (TDDFT) framework, in the solvent-phase, at the more refined CAM-B3LYP level of theory with the large 6-311+G(2d,2p) BS.[30-36]

It is our experience that the combination of extended BSs with a long-range functional for TDDFT calculations is essential to accurately describe the electronic structures of systems likely to show marked charge-transfer excitations.[37,38]

The complexes are formed in DMSO and the solvent effects on both the geometry optimizations and TDDFT calculations have been taken into account by the polarisable continuum model (PCM).[39] In PCM, one usually divides the problem into a solute part (the complex) lying inside a cavity, and a solvent part. By solving the Poisson's at the interface, PCM gives a valid approximation of solvent effects. For the vertical excitation energies, we have selected the so-called non-equilibrium PCM solutions.[40]

G shows two positive pKas estimated at 3.2 and 0.9 in water.[41] At pH = 0.3, we have two basic sites that are protonated (to give $GH_2^{2+}$), as depicted in Figure 1.

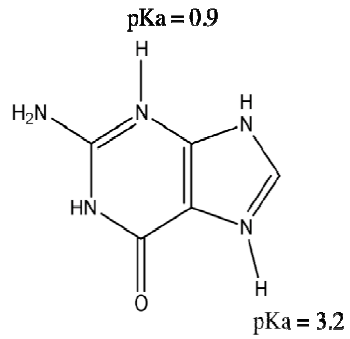


**Figure 1 -** Molecular structure for $GH_2^{2+}$ and the two protonated basic sites.

In the present contribution, we did focus on three different EDOT:$GH_2^{2+}$ (1:1) complexes:

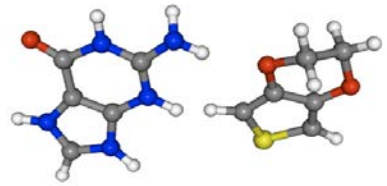

**C-1**

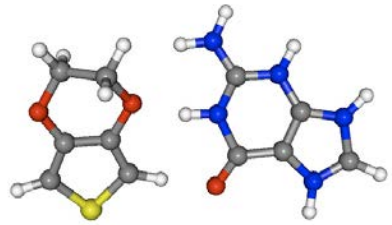

**C-2**

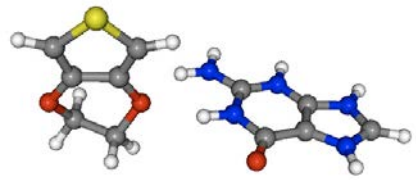

**C-3**

**Figure 2 -** Molecular structure of the initial conformation of the three EDOT:$GH_2^{2+}$ complexes of interest C-1, C-2, C-3.

C-1, -2 and -3 have been chosen as starting conformations because it has been previously shown that the corresponding neutral forms (*i.e.* EDOT:G complexes) show the best stability in both gas- and solvent-phase.[18]

### 4.3.3 – Results and Discussion

*Experimental measures.* Figure 3 shows the absorption spectra recorded for diluted solutions of EDOT, $GH_2^{2+}$ and EDOT:$GH_2^{2+}$ (1:1 mass ratio), the curves resulting from the deconvolution process being included in each case. Satisfactory statistical parameters [*i.e.* correlation coefficient $r^2$ > 0.98 and standard error *s.e.* < 0.005) were obtained by considering 2, 2 and 3 isolated curves in the deconvolution of EDOT, $GH_2^{2+}$ and EDOT:$GH_2^{2+}$ spectra, respectively.

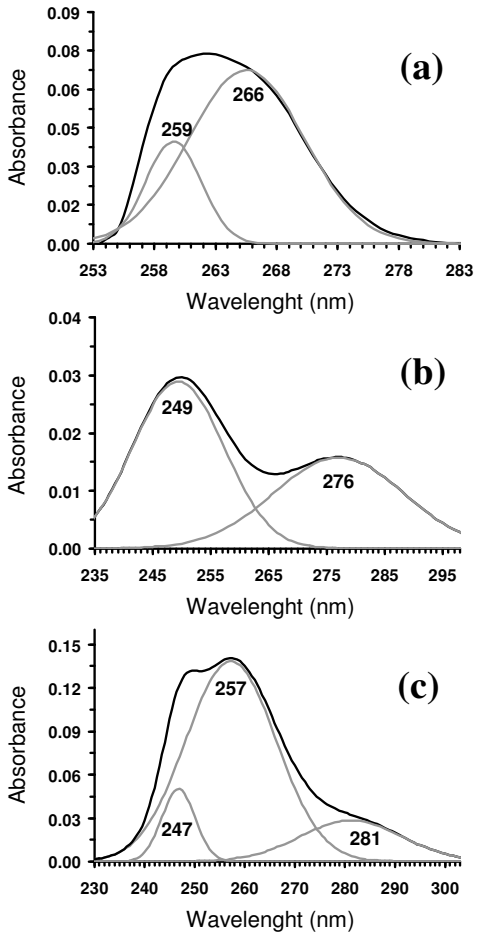


**Figure 3 -** Absorption spectra (black lines) of (a) EDOT, (b) $GH_2^{2+}$ and (c) EDOT:$GH_2^{2+}$ (1:1 mass ratio) determined in dilute solution (see Methods). The curves and wavelength at the maxima resulting from the deconvolution process are also shown for each spectrum (gray lines).

As it can be seen, diluted EDOT shows two important transitions at 259 and 266 nm, while the transitions of $GH_2^{2+}$ are observed at 249 and 276 nm. For the complex, the deconvolution process led to three peaks centred at 247, 257 and 281 nm. It should be mentioned that the shoulder observed at the largest wavelength region precludes any reasonable fitting with a lower number of curves. Accordingly, the interactions between the two species, which are responsible of the formation of the complex, affected considerably one of the transitions. Thus, although the peaks at 259 and 249 nm for EDOT and $GH_2^{2+}$, respectively, undergo a change upon complexation (*i.e.* a blue shift of 2 nm is detected), the peaks at 266 and 276 nm merge and red-shift to 281 nm. Results obtained for complexes with 1:2, 2:1 and 1:4 mass ratios are very similar to those displayed in Figure 3c (data not shown). In order to interpret the transitions displayed in Figure 3, quantum mechanical calculations were performed on EDOT, $GH_2^{2+}$ and EDOT:$GH_2^{2+}$.

*Quantum mechanical calculations.* Table 1 provides the binding energies and free enthalpies of complexation for the three above-evoked systems C-1, C-2 and C-3. The three systems present both binding energy and free enthalpies of complexation values in the same order of magnitude, from 0.91 to 0.95 eV for B and from 0.25 to 0.28 eV for ΔG.

**Table 1 –** Theoretical binding energies (B) and free enthalpies of complexation (ΔG) (in eV) for the three complexes (G//EDOT) 1:1 in DMSO.

| Compounds | B | ΔG |
|---|---|---|
| C-1 | 0.91 | 0.25 |
| C-2 | 0.94 | 0.28 |
| C-3 | 0.95 | 0.28 |

This can be related to the fact that for the three final structures, we have two hydrogen-bonds (H-bonds), implying an EDOT oxygen and the –NH and $–NH_2$ functions of $GH_2^{2+}$. Since C-2 and -3 present a similar structure after optimization, we compute equivalent B and ΔG values. For C-1, however, the optimized EDOT:$GH_2^{2+}$ configuration is quite different in regards to the two last ones (Figure 4), *i. e.* the $GH_2^{2+}$ carbonyl group is far from the guanine moiety, and it results a increase (decrease) of the $–NH_2$---O (–NH---O) H-bond length.

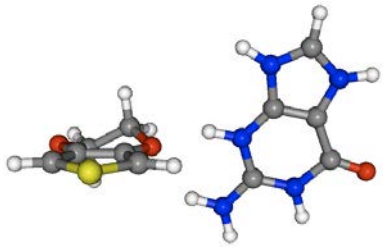

C-1

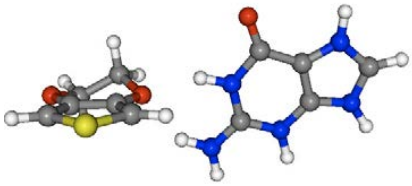

C-2

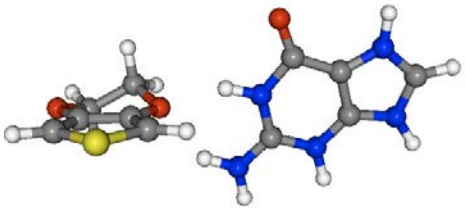

C-3

**Figure 4 -** Molecular structure of the final conformation of the three EDOT:$GH_2^{2+}$ complexes of interest C-1, C-2, C-3.

The theoretical excitation energies for the $GH_2^{2+}$, EDOT and C-1 to -3 systems are listed and confronted to the experimental data in Table 2. For both the four considered systems, TDDFT systematically provides two peaks ($\lambda^{(1)}$, $\lambda^{(2)}$) in the high energetic region of the UV-Vis spectrum.

For both $GH_2^{2+}$ and EDOT, the absorption band of higher energy ($\lambda^{(1)}$) corresponds to a HOMO $\rightarrow$ LUMO transition. For $GH_2^{2+}$, The MOs in Table 3 clearly show that $\lambda^{(1)}$ is related to an intramolecular charge transfer (CT) from the $-NH_2$ to the carbonyl whereas for the second absorption band HOMO $\rightarrow$ LUMO+1 transition), the charge transfer occurs in the opposite

direction (*i. e.* we have a $–NH_2 \rightarrow –C=O$ photoinduced intramolecular CT). The nature of the CT is less obvious in the EDOT case but the MOs analysis lets us suggest that for $\lambda^{(1)}$, the charge transfer takes place from the oxygen atoms in the heterocycle to the aromatic moiety (the MO is mainly localized on the C-H bond) whereas for $\lambda^{(1)}$ we have a HOMO-1→ LUMO CT from the oxygen atoms to the sulfur atom.

**Table 2 –** Comparison between experimental and theoretical UV-vis absorption bands, λ in eV [in nm] for the doubly-protonated Guanine ($GH_2^{2+}$), EDOT and three complexes (C-1, -2, and -3) 1:1 in DMSO. Δ is the absolute energy difference between the first and second excitation, in eV [in nm]. We also provide the oscillator strength f related the theoretical $\lambda^{(1)}$, $\lambda^{(2)}$ and the related molecular orbitals (MOs) labels.

| Compounds | Experiment | | Theory (f) | |
|---|---|---|---|---|
| | $\lambda^{(1)}, \lambda^{(2)}$ | Δ | $\lambda^{(1)}, \lambda^{(2)}$ | Δ |
| $GH_2^{2+}$ | 4.49, 4.98 | 0.49 | 5.37 (0.22), 5.83 (0.35) | 0.46 |
| | [276, 249] | [27] | [231, 213] | [18] |
| EDOT | 4.66, 4.78 | 0.12 | 5.23 (0.24), 5.39 (0.10) | 0.16 |
| | [266, 259] | [7] | [237, 230] | [7] |
| C-1 | | | 5.26 (0.24), 5.32 (0.17) | 0.06 |
| | 4.41, 4.82, 5.02 | 0.41 | [236, 233] | [3] |
| C-2 | [281, 257, 247] | [24] | 5.26 (0.24), 5.37 (0.21) | 0.11 |
| | | | [236, 231] | [5] |
| C-3 | | | 5.26 (0.24), 5.37 (0.21) | 11 |
| | | | [236, 231] | [5] |
| | MOs labels $\lambda^{(1)}, \lambda^{(2)}$ | | | |
| $GH_2^{2+}$ | HOMO → LUMO, HOMO → LUMO+1 | | | |
| EDOT | HOMO → LUMO, HOMO-1→ LUMO | | | |
| C-1 | HOMO → LUMO+4, HOMO-2 → LUMO | | | |
| C-2 | HOMO → LUMO+4, HOMO-2 → LUMO | | | |
| C-3 | HOMO → LUMO+4, HOMO-2 → LUMO | | | |

Concerning the complexes, Table 3 reveals the intermolecular nature of the CT involved in the first excitation. Clearly, the HOMO → LUMO+4 transition is predominantly localized on EDOT but with a slight contribution of the $–NH_2$ as well as the NH functions of $GH_2^{2+}$ (LUMO+4). On the contrary, $\lambda^{(2)}$ is characterized by a pure intramolecular CT localized on the protonated guanine and C-1 $\lambda^{(2)}$ MOs' topology nature is similar to the one observed for the first excitation of isolated $GH_2^{2+}$, *i. e.* a $–NH_2 \rightarrow –C=O$ photoinduced intramolecular

CT. The similarity between the MOs involved in the $GH_2^{2+}$ HOMO → LUMO transition and in the C-1 HOMO-2 → LUMO can explain the similar excitation energies and oscillator strength computed for $GH_2^{2+}$ $\lambda^{(1)}$ (5.37 eV, f=0.22) and C-1, -2 and -3 $\lambda^{(2)}$ (5.32 and 5.7 eV, f=0.17 and 0.21).

**Table 3 –** Shape of the MOs (and their labels) involved in the $\lambda^{(1)}$ and $\lambda^{(2)}$ for $GH_2^{2+}$, EDOT and C-1, respectively. They have been obtained at the PCM(DMSO)-B3LYP/6-311G(d,p) level of theory with a contour threshold fixed at 0.05 $|e|$.

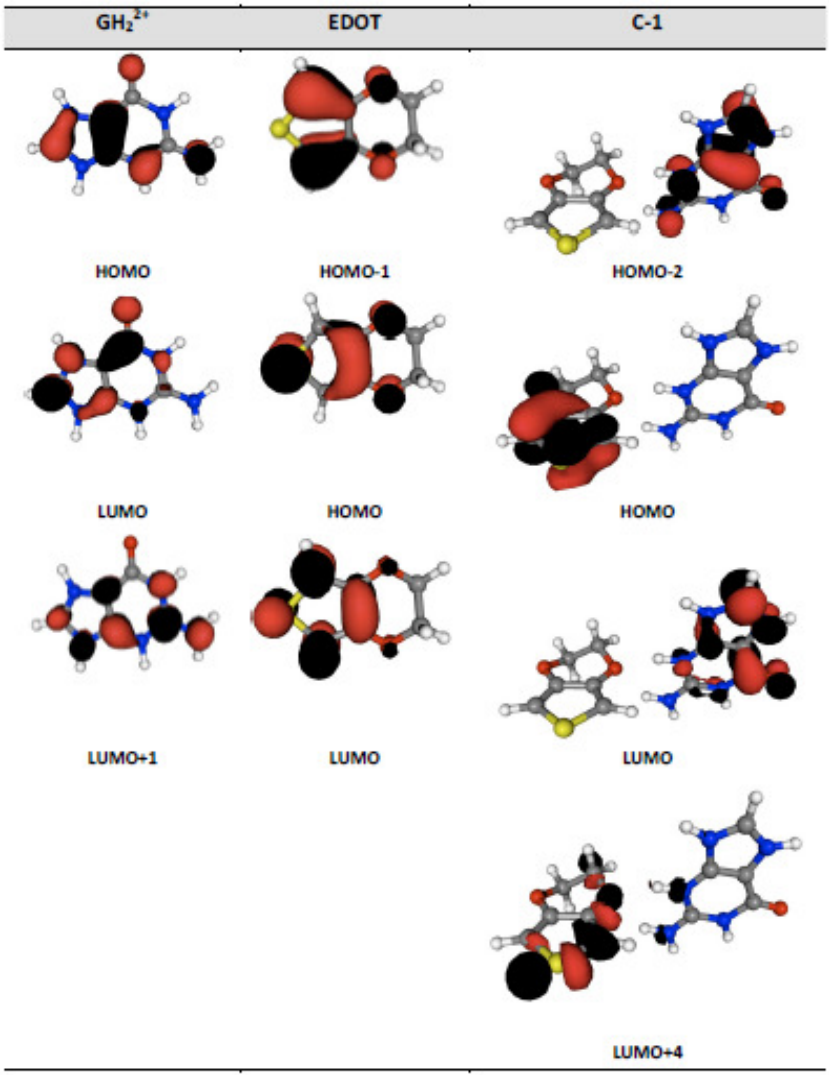

For $GH_2^{2+}$ and EDOT, our TDDFT procedure is able to reproduce the $\lambda^{(1)}$-$\lambda^{(2)}$ energy gap ($\Delta$) and the relative $\lambda^{(1)}$-$\lambda^{(2)}$ oscillator strength magnitude. Indeed, $\Delta$ is calculated at 0.46 and 0.16 eV for $GH_2^{2+}$ and EDOT, respectively whereas these gaps are measured at 0.49 and 0.12 eV. On the other hand, the relative $f^{(1)}/f^{(2)}$ parameter is estimated at 0.63 and 2.40 for $GH_2^{2+}$ and EDOT, respectively in qualitative agreement with experimental trends. Indeed, for EDOT the peaks at 259 and 266 nm present absorbance of 0.038 and 0.067, and the ratio $f^{(1)}/f^{(2)}$ values 0.57 whereas for $GH_2^{2+}$, it is computed at ca. 1.84 with peaks at 249 and 276 nm presenting measured absorbance of 0.029 and 0.016. If the theory successfully characterizes the UV-Vis spectra of the isolated $GH_2^{2+}$ and EDOT, the analysis of the TDDFT results is quite problematic for the complexed form. Indeed, whereas TDDFT provides two absorption bands, the deconvolution reveals three peaks at 4.41, 4.82 and 5.02 eV (281, 257 and 247 nm, respectively). Obviously, a characteristic feature of the absorption spectrum of the EDOT:$GH_2^{2+}$ complex is the existence of several maxima in the short-wave band. Although many speculations can be held to elucidate this spectral pattern, our favor goes to the vibrational coupling hypothesis because the distance between the two neighbouring peaks at 257 and 247 nm sticks to an IR frequency. For instance, one can check that the typical ~1600-1700 $cm^{-1}$ stretching of carbonyl or ethylene side groups corresponds to 0.20 eV separation experimentally observed for the complex. Note that the gap between the peaks at 281 and 247 nm is superior to 0.60 eV and corresponds to ca. 5000 $cm^{-1}$ separation, which is out of the infrared energetic region. The IR spectrum for C-1 clearly shows an absorption band of high intensity at 1720 $cm^{-1}$ which corresponds to the stretching of the $GH_2^{2+}$ carbonyle. In such a context, we can associate the second excitation to the experimental UV-Vis peak that presents the highest intensity after deconvolution, *i.e.* the band at 257 nm (4.82 eV).

The results discussed in this work confirm that G and EDOT interact through specific N-H···O secondary bonds. It should be noted that, although the existence of weak hydrogen bonding interactions was proposed in previous studies describing PEDOT:DNA complexes, no direct experimental evidence about their existence was obtained.[16,18-20] Thus, the fast formation of PEDOT:DNA adducts was governed by electrostatic attraction between the positively charged polymer molecules (*i.e.* +0.5 per repeating unit was measured for oxidized PEDOT) and the negatively charged phosphate groups of the DNA.[25] However, the presence of weak interactions with specific nucleotide sequences was postulated to explanation both

the protection imparted by the PEDOT to the DNA digestion in presence of selected restriction enzymes and the formation of stable complexes when the charge of PEDOT was electrochemically reduced from +0.5 to +0.1 per repeating unit.[16,18,19] In this work, strong electrostatic interactions are not possible because of the lack of both negatively charged phosphate groups and oxidized EDOT units. DFT calculations show that the building blocks studied in this work form complexes stabilized through specific N-H···O interactions. The agreement between the experimental and calculated absorption spectra proves the importance of the latter interactions in complexes formed by PEDOT and plasmid DNA.

### 4.3.4 – Conclusions

This works examines the specific interactions in complexes formed by between $GH_2^{2+}$ and EDOT, which should be considered as building blocks of plasmid DNA and PEDOT, respectively, using UV-Vis spectroscopy and quantum mechanical calculations. In order to prepare EDOT:$GH_2^{2+}$ mixtures with mass ratios 1:1, 1:2, 2:1 and 1:4, an acid pH was required, which provoked the protonation of G. In spite of this, EDOT:$GH_2^{2+}$ should be considered as reliable model compounds since the co-existence of negatively charged phosphate groups in DNA and the positive charges of the oxidized polymer is avoided.

DFT calculations indicate that EDOT:$GH_2^{2+}$ complexes are stabilized by N-H···O interactions, involving an EDOT oxygen and the –NH and $–NH_2$ moieties of $GH_2^{2+}$. Furthermore, TDDTF calculations have allowed us to reproduce the absorption spectra (both energy gaps and relative oscillator strength magnitudes) of EDOT and $GH_2^{2+}$ but also of the complex. In summary, results provide evidence about the existence of specific N-H···O interaction in the systems under study, allowing us to confirm our previous hypothesis and to explain previous experimental observations.

### 4.3.5 – References

[1] J. W. Lee, F. Serna, J. Nickels, C. E. Schmidt, *Biomacromolecules* 7 (2006) 1692.

[2] L. J. del Valle, F. Estrany, E. Armelin, R. Oliver, C. Alemán, *Macromol. Biosci.* 8 (2008) 1144.

[3] A. Azioune, M. M. Chehimi, B. Miksa, T. Basinska, S. Slomkowski, *Langmuir* 18 (2002) 1150.

[4] A. B. Sanghvi, K. P. H. Miller, A. M. Belcher, C. E. Schmidt, *Nat. Mat.* 4 (2005) 496.

[5] H. Peng, L. Zhang, J. Spires, C. Soeller, J. Travas-Sejdic, *Polymer* 48 (2007) 3413.

[6] Y. Fan, X. T. Chen, A. D. Trigg, C. H. Tung, J. M. Kong, Z. Q. Gao, *J. Am. Chem. Soc.* 129 (2007) 5437.

[7] A. Dawn, A. K. Nandi, *Macromolecules* 38 (2005) 10067.

[8] Q. H. Xu, B. S. Gaylord, S. Wang, G. C. Bazan, D. Moses, A. J. Heeger, *Proc. Natl. Acad. Sci. U.S.A.* 101 (2004) 11634.

[9] Q. H. Xu, S. Wang, D. Korystov, A. Mikhailovsky, G. C. Bazan, D. Moses, A. J. Heeger, *Proc. Natl. Acad. Sci. U.S.A.* 102 (2005) 530.

[10] B. S. Gaylord, A. J. Heeger, G. C. Bazan, *J. Am. Chem. Soc.* 125 (2003) 896.

[11] S. Wang, B. Liu, B. S. Gaylord, G. C. Bazan, *Adv. Funct. Mater.* 13 (2003) 463.

[12] F. Xia, Z. Xiaolei, R. Yang, Y. Xiao, D. Kang, A. Vallée-Bélise, X. Gong, A. J. Heeger, K. V. Plaxco, *J. Am. Chem. Soc.* 132 (2010) 1252.

[13] Y. Kim, J. E. Whitten, T. M. Swager, *J. Am. Chem. Soc.* 127 (2005) 12122.

[14] P. Pfeiffer, E. Armelin, F. Estrany, L. J. del Valle, L. Y. Cho, C. Alemán, *J. Polym. Res.* 15 (2008) 225.

[15] D. Zanuy, C. Alemán, *J. Phys. Chem. B* 112 (2008) 3222.

[16] C. Ocampo, E. Armelin, F. Estrany, L. J. del Valle, R. Oliver, F. Sepulcre, C. Alemán, *Macromol. Mater. Eng.* 292 (2007) 85.

[17] B. Teixeira-Dias, L. J. del Valle, F. Estrany, E. Armelin, R. Oliver, C. Alemán, *Eur. Polym. J.* 44 (2008) 3700.

[18] C. Alemán, B. Teixeira-Dias, D. Zanuy, F. Estrany, E. Armelin, L. J. del Valle, *Polymer* 50 (2009) 1965.

[19] B. Teixeira-Dias, D. Zanuy, L. J. del Valle, F. Estrany, E. Armelin, C. Alemán, *Macromol. Chem. Phys.* 211 (2010) 1117.

[20] J. Preat, D. Zanuy, E. A. Perpète, C. Alemán, *Biomacromolecules* 12 (2011) 1298.

[21] R. Kircheis, T. Blessing, S. Brunner, L. Wightman, E. Wagner, *J. Controlled Release* 7 (2001) 165.

[22] M. A. Wolfert, P. R. Dash, O. Navarova, D. Oupicky, L. W. Seymour, S. Smart, J. Strohalm, K. M. A. Ulbrich, *Bioconjugate Chem.* 10 (1999) 993.

[23] G. Heywang, F. Jonas, *Adv. Mater.* 4 (1992) 116.

[24] M. Dietrich, J. Heinze, G. Heywang, F. Jonas, *J. Electroanal. Chem.* 369 (1994) 87.

[25] C. Ocampo, R. Oliver, E. Armelin, C. Alemán, F. Estrany, *J. Polym. Res.* 13 (2006) 193.

[26] E. Tamburri, S. Orlanducci, F. Toschi, M. L. Terranova, D. Passeri, *Synth. Met.* 159 (2009) 406.

[27] L. J. del Valle, D. Aradilla, R. Oliver, F. Sepulcre, A. Gamez, E. Armelin, C. Alemán, F. Estrany, *Eur. Polym. J.* 43 (2007) 2342.

[28] M. J. Frisch, G. W. Trucks, H. B. Schlegel, G. E. Scuseria, M. A. Robb, J. R. Cheeseman, G. Scalmani, V. Barone, B. Mennucci, G. A. Petersson, H. Nakatsuji, M. Caricato, X. Li, H. P. Hratchian, A. F. Izmaylov, J. Bloino, G. Zheng, J. L. Sonnenberg, M. Hada, M. Ehara, K. Toyota, R. Fukuda, J. Hasegawa, M. Ishida, T. Nakajima, Y. Honda, O. Kitao, H. Nakai, T. Vreven, J. A. Montgomery, Jr., J. E. Peralta, F. Ogliaro, M. Bearpark, J. J. Heyd, E. Brothers, K. N. Kudin, V. N. Staroverov, R. Kobayashi, J. Normand, K. Raghavachari, A. Rendell, J. C. Burant, S. S. Iyengar, J. Tomasi, M. Cossi, N. Rega, J. M. Millam, M. Klene, J. E. Knox, J. B. Cross, V. Bakken, C. Adamo, J. Jaramillo, R. Gomperts, R. E. Stratmann, O. Yazyev, A. J. Austin, R. Cammi, C. Pomelli, J. W. Ochterski, R. L. Martin, K. Morokuma, V. G. Zakrzewski, G. A. Voth, P. Salvador, J. J. Dannenberg, S. Dapprich, A. D. Daniels, Ö. Farkas, J. B. Foresman, J. V. Ortiz, J. Cioslowski, and D. J. Fox, Gaussian 09, Revision A.1, Gaussian, Inc., Wallingford CT, 2009.

[29] A. D. Becke, *J. Chem. Phys.* 98 (1993) 5648.

[30] M. J. Frish, J. A. Pople, J. S. Binkley, *J. Chem. Phys.* 80 (1984) 3265.

[31] J. Preat, C. Michaux, A. Lewalle, E. A. Perpète, D. Jacquemin, *Chem. Phys. Lett.* 451 (2008) 37.

[32] J. Preat, P. F. Loos, X. Assfeld, D. Jacquemin, E. A. Perpète, *Int. J. Quantum Chem.* 107 (2007) 574.

[33] J. Preat, D. Jacquemin, V. Wathelet, J. M. André, E. A. Perpète, *Chem. Phys.* 335 (2007) 177.

[34] F. Furche, R. Ahlrichs, *J. Chem. Phys.* 117 (2002) 7433.

[35] G. Scalmani, M. J. Frisch, B. Mennucci, J. Tomasi, R. Cammi, V. Barone, *J. Chem. Phys.* 124 (2006) 094107.

[36] T. Yanai, D. Tew, N. Handy, *Chem. Phys. Lett.* 393 (2004) 51.

[37] J. Preat, *J. Phys. Chem. C* 114 (2010) 16716.

[38] D. Jacquemin, J. Preat, E. A. Perpète, *Chem. Phys. Lett.* 410 (2005) 254.

[39] J. Tomasi, B. Mennucci, R. Cammi, *Chem. Rev.* 105 (2005) 2999.

[40] M. Cossi, V. Barone, *J. Chem. Phys.* 115 (2001) 4708.

[41] http://aceorganic.pearsoncmg.com

## 4.4 – Binding of 6-mer single-stranded homo-nucleotides to poly(3,4-ethylenedioxythiophene): Specific hydrogen bonds with guanine

Complexes formed by 6-mer of single-stranded homo-nucleotides and poly(3,4-ethylenedioxythiophene), a π-conjugated polymer, have been investigated from both experimental and theoretical points of view. UV-Vis absorption and circular dichroism spectra indicate that adenine and cytosine homo-nucleotides form stable and compact adducts with the conducting polymer, which are stabilized by non-specific electrostatic interactions. In contrast, complexes involving the guanine homonucleotide are clearly dominated by specific hydrogen bonds. A hierarchical modeling approach has been used to gain some information of the complex formed by the homo-nucleotide of guanine and the polymer at both the molecular and electronic levels. Atomistic molecular dynamics simulations reveal that upon complexation the B-DNA conformation of the homo-nucleotide unfolds into a completely disordered arrangement, which allows the simultaneous formation of N-H···O and N-H···S hydrogen bonds, N-H···π, π-π stacking and electrostatic interactions with the extended polymer molecule. In spite of such variety of interactions, specific hydrogen bonds have been found to be the most abundant and decisive in this complex. The study has been complemented by ab initio and density functional theory calculations to examine the specific interactions between 1-methylguanine and 3,4-ethylene-dioxythiophene (G:EDOT). The energy decomposition analyses performed show that the stability of the different structures is governed by the attractive electrostatic interaction and reveal the reason why the N–H···O hydrogen bond is the strongest specific interaction between these two molecules.[*]

[*] - Results described in this section have been accepted for publication in *Soft Matter*. Force-field simulations were performed by D. Zanuy, while quantum mechanical calculations were carried out by J. Poater and M. Solà.

### 4.4.1 – Introduction

CPs bearing polar functional groups form specific interactions with well-defined nucleotide sequences of plasmid DNA, which have been proposed to be hydrogen bonds.[1-5] In contrast, interactions between DNA and CPs without groups able to act as hydrogen bonding donors and/or acceptors, as for example poly(3-methylthiophene) and polythiophene, are non-specific, even though stable adducts were detected.[3,5,6] These features suggest that the role played by hydrogen bonds in CP···DNA molecular recognition processes is crucial with respect to that showed by other less specific weak interactions (*e.g.* π-π stacking and hydrophobic) and by strong electrostatic interactions.

The CPs used in our investigations are usually in a highly oxidized (doped) state.[1,3-5] Spontaneous interpolymer complexation between cationic polyelectrolytes and DNA is a

well-known process, which results from cooperative electrostatic forces.[7,8] Accordingly, the unequivocal formation of electrostatic interactions between positively charged CPs and negatively charged DNA is expected to be essential for the formation and stability of the adducts. In a very recent study we investigated the influence of the doping level in the formation of specific interactions between DNA and CPs bearing polar functional groups.[9] Specifically, we considered a polymer in different oxidized states (1.0 and 0.5 positive charges per repeating unit) and in a reduced state (0.1 charges per repeating unit) states. Results allowed us to propose a mechanism for the formation of the adducts with DNA, which consists of an initial stabilization of the complexes through non-specific electrostatic interactions, followed by small structural re-arrangements that allow establishing specific hydrogen bonds between the polar groups of the CP and selected DNA bases. This process requires a structural alteration of the B-DNA double helix, which unfolds into two separated strands as was observed by circular dichroism and UV-Vis spectroscopy.[4,9] The proposed mechanism was confirmed in a very recent study, in which the binding of an oxidized CP to a single-stranded DNA featuring the Dickerson's dodecamer sequence was examined using Molecular Dynamics (MD) simulations. [10]

Among CP, poly(3,4-ethylenedioxythiophene), hereafter abbreviated PEDOT (Scheme 1), has attracted considerable interest due to a combination of properties: low oxidation potential, good optical transparency, high conductivity (up to 500 S/cm), exceptional thermal and chemical stabilities, fast doping-undoping processes, and excellent biocompatibility.[11-15] Electrophoretic and spectroscopic studies on mixtures of plasmid DNA and both oxidized and reduced PEDOT showed the formation of stable adducts, the formation of interactions with specific nucleotide sequences being evidenced through the protection imparted by this material against restriction enzymes.[3,5,9] Moreover, first principle calculations using the MP2 quantum mechanical method indicated that the binding strength between 3,4-ethylenedioxythiophene (EDOT) monomeric units in the neutral state and DNA bases grows in the following order: Adenine (A) < Cytosine (C) < Thymine (T) ≈ Guanine (G).[5] These preferences were confirmed in a very recent MD study, in which the interaction between an oxidized PEDOT chain and a single-stranded DNA molecule with sequence 5'-CGCGAATTCGCG-3' was investigated at the atomistic level.[10] Results revealed the formation of specific O···H and S···H hydrogen bonds, π-π stacking, and N-H···π interactions, in addition to the expected electrostatic interactions. In general, O···H

hydrogen bonds were found to be very abundant showing relatively large accumulated lifetimes, these specific interactions being more frequent with G than with the other bases.

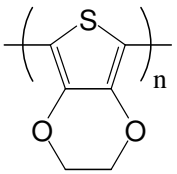


PEDOT

**Scheme 1**

In this work we focused on the interaction between PEDOT and the four DNA bases considering short single-stranded homo-nucleotides (ss-hn). The possible existence of hydrogen bonding and/or π-π stacking interactions in adducts involving such CP and different ss-hn have been studied using UV-Vis spectroscopy and circular dichroism (CD). Specifically, the 6-mer ss-hn of A, T, C and G, hereafter denoted ss-dA6, ss-dT6, ss-dC6 and ss-dG6, respectively, have been used for the present study. In addition to their important role in biology (*e.g.* microRNA and understanding single-stranded DNA-binding proteins important in DNA replication) and technology (e.g. biodetection and development of new materials) short ss-hn should be considered as important models to explain and improve molecular recognition of DNA.[16-19] Experimental measurements have allowed us to demonstrate the presence of specific hydrogen bonds in the complexes formed by PEDOT and ss-dG6. Furthermore, a top-down hierarchical modeling approach has been used to provide a comprehensive picture of the experimental observations obtained for the latter complexes. Thus, in order to provide a description of both the molecular topology and the dynamical characteristics of the interactions in ss-dG6:PEDOT, atomistic MD simulations have been carried out. Finally, quantum mechanical calculations on small model complexes formed by a guanine base and a single EDOT unit have been used to rationalize at the electronic level the differences among all the possible interaction patterns, which have been generated by combining the interaction sites of the two molecules.

### 4.4.2 – Methods

*Synthesis of the conducting polymer.* EDOT monomer was purchased from Aldrich and used as received. Anhydrous $LiClO_4$, analytical reagent grade from Aldrich, was stored in an oven at 80 ºC before use in the electrochemical trials.

PEDOT was prepared by chronoamperometry (CA) under a constant potential of 1.40 V using a polymerization time of 900 s. Anodic electropolymerization was performed on a VersaStat II potenciostat-galvanostat using a three-electrode compartment cell under nitrogen atmosphere at 25 ˚C. The anodic compartment was filled with 40 mL of a 10 mM monomer solution in acetonitrile containing 0.1 M $LiClO_4$ as supporting electrolyte, while the cathodic compartment contained 10 mL of the same electrolyte solution. Steel AISI 316 sheets of 1 $cm^2$ area were employed as working and counter electrodes. The reference electrode was an Ag|AgCl electrode containing a KCl saturated aqueous solution.

Ultrafine particles of polymer were used to interact with ss-hn. These were obtained by applying ultrasounds to a polymer solution (0.5 μg polymer/μL; milliQ water), which was prepared by considering the polymer samples grinded with a mortar. The dimensions of the resulting particles were analyzed using scanning electron microscopy (SEM) with a JSM-6400 JEOL microscope.

*Formation of DNA:PEDOT complexes.* dA6, dT6, dC6 and dG6 were purchased from Sigma, re-dissolved in milliQ water to 100 uM, and diluted 10 times before use. Complexes with different mass ratios (1:0, 1:1 and 1:5) were prepared by mixing 166.7 μL of dA6 (0.018 μg/μL), dT6 (0.017 μg/μL), dC6 (0.017 μg/μL) or dG6 (0.019 μg/μL) aqueous solutions and a volume *V* of a polymer solution (0.50 μg/μL), were *V* was 6.0, 5.6, 5.9 or 6.3 μL, respectively, for the 1:1 complexes and 29.9, 27.8, 29.3 or 31.7 μL for the 1:5 ones. Final volumes were raised to 500 μL with sterile milliQ water.

*Nature of intermolecular interactions in DNA:PEDOT complexes.* Formaldehyde (FA) and ethylene glycol (EG), which promote hydrogen bonding and stacking interactions, respectively, were used to determine the chemical nature of the weak intermolecular interactions in dG6:PEDOT complexes.[20] For this purpose, dG6:FA:PEDOT and dG6:EG:PEDOT complexes were prepared in aqueous solution by mixing 166.7 μL of dG6

(0.019 μg/μL, respectively), 5-15 μL (1%-3% v/v) of FA or EG, and the volume of polymer solution (0.5.00 μg/μL) necessary to reach the 1:1, 1:2, 1:3, 1:4 and 1:5 dG6:PEDOT mass ratio (6.3, 12.7, 19.0, 25.4 and 31.7 μL, respectively). Final volumes were raised to 500 μL with sterile milliQ water. Initially, FA and EG solutions were incubated with dG6 for 30 min, PEDOT solutions being added after such time. Then, the three-component solutions were incubated overnight at 37 ˚C. Finally, samples were centrifuged for 10 min and the supernatants were analysed by UV-Vis spectroscopy.

*Spectroscopic studies.* An UV-3600 (Shimadzu) UV-Vis/NIR spectrophotometer controlled by the UVProbe V2.31 software was used to record UV-Vis spectra at room temperature, in the 220-350 nm range, with a bandwidth of 2 mm, a scan speed of 600 nm/min. Light scattering effects were avoided by correcting the maximum absorbance of dA6, dC6, dG6 and dT6 at 262 ($A_{262}$), 275 ($A_{275}$), 250 ($A_{250}$) and 265 nm ($A_{265}$), respectively, with respect to the absorbance at 350 nm ($A_{350}$).

CD measurements were carried out in a Jasco J-810 spectropolarimeter at 22 ˚C using a quartz cuvette. The CD data were recorded with standard sensitivity (100 mdeg), in the 170-400 nm range, with bandwidth of 2 mm, response time of 0.5 s and scanning speed of 200 nm/min. The reported spectra correspond to the average of five scans, the raw spectra being smoothed by applying the Savitsky-Golay algorithm. For each sample, the CD spectrum of the polymer was subtracted from that of the homo-oligonucleotide:PEDOT complex, and compared with the CD spectrum of the corresponding ss-hn.

*Molecular Dynamics simulations.* MD simulations were performed to propose an atomistic model of the interaction between PEDOT and dG6. PEDOT was represented by an oligomer of 12 repeating units in the oxidized state, a net positive charge being located at every two repeating units. The number of positive charges supported by each monomeric unit of PEDOT produced under identical experimental conditions that those used in this work was found to be +0.549.[13] It should be noted that this oxidation degree, which was determined by standard ion chromatography, is accurately reproduced by the model used in this work for PEDOT *i.e.* $[(EDOT^{0.539+})_n(ClO_4^-)_{0.539n}]_{solid} \approx [(EDOT_2)^+Cl^-]_n$ where $ClO_4^-$ refers to the counterions used in the experiments. Recent studies based on PEDOT samples with oxidation degrees ranging from +0.14 to +1.05 positive charges per repeating units, which

were obtained by modifying (reducing and oxidizing, respectively) the polymer after electrodeposition, indicated that the interaction with DNA is affected by the doping level.[9] However, in this work we only considered the chemical characteristics of PEDOT as frequently prepared (*i.e.* the conditions used in reference 13). On the other hand, the 5'-GGGGGG-3' sequence, where both 5' and 3' terminal positions refer to hydroxyl groups, was used to represent dG6.

The PEDOT and dG6 molecules were initially placed at 12 Å of distance, being allowed to evolve freely during the equilibration period (see below). Both molecules together were placed in the center of a tetragonal simulation box with dimensions $85.0 \times 85.0 \times 125.0$ Å$^3$, full of previously equilibrated (1 atm and 298 K) water molecules. The box dimensions were chosen to avoid biased results that would result of the violation of periodic boundary conditions. The solvent consists of 28342 water molecules, which were represented using the TIP3 model.[21] In order to reach both the electric neutrality and the physiological strength, forty six positively charged sodium atoms and forty seven negative charged chloride atoms were added to the simulation box.

The potential energy of the simulated system was computed using Amber force field.[22] All bonding and non bonding parameters were extracted from Amber libraries except for those describing PEDOT, that were previously reported.[10,22] MD simulations were performed using the NAMD program.[23] Atom pair distance cut-offs were applied at 14.0 Å to compute the van der Waals interactions. In order to avoid discontinuities in the Lennard-Jones potential, a switch function was applied to allow a continuum decay of the energy when the atom pair distances are larger than 12.0 Å. For electrostatic interactions we computed the non-truncated electrostatic potential throughout Ewald Summations.[24] The real space term was determined by the van der Waals cut off (14 Å), while the reciprocal term was estimated by interpolation of the effective charge into a charge mesh with a grid thickness of 5 points per volume unit, *i.e.* Particle-Mesh Ewald (PME) method.[24] Both temperature and pressure were controlled by the weak coupling method, the Berendsen thermobarostat, using a time constant for heat bath coupling and a pressure relaxation time of 1 ps. Bond lengths were constrained using the SHAKE algorithm with a numerical integration step of 1 fs. Periodic boundary conditions were applied using the nearest image convention, and the nonbonded pair list was updated every 1000 steps (1 ps).[25,26]

Before starting the MD run series, $5 \cdot 10^3$ steps of energy minimization were performed to relax conformational and structural tensions. Then the system was heated and equilibrated by a series of consecutive MD runs. Thus, 0.1 ns of NVT (constant volume and temperature) MD at 500 K were used to homogeneously distribute the solvent and ion in the box, while keeping the dG6 and PEDOT affixed. Next, thermal equilibration for 0.2 ns in the constant NVT ensemble at 298 K, and a density relaxation for 0.4 ns in the constant NPT (constant pressure and temperature) ensemble at 298 K were performed. The last snapshot of the NPT MD was used as the starting point for the production series. Coordinates were saved every 1 ps for further analysis for simulation length of 20 ns.

*Quantum mechanical calculations.* In a previous work by some of us, seven minimum energy complexes G:EDOT were obtained through geometry optimization at the MP2/6-31G(d) level of theory.[5] In the present work, energy decomposition analyses (EDA) have been performed on these MP2/6-31G(d) optimized geometries by means of the Amsterdam Density Functional package (ADF).[27-42] The EDA have been performed with the TZ2P basis set of Slater type orbitals (STOs) of triple-$\zeta$ quality containing with two sets of polarization functions.[40] The core shells of carbon, nitrogen, oxygen and sulfur were treated by the frozen-core approximation.[33] Energies were calculated with the generalized gradient approximation (GGA) with the PBE-D functional, which includes the dispersion-correction as developed by Grimme for a correct treatment of the stacking interactions.[43-46]

In the EDA analysis, the total binding energy (ΔE) corresponds to the formation of the complex G:EDOT, and through EDA it is decomposed into two terms, the preparation and the interaction energies: $\Delta E=\Delta E_{prep}+\Delta E_{int}$. The preparation energy ($\Delta E_{prep}$) is the amount of energy required to deform G and EDOT from their equilibrium structure to the geometry that they acquire in the complex; whereas the interaction energy ($\Delta E_{int}$) corresponds to the actual energy change when these geometrically deformed G and EDOT are combined to form the G:EDOT complex. $\Delta E_{int}$ is analyzed in the framework of the Kohn-Sham molecular orbital model using a quantitative decomposition of the bond into electrostatic interaction, Pauli repulsion, orbital interactions and dispersion energy terms represented as: $\Delta E_{int}=\Delta E_{Pauli}+\Delta V_{elstat}+\Delta E_{oi}+\Delta E_{disp}$.[27-30]

### 4.4.3 – Results and Discussion

*Experimental measures.* Figure 1 (curve 1) shows the absorption spectra of the four ss-hn. The maximum of absorbance appears at 253, 266, 257 and 274 nm for dG6, dT6, dA6 and dC6, respectively. In addition, the spectrum of dG6 shows a characteristic shoulder around 285 nm. Figure 1 (curve 2) also includes the spectra of ss-hn:PEDOT mixtures considering 1:1 and 1:5 mass ratios. The interaction between the CP and the four ss-hn is evidenced by a reduction in the absorbance reflecting a hypochromic shift (*i.e.* the exposition of the nitrogen bases decreases). In many cases such reduction is moderate, as for example in all the 1:1 mixtures, which may be due to the participation of weak specific interactions (*i.e.* hydrogen bonds and/or π-π stacking) in the formation of ss-hn:PEDOT adducts. However, in some other cases, as for example in dA6:PEDOT with 1:5 mass ratios, the absorbance vanishes reflecting that the formation of compact adducts dominated strong non-specific interactions (*e.g.* electrostatic) in which the nitrogen bases are completely screened by the CP.

In order to determine the existence of weak specific interactions in complexes that undergone a moderate reduction in the absorbance, mixtures were submitted to a thermal denaturalization process (*i.e.* samples were heated at 94 ˚C for 15 min producing exposition of all the nitrogen bases). Figure 1 (curve 3) shows the UV-Vis spectra recorded immediately after such thermal treatment. The annihilation of the absorbance displayed by denaturalized dC6:PEDOT (both 1:1 and 1:5 mass ratios) and dA6:PEDOT (1:5 mass ratio) evidence that complexes involving such ss-hn are dominated by strong non-specific interactions. In contrast, the role played by weak specific interactions was found to be relevant in dT6:PEDOT and, especially, dG6:PEDOT complexes since the absorbance is similar before and after the denaturalization process. It is worth noting that the absorbance of dG6 is higher after thermal denaturalization than before (1:5 mass ratios), which is fully consistent with the formation of specific interactions. These spectroscopic observations are in agreement with previously reported quantum mechanical calculations on model complexes formed by EDOT and DNA nitrogen bases, which allowed to predict the stabilizing effect of specific interactions involving G and T with respect to those with A and C.[5]

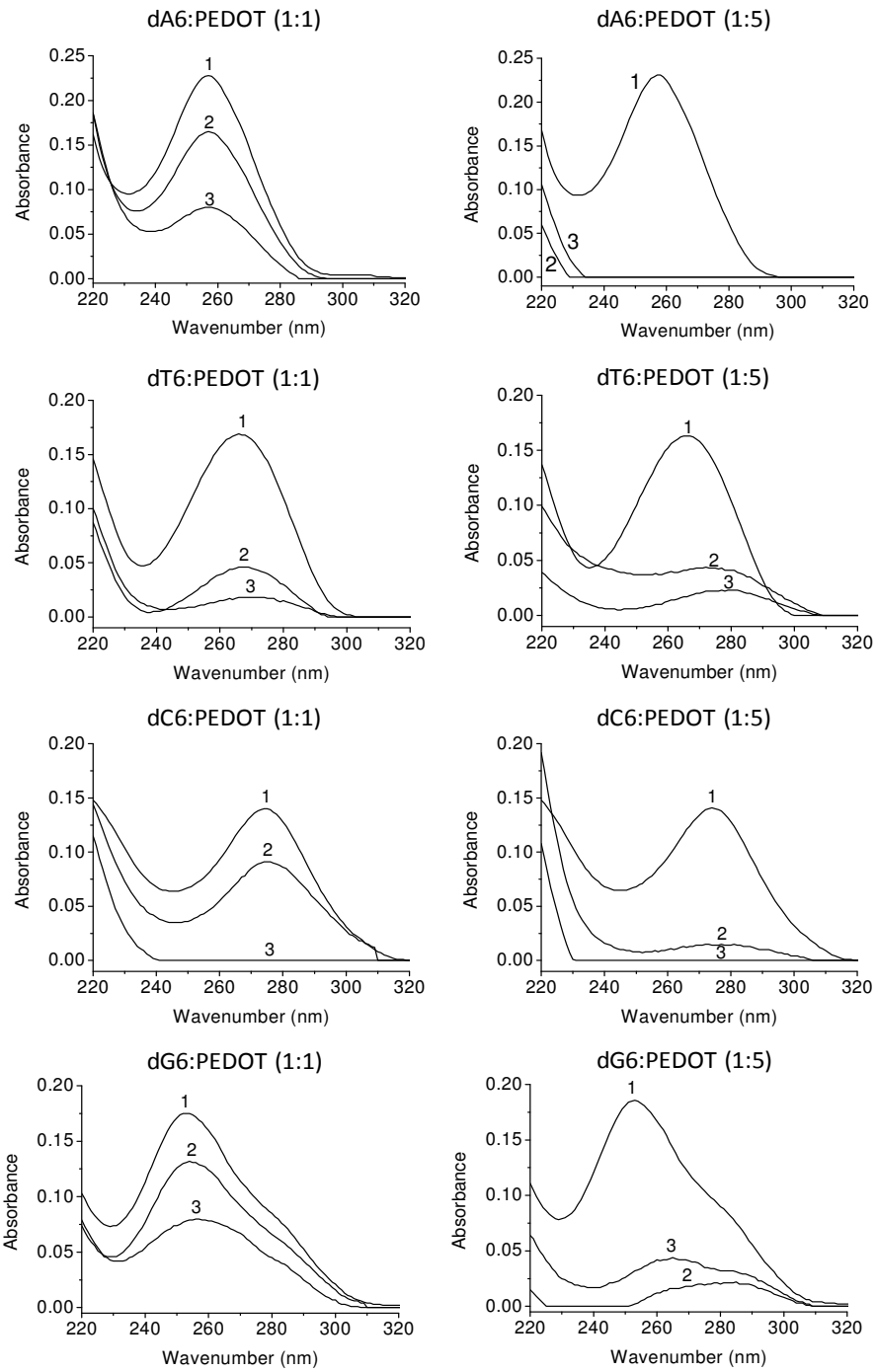


**Figure 1 –** UV-Vis spectra of ss-hn in dilute solution (curve 1), mixtures with PEDOT considering 1:1 and 1:5 mass ratios (curve 2) and after thermal denaturalization (heating at 94 ˚C for 15 min) of the mixtures with PEDOT considering 1:1 and 1:5 mass ratios (curve 3).

Time resolved UV-Vis spectroscopy has been used to obtain kinetic information about the interaction of the ss-hn and PEDOT. Figure 2 represents the evolution of $1-\left(\frac{A_0-A}{A_0}\right)$ against the time (*t*), where $A_0$ corresponds to the absorbance of the ss-hn in solution (1:0 ss-hn:PEDOT ratio) at the initial time (*t*= 0 min) and *A* is the absorbance of nitrogen bases in ss-hn:PEDOT mixtures measured at different times (cycles).

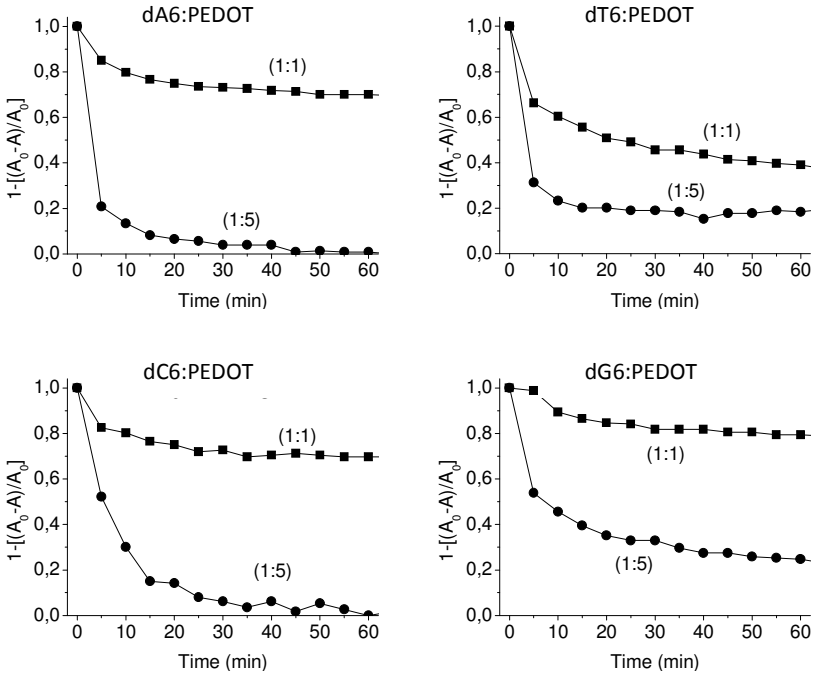


**Figure 2 –** Temporal evolution of dA6:PEDOT, dT6:PEDOT, dC6:PEDOT and dG6:PEDOT mixtures with 1:1 and 1:5 mass ratios followed by UV–Vis spectroscopy (see text). Spectra were recorded during 12 cycles, two consecutive cycles being separated by a 5 min interval.

As it can be seen, the absorbance decay follows an exponential behaviour in all cases, which have been used to derive the velocity of the interaction (Table 1) by fitting these data to the following equation:

$$y = C \cdot e^{-x \cdot k} + y_o \qquad (1)$$

where *y* and *x* correspond to $1-\left(\frac{A_0-A}{A_0}\right)$ and the time, respectively, *k* is the constant of velocity, and $y_0$ is the maximum decay.

**Table 1 –** Kinetic parameters for the hypochromic effect observed in ss-hn:PEDOT mixtures (see Eqn 1): *k*, $y_0$ and $R^2$ refer to the constant of velocity, the maximum decay (value ± standard deviation) and correlation coefficient.

| Mixture | k ($min^{-1}$) | $y_0$ | $R^2$ |
|---|---|---|---|
| dA6:PEDOT (1:1) | 0.107 | 0.030 ± 0.008 | 0.9844 |
| dA6:PEDOT (1:5) | 0.394 | 0.785 ± 0.007 | 0.9613 |
| dC6:PEDOT (1:1) | 0.112 | 0.701 ± 0.005 | 0.9654 |
| dC6:PEDOT (1:5) | 0.126 | 0.025 ± 0.007 | 0.9929 |
| dT6:PEDOT (1:1) | 0.095 | 0.402 ± 0.013 | 0.9504 |
| dT6:PEDOT (1:5) | 0.363 | 0.189 ± 0.004 | 0.9950 |
| dG6:PEDOT (1:1) | 0.059 | 0.785 ± 0.007 | 0.9613 |
| dG6:PEDOT (1:5) | 0.136 | 0.266 ± 0.013 | 0.9562 |

The regression coefficients indicate an excellent correlation in all cases ($R^2$ > 0.95). Faster interactions occur for dA6 and dC6, which is consistent with the formation of aggregates stabilized by non-specific electrostatic interactions between the CP and the phosphate scaffold, while the slowest association process corresponds to dG6. The latter is also evidenced by the values of $y_0$, which are higher for dG6:PEDOT than for dA6:PEDOT and dC6:PEDOT. Accordingly, the achievement of association geometries for the formation of specific interactions needs larger times than those required by non-specific interactions. Finally, the results obtained for dT6:PEDOT are half-way between those of dG6:PEDOT and those of the mixtures involving dA6 and dC6.

CD spectroscopic analyses were carried out to examine the structural alteration undergone by ss-hn when they bound to the CP. The CD spectra of both the ss-hn without CP (1:0 mass ratio) and the ss-hn:PEDOT mixtures (both 1:1 and 1:5 mass ratios) are compared in Figure 3. It should be emphasized that, as was mentioned in the Methods section, in order to allow detection of structural changes in ss-hn, the CD spectrum of the polymer was

subtracted from the CD spectra of the ss-hn:PEDOT complexes. Results indicate that 1:0 ss-hn presents a high degree of secondary structure, which previous studies attributed to highly stacked configurations somewhat close to the conventional B-DNA structure.[47,48] The spectra of the mixtures reflect the structural alterations produced in the ss-hn by the interactions with the CP. These alterations grow with the concentration of PEDOT. Thus, the reduction of the CD signal observed in Figure 3 for the 1:5 mixtures should be attributed to a significant loss of secondary structure. Indeed, dG6 is the only template able to retain the CD signal of its secondary structure for both 1:1 and 1:5 mixtures. The lost of secondary structure in dA6:PEDOT, dC6:PEDOT and dT6:PEDOT mixtures has been attributed to the intercalation of planar polymer molecules between neighboring bases.[49] It is worth noting that CD results are in excellent agreement with the conclusions extracted from the UV-Vis spectra (Figures 1 and 2).

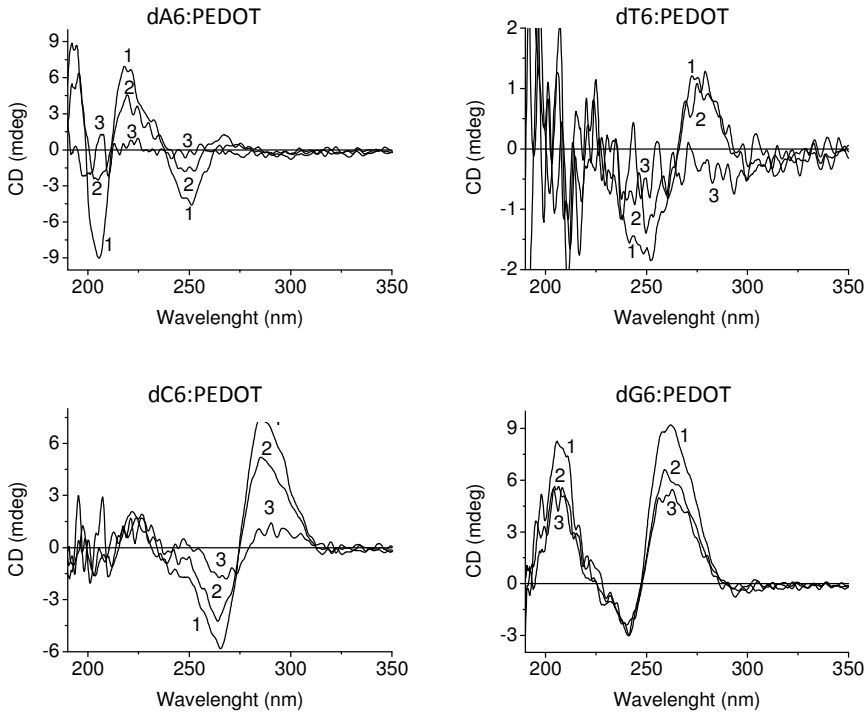


**Figure 3 –** CD spectra of ss-hn:PEDOT complexes to study structural alterations of DNA: (i) ss-hn in dilute solution (curve 1); and (ii) ss-hn:PEDOT mixtures with 1:1 and 1:5 mass ratios (curves 2 and 3, respectively). In all cases the CD spectrum of PEDOT was subtracted from the CD spectra of the mixtures.

The interaction between dG6 and PEDOT has been examined using FA and EG, which promote hydrogen bonding and stacking interactions, respectively. Figure 4a shows the curves obtained from the deconvolution of the UV-Vis spectrum of dG6, evidencing two important peaks at 250 and 275 nm. These transitions are in agreement with those reported in the literature for nucleotide bases.[50] Incubation of dG6 with EG 1% and 3% w/w did not produce any change in the absorption spectrum (data not shown) indicating the absence of new stacking interactions. Thus, in all cases transitions remained at 250 and 275 nm indicating that intramolecular stacking interactions are more stable than those that could be promoted by the EG molecules.

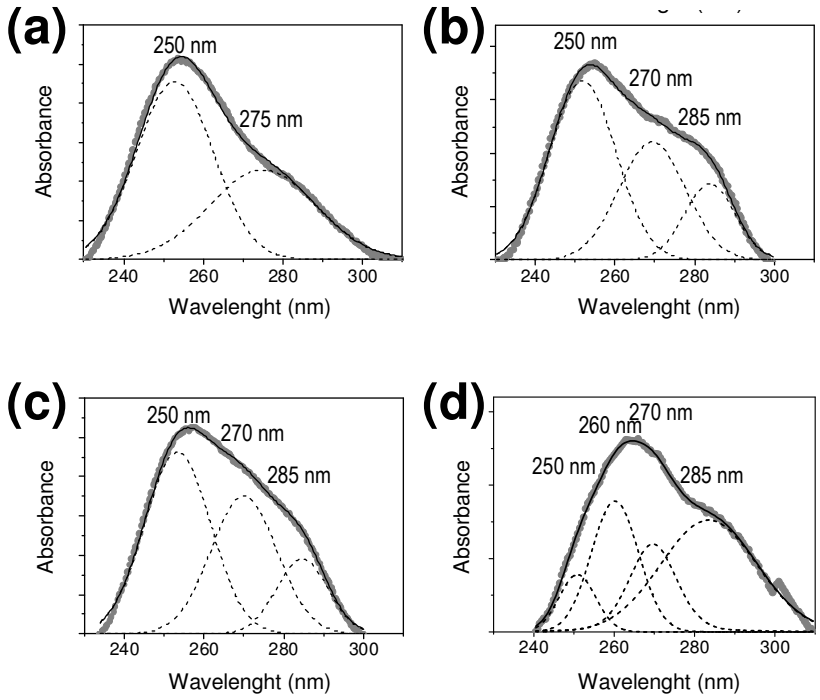


**Figure 4 –** Deconvoluted absorption spectra of: (a) dG6; (b) dG6 incubated with 1% w/w FA; c) dG6 incubated with 3% w/w FA; and d) dG6:PEDOT mixture (1:5 mass ratio) incubated with 1% w/w FA. Thick gray line refers to the recorded spectra, while thin black lines correspond to the fitted model. The components derived from the deconvolution process are indicated by dashed lines.

In contrast, the UV-Vis spectra of dG6 incubated with FA 1% and 3% w/w show a new transition at 285 nm (Figures 4b and 4c, respectively), which reflects the formation of hydrogen bonding interactions. The peak at 285 nm, which increases with the concentration of FA, should be attributed to the $n \rightarrow \pi^*$ transition of FA molecules. Furthermore, the peak found at 275 nm undergoes a blue shift at 270 nm, the shape of the spectrum changing because of the loss of the inflection point.

On the other hand, deconvolution of the spectra recorded for dG6:PEDOT mixture (1:5 mass ratio) after incubation with FA 1% w/w (Figure 4d) evidences the presence of the two peaks of dG6 at 250 and 270 nm, the peak of PEDOT at 260 nm, and the transition of FA at 285 nm. On the other hand, the spectrum of PEDOT shows a unique peak at 264 nm (data not shown), which corresponds to the $n \rightarrow \pi^*$ transition. Incubation of PEDOT with FA shows two transitions at 260 and 285 nm (data not shown), the latter being attributed to the formation of hydrogen bonding interactions between the two species. Furthermore, these interactions are also responsible of the blue shift (4 nm) detected in $n \rightarrow \pi^*$ transition of PEDOT. Overall these results demonstrate that both dG6 and PEDOT interact with FA through hydrogen bonds.

Additional experiments were performed to compare the relative ability of dG6 and PEDOT to form hydrogen bonds. More specifically, the competition between FA and PEDOT for the formation of hydrogen bonds with dG6 was examined by keeping constant the concentration of FA and increasing progressively the concentration of PEDOT to change the dG6:PEDOT mass ratio. The variation of the relative area of the different bands derived from the spectra is represented in Figure 5 considering both 1% and 3% w/w FA concentrations. The area of the transition at 285 nm increases from 44% to 50% when the dG6:PEDOT mass ratio varied from 1:1 to 1:4 (Figure 5b). A very similar scenario is depicted in Figure 5a for the 1% w/w FA concentration, even though in this case the increase of the area of the band at 285 nm is more progressive. According to these results, interactions between PEDOT and FA are the most abundant indicating that the tendency to form hydrogen bonds is higher for the CP polymer than for dG6.

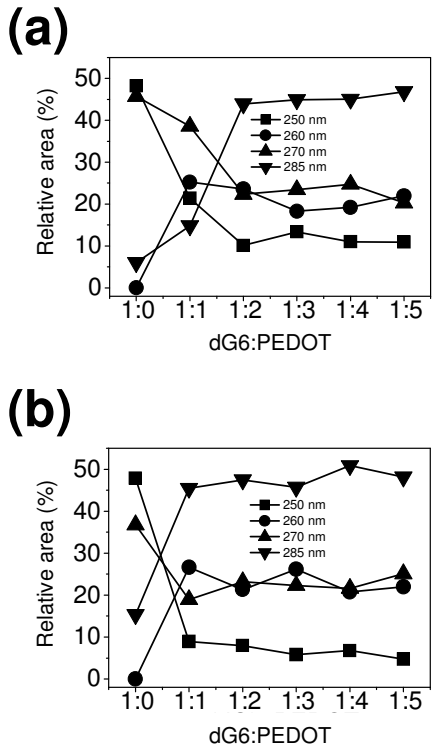


**Figure 5 –** Variation of the relative area (in %) of the absorption bands identified for the dG6:PEDOT mixture in presence of (a) 1% and (b) 3% of FA against the mass ratio.

*Modelling of dG6:PEDOT complexes.* MD simulations of a complex formed by a single stranded dG6 and a PEDOT chain represented by twelve repeating units in aqueous solution were carried out to examine the specific interactions described in the previous sub-section at the atomistic level. The temporal evolution of the intermolecular distance, which has been determined by measuring the distance between the centre of masses of the dG6 and PEDOT chains ($d_{cm\text{-}cm}$), is represented in Figure 6a. As it can be seen, $d_{cm\text{-}cm}$ remains stable during the whole simulation. This stability, which is also reflected by the low standard deviation of the average value, $\bar{d}_{cm\text{-}cm}$ = 6.25±0.56 Å, indicates that the two molecules form a very stable adduct at the first stages of the simulation. Indeed, such adduct is formed during the equilibration period (*i.e.* $d_{cm\text{-}cm}$= 12.0 Å at the beginning of the simulation) remaining practically unperturbed during the 20 ns simulation.

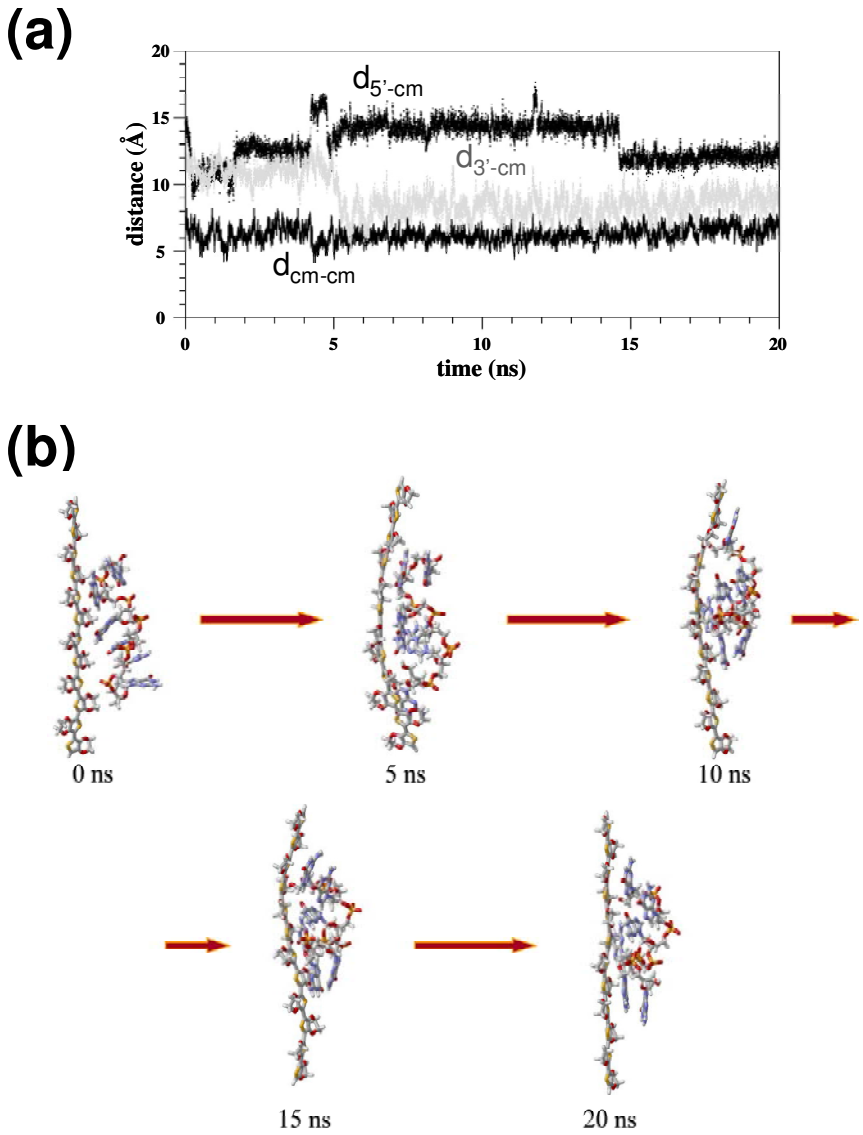


**Figure 6 –** From the MD simulation of the dG6:PEDOT complex: (a) temporal evolution of the distance between the center of masses of the two molecules ($d_{cm\text{-}cm}$, solid black line), the distance between the 3' edge of dG6 and the center of mass of PEDOT ($d_{3'\text{-}cm}$, solid light gray), and the distance between the 5' edge of dG6 and the center of mass of PEDOT ($d_{5'\text{-}cm}$, dashed black line); (b) selected snapshots of the complex.

Figure 6a includes the evolution along the 20 ns trajectory of the distance between the 3' and the 5' edges of the homo-oligonucleotide and the centre of mass of the PEDOT chain

($d_{3'\text{-cm}}$ and $d_{5'\text{-cm}}$, respectively). Both distances show fast and abrupt re-organizations during the trajectory, which occur at 5.0 ns for $d_{3'\text{-cm}}$ and at 4.1 and 14.6 ns for $d_{5'\text{-cm}}$. Thus, although the adduct remains stable through the whole simulation, the tails of the homo-oligonucleotide undergo some re-arrangements, as it is schematically represented in Figure 6b. As it can be seen, the PEDOT chain retains the initial all-*anti* conformation during the whole trajectory while the B-DNA shape of dG6 transformed into a disordered conformation at the first stages of the simulation (*i.e.* when the complex was formed during the equilibration period).

Analysis of the trajectory led to identify four different types of weak specific interactions. These consist of: (1) conventional N-H···O hydrogen bonds involving the oxygen atom of PEDOT; (2) N-H···S hydrogen bonds involving the thiophene rings of PEDOT, which were reported to be significantly weaker than the N-H···O interactions; (3) N-H···π interactions; and (4) π-π stacking interactions.[5] Additionally, non-specific electrostatic interactions involving the phosphate groups of dG6 have been also detected. The identification of the interactions was based on the following geometric criteria: (a) for hydrogen bonds, the O···H or S···H distance is shorter than 3.0 Å; (b) for N-H···π interactions, the distance between the hydrogen atom and the center of mass of the ring is shorter than 3.0 Å; (c) or π-π stacking, the distance between the centers of mass of the stacked rings is shorter than 4.0 Å; and (d) for electrostatic interactions between the EDOT units and the phosphate groups, the distance between the interacting atoms is shorter than 6.5 Å. Table 2 lists the average distance between the groups participating in such interactions for each of the six nucleotide bases. As it can be seen, only four of the six bases participate in the intermolecular interactions, the second and the sixth bases being important to adapt the conformation of the ss-hn and allow the formation of specific interactions between PEDOT and the other four bases. Inspection of the distances displayed in Table 2 clearly indicates that both specific N-H···O and N-H···S hydrogen bonds are stronger for the bases located at the central tract (*i.e.* third and fourth bases), while the first and the fifth guanines participate in the stronger π-π stacking. On the other hand, a more detailed analysis of both the two types of hydrogen bonds indicates that $N_{ring}$-H···O and $N_{ring}$-H···S intermolecular distances, where $N_{ring}$ refers to the endocyclic nitrogen atom, are in average 0.04 Å shorter than those involving the exocyclic $NH_2$ group.

**Table 2 –** Averaged intermolecular distances and the corresponding standard deviations (both in Å) for the specific and non-specific interactions detected by MD simulations between each of the six nucleotide bases of dG6 and PEDOT.

| Interaction | G1 | G2 | G3 | G4 | G5 | G6 |
|---|---|---|---|---|---|---|
| N-H···O[a] | 2.895±0.067 | - | 2.846±0.118 | 2.824±0.111 | 2.908±0.072 | - |
| N-H···S[a] | 2.919±0.066 | - | 2.811±0.147 | 2.834±0.111 | 2.920±0.065 | - |
| N-H···π[c] | 2.944±0.045 | | 2.892±0.094 | 2.860±0.092 | 2.895±0.073 | - |
| π-π[d] | 3.781±0.149 | - | 3.984±0.016 | 3.882±0.097 | 3.777±0.100 | - |
| Electrostatic[e] | 6.257±0.168 | - | - | 6.219±0.186 | 6.337±0.125 | - |

[a] Distance between the hydrogen atom of guanine and the oxygen or sulfur atom of PEDOT. [c] Distance between the hydrogen atom of guanine and the center of mass of the thiophene ring in EDOT units. [d] Distance between the centers of mass of the two interacting rings. [e] Distance between the oxygen atom of the charged phosphate group and the closest atom of PEDOT.

Table 3 lists the average residence time ($\tau$) and the maximum residence time ($\tau_{max}$) for each type of interaction.

**Table 3 –** Averaged residence time ($\tau$; in ps) and maximum residence time ($\tau_{max}$; in ps) for the specific and non-specific interactions detected by MD simulations between each of the six nucleotide bases of dG6 and PEDOT.

| Interaction | G1 | | G2 | | G3 | | G4 | | G5 | | G6 | |
|---|---|---|---|---|---|---|---|---|---|---|---|---|
| | $\tau$ | $\tau_{max}$ | $\tau$ | $\tau_{max}$ | $\tau$ | $\tau_{max}$ | $\tau$ | $\tau_{max}$ | $\tau$ | $\tau_{max}$ | $\tau$ | $\tau_{max}$ |
| N-H···O[a] | 1.0 | 3 | - | - | 1.6 | 23 | 1.5 | 18 | 1.5 | 4 | - | - |
| N-H···S[a] | 1.0 | 3 | - | - | 1.9 | 191 | 2.0 | 29 | 1.0 | 2 | - | - |
| N-H···π[c] | 1.0 | 2 | - | - | 1.2 | 11 | 1.2 | 5 | 1.3 | 3 | - | - |
| π-π[d] | 4.9 | 123 | - | - | 1.0 | 1 | 1.4 | 5 | 7.9 | 269 | - | - |
| Electrostatic[e] | 2.5 | 36 | - | - | - | - | 4.1 | 417 | 1.9 | 33 | - | - |

[a] Distance between the hydrogen atom of guanine and the oxygen or sulfur atom of PEDOT. [c] Distance between the hydrogen atom of guanine and the center of mass of the thiophene ring in EDOT units. [d] Distance between the centers of mass of the two interacting rings. [e] Shortest distance between an oxygen atom of the charged phosphate group and an atom located at the thiophene rings of PEDOT.

As it can be seen, some interactions present values of $\tau_{max}$ relatively large, as for example the electrostatic (417 ps with G4), the π-π stacking (269 ps with G5) and the N-H···S hydrogen bond (191 ps with G3). However, in spite of this, the τ values are considerably low in all cases, independently of the interaction type and nucleotide base, reflecting the dynamic behaviour of the complex. Thus, thermal fluctuations induce the fast formation and disruption of both specific and non-specific interactions along the whole trajectory. Accordingly, interactions are frequently detected but with short life times, which explains the existence of multiple interaction types between PEDOT and each of the six bases of the ss-hn (Tables 2 and 3). Comparison of the hydrogen bonds involving the $N_{ring}$-H and the amino N-H does not reveal any significant different in terms of τ and $\tau_{max}$ values (data not shown).

Figure 7 represents the accumulated life times in each of the six bases of dG6 for the four types of weak specific interactions as well as for the electrostatic ones. It should be noted that a given base may participate in more than one specific interaction simultaneously.

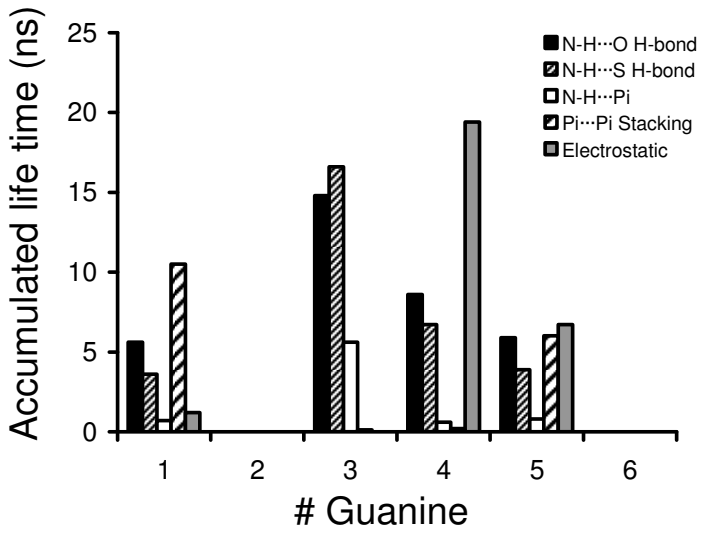


**Figure 7 –** Accumulated life time (in ns) of the different types of interactions (N-H···O and N-H···S hydrogen bonds, N-H···π, π-π stacking and electrostatic) identified in the MD simulation of the dG6:PEDOT complex. The accumulated life times are indicated for each of the six nucleotide bases of dG6. Each base may participate in more than one specific interaction simultaneously.

The two hydrogen bonds involving the third base and the π-π stacking involving the first base remain formed during more than a half of the whole trajectory, evidencing the high stability of these interactions. However, it should be remarked that the dG6:PEDOT complex is completely dominated by the hydrogen bonding interactions, the accumulated life time of the π-π stacking being relatively small. Thus, the total accumulated life time considering the six bases is 34.9, 30.8, 7.7, 16.8 and 27.3 ns for N-H···O, N-H···S, N-H···π, π-π stacking and electrostatic interactions, respectively. These results are fully consistent with the experimental evidences obtained above using EG and FA. Furthermore, it is particularly noticeable that the first and third bases interact with the PEDOT chain through weak interactions during the 20 ns trajectory, whereas the presence of weak interactions accumulates by 16.1 and 16.6 ns for the fourth and fifths bases, respectively. In contrast, the presence of electrostatic interactions is only remarkable for the fourth and fifth bases (*i.e.* 19.4 and 6.7 ns, respectively), being null or practically negligible for all the others. It should be mentioned that the accumulated life times of $N_{ring}$-H···O and $N_{ring}$-H···S was ~20% larger than those of the hydrogen bonds involves the exocyclic $NH_2$ group.

*Electronic nature of the interactions in dG6:PEDOT complexes.* In order to provide a deeper understanding of the specific interactions found in dG6:PEDOT complexes, a top-down hierarchical modelling approach has been applied. Specifically, quantum mechanical calculations have been performed on model systems formed by guanine and a single 3,4-ethylenedioxythiophene unit (G:EDOT), the different possible interaction patterns being considered. The resulting binding energies have been analyzed to determine the influence of the different contributions at the electronic level. Results allow to complete the molecular model described in the previous section for dG6:PEDOT complexes through an electronic description of the individual interactions.

As said above, seven minimum energy complexes G:EDOT were previously obtained through geometry optimization at the MP2/6-31G(d) level of theory (labeled as Im-G – VIIm-G in Figure 9 of reference 5). All systems, except VIIm-G, present an N-H···O interaction; in addition, IIm-G has an N-H···π, Vm-G a C-H···O, and IVm-G and VImG a CH···N interactions; whereas VIIm-G only presents an N-H···π interaction. Unfortunately, the electronic study of the N-H···S hydrogen bond has not been possible in the current work because MP2 geometry optimizations in the gas-phase of the G:EDOT model complex did not lead to any structure

stabilized by such specific interaction. Table 4 encloses the different terms of the EDA carried out on these systems at the PBE-D/TZ2P//MP2/6-31G(d) level. First, it is noticeable the good correlation of the binding energies between the MP2 (previous work) and the present PBE-D values.[5] PBE-D binding energies are always somewhat bigger than the MP2/6-31G(d) ones, although the differences are never larger than 2.5 kcal/mol. The ordering of the interactions given by the two methodologies is the same except for the VmG-E that is considered slightly more stable than the IImG-E and IVmG-E at the MP2/6-31G(d) level.

**Table 4 –** Energy decomposition analysis in kcal/mol at the PBE-D/TZ2P//MP2/6-31G(d) level. Relative energies with respect to ImG-E in parenthesis. See Figure 9 of reference 5 for nomenclature.

| | $\Delta E_{Pauli}$ | $\Delta V_{elstat}$ | $\Delta E_{oi}$ | $\Delta E_{disp}$ | $\Delta E_{int}$ | $\Delta E_{prep}$ | $\Delta E$ | $\Delta E_{MP2}$[a] |
|---|---|---|---|---|---|---|---|---|
| ImG-E | 14.92 | -14.53 | -8.58 | -4.00 | -12.19 | 0.67 | -11.52 *(0.00)* | -9.8 |
| IImG-E | 13.00 | -8.95 | -8.08 | -6.06 | -10.10 | 0.17 | -9.93 *(1.59)* | -7.4 |
| IIImG-E | 14.51 | -13.40 | -8.05 | -4.30 | -11.24 | 0.40 | -10.84 *(0.68)* | -8.6 |
| IVmG-E | 13.95 | -11.42 | -5.89 | -6.05 | -9.41 | 0.10 | -9.30 *(2.22)* | -7.0 |
| VmG-E | 11.76 | -10.82 | -7.15 | -3.33 | -9.54 | 0.65 | -8.89 *(2.63)* | -7.5 |
| VImG-E | 9.46 | -9.01 | -5.05 | -3.10 | -7.70 | 0.03 | -7.67 *(3.85)* | -5.9 |
| VIImG-E | 8.43 | -7.38 | -3.75 | -3.50 | -6.20 | -0.07 | -6.27 *(5.25)* | -4.4 |

[a] From ref. 5.

Next, we go into the discussion of the different terms of the EDA in order to justify the differences, always taking compound ImG-E as reference because it is the most stable. First, we observe how the preparation energies have only a minor influence; they are always less than 1 kcal/mol. There is one system (VIImG-E) with negative preparation energy, and the reason is that EDA comes from single point energy calculations performed at the PBE-D/TZ2P level with the MP2/6-31G(d) optimized geometries. After, the most important attractive interactions in these complexes are the electrostatic ones that represent between 54% and 39% of the total attractive forces (electrostatic+orbital interaction+dispersion). This $\Delta V_{elstat}$ term is in general the most important in order to explain the differences among the

conformers. This is not surprising in the case of the hydrogen bonds, since it is well-known that the electrostatic interactions are the dominant ones in hydrogen bonded species.[51] The larger electrostatic contribution takes place in the species with $N_{ring}$-H···O hydrogen bonds (systems ImG-E and IIImG-E). This increase in the electrostatic contribution has to be attributed to the larger positive charge of the H attached to the N of the ring as compared to those of the $NH_2$ group. The reason for this is the relative importance of resonance form B in guanine that leads to an aromatic six-membered ring (Scheme 2). Indeed, formation of the hydrogen bond in these complexes increase the importance of resonance form B in guanine, as can be proved from the fact that the aromaticity of the free 1-methylguanine is lower than that of the ImG-E and IIImG-E complexes (the HOMA value is 0.679 for the former and 0.734 and 0.718 for the two latter while NICS results given in the SI lead to the same conclusion). Therefore these $N_{ring}$–H···O hydrogen bonds have to be considered resonance assisted hydrogen bonds (RAHB).[52,53] In general, the shorter the distance between the G and EDOT fragments (systems ImG-E and IIImG-E having RAHB), the higher the electrostatic interaction (in absolute value) and the Pauli repulsion. On the contrary, systems with planar conformation or with N-H···π interaction, which have longer G–EDOT distances present lower $\Delta V_{elstat}$ values (in absolute value) and Pauli repulsions (II, V, VI and VIImG-E). Interestingly, hydrogen bonding involving the $NH_2$ substituent of guanine (IVmG-E) is less stabilizing than the one involving an $N_{ring}$H group of the guanine ring (ImG-E or IIImG-E). The reason is the above mentioned RAHB present in the $N_{ring}$–H···O hydrogen bonds.

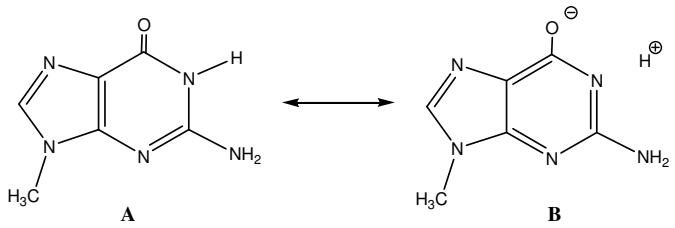


**Scheme 2 -** Representative canonical forms of 1-methylguanine.

Comparison of ImG-E (or IIImG-E) and IVmG-E conformers shows that the main difference in this case comes from both the orbital interaction and the electrostatic terms that are more stabilizing for the ImG-E (or IIImG-E) conformer. On the other hand, comparison of ImG-E (or IIImG-E) and IImG-E indicates that the main difference in this case

comes from the electrostatic term, however, in the latter an N-H···π interaction is also involved and a comparison of the two isolated hydrogen bond interactions is not possible. Finally, the dispersion term is quite constant although somewhat higher (about 2 kcal/mol) for the II-mGE and IV-mGE that have N-H···π or C-H···N interactions. As a whole, this EDA analysis shows that the most stabilizing interaction of the G:EDOT complex comes from the $N_{ring}$–H···O hydrogen bond due to formation of a RAHB.

### 4.4.4 – Conclusions

Both the existence and identification of weak specific interactions between ss-hn and PEDOT have been investigated using experimental and theoretical approaches. Both UV-Vis and CD spectra indicate that dG6 interact with this CP through weak specific interactions, which do not produce major alterations in the secondary structure of the ss-hn. In contrast, dA6:PEDOT and dC6:PEDOT adducts are made of compact structures stabilized by strong electrostatic interactions, giving place to the loss of the ss-hn secondary structure. The characteristics of dT6:PEDOT complexes are half-way between those of dG6:PEDOT and the electrostatic adducts involving dA6 or dC6. Thus, experimental results for dT6:PEDOT complexes suggest that, although electrostatic interaction play an important role in their stabilization, weak specific interactions also participate in their final organization. The velocity of the association processes, which have been determined using time resolved UV-Vis spectroscopy, are fully consistent with these features. Thus, the association of PEDOT with dA6 or dC6 is significantly faster than with dG6, whereas a half-way velocity was measured for dT6:PEDOT complexes. Incubation of dG6:PEDOT mixtures with different concentrations of EG and FA, which promote the formation of stacking and hydrogen bonds, respectively, confirmed the presence of the latter interactions in the complexes while the π-π stacking are undetectable.

On the other hand, atomistic MD simulations indicated that the dG6:PEDOT complex is formed very rapidly, which should be attributed to the electrostatic attraction of the negatively charged phosphate groups and the oxidized polymer. This produces the unfolding of the dG6 molecule, which abandons the B-DNA shape and adopts a disordered conformation, while the PEDOT chain retain the all-*anti* conformation. The complex was found to remain stable during the whole trajectory, even though small re-organizations were

detected at both the 3' and 5' edges. In addition to the electrostatic interactions, four weak specific interactions were detected: N-H···O and N-H···S hydrogen bonds, N-H···π and π-π stacking. Analyses of the strength, residence times and accumulated life times indicate that the dG6:PEDOT complex is dominated by hydrogen bonds, which are the most populated and frequent interactions. Finally, the EDA analyses show that the most stabilizing interaction in the G:EDOT complex corresponds to the $N_{ring}$–H···O hydrogen bond that is especially favored by resonance assistance.

### 4.4.5 – References

[1] P. Pfeiffer, E. Armelin, F. Estrany, L. J. del Valle, L. Y. Cho, C. Alemán, *J. Polym. Res.* 15 (2008) 225.

[2] D. Zanuy, C. Alemán, *J. Phys. Chem. B* 112 (2008) 3222.

[3] C. Ocampo, E. Armelin, F. Estrany, L. J. del Valle, R. Oliver, F. Sepulcre, C. Alemán, *Macromol. Mater. Eng.* 292 (2007) 85.

[4] B. Teixeira-Dias, L. J. del Valle, F. Estrany, E. Armelin, R. Oliver, C. Alemán, *Eur. Polym. J.* 44 (2008) 3700.

[5] Alemán, C.; Teixeira-Dias, B.; Zanuy, D.; Estrany, F.; Armelin, E.; del Valle, L. J. *Polymer* 2009, *50*, 1965.

[6] H. Peng, L. Zhang, J. Spires, C. Soeller, J. Travas-Sejdic, *Polymer* 48 (2007) 3413.

[7] R. Kircheis, T. Blessing, S. Brunner, L. Wightman, E. Wagner, *J. Controlled Release* 7 (2001) 165.

[8] M. A. Wolfert, P. R. Dash, O. Navarova, D. Oupicky, L. W. Seymour, S. Smart, J. Strohalm, K. M. A. Ulbrich, *Bioconjugate Chem.* 10 (1999) 993.

[9] B. Teixeira-Dias, D. Zanuy, L. J. del Valle, F. Estrany, E. Armelin, C. Alemán, *Macromol. Chem. Phys.* 211 (2010) 1117.

[10] J. Preat, D. Zanuy, E. A. Perpète, C. Alemán, *Biomacromolecules* 12 (2011) 1298.

[11] G. Heywang, F. Jonas, *Adv. Mater.* 4 (1992) 116.

[12] M. Dietrich, J. Heinze, G. Heywang, F. Jonas, *J. Electroanal. Chem.* 369 (1994) 87.

[13] C. Ocampo, R. Oliver, E. Armelin, C. Alemán, F. Estrany, *J. Polym. Res.* 13 (2006) 193.

[14] E. Tamburri, S. Orlanducci, F. Toschi, M. L. Terranova, D. Passeri, *Synth. Met.* 159 (2009) 406.

[15] L. J. del Valle, D. Aradilla, R. Oliver, F. Sepulcre, A. Gamez, E. Armelin, C. Alemán, F. Estrany, *Eur. Polym. J.* 43 (2007) 2342.

[16] G. Ruvkun, *Science* 294 (2001) 797.

[17] Y. T. Kim, S. Tabor, C. Bortner, J. D. Griffith, C. C. Richardson, *J. Biol. Chem.* 267 (1992) 15022.

[18] P. Kohli, C. C. Harrell, Z. Cao, R. Gasparac, W. Tan, C. R. Martin, *Science* 305 (2004**)** 984.

[19] N. C. Seeman, *Nature* 421 (2003) 427.

[20] J. D. McGhee, P. H. von Hippel, *Biochemistry* 14 (1975) 1281.

[21] W. L. Jorgensen, J. Chandrasekhar, J. D. Madura, R. W. Impey, M. L. Klein, *J. Chem. Phys.* 79 (1983) 926.

[22] W. D. Cornell, P. Cieplak, C. I. Bayly, I. R. Gould, K. M. Merz, D. M. Ferguson, D. C. Spellmeyer, T. Fox, J. W. Caldwell, P. A. Kollman, *J. Am. Chem. Soc.* 117 (1995) 5179.

[23] J. C. Phillips, R. Braun, W. Wang, J. Gumbart, E. Tajkhorshid, E. Villa, C. Chipot, R. D. Skeel, L. Kale, K. Schulten, *J. Comput. Chem.* 26 (2005) 1781.

[24] H. J. C. Berendsen, J. P. M. Postma, W. F. van Gunsteren, A. DiNola, J. R. Haak, *J. Chem. Phys.* 81 (1984) 3684.

[25] J. P. Ryckaert, G. Ciccotti, H. J. C. Berendsen, *J. Comput. Phys.* 23 (1977) 327.

[26] T. Darden, D. York, L. Pedersen, *J. Chem. Phys*. 98 (1993) 10089.

[27] K. Morokuma, *Acc. Chem. Res.* 10 (1977) 294.

[28] K. Kitaura, K. Morokuma, *Int. J. Quantum Chem.* 10 (1976) 325.

[29] T. Ziegler, A. Rauk, *Theor. Chim. Acta* 46 (1977) 1.

[30] T. Ziegler, A. Rauk, *Inorg. Chem.* 18 (1979) 1755.

[31] E. J. Baerends, J. Autschbach, A. Bérces, F. M. Bickelhaupt, C. Bo, P. M. Boerrigter, L. Cavallo, D. P. Chong, L. Deng, R. M. Dickson, D. E. Ellis, M. van Faassen, L. Fan, T. H. Fischer, C. Fonseca Guerra, S. J. A. van Gisbergen, A. W. Götz, J. A. Groeneveld, O. V. Gritsenko, M. Grüning, F. E. Harris, P. van den Hoek, C. R. Jacob, H. Jacobsen, L. Jensen, G. van Kessel, F. Kootstra, M. V. Krykunov, E. van Lenthe, D. A. McCormack, A. Michalak, J. Neugebauer, V. P. Nicu, V. P. Osinga, S. Patchkovskii, P. H. T. Philipsen, D. Post, C. C. Pye, W. Ravenek, J. I. Rodriguez, P. Ros, P. R. T. Schipper, G. Schreckenbach, J. G. Snijders, M. Solà, M. Swart, D. Swerhone, G. te Velde, P. Vernooijs, L. Versluis, L. Visscher, O. Visser, F. Wang, T. A. Wesolowski, E. M. van Wezenbeek, G. Wiesenekker, S.

K. Wolff, T. K. Woo, A. L. Yakovlev, T. Ziegler, ADF2008.01, SCM, Theoretical Chemistry, Vrije Universiteit, Amsterdam, The Netherlands, http://www.scm.com

[32] G. te Velde, F. M. Bickelhaupt, E. J. Baerends, C. Fonseca Guerra, S. J. A. van Gisbergen, J. G. Snijders, T. Ziegler, *J Comput. Chem.* 22 (2001) 931.

[33] C. Fonseca Guerra, O. Visser, J. G. Snijders, G. te Velde, E. J. Baerends, In: E. Clementi, G. Corongiu, (eds) *Methods and Techniques for Computational Chemistry*, STEF, Cagliari (1995) 305.

[34] E. J. Baerends, D. E. Ellis, P. Ros, *Chem. Phys.* 2 (1973) 41.

[35] E. J. Baerends, P. Ros, *Chem. Phys.* 8 (1975) 412.

[36] E. J. Baerends, P. Ros, *Int. J. Quantum Chem. Symp.* 12 (1978) 169.

[37] C. Fonseca Guerra, J. G. Snijders, G. te Velde, E. J. Baerends, *Theor. Chem. Acc.* 99 (1998) 391.

[38] P. M. Boerrigter, G. te Velde, E. J. Baerends, *Int. J. Quantum Chem.* 33 (1998) 87.

[39] G. te Velde, E. J. Baerends, *J. Comp. Phys.* 99 (1992) 84.

[40] J. G. Snijders, P. Vernooijs, E. J. Baerends, *At. Nucl. Data Tables* 26 (1981) 483.

[41] J. Krijn, E. J. Baerends, *Fit-Functions in the HFS-Method*; Internal Report (in Dutch), Vrije Universiteit, Amsterdam (1984).

[42] L. Versluis, T. Ziegler, *J. Chem. Phys.* 88 (1988) 322.

[43] J. P. Perdew, K. Burke, M. Ernzerhof, *Phys. Rev. Lett.* 77 (1996) 3865.

[44] J. P. Perdew, K. Burke, Y. Wang, *Phys. Rev.* B54 (1996) 16533.

[45] S. Grimme, *J. Comput. Chem.* 25 (2004) 1463.

[46] S. Grimme, *J. Comput. Chem.* 27 (2006) 1787.

[47] C. S. M. Olsthoorn, L. J. Bostelaar, J. F. M De Rooij, J. H. Van Boom, C. Altona, *Eur. J. Biochem.* 115 (1981) 309.

[48] S. Tonzani, G. C. Schatz, *J. Am. Chem. Soc.* 130 (2006) 7607.

[49] L. Mikelson, C. Carra, M. Shaw, C. Schweitzer, J. C. Scaiano, *Photochem. Photobiol. Sci.* 4 (2005) 798.

[50] M. P. Fülscher, L. Serrano-Andrés, B. O. Roos, *J. Am. Chem. Soc.* 119 (1997) 6168.

[51] J. Poater, X. Fradera, M. Solà, M. Duran, S. Simon, *Chem. Phys. Lett.* 369 (2003) 248.

[52] G. Gilli, F. Bellucci, V. Ferretti, V. Bertolasi, *J. Am. Chem. Soc.* 111 (1989) 1023.

[53] M. Palusiak, S. Simon, M. Solà, *J. Org. Chem.* 71 (2006) 5241.

## 4.5 – Specific interactions in complexes formed by polythiophene derivatives bearing polar side groups and plasmid DNA

The interaction between plasmid DNA and polythiophene derivatives bearing substituents with polar groups has been examined using electrophoresis assays, and both UV-Vis and CD spectroscopies. Results clearly indicate that such CPs form stable adducts with DNA, even although the interactions strongly depend on the chemical constitution of the polymers. Furthermore, digestion assays with *Eco*RI and *Bam*HI evidence that the polymers form specific interactions with the DNA, protecting the target nucleotide sequences of these restriction enzymes. On the other hand, UV-Vis and CD spectra show that the interactions induce a fast and very significant exposition of the nitrogen bases, which is consequence of the structural alterations induced in the circular DNA. These results have been compared with those previously reported for polypyrrole, poly(3,4-ethylendioxythiophene) and poly(3-methylthiophene). Finally, a model based on the intercalation of the conducting polymer between the two DNA strands has been proposed.*

* - Results described in this section previously appeared in *European Polymer Journal* 44 (2008) 3700.

### 4.5.1 – Introduction

The interaction of conducting electroactive polymers, such as PTh, PPy and their derivatives, with selected bioentities (*e.g.* amino acids, proteins, DNA and oligonucleotides, and living cells) is a subject of increasing interest.[1-21] The quest to interact more efficiently with biosystems, to obtain information related to system performance and to control that performance remains not only an exciting but also an essential area of research. Thus, the development of biotechnological applications based CPs greatly depends on the control of such interactions.

Within this area of research we are particularly interested in the interaction of CPs with DNA sequences, which may have great implications in numerous medical applications ranging from diagnosis to gene therapy.[8-16,21,22] The interaction of p-doped electroactive materials with DNA has been traditionally attributed to the tendency of the latter to interact with positively charged molecules. However, in recent studies we found that poly(3,4-ethylenedioxythiophene), a widely used PTh derivative hereafter abbreviated PEDOT (Scheme 1), as well as PPy are able to bound forming specific interactions with well-defined nucleotide sequences of plasmid DNA.[10,16] The formation of specific interactions suggest that polymer:DNA adducts are stabilized not only by electrostatic interactions but also by

other kind of interactions. Thus, the importance of specific hydrogen bonding interactions in these complexes is expected to be significantly greater than those that are of non-specific, *e.g.* stacking, van der Waals and charge-transfer interactions. Indeed, the N-H groups of PPy and the dioxane oxygen atoms of PEDOT are excellent donors and acceptors of hydrogen bonds, respectively. Consistently, although plasmid DNA and poly(3-methylthiophene) (P3MT), a PTh derivative without hydrogen bonding donors and acceptors, form stable adducts, specific interactions are significantly weaker in DNA:P3MT than in DNA:PEDOT. In addition, we recently used advanced theoretical calculations to demonstrate that hydrogen bonding interactions between DNA bases and PPy are significantly stronger than interactions between DNA bases and PTh derivatives without hydrogen bonding donors and acceptors.[22]

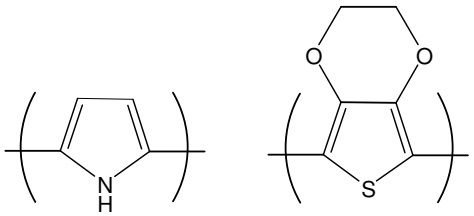


PPy PEDOT

**Scheme 1**

Attracted by this field, we recently developed two PTh derivatives bearing carboxylate groups in the 3-position of the thiophene ring (Scheme 2).[23,24] These materials, which are expected to interact specifically with DNA through the oxygen atoms of the side groups, are the poly(3-thiophen-3-yl-acrylic acid methyl ester) and the poly(2-thiophen-3-yl-malonic acid dimethyl ester), hereafter abbreviated PT3AME and PT3MDE, respectively.

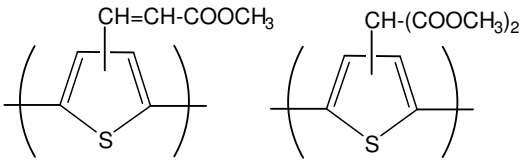


PT3AME PT3MDE

**Scheme 2**

PT3MDE presents better solubility properties than PT3AME, which should be attributed to the presence of two polar groups in the chemical repeating unit of the former polymer. Thus, the malonic ester derivative is soluble not only in polar organic solvents, as the acrylate derivative, but also in aqueous base solutions. On the other hand, PT3AME exhibits high electrical conductivity, even although this property decreases very fast with the time.

In this work we present a complete study about the interaction of PT3AME and PT3MDE with plasmid DNA using electrophoretic analyses, and UV-Vis and circular dichroism (CD) spectroscopies. The possible formation of specific interactions have been examined by adding restriction enzymes, which cut off at specific nucleotide sequences, to the DNA:polymer mixtures. Thus, DNA is protected from digestion when the interactions with the CP occur specifically at the restriction sites. Results indicate that these polymers provide different interactions with DNA, a mechanism for the formation of stable DNA:polymer adducts being finally proposed.

### 4.5.2 – Methods

*Polymer synthesis.* The synthesis of PT3AME and PT3MDE were detailed in previous works.[23,24] The synthetic procedure is briefly summarized in Scheme 3. 3-Thiophen-3-yl-acrylic acid and 2-thiophen-3-yl-malonic acid (3g) were refluxed in dry methanol (15mL) with one-two drops of concentrated sulfuric acid for 24 hours, to give 3-thiophen-3-yl-acrylic acid methyl ester (99.9 % of yield) and 2-thiophen-3-yl-malonic acid dimethyl ester (90% of yield), respectively. After purification by the evaporation of methanol and successive extraction with diethyl ether, polymerization of the protected monomers was performed by chemical oxidative coupling in dry chloroform using anhydrous ferric chloride. The oxidant:monomer molar ratio was 4:1, as was suggested in the literature.[25] After precipitation in a large excess of methanol, the resulting polymers were recovered in chloroform and successively washed with methanol to remove the residual $FeCl_3$, monomers and small oligomers. Products were obtained with a yield between 60-75% after drying under vacuum at 40 °C for 72 hours.

It should be noted that, in order to reduce the importance of the electrostatic interactions in the formation of stable DNA:PT3AME and DNA:PT3MDE complexes, the polymers produced using the procedure indicated in Scheme 3 were not subjected to a doping process with $LiClO_4$. Thus, PT3AME and PT3MDE were used as produced, *i.e.* oxidized

with $Cl^-$ acting as counter-anion. It should be noted that replacement of $Cl^-$ by $ClO_4^-$ dopant ions enhances the p-doping state of polymer chains since the charge separation is significantly promoted by the latter anion with respect to the former one.[26,27]

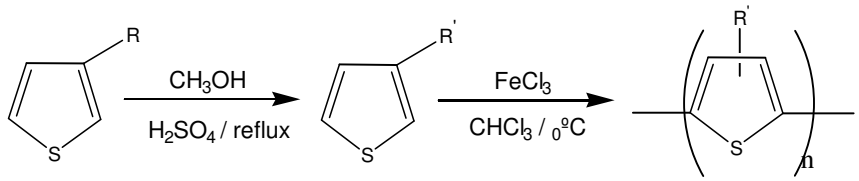


**1.** R= -CH=CH-COOH
**2.** R= -CH-(COOH)$_2$

**1.** R'= -CH=CH-COOCH$_3$
**2.** R'= -CH-(COOCH$_3$)$_2$

**1. PT3MDE**: R'= -CH=CH-COOCH$_3$
**2. PT3AME**: R'= -CH-(COOCH$_3$)$_2$

**Scheme 3**

*Polymer Characterization.* The structural characterization of PT3AME and PT3MDE was detailed in our previous works, a brief summary being provided in this section.[23,24] Specifically, the spectral properties recorded for the two materials were consistent with their structures. Analysis of the protons from 3.7 to 3.0 ppm region in the $^1$H-NMR spectra showed that the head-to-tail is the predominant linkage (~ 75%-80%) for the polymers, the remaining ones being of head-to-head type. On the other hand, the $\pi$-$\pi^*$ lowest transition energy ($\varepsilon_g$) of the two polymers was derived in different environments using UV-Vis spectroscopy. The $\varepsilon_g$ values obtained for PT3AME in acetone and DMSO were 2.54 eV and 2.48 eV, respectively, while the values determined for PT3MDE in the same solvents were 2.52 and 2.36 eV.

Unfortunately, determination of the molecular weight by GPC analyses using polystyrene standards and hexafluoro-2-propanol as solvent did not led to any conclusive result. We also tried to perform MALDI-TOFF mass spectrometry in several types of matrices (dihydrobenzoic acid, dithranol, sinapinic acid, etc) but, again, all the polymers gave variable and inaccurate results. However, inspection to the $^1$H-NMR spectra recorded after the polymerization processes indicated the presence of shoulders at the ring proton multiple region, which were attributed to the remaining α-H. This is usually associated to low molecular weight polymer chains.

The electrical conductivities of PT3AME and PT3MDE, which were determined using the standard four probe technique, were significantly high, *i.e.* 15 S/cm and 6 S/cm

respectively. However, such remarkable electrical properties decreased very fast, *i.e.* in about 24 hours.

*Formation of DNA:polymer complexes and electrophoretic assays.* Polymers were dissolved in milliQ water (0.5 µg polymer/µl) for biological assays. Due to the difficulties associated to the solubilisation of PT3MDE in neutral water, 10% of acetone was included in the final volume. In order to guarantee a homogeneous solution, PT3AME was subjected to ultra-sounds.

DNA:polymer complexes were prepared upon aqueous solutions by mixing 4 µl of plasmid pMT4 (0.5 µg/µl) with 0.00, 0.05, 0.50, 5.00 and 10.00 µl of polymer solution (5 µg/µl), which corresponded to the desired DNA:polymer ratios (1:0, 1:1, 1:10, 1:100, 1:200, respectively).[28] Total volumes were raised to 13 µl with sterile milliQ water. The mixtures were incubated for 3 h at 37 ˚C, and an aliquot (20 µl) of 6× gel loading buffer (2% (wt/vol) SDS, 10% (vol/vol) glycerol, 62.5 mM Tris-HCl, 5% (vol/vol) β-mercaptoethanol, and 0.001% (vol/vol) bromphenol blue) was added and centrifuged for 10 min. The supernatant was then analysed by electrophoresis with 1% of agarose gel containing ethidium bromide (0.5 µg/ml of gel) in 1×tris-acetate-EDTA buffer (TAE). The cleavage of pMT4 with *Eco*RI and *Bam*HI in DNA:polymer complexes was evaluated by adding 10 U of restriction enzyme in 1.56 µl of 10× enzyme buffer to the samples previously incubated. The composition of the 10× buffer for *Eco*RI and *Bam*HI was 0.5 M Tris-HCl, 1M NaCl, 100 mM $MgCl_2$ and 10 mM DTE (pH= 7.5 at 37 ˚C) and 100 mM Tris-HCl, 1M NaCl, 50 mM $MgCl_2$ and 10 mM 2-mercaptoethanol (pH= 8.0 at 37 ˚C), respectively, The digestion process was carried out at 37 ˚C for 1 h, the resulting products being analysed by electrophoresis.

*Characterization techniques.* A Nicolet Evolution 300 (Thermo Electron Co.) spectrophotometer controlled by the Vision Pro software was used to record UV-Vis spectra of DNA:PT3AME and DNA:PT3MDE complexes with ratios 1:1 and 1:200 at 22 ˚C, in the 200-1000 nm range, with a bandwidth of 2 mm and a scan speed of 600 nm/min. For each sample, 15 cycles separated by an interval of 2 min between consecutive cycles were recorded.

Circular dichroism (CD) measurements were carried out in a Jasco J-810 spectropolarimeter at 22 ˚C using a quartz cuvette. The CD data were recorded with standard sensitivity (100 mdeg), in the 170-360 nm range, with bandwidth of 2 mm,

response time of 0.5 s and scanning speed of 500 nm/min. The reported spectra correspond to the average of five scans, the raw spectra being smoothed by the Savitsky-Golay algorithm and deconvolutioned for analysis and interpretation. For each sample, the CD spectrum of the polymer was subtracted from that of the DNA:polymer complex, and compared with the CD spectrum of the plasmid DNA.

### 4.5.3 – Results and Discussion

*Electrophoretic analyses of DNA:polymer complexes.* The interaction of PT3AME and PT3MDE with plasmid DNA to form DNA:PT3AME and DNA:PT3MDE complexes was investigated using electrophoretic assays. For this purpose, polymer solutions were mixed with plasmid DNA (0.5 μg) considering different DNA:polymer ratios, *i.e.* 1:0, 1:1, 1:10, 1:100 and 1:200, followed by homogeneization and equilibration for 3h in a shaking plate at 37 ˚C. The electrophoretograms obtained for DNA:PT3AME and DNA:PT3MDE complexes at different DNA:polymer ratios are displayed in Figure 1.

Lane 1 in Figures 1a and 1b, which corresponds to the plasmid (1:0 DNA:polymer ratio), shows the typical mixture of the supercoiled form I (bottom or band at the front) and the singly nicked form II (top or band at the back). Lanes 2-5 display the interactions between DNA and polymers at increasing DNA:polymer ratios. As can be seen, both PT3AME and PT3MDE are able to interact with DNA, the formation of adducts being evidenced by significant alterations in the bands associated to the plasmid DNA (forms I and II). The formation of complexes retards the mobility of form I and enhances slightly the mobility of form II. Furthermore, the interaction between DNA and polymers produces changes in the intensity of the bands. Specifically, the intensity decreases and increases for forms I and II, respectively. Caution is required to analyze the fluorescence of DNA because the variation of this property during experiments involving formation of adducts cannot be related with the amount of interacting plasmid. However, CPs may induce conformational changes in plasmid DNA during the formation of the corresponding complexes, which could explain the variations in the mobility and intensity undergone by the two bands. Therefore, hereafter forms I' and II' will refer to forms I and II, respectively, after undergo alterations in the mobility due to the formation of adducts.

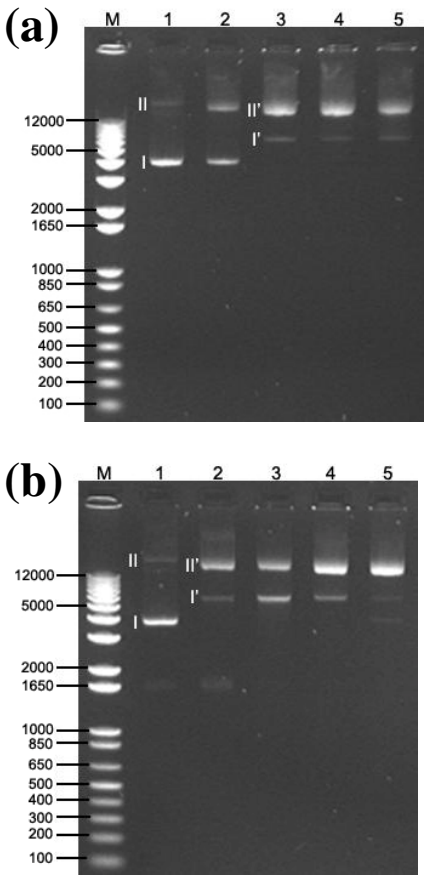


**Figure 1 –** Interaction of pMT4 plasmid DNA and increasing concentration of PT3AME (a) and PT3MDE (b) after their incubation for 3h at 37 ˚C. Lane M: molecular weight marker (1 Kb Plus DNA Ladder). Lane 1: pMT4 plasmid DNA (1:0 DNA:polymer ratio). Lanes 2-5: 1:1, 1:10, 1:100 and 1:200 DNA:polymer ratios. Labels I and II indicate form I and II of pMT4 plasmid DNA, respectively. Labels I' and II' refer to the forms I an II of plasmid DNA, respectively, that underwent alterations in the mobility after interact with the CP.

On the other hand, a detailed inspection of Figure 1 reveals that the interaction between the plasmid DNA and the CP may be different in DNA:PT3AME and DNA:PT3MDE complexes. This is because no interaction is detected for PT3AME at the 1:1 ratio, the absence of adduct being evidenced by the lack of mobility in the two bands (Figure 1a, lane 2). Furthermore, after formation of the complex, which occurs at the 1:10 DNA:PT3AME ratio (Figure 1a, lane 3), the mobility of the bands is similar in all cases, independently of the concentration of CP. In contrast, DNA:PT3MDE complexes are detected for all the ratios

examined, even although the alteration in the mobility clearly depends on the concentration of PT3MDE (Figure 1b, lanes 2-5).

In order to look for specific interactions between plasmid DNA and the CPs investigated in this work, additional assays were performed adding restriction enzymes. Specifically, the two enzymes considered in this work were *Eco*RI and *Bam*HI, the digestion period being 1 h after the formation of the DNA:polymer adducts. These restriction enzymes cut off at specific nucleotide sequences: 5'-G/AATTC-3' (*Eco*RI) and 5'-G/GATCC-3' (*Bam*HI). The pMT4 plasmid contains one and three restriction sites for *Eco*RI and *Bam*HI, respectively. The digestion with *Eco*RI converts supercoiled form I and single nicked circular form II of DNA into linear form III, while *Bam*HI produces three DNA fragments named F1, F2 and F3. The molecular weights of F1 and F2 are similar, their mobility in the agarose gel being associated to a unique band. Fragment F3 presents the lowest molecular weight, which is evidenced the fastest mobility. However, *Bam*HI produces form III when it makes only one cut in the plasmid DNA.

Figure 2 shows the gel electrophoresis results for DNA:PT3AME (Figure 2a) and DNA:PT3MDE (Figure 2b) complexes after digestion with *Eco*RI and *Bam*HI. For both complexes, lane 1 corresponds to the untreated and undigested pMT4 plasmid DNA, while lanes 2 and 7 display the plasmid DNA (1:0 DNA:polymer ratio) digested with *Eco*RI and *Bam*HI, respectively. Finally, lanes 3-6 and 8-11 correspond to increasing DNA:polymer ratios (1:1, 1:10, 1:100 and 1:200) digested with *Eco*RI and *Bam*HI restriction enzymes, respectively.

The band patterns obtained for DNA:PT3AME and DNA:PT3MDE complexes after digestion with *Eco*RI depends on the polymer concentration (Figure 2). As can be seen, digestion produced a unique band associated to linear DNA (form III) for complexes formed using 1:1 to 1:200 ratios. In general, the band intensity of form II decreases when the concentration of CP increases. This is a direct evidence that PT3AME and PT3MDE polymers protect the restriction site of *Eco*RI (5'-G/AATTC-3' sequence). Furthermore, others bands associated to supramolecular structures with high molecular weights are also observed. Specifically these bands, which are explicitly marked in Figure 2, should be attributed to complexes formed by polymers and linear DNA molecules. This is consistent with the lack of

detection of such bands when the polymers interact with circular DNA (Figure 1).

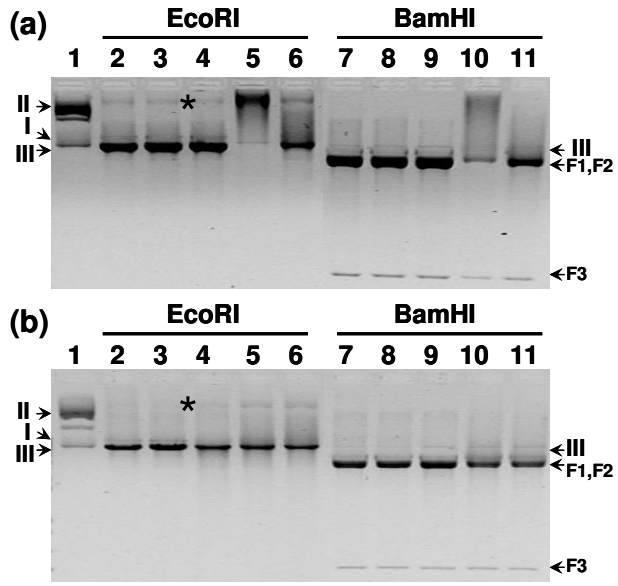


**Figure 2 –** Enzymatic digestion with *Eco*RI and *Bam*HI of DNA:PT3AME (a) and DNA:PT3MDE (b) complexes. Different DNA:polymer ratios (1:0, 1:1, 1:10, 1:100 and 1:200) were incubated for 3 h at 37 ˚C to promote the formation of complexes, followed by their enzymatic digestion for a period of 1 h at 37 ˚C. Lane 1: undigested and untreated pMT4 plasmid. Lanes 2-6 and 7-11: 1:0, 1:1, 1:10, 1:100, 1:200 DNA:polymer ratios after enzymatic digestion. Labels I, II and III correspond to the forms I, II and III of pMT4 plasmid DNA, respectively. Labels F1, F2 and F3 refer to the three produced fragments by enzymatic digestion with *Bam*HI restriction enzyme. The asterisks indicate the bands associated to supramolecular structures with high molecular weight (see text).

On the other hand, enzymatic digestion with *Eco*RI of the 1:100 DNA:PT3AME complexes is particularly interesting (Figure 2a, lane 5). This ratio favours interchain interactions giving place to the formation of supramolecular adducts or products with high molecular weights. This result, which is fully consistent with that obtained when the digestion is carried out with *Bam*HI (Figure 2a, lane 10), suggests that the 1:100 is the optimum DNA:PT3AME ratio. Thus, the formation of DNA:PT3AME adducts depends on the DNA:polymer ratio, and the effects of the interaction between the two systems may follow a normal distribution.

Digestion experiments with *Bam*HI on DNA:PT3AME complexes demonstrate a protective effect that depends on the ratio (Figure 2a). This fact is evidenced by the reduction in the intensity of the band associated to the F1 and F2 fragments. Furthermore, linear DNA or form III, which is produced by one cut-off, appears in the 1:100 and 1:200 ratios. These results clearly indicate that PT3AME protects the target sequence of *Bam*HI (5'-G/GATCC-3'). Figure 2b shows the results obtained for DNA:PT3MDE complexes with *Eco*RI and *Bam*HI. The results are similar to those described for DNA:PT3AME. Thus, PT3MDE interacts specifically with the sequences of circular DNA that are targets of the restriction enzymes.

*UV-Vis spectroscopy of DNA:polymer complexes.* In order to provide a better understanding of the interactions between plasmid DNA and the two CPs examined in this work, the behaviour of the nucleotide bases was investigated during the formation of the adducts by UV-Vis spectroscopy. Light scattering effects were avoided by correcting the maximum absorbance of nucleotide bases in DNA, which is 260 nm ($A_{260nm}$), with respect to the absorbance at 350 nm ($A_{350nm}$). The absorbance of the bases was recorded during 15 cycles separated by 2 min for the DNA:polymer mixtures with the 1:1 and 1:200 ratios. Figure 3 represents the evolution of $(A-A_0)/A_{max}$ against the time ($t$), where $A_0$ corresponds to the absorbance of DNA in solution (1:0 DNA:polymer ratio) at the initial time ($t$= 0 min), $A_{max}$ is the absorbance of the bases in the DNA:polymer mixture after thermal denaturalization of DNA by heating the sample at 94 ˚C during 15 min, *i.e.* when 100% of DNA bases are exposed, and $A$ is the absorbance of nitrogen bases in DNA:polymer mixtures measured at different times (cycles).

Results displayed in Figure 3a, which correspond to the 1:1 DNA:polymer ratio, reveal different behaviours for PT3AME and PT3MDE. The latter interacts very rapidly with plasmid DNA, *i.e.* the maximum of the profile is reached in two minutes (second cycle). In opposition, the value of $(A-A_0)/A_{max}$ remains at zero during 30 min for the DNA:PT3AME mixture. This feature is consistent with the lack of interaction between the plasmid DNA and the PT3AME, this result being in agreement with electrophoretic observations (Figure 1a, lane 2). Inspection to the results obtained for the 1:200 DNA:polymer ratio, which are displayed in Figure 3b, reveals a significant change for the DNA:PT3AME mixture. Thus the interaction between the plasmid DNA and the CP induce a fast and very significant exposition of the

nitrogen bases. This dependence on the DNA:PT3AME ratio is fully consistent with the electrophoresis results displayed in Figure 1. On the other hand, the behaviour showed by the DNA:PT3MDE mixture is very similar for both the 1:1 and 1:200 ratios, as is evidenced by the immediate formation of DNA:PT3MDE adducts. Moreover, Figure 3b clearly shows that the exposition of DNA bases is considerably smaller in DNA:PT3MDE complexes than in DNA:PT3AME complexes.

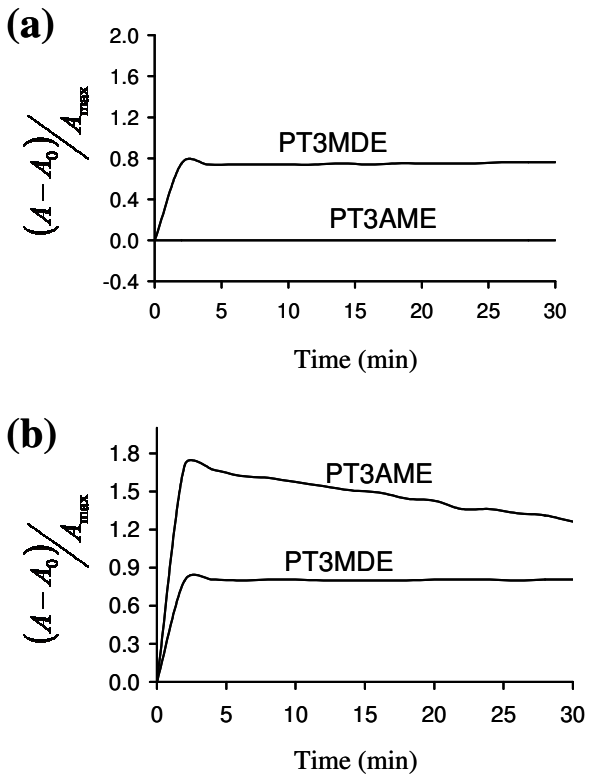


**Figure 3 –** Temporal evolution of DNA:PT3MDE and DNA:PT3AME mixtures with 1:1 (a) and 1:200 (b) DNA:polymer ratios followed by UV-Visible spectroscopy (see text). Spectra were recorded during the 15 cycles, two consecutive cycles being separated by a 2 min interval. For the 1:1 DNA:PT3AME ratio no interaction was detected, the profile being a straight line with all the values at zero.

The results provided by UV-Vis spectroscopy and electrophoretic assays indicate that the interaction between the plasmid DNA and the CPs to form DNA:PT3AME and DNA:PT3MDE adducts depends on the chemical nature of the polymer. Thus, the two polymers provide different interactions with DNA as is evidenced by the following

observations: (1) no DNA:PT3AME adduct was identified at the 1:1 ratio while, in contrast, the DNA:PT3MDE complex was clearly detected for the same ratio; and (2) for the 1:200 ratio, the exposition of nitrogen bases is considerably higher in DNA:PT3AME than in DNA:PT3MDE complexes.

*Structure of DNA: A circular dichroism study.* The objective of the CD investigation presented in this section was to examine the structural alterations undergone by the plasmid DNA when it is bound to the CPs. For this purpose, CD spectroscopic analyses were performed on solutions containing plasmid DNA (1:0 DNA:polymer ratio) and DNA:polymer mixtures with 1:1 and 1:200 ratios. Results are provided in Figure 4. It should be emphasized that, as was mentioned in the Methods section, the CD spectrum of the polymer was subtracted from the CD spectra of the DNA:polymer adducts. This allowed detect structural changes in DNA.

The plasmid is a supercoiling circular DNA and its ellipiticity is negative. The raw CD spectra recorded between 200 and 360 nm show ellipiticity changes as well as lost of supercoiling for the DNA:PT3AME and DNA:PT3MDE complexes (data not shown). The supercoiling was lost in the 1:200 DNA:PT3AME mixture, while positive ellipiticity was obtained for the 1:1 ratio (Figure 4a). For DNA:PT3MDE mixtures, both ratios provided lost of supercoiling and negative ellipiticity (Figure 4b).

DNA adopts the B-form in aqueous solution, the CD signals typically found for the canonical structure being as follow: positive band at 275 nm, negative band at 245 nm and crossover point near 258 nm.[29,30] As can be seen in Figure 4, the characteristic features of the DNA plasmid correspond to the B-form, even although small differences are detected with respect to the canonical form: positive band at 280 nm, negative signal at 257 nm, and crossover point near 272 nm. The DNA:PT3AME and DNA:PT3MDE complexes show that the CD of plasmid DNA is significantly perturbed when it interacts with the two CPs (Figure 4a and 4b, respectively). Changes include a significant reduction in the intensity of the negative and positive bands. Although these changes correspond to conformational variations, the structure of the DNA in the complexes cannot be clearly defined due to the presence of the light scattering of spectral tails. Thus, the size of the complexes can contribute to the light scattering.[30] However, the changes observed by CD spectroscopy together with the increase in absorbance evidenced by UV-Vis spectroscopy and the protective effect in the restriction

cleavage clearly indicate that the formation of DNA:PT3AME and DNA:PT3MDE complexes involve structural alterations in the DNA.

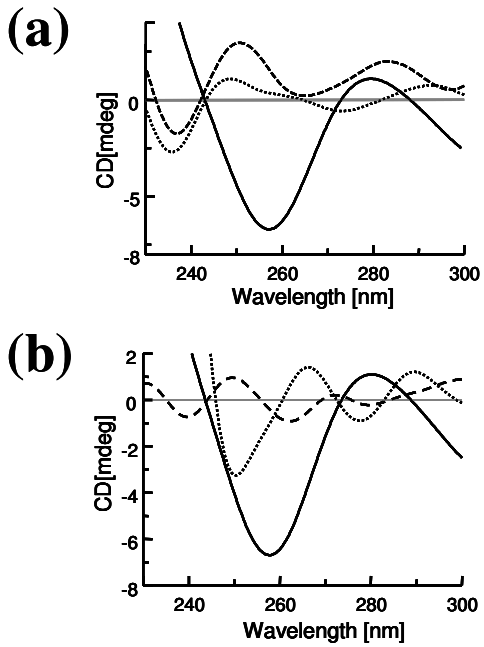


**Figure 4 –** CD spectra of DNA:polymer complexes to study structural alterations of DNA: (a) DNA:PT3AME and (b) DNA:PT3MDE complexes with 1:1 (dashed line) and 1:200 (dotted line) DNA:polymer ratios. In all cases the CD spectrum of the corresponding CP was subtracted from the CD spectra of the DNA:polymer complexes. The spectrum recorded the pMT4 plasmid DNA represented by the solid line.

These results allow conclude that the interaction between the plasmid DNA and the two CPs produces ellipiticity changes and alteration in the secondary structure of DNA. The immediate consequence of this structural alteration is the exposition of the DNA bases allowing the rapid interaction with the polymer molecules.

### 4.5.4 – Conclusions

This work provides reliable information about the interaction of plasmid DNA with two PTh derivatives, PT3AME and PT3MDE, bearing polar side groups, these results being complementary to those previously reported for PPy, PEDOT and P3MT.[10,16] The two CPs used in this work were prepared by chemical oxidation using $FeCl_3$. Therefore, the oxidation

degrees of PT3AME and PT3MDE are significantly lower than those of the CPs used in our previous works, which were doped with $LiClO_4$. In spite of this, both PT3AME and PT3MDE are able to form adducts, even although a relatively high concentration of CP is required for the formation of DNA:PT3AME complexes.

The ability of positively charged molecules to interact with DNA is based on the propensity of the latter to form adducts with cationic species.[31] However, the interactions of CPs with specific nucleotide sequences, like those found for the 5'-G/AATTC-3' (target for *Eco*RI) and 5'-G/GATCC-3' (target for *Bam*HI) sequences with both PT3AME and PT3MDE, require the formation of directional and specific interactions like hydrogen bonds. This allows to conclude that the formation of specific interactions with DNA depends on the chemical nature of the CP, which is fully consistent with the results provided not only in this but also in our previous works.[10,16] In particular, PPy, PEDOT, PT3AME and PT3MDE, which contain acceptors or donors of hydrogen bonds, have been found to form specific interactions with DNA, while this kind of interaction was weak and poorly detected for P3MT and PTh derivatives without donor and acceptors of hydrogen bonds.

Finally, UV-Vis results revealed significant differences in the interaction pattern of PT3AME and PT3MDE with DNA. The first one was mentioned above and refers to the concentration of CP required for the formation of the DNA:PT3AME and DNA:PT3MDE. Taken into account that the oxidation level is similar for the two polymers, this should be attributed to the chemical constitution of PT3AME and PT3MDE, which involve one and two polar groups per repeating unit, respectively. The second difference refers to the exposition of the DNA bases to radiation, which is higher in DNA:PT3AME than in DNA:PT3MDE complexes. This should be also related with the different capabilities of the two CPs to act as hydrogen bonding acceptors. Thus, the degree of interaction between the nitrogen bases and the CP is higher for PT3MDE than for PT3AME. Moreover, CD spectra clearly show that the interaction with the CPs provokes an alteration in the secondary structure of DNA, *i.e.* the unfolding of the double helix.

The overall of these results lead us to propose the following hypothesis for the interaction of DNA with both PT3AME and PT3MDE: these polymers produce the unfolding of the double helix promoting the intercalation of the CP molecules between the DNA strands. This leads to enhance the exposition of the DNA bases, the degree of such exposition depending on the number of hydrogen bonding interactions between the bases

and the polar groups. A schematic description of the proposed mechanism is provided in Figure 5.

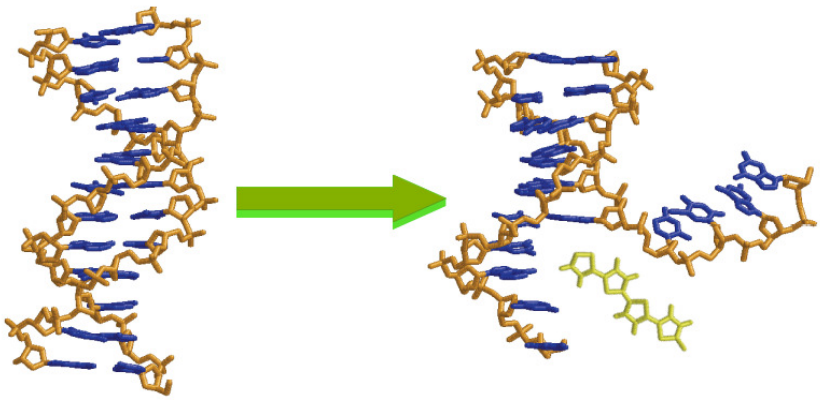

**Figure 5 –** Schematic view of the proposed mechanism for the interaction between plasmid DNA and the two PTh derivatives under consideration, which is based on the intercalation of the polymer between the two strands of DNA.

### 4.5.5 – References

[1] H. Chriswanto, G. G. Wallace, *J. Liq. Chromatogr.* 19 (1996) 2457.

[2] L. L. Miller, B. Zinger, O. X. Zhou, *J. Am. Chem. Soc.* 109 (1987) 2267.

[3] H. Guo, C. M. Knobler, R. B. Kaner, *Synt. Met.* 101 (1999) 44.

[4] P. Englebienne, *J. Mater. Chem.* 9 (1999) 1043.

[5] A. Kros, S. W. F. M. van Howell, N. A. S. M. Sommerdijk, R. J. M. Nolte, *Adv. Mater.* 13 (2001) 1555.

[6] G. F. Khan, W. Wernet, *Thin Solid Films* 300 (1997) 265.

[7] A. Azioune, M. M. Chehimi, B. Miksa, T. Basinska, S. Slomkowski, *Langmuir* 18 (2002) 1150.

[8] V. Misoska, W. E. Prize, S. Ralph, G. G. Wallace, *Synth. Met.* 123 (2001) 279.

[9] J. Wang, M. Jiang, *Electroanalysis* 13 (2001) 537.

[10] C. Ocampo, E. Armelin, F. Estrany, L. J. del Valle, R. Oliver, F. Sepulcro, C. Alemán, *Macromol. Mat. Engin.* 292 (2007) 85.

[11] H.-A. Ho, M. Boissinot, M. G. Bergeron, G. Corbeil, K. Dore, D. Boudreau, M. Leclerc, *Angew Chem. Int. Ed.* 41 (2002) 1548.

[12] D. S. Minehan, K. A. Marx, S. K. Tripathy, *Macromolecules* 27 (1994) 777.

[13] A.-H. Bae, T. Hatano, M. Numata, M. Takeuchi, S. Shinkai, *Macromolecules* 38 (2005) 1609.

[14] H. Peng, L. Zhang, J. Spires, C. Soeller, J. Travas-Sejdic, *Polymer* 48 (2007) 3413.

[15] T. Yamamoto, T. Shimizu, E. Kurokawa, *React. Funct. Polym.* 43 (2000) 79.

[16] P. Pfeiffer, E. Armelin, F. Estrany, L. J. del Valle, L. Y. Cho, C. Alemán, *J. Polym. Res.* 15 (2008) 225.

[17] B. Liu, G. C. Bazán, *Chem. Mater.* 16 (2004) 4467.

[18] C. E. Schmidt, V. Shastri, J. P. Vacanti, R. Langer, *Proc. Natl. Acad. Sci. USA* 94 (1997) 8948.

[19] A. Kotwal, C. E. Schmidt, *Biomaterials* 22 (2001) 1055.

[20] L. J. del Valle, D. Aradilla, R. Oliver, F. Sepulcro, A. Gamez, E. Armelin, C. Alemán, F. Estrany, *Eur. Polym. J.* 43 (2007) 2342.

[21] G. G. Wallace, L. A. P. Kane-Maguire, *Adv. Mat.* 14 (2002) 953.

[22] D. Zanuy, C. Alemán, *J. Phys. Chem. B* 112 (2008) 3222.

[23] O. Bertran, P. Pfeiffer, J. Torras, E. Armelin, F. Estrany, C. Alemán, *Polymer* 48 (2007) 6955.

[24] V. Lingua, J. Gómez, S. García-Gil, *Master Thesis* 2007, EUETIB, Universitat Politécnica de Catalunya 2007.

[25] B. Kim, L. Chen, J. Gong, Y. Osada, *Macromolecules* 32 (1999) 3964.

[26] C. Alemán, R. Oliver, E. Brillas, J. Casanovas, F. Estrany, *Chem. Phys.* 323 (2006) 407.

[27] C. Alemán, R. Oliver, E. Brillas, J. Casanovas, F. Estrany, Chem. Phys. 314 (2005) 1.

[28] L. Ferretti, S. S. Karnik, H. G. Khorana, M. Nassal, D. D. Oprian, *Proc. Natl. Acad. Sci. USA* 83 (1986) 599.

[29] K. Nejedly, J. Chládková, M. Vorlícková, I. Hrabcová, *J. Kypr, Nuc. Acids. Res.* 33 (2005) e5.

[30] C. S. Braun, G. S. Jas, S. Choosakoonkriang, G. S. Koe, J. G. Smith, C. R. Middaugh, *Biophys. J.* 84 (2003) 1114.

[31] W. D. Wilson, L. Stertkowski, F. A. Tanious, R. A. Watson, J. L. Mokrosz, A. Strekowska, G. D. Webster, S. Neidle, *J. Am. Chem. Soc.* 110 (1988) 8292.

# Chapter 5

# Drug Detection

# 5.1 – Microstructures of poly(*N*-methylpyrrole) and their interaction with morphine

Microstructures of poly(*N*-methylpyrrole) have been generated by direct electrochemical oxidation of N-methylpyrrole with poly(styrenesulfonic acid) in aqueous solution, using a micelle formation mechanism with gas bubble templates. These microstructures present a "doughnut"-like morphology with diameters ranging from 20 to 100 μm. Other anionic surfactants, such as camphorsulfonic acid and $\beta$-naphthalenesulfonic acid, have been also employed, results evidencing that the morphology of the microstructures depends on the nature of the surfactant electrolytes. The dimensions, abundance and texture of the microstructures have been modulated by varying the surfactant molecules, the electrochemical technique, and the distance between the working and counter-electrode. The generated microstructures have been characterized using electrochemical techniques, RAMAN and infrared spectroscopies, scanning electron microscopy and atomic force microscopy. Hollow microstructures-containing films made of poly(*N*-methylpyrrole)/poly(styrenesulfonic acid), which present remarkable electroactivity and electrostability, has been proved to interact with morphine molecules. Thus, systems based on this prominent material show a high ability to capture the drug molecules and to retain them for a long period of time.[*]

[*] - Results described in this section previously appeared in *Electrochimica Acta* 56 (2011) 5836.

## 5.1.1 – Introduction

Many of the nanostructured materials currently under development draw their inspiration from the structures found in nature.[1-3] Highly sophisticated morphologies and functions have been achieved using supramolecular architectures of polymer structures.[4] Within this context, micro- and nanostructures based on CPs are a class of important materials with many potential applications because of their low density, large specific area, high stability and surface permeability, and good electrochemical properties.

In recent years, a new approach for the fabrication of CP micro- and nanostructures has emerged. The general process can be described as the one-step electrochemical generation of the CP in a solid substrate assisted by a solid or soft template mechanism. Thus, this method can be applied using solid templates with well defined shapes (*e.g.* porous alumina membranes and polystyrene colloidal particles) limiting the size of the materials, or "soft" templates formed by assemblies of molecules (*e.g.* surfactants and gases) in solution or solid surface.[5-8] In this field, the research developed by Gaoquan Shi and co-workers in complex systems based on CPs was a brilliant and pioneering

contribution.[9-17] These authors reported microspheres, microcrocks, microbowls, microbarrels and micropumpkins made of PPy, all them showing remarkable thermal stability and distinct cation-exchange behaviour during the redox processes. The most recent advances in the study of micro- and nanostructures prepared by electrosynthesis, as well as the future research directions in the field, were recently reviewed by Shi *et. al*..[18]

In this work we apply the electrochemical method developed by Shi and co-workers, and based on "soap bubble" templates, to generate microstructures made of poly(*N*-methylpyrrole) (PNMPy). The most relevant characteristic of this approach is the use of gas molecules as templates, in spite of the solid templates frequently used.[19] Typically, the fabrication of micro- and nanostructures starts with a very fine electrodeposition of a polymer film on a metal surface. After this, the CP grows in the bubble surface assisted by anionic surfactants as electrolytes.[9,13-14,20] The formation of microstructures using this method with gas templates presents some advantages. More specifically, the control of the electrochemical process is very easy and the production of intact microstructures requires only one step of synthesis without any intermediate stages.[21-24]

In this work we explore the synthesis of PNMPy hollow microstructures using three different organic acid surfactants as supporting electrolytes: (1) poly(styrenesulfonic acid) (PSSA), a dopant agent that can be immobilized in the polymer matrix and shows cation-exchange properties during the redox properties, which are due to the large size of poly(styrene sulfonate) ($PSS^-$) chains; (2) (±)-camphorsulfonic acid (CSA), a low molecular weight surfactant that is expected to enhance the mobility and capacity of the ionic species; and (3) $\beta$-naphthalenesulfonic acid ($\beta$-NSA), whose large aromatic rings are expected to stabilize the cation radicals and to reduce the oxidation potential of the monomer.[18] The morphology and dimensions of the resulting PNMPy hollow microstructures are discussed and compared with those obtained using PPy. Finally, we examine the ability of these microstructures to detect morphine, a drug with well-known anaesthetic properties and, recently, associated to cardiovascular protective effects.[25] The detection of morphine using PPy modified electrodes was early described by Johnson and Kriz in 1997.[26] These authors showed that the current response of the polymer increased with the increase concentration of the drug. The overall of the results reported in this work suggests that the electrochemical generation assisted by gas templates is a successful method for the preparation of microstructured materials, including capsules, nanotubes and biomimetic

structures, which have many potential applications (*e.g.* drug detection, sensors, microreactors, mechanisms for the adsorption or immobilization of organic and inorganic molecules, catalysis).

### 5.1.2 – Methods

*Reagents. N*-methylpyrrole (NMPy) and Py were purchased from Sigma Aldrich Química S.A. and distilled before use. PSSA, 18 wt% in aqueous solution ($M_w$ ~75000) and $\beta$-NSA (M= 208.24 g/mol) were purchased from Aldrich and used as received. CSA (M= 232.3 g/mol) was purchased from Fluka Analytical and used as received.

*Equipments.* Electrochemical experiments were recorded with an Autolab PGSTAT302N (Ecochimie, The Netherlands) potenciostat-galvanostat equipped with GPES and FRA software, and using a conventional three-electrode system. Electrochemical characterization was performed by cyclic voltammetry (CV) in the potential range of -1.00 to 1.00 V at a scanning rate of 50 mV/s for consecutive oxidation-reduction cycles.

FTIR-ATR spectra were obtained using a 4100 Jasco spectrophotometer equipped with an ATR MKII Golden Gate Heated Single Reflection Diamond Specac model. RAMAN spectra were recorded with a Dilor Jobin Yvon dispersive spectrometer equipped with a 1024 diodes multichannel detector using a He/Ne laser (20 mW) with 633 nm of excitation wavelength.

Optical photographs were carried out using an optical microscope Olympus BX51 with a digital camera and software AnalSIS. Scanning electron microscopy (SEM) photographs were obtained using a JEOL JSM-6400 scanning electron microscope equipped with EDS Oxford analyzer. Tapping-mode atomic force microscopy (AFM) measurements were carried out with a Molecular Imaging PicoSPM using a NanoScope IIIa controller in ambient conditions.

*Electrochemical polymerization.* All microstructures based on PNMPy and PPy were prepared by anodic polymerization using an Autolab PGSTAT 302N potenciostat-galvanostat equipped with the GPES software. Electrochemical experiments were conducted in three-electrode two-compartment cells under nitrogen atmosphere (99.995% in purity). Steel AISI

316 sheets of 4 $cm^2$ areas were employed as working (WE) and counter electrodes (CE), both electrodes being separated with a distance of 0.5 cm and arranged face-to-face. The reference electrode (RE) was Ag/AgCl (3 M KCl) electrode in all cases.

In order to generate enough gas bubbles as templates, the solution was pre-treated by CV scanning before the electrochemical generation of the CPs, as was recommended in reference.[12] The synthesis of PNMPy and PPy microstructures was performed by CV scanning over the potential range of 0.00-1.00 V in the case of the PSSA electrolyte, and in the range 0.00-0.90 V for CSA and $\beta$-NSA at a scanning rate of 20 mV/s for 2 cycles. This was followed by a chronoamperometry (CA) with a constant potential of 1.00 V (PSSA) or 0.90 V (CSA and $\beta$-NSA), the time of polymerization being 240 seconds. The electrochemical media were aqueous solutions of Py or NMPy monomers (0.5 M) and PSSA, CSA or $\beta$-NSA surfactant electrolytes (0.5 M). Experiments were performed at room temperature in all cases.

*Morphine detection.* Electrochemical impedance spectroscopy (EIS) was carried out in a two-compartment cell with a three-electrode configuration, using an Autolab 302N potentiostat/galvanostat with the FRA software program. PNMPy/PSSA microstructures were electrogenerated (see section *2.3*) on the surface of a 2 $cm^2$ AISI 316 sheet (WE), an identical sheet of AISI 316 being used as CE. The cell was filled with 40 ml of PSSA (0.5 M) aqueous solution and all the measurements were performed at room temperature.

EIS measurements were carried out in the 1 kHz – 10 mHz frequency range and sinusoidal voltage amplitude of $\pm$5 mV for 70 frequencies. EIS data were plotted in terms of real and imaginary parts of the impedance (Z' and –Z'', respectively). This procedure was employed for the analysis of the experimental impedance spectra of PNMPy/PSSA microstructures, before and after the incubation of the modified WEs with morphine solution (30 µM) for 0 h, 3 h and 24 h.

### 5.1.3 – Results and Discussion

*Synthesis of PNMPy and PPy microstructures.* Initial CVs of stainless steel electrodes in aqueous solutions of NMPy and Py with organic acid surfactants as supporting electrolytes are displayed in the Figure 1. According to Shi and co-workers, the monomer/electrolyte

solution pretreatment produced gas bubbles from water decomposition and a very thin film of polymer in the working electrode (data not shown).[9-17] In the subsequent electrochemical polymerization of NMPy monomers by CV (Figure 1a), we observe a steep increase of the current density at about $E_{Ag/AgCl}$ = 0.78 V and 0.86 V in the positive going scan for $\beta$-NSA and CSA electrolytes, respectively. In the negative going scan a trace crossing occurs for NMPy at $E_{Ag/AgCl}$ = 0.72 V and 0.84 V for $\beta$-NSA and CSA electrolytes, respectively. It has been suggested that trace crossing may be due to nucleation overpotential, previously described in many works or, alternatively, to a local increase in concentration of oligomers easier to oxidize (*i.e.* at lower electrode potentials) close to the electrode.[27-30] Recently, this phenomenon has been also attributed to a comproportionation reaction between oligomeric reaction products and starting monomer molecules at the solution/metal interface.[31] No trace crossing was obtained for NMPy/PSSA system. In spite of this, NMPy/PSSA complex showed better electrochemical response than $\beta$-NSA and CSA electrolytes, with two positive potentials at $E_{Ag/AgCl}$ = 0.63 V and 0.90 V. This behaviour may be attributed to the fact that NMPy was better stabilized by a polymer with high molecular weight as electrolyte than by small surfactant molecules or to an overall faster reaction resulting in higher concentrations of reactive species migrating to the working electrode. The first potential is associated to polaron species initially formed at the electrode surface, their subsequently transformation into bipolaron species, and finally the polymerization of the latter at the WE surface. In contrast, the CVs obtained during electropolymerization of the Py monomer (Figure 1b) did not show oxidation processes associated to a polaron or bipolaron species in the employed potential range.[32] The oxidation wave of PPy and the passivation wave of the electrode were too weak to be clearly identified from these curves. Py monomers usually need less positive potentials than NMPy for their polymerization at the stainless steel surface in acetonitrile or acid aqueous solutions.[32] In spite of this, the PNMPy/PSSA system presented easier oxidation behaviour than PPy/PSSA systems. The later needs higher electrogeneration potential than PNMPy (Figure 1). However, we can not use more positive potentials than 1.00 V in aqueous solutions due to the extremely high concentration of oxygen molecules from water electrolysis produced at $E_{Ag/AgCl}$ = 1.00 V or $E_{Ag/AgCl}$ = 1.23 V. Another limiting factor for the electropolymerization of NMPy and Py in aqueous solution was the pH of the surfactant solutions.

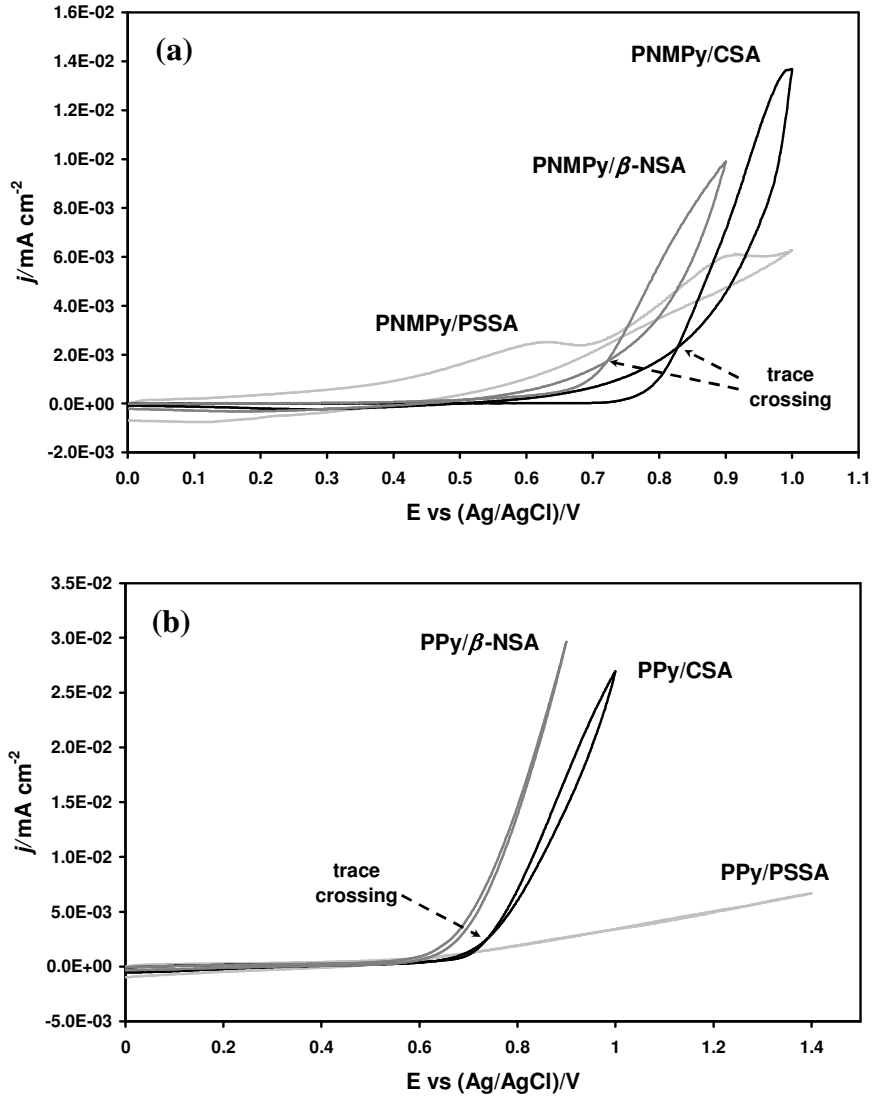


**Figure 1 –** Electropolymerization of (a) NMPy and (b) Py monomers in aqueous solutions of organic acid surfactants by two CV scans. PNMPy/PSSA, and PNMPy/CSA were generated from 0.00 to 1.00 V, while NMPy/$\beta$-NSA was generated from 0.0 to 0.90 V. PPy/PSSA was generated from 0.00 to 1.40 V, while PPy/CSA or $\beta$-NSA were generated with the same CV parameters than PNMPy. Scan rate: 20 mV/s. All potentials are referred to Ag/AgCl (KCl saturated) electrode.

In this case, CVs in the potential range of -0.50 to 1.00 V (data not shown) of the stainless steel electrodes in surfactant aqueous solutions (*i.e* in the absence of the monomer) show oxidation processes at -0.10 V for $\beta$-NSA (pH = 1.48) and CSA (pH = 1.50), which were

associated with the vigorous formation of hydrogen gas burbles in the anode electrode that migrate to the cathode electrode.[11] However, PSSA electrolyte (pH = 2.50) did not show oxidation/reduction processes in the same conditions (data not shown). We associate this behaviour to the higher molecular weight of PSSA molecules, which prevent the fast $H_2$ gas migration towards the WE, as occurs with $\beta$-NSA and CSA.

Our results indicate that the CV followed by the CA produces PNMPy stable films at the electrode surface, *i.e.* not powdery deposit, and that the adhesion of the film to the WE depends on the chemical composition of the surfactant molecules. PNMPy presents better film forming properties in PSSA aqueous solutions with high thickness and weak adhesion to the substrate, whereas $\beta$-NSA and CSA produce lower thickness and stronger adhesion to the substrate. However, PPy films obtained with these two techniques were very thin evidencing that these system require more positive potential than PNMPy. Therefore, from an electrochemical point of view, PNMPy and PSSA, as organic acid surfactant, complexes seem to be interesting systems with low potentiostatic requirements for their generation.

Electrochemical characterization of the PNMPy-surfactant complexes was performed using cyclic voltammetry control (CVC), results being displayed in the Figure 2. The oxidation of PNMPy/$\beta$-NSA and PNMPy/CSA films generates a significant amount of $H_2$ gas burbles due to the chemical characteristics of the surfactants (*i.e.* low molecular weight and high concentration of hydrogen protons). This phenomenon increases with the number of CVC cycles. Furthermore, these systems do not show a well defined reversibility (Figure 2). The oxidation potential occur as a shoulder at $E_{Ag/AgCl}$ = 0.63-0.70 V at a scan rate of 50 $mV \cdot s^{-1}$ in both cases, whereas the reduction potentials are observed at $E_{Ag/AgCl}$ = -5 mV and -0.23 V for $\beta$-NSA and CSA, respectively. Finally, a complete loss of electroactivity is observed for both PNMPy/$\beta$-NSA and PNMPy/CSA complexes after 10 cycles. On the other hand, PNMPy/PSSA films showed high reversibility with well defined oxidation-reduction peaks at $E_{Ag/AgCl}$ = 0.80 V and $E_{Ag/AgCl}$ = -0.28 V, respectively, at a scan rate of 50 $mV \cdot s^{-1}$. As it can be seen, in spite of the electrochemical stability decreases from the first to the tenth cycle, the material is able to maintain its redox reversibility and electroactivity. This should be attributed to the role of the PSSA molecules as dopant and counter-ion incorporated and stabilized inside the PNMPy film during the electropolymerization process.

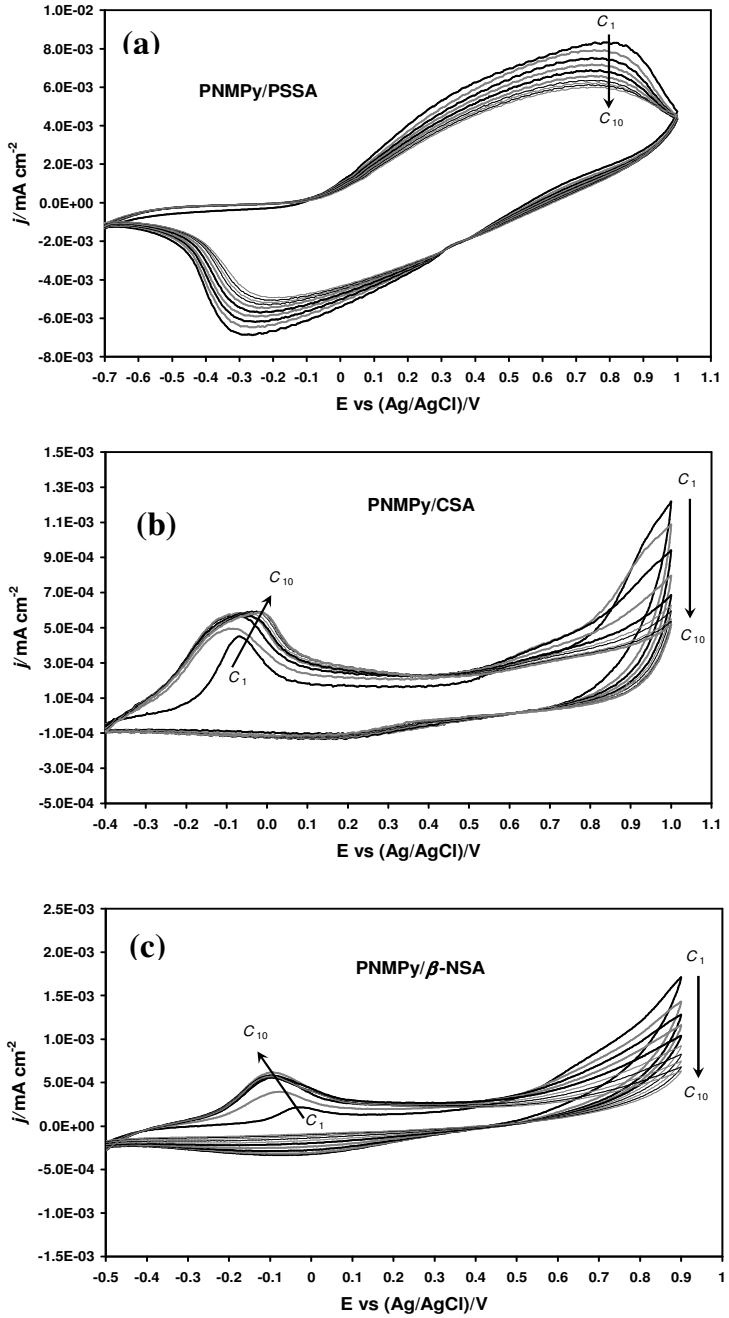


**Figure 2 –** Control voltammograms for 10 consecutive oxidation-reduction cycles of PNMPy/organic acid surfactants microstructures prepared using two cycles of CV and followed by a CA. The CV range varied from -0.70 to 1.00 V for (a) PNMPy/PSSA and (b) PNMPy/CSA; and from -0.40 V to 0.90 V for (c) PNMPy/$\beta$-NSA microstructures. Labels $c_1$ and $c_{10}$ refer to the voltammograms recorded in the first and tenth cycles, respectively.

Thus, PSSA surfactant shows electrocatalytic properties during the preparation of the PNMPy hollow microstructures, activating the NMPy monomers and lowering their oxidation potential. As the electrochemical properties of PNMPy/PSSA are better than those of PNMPy/$\beta$-NSA and PNMPy/CSA, characterization and application studies have been focused in the former complex. The hollow microstructures obtained with two cycles of CVs followed by CA techniques will be discussed in morphological characterization section.

*Spectroscopic characterization.* The IR spectra displayed in Figure 3a show the main absorption bands for the NMPy monomer and the PNMPy/PSSA microstructures. It should be remarked that the characterization of CPs by IR spectroscopy is a difficult task compared to conventional and insulating polymers. Thus, the effect of polymerization and the presence of charges in heterocyclic rings and dopant ions cause a general broadening and overlapping of some absorption bands.[33] In spite of this, an approach in terms of chemical groups can be provided. The absorbance of the aromatic C-H stretch of the Py ring (α C-H and β C-H) sometimes does not appear in the IR spectrum and, therefore, this band is not typically for C-H identification. However, in this case we observe a very weak peak at ~3103 $cm^{-1}$ in the NMPy monomer, which can be attributed to the α -hydrogen position of the aromatic ring (Figure 3a).[34] On the other hand, the β C-H out-of-plane deformation was observed as a medium peak at 968 $cm^{-1}$ while the α C-H out-of-plane deformation appeared as a very sharp band at 720 $cm^{-1}$. As it was expected, the weak peak at ~3103 $cm^{-1}$ and the strong peak at 720 $cm^{-1}$ of the α C-H groups disappear in the spectrum of the PNMPy/PSSA microstructure, indicating that the α positions (2- and 5- positions, alternatively) of NMPy ring have been successfully bonded. Additionally, the absence of the ring deformation band at 1510 $cm^{-1}$ (C=C, non-conjugated diene) in the PNMPy/PSSA spectrum also reflect the NMPy polymerization.

The FTIR-ATR spectrum of the oxidized material also reflects the existence of degradation processes affecting the polymerization of NMPy. Thus, a strong band from C=O carbonyl groups, which is produced by polymer oxidation, can be appreciated at 1745 $cm^{-1}$. The overoxidation undergone by CPs, which has been extensively described in the literature, is a well known process difficult to avoid.[35-37]

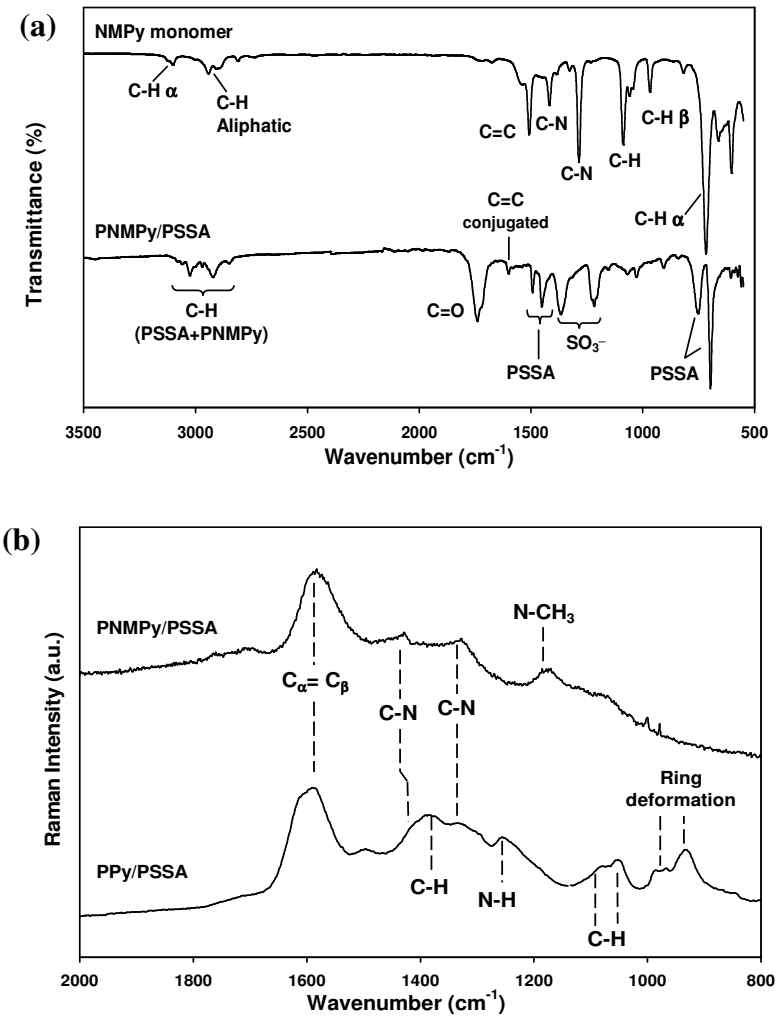


**Figure 3 –** (a) FTIR-ATR spectra of the NMPy monomer freshly distilled and the PNMPy/PSSA hollow microstructures. (b) Raman spectra of PNMPy/PSSA and PPy/PSSA hollow microstructures. Exciting radiation: 632.8 nm.

Analysis of the spectrum of PNMPy/PSSA microstructures allows confirm that PSSA was successfully incorporated into the CP as anionic dopant. In fact, the major absorption bands observed in the spectrum are related with the PSSA molecules. The mean peaks of PSSA are observed at 3030 and 2932 $cm^{-1}$ (C-H aromatic and aliphatic stretching), 1494 and 1454 $cm^{-1}$ (C=C aromatic stretching), 1032 and 916 $cm^{-1}$ (C-H in-plane and out-of-plane bending), and two intense absorption bands at 759 and 698 $cm^{-1}$ (substituted benzene rings).

The $SO_3^-$ group is observed as two intense peaks at 1368 and 1218 $cm^{-1}$ (Figure 3a), which correspond to the asymmetric and symmetric SO stretching vibrations, respectively.[38] On the other hand, the C=C stretching band from the PNMPy conjugated system was observed as a very weak band at 1604 $cm^{-1}$.

Fortunately, absorption bands corresponding to non-polar or weakly polar groups (*e.g.* C=C and N-C) can be identified by RAMAN spectroscopy. The bands corresponding to the CP are increased by the Raman resonant effect; while the bands of the dopant molecules are not in resonance conditions.[35] Therefore, PNMPy/PSSA and PPy/PSSA microstructures were characterized by Raman analysis, their spectra being displayed in Figure 3b. Comparison of the two spectra allows identify the absorption bands corresponding to $N\text{-}CH_3$ and N-H deformations at 1175 $cm^{-1}$ and 1250 $cm^{-1}$, respectively. Furthermore, we can observe strong bands at 1578 $cm^{-1}$ ($C^{\alpha}=C^{\beta}$ ring stretching), 1425 and 1327 $cm^{-1}$ (C-N antisymmetrical stretching) and duplicated peaks associated to partially doped polymer chains in the 1200-900 $cm^{-1}$ region. These duplicated peaks have been related with the bipolaron and polaron structures formed after the incorporation of the PSSA dopant into the CP.[17,39-40] However, the peaks assigned to the $C^{\beta}$-H bending vibrations at 1080-1040 $cm^{-1}$ and the duplicated $C^{\beta}=C^{\beta}$ ring bending at 970-925 $cm^{-1}$ are not detected in the Raman spectra of the PNMPy/PSSA microstructures. This phenomenon was attributed to the noise of the spectrum (*i.e.* only a small shoulder is observed at ~1065 $cm^{-1}$) in previous works.[44] However, in this case we relate such disappearance with the polymer backbone overoxidation of the C-H (β) position in the NMPy ring, which is consistent with our previous observations in the FTIR spectrum.

*Morphological characterization.* The morphology of the microstructures was studied by SEM and AFM. Figure 4 evidences the "doughnut"-like morphology of the hollow microstructures obtained when PNMPy/PSSA is prepared by CV followed by CA techniques. The concentration of PNMPy/PSSA microstructures can be controlled through the distance between the WE and the CE. Thus, abundant microstructures, which tend to collapse (Figure 4a), are produced when the separation between the two electrodes is higher than 1.5 cm. Figure 4b shows some microstructures with a diameter ranging from 15 to 35 µm and hollow interiors with diameters of ~15 µm. The deep and wall thickness were around 12 µm and 7-8 µm, respectively. Figure 4b also evidences that the "doughnut"-like microstructures are well

adhered and incorporated on the surface of the PNMPy flat films, which present a thickness of ~12 µm. However, in some cases we obtain bigger "doughnut" structures with diameter of ~60 µm (Figure 4c). In contrast, individually separated "doughnuts" with an average diameter of 30 ± 5.0 µm are produced when the distance between WE and CE is reduced to 0.5 cm, which is consequence of the small size of the gas bubbles formed in these conditions. Independently of the distance between the electrodes, the PNMPy/PSSA microstructures present rough walls and surface (Figure 4c). The texture of the surface has been characterized at the nanometric scale using AFM (Figure 4d).

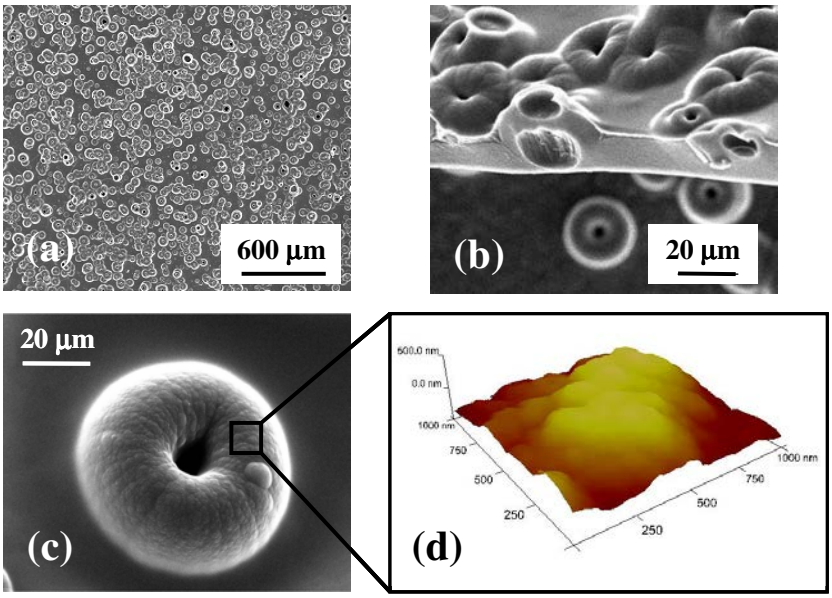


**Figure 4 –** SEM images of PNMPy/PSSA "doughnuts"-like microstructures obtained by electropolymerization in aqueous solution with a separation of 1.7 cm between the WE and CE: (a) low magnification; (b) high magnification and transversal section; (c) high magnification of an individual "doughnut"; and (d) AFM image of the "doughnut" surface.

On the other hand, the morphologies of the PNMPy microstructures obtained using $\beta$-NSA and CSA electrolytes were completely different to the "doughnut" displayed in Figure 4. As it can be seen in Figure 5a, the PNMPy microstructures produced using such two low molecular weight electrolytes present a brain-like morphology forming a wrinkle network system. According to our observations, the formation of microstructures with such morphology may be attributed to different factors. The first is related with the limited

capability of the low molecular weight surfactants to surround the gas bubble template (*i.e.* no regular spherical structure reaches the WE surface). Another hypothesis we have considered is that both the acidity and hydrogen gas production is higher for the $\beta$-NSA and CSA electrolytes than for the PSSA one (as mentioned in the synthesis section), which causes a larger concentration of gas molecules coalescing together at the metal surface followed by the polymer deposition. Finally, we should point out that the oxidizing ability of $\beta$-NSA and CSA is lower than PSSA, limiting the formation of the "doughnuts" in the former cases.

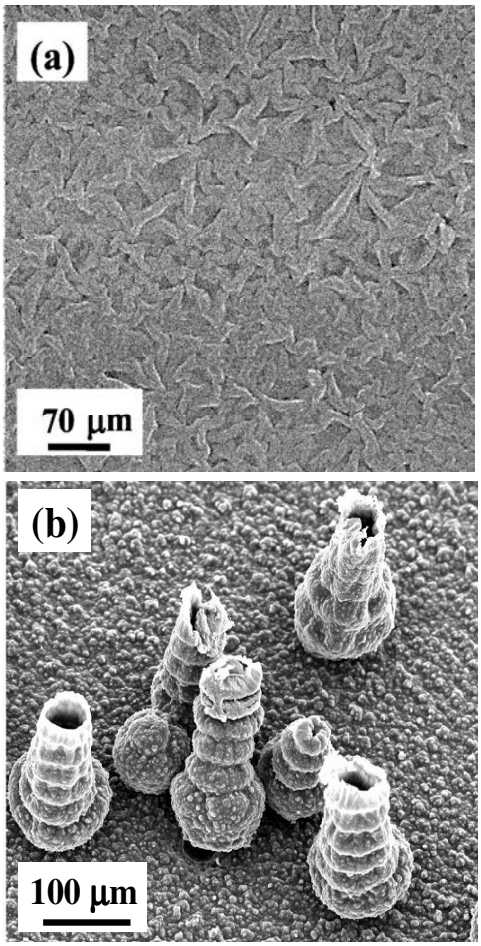


**Figure 5 –** SEM images of (a) PNMPy/CSA wrinkle films after two cycles of CV in the potential range of 0.00-1.00 V and one CA at 1.00 V for 240s, and (b) PPy/CSA bottle structures obtained after seven cycles of CV in the potential range of 0.00-1.20 V. Scan rate: 20 mV/s in both cases.

The electrochemical techniques used to generate PNMPy/PSSA microstructures were not efficient to obtain PPy/organic acid electrolytes microstructures. However, PPy/CSA was easily obtained following the same conditions employed by Qu and co-workers (*i.e.* applying seven CV scanning in the potential range of 0.00-1.20 V and at a scan rate of 20 mV/s).[12] As it can be seen in Figure 5b, "micro-bottles" grew from the bottom to the top, the number of rings being consistent with the number of CV cycles. These microstructures are randomly distributed in the surface of the film without following any regular apparition pattern. However, the PPy/CSA microstructures do not have good adhesion to the surface of the PNMPy membrane, being easily removed from the polymer film by ultrasonic treatment. This system showed better electrochemical stability than the PPy/PSSA complexes obtained after two CV scanning and CA.

In summary, the overall of these results allow state that the high electrochemical stability observed for the PNMPy/PSSA system is due to the large surface area generated when regular microstructures are formed. However, characteristics like the permeability and the shape of these microstructures may also contribute to the improvement of the electrochemical stability.

*On the use of PNMPy/PSSA microstructures for the electrochemical detection of morphine.* EIS was employed to investigate the interaction of morphine with PNMPy/PSSA electrodes immersed in a PSSA (0.5 M) aqueous solution. Figure 6 shows the Nyquist (6a) and Bode plots (6b) of the stainless steel coated electrodes obtained in the absence and presence of morphine. After initial exposure of the PNMPy film to the PSSA electrolyte, diffusion of water molecules and ions into the "doughnuts" (Figure 4b) and the porous of the film take place. Figure 6a inset show the Nyquist plot detail for high frequency time constant.

The experimental EIS plots were fitted using an equivalent circuit (EC) composed of two time constants (Figure 6c), as reported previously in the case of a coated glassy carbon electrodes.[42] The proposed EC is given by $R_s(CPE_c[R_{po}(CPE_{dl}R_{ct})])$, where $R_s$ represents the ohmic resistance between the working and the reference electrodes, $R_{po}$ the pore resistance of the polymer layer and $R_{ct}$ the charge transfer resistance, whereas $CPE_c$ and $CPE_{dl}$ correspond to the capacitance of the polymer film and of the double layer, respectively.

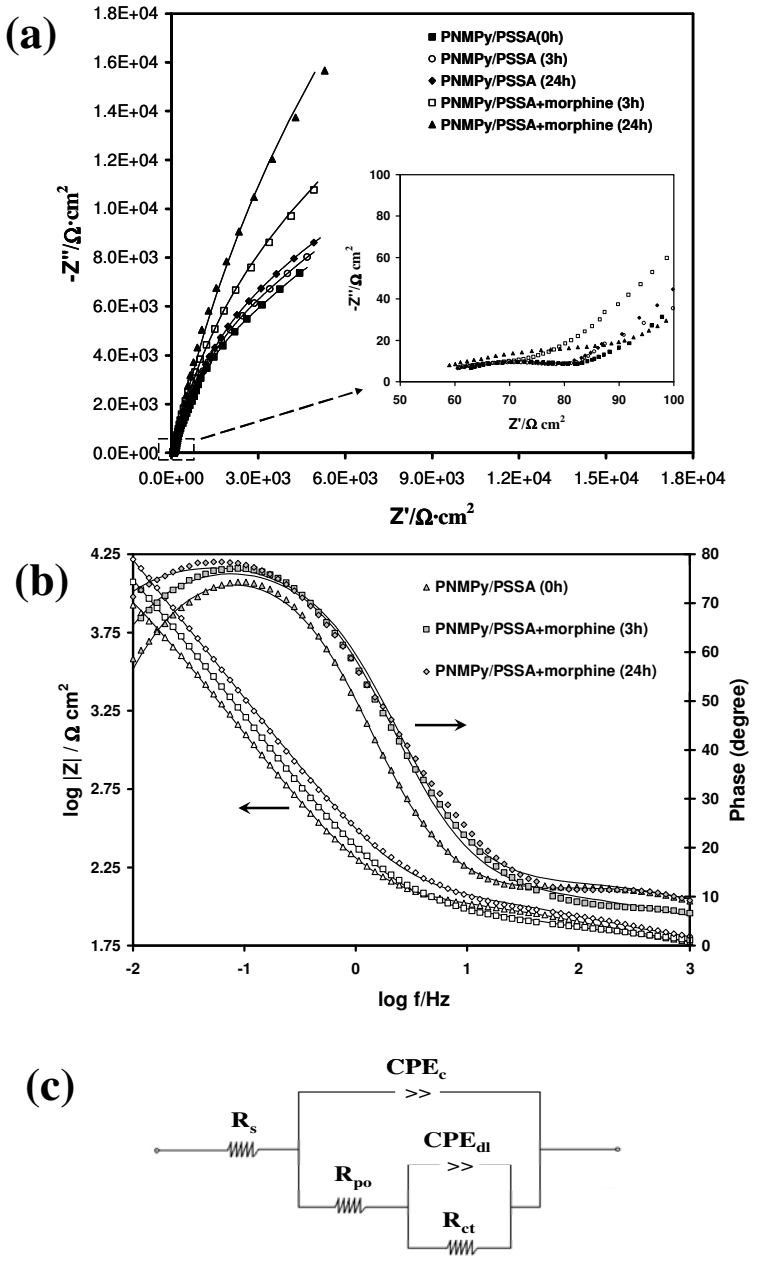


**Figure 6 –** Nyquist (a) and Bode (b) plots showing the evolution of the impedance data, before and after morphine incubation, on PNMPy/PSSA "doughnuts"-like microstructures. Points represent the experimental data, while the full lines correspond to the fitting of such data using the equivalent circuit model depicted on (c). The inset in (a) corresponds to the high frequency in the Nyquist plot.

Thus, the time constants at the high and the low frequencies were related to the polymer layer and the interfacial layer, respectively. These time constants were affected by the presence of pores on the polymer layer through which the solution can reach the metallic surface. The capacitance was replaced by a constant phase element (*CPE*) that describes a non-ideal capacitor when the phase angle is different from –90°. The *CPE* impedance is attributed to the distributed surface reactivity, surface heterogeneity, and roughness of the current and potential distribution, which in turn are related to the electrode geometry and the electrode porosity, being expressed as $Z_{CPE} = [Q\ (j\omega)^{n}]^{-1}$; where Q is a frequency-independent constant, ω is the angular frequency and n values are the correlation coefficients for the CPE.[43]

The CPE represents a capacitor for n = 1, a resistor when n= 0 and if n= 0.5, the CPE is associated with a diffusion process. Table 1 shows the values of the equivalent circuit elements obtained by fitting the experimental results. The fitting quality was judged according to the error percentage associated to each circuit component, showing errors smaller than 5%.

**Table 1 –** Fitting parameters used to simulate the EIS data obtained for the systems studied in this work.

| Sample | Time | Fitting Parameters | Data | Sample | Time | Fitting Parameters | Data |
|---|---|---|---|---|---|---|---|
| **PNMPy/PSSA** (Blank control) | **0 h** | $R_s$ / Ω·cm$^2$ | 56.1 | | | | |
| | | $R_{po}$ / Ω·cm$^2$ | 68.2 | | | | |
| | | $CPE_c$ / F cm$^{-2}$ | 0.29x10$^{-3}$ | | | | |
| | | n | 0.64 | | | | |
| | | $R_{ct}$ / Ω·cm$^2$ | 32.95x10$^3$ | | | | |
| | | $CPE_{dl}$ / F cm$^{-2}$ | 18.30x10$^{-4}$ | | | | |
| | | n | 0.87 | | | | |
| **PNMPy/PSSA** (Blank control) | **3 h** | $R_s$ / Ω·cm$^2$ | 51.0 | **PNMPy/PSSA + Morphine** | **3 h** | $R_s$ / Ω·cm$^2$ | 49.8 |
| | | $R_{po}$ / Ω·cm$^2$ | 73.0 | | | $R_{po}$ / Ω·cm$^2$ | 52.0 |
| | | $CPE_c$ / F cm$^{-2}$ | 0.17x10$^{-4}$ | | | $CPE_c$ / F cm$^{-2}$ | 1.82x10$^{-3}$ |
| | | n | 0.69 | | | n | 0.50 |
| | | $R_{ct}$ / Ω·cm$^2$ | 24.50x10$^3$ | | | $R_{ct}$ / Ω·cm$^2$ | 43.90x10$^3$ |
| | | $CPE_{dl}$ / F cm$^{-2}$ | 19.21x10$^{-4}$ | | | $CPE_{dl}$ / F cm$^{-2}$ | 9.40x10$^{-4}$ |
| | | n | 0.88 | | | n | 0.90 |
| **PNMPy/PSSA** (Blank control) | **24 h** | $R_s$ / Ω·cm$^2$ | 51.1 | **PNMPy/PSSA + Morphine** | **24 h** | $R_s$ / Ω·cm$^2$ | 49.8 |
| | | $R_{po}$ / Ω·cm$^2$ | 72.2 | | | $R_{po}$ / Ω·cm$^2$ | 80.0 |
| | | $CPE_c$ / F cm$^{-2}$ | 0.58x10$^{-4}$ | | | $CPE_c$ / F cm$^{-2}$ | 0.98x10$^{-3}$ |
| | | n | 0.67 | | | n | 0.43 |
| | | $R_{ct}$ / Ω·cm$^2$ | 29.50 x10$^3$ | | | $R_{ct}$ / Ω·cm$^2$ | 114.3 x10$^3$ |
| | | $CPE_{dl}$ / F cm$^{-2}$ | 17.51x10$^{-4}$ | | | $CPE_{dl}$ / F cm$^{-2}$ | 7.14x10$^{-4}$ |
| | | n | 0.88 | | | n | 0.90 |

The coating capacitance ($CPE_c$) exponent values (n) are around 0.50-0.60 for all samples which were ascribed to a diffusion process taking place at the [$PNMPy^+/PSS^-$] microstructures. The pore resistance ($R_{po}$) are low, varying from 68.2 ohm·$cm^2$ in the absence of morphine to 80 ohm·$cm^2$ after 24 hours incubation in a solution containing morphine. As the CP presents interconnected conductive paths promoted by the electrolyte filled micropores, diffusion through the polymer film can occur at high frequencies. This phenomenon is consequence of the difference between the chemical potentials of the outer (solution side) and inner (phase boundary side between the polymer film and the steel test panel) regions. In addition, this behaviour is attributed to the diffusion of PSSA electrolyte in the polymer film. The blank control referred to the PNMPy/PSSA microstructures without morphine and incubated for 3 and 24 h in PSSA solutions do not show variations in the Nyquist plot respect to the blank control at 0 h (directly after electropolymerization) (Figure 6a), as expected, and proving that changes observed after morphine incubation are not related with the displacement of PSSA molecules by morphine.

The low frequency time constant shows a nearly capacitive behaviour with the double layer capacitance ($CPE_{dl}$) exponent values close to 0.90. On the other hand, charge transfer resistance ($R_{ct}$) increased from ~25 kohm·$cm^2$ in the solution without morphine to ~100 kohm·$cm^2$ after 24 h of incubation in a morphine solution, indicating that the polymer matrix is saturated with morphine molecules leading to an enhanced resistance. The bode plots, illustrated in the Figure 6b (data for blank control at 3 h and 24 h were not plotted for better visualization), show a perfect correlation between the experimental data and the simulated curves.

The effect of the incubation time with morphine on the overall impedance illustrates how fast the drug is captured by the polymer matrix, reducing the electron-transfer capability of the hollow microstructures-containing PNMPy/PSSA film. The mechanism of the morphine capture inside the PNMPy/PSSA matrix is predominantly adsorption followed by the occlusion inside the film. No detachment of morphine molecules was observed after washing repeatedly with water.

In the mentioned circuit, the charge transfer resistance ($R_{ct}$) of the electrode is the only circuit element that as a simple physical meaning describing how fast the rate of charge transfer, during morphine adsorption, changes with the time.

### 5.1.4 – Conclusions

This work reports the electrochemical preparation of PNMPy/PSSA microstructures using gas templates. The formation of the microstructures occurs through a versatile and fast process, which allows modulate their dimensions, abundance and texture by controlling the monomer and electrolyte concentrations, the type of anionic surfactant molecules, and the distance between the WE and the CE. The stability of the CP film in an aqueous solution was improved when an appropriate surfactant counterion was used. The high electrochemical stability of PNMPy/PSSA systems can be attributed to the "doughnut" morphology of their microstructures, which present an extremely high surface area and good ability to release and to catch the ions molecules during the anodic and cathodic current charging. These characteristics also explain the interaction of this system with morphine molecules, as proved by EIS measurements. The electrochemical results displayed in this work indicate that electrodes modified PNMPy/PSSA microstructures are potential candidates for the development of new chemo- and bio-sensors, including drugs detectors.

### 5.1.5 – References

[1] B. Städler, A. D. Price, R. Chandrawati, L. Hosta-Rigau, A. N. Zelikin, F. Caruso, *Nanoscale* 1 (2009) 68.

[2] Y. Wang, A. S. Angelatos, F. Caruso, *Chem. Mat.* 20 (2008) 848.

[3] J. F. Quinn, A. P. R. Johnston, G. K. Such, A. N. Zelikin, F. Caruso, *Chem. Soc. Rev.* 36 (2007) 707.

[4] M. Wan, *Macromol. Rapid Commun.* 30 (2009) 963.

[5] R. V. Parthasarathy, C. R. Martin, *J. Appl. Polym. Sci.* 62 (1996) 875.

[6] J. Jang, J. H. Oh, J. Li, *Mater. Chem.* 14 (2004) 2872.

[7] J. Jang, J. H. Oh, *Adv. Mater.* 15 (2003) 977.

[8] H. B. Xia, D. M. Cheng, C. Y. Xiao, H. S. O. Chan, *J. Mat. Chem.* 15 (2005) 4161.

[9] L. Qu, G. Shi, F. Chen, J. Zhang, *Macromolecules* 36 (2003) 1063.

[10] L. Qu, G. Shi, *Chem. Commun.* (2003) 206.

[11] J. Yuan, D. Zhang, L. Qu, G. Shi, X. Hong, *Polym. Int.* 53 (2004) 2125.

[12] L. Qu, G. Shi, J. Yuan, G. Han, F. Chen, *J. Electroanal. Chem.* 561 (2004) 149.

[13] L. Qu, G. Shi, J. *Polym. Sci. Pol. Chem.* 42 (2004) 3170.

[14] M. Ma, L. Qu, G. Shi, *J. Appl. Polym. Sci.* 98 (2005) 2550.

[15] Y. Gao, L. Zhao, H. Bai, Q. Chen, G. Shi, *J. Electroanal. Chem.* 597 (2006) 13.

[16] X. He, C. Li, F. Chen, G. Shi*, Adv. Funct. Mater.* 17 (2007) 2911.

[17] M. Li, J. Yuan, G. Shi, *Thin Sol. Films* 516 (2008) 3836.

[18] C. Li, H. Bai, G. Shi, *Chem. Soc. Rev.* 38 (2009) 2397.

[19] P. Hammond, *Adv. Mat.* 16 (2004) 1271.

[20] D. G. Shchukin, K. Köhler, H. Möhwald, *J. Am. Chem. Soc.* 128 (2006) 4560.

[21] V. Bajpai, P. He, L. Dai, *Adv. Funct. Mater.* 14 (2004) 145.

[22] J. Yuan, L. Qu, D. Zhang, G. Shi, *Chem. Commun.* 8 (2004) 994.

[23] B. Parakhonskiy, D. Andreeva, H. Möhwald, D. G. Shchukin, *Langmuir* 25 (2009) 4780.

[24] D. V. Andreeva, D. A. Gorin, D. G. Shchukin, G. B. Sukhorukov, *Macromol. Rapid Commun.* 27 (2006) 931.

[25] F. N. Obame, C. Plin-Mercier, R. Assaly, R. Zini, J. L. Dubois-Rande, A. Berdeaux, D. Morin, *J. Pharm. Exp. Therap.* 326 (2008) 252.

[26] K. A. Johnson, D. Kriz, *Instrum. Sci. & Techn.* 25 (1997) 29.

[27] B. R. Scharifker, D. J. Fermin, *J. Electroanal. Chem.* 365 (1994) 35.

[28] O. Schneider, G. Schwitzgebel, *Synth. Met.* 93 (1998) 219.

[29] S. Fletcher, C. S. Halliday, D. Gates, M. Westcott, T. Lwin, G. Nelson, *J. Electroanal. Chem.* 159 (1983) 267.

[30] J. Arjomandi, R. Holze, *Synth. Met.* 157 (2007) 1021.

[31] J. Heinze, A. Rasche, M. Pagels, B. Geschke, *J. Phys. Chem.* B 111 (2007) 989.

[32] C. Alemán, J. Casanovas, J. Torras, O. Bertran, E. Armelin, R. Oliver, F. Estrany, *Polymer* 49 (2008) 1066.

[33] J. Haslam, H. A. Willis, *Identification and Analysis of Plastics*, *2nd. Ed.*, Iliffe Books Ltd. Ed. (1967) p.28.

[34] C. Ocampo, C. Alemán, R. Oliver, M. L. Arnedillo, O. Ruíz, F. Estrany, *Polym. Int.* 56 **(**2007) 803.

[35] L. H. Dall'Antonia, M. E. Vidotti, S. I. Córdoba de Torresi, R. M. Torresi, *Electroanal.* 14 (2002) 1577.

[36] A. Cambra, M. I. Redondo, M. J. Gonzalez-Tejera, *Synth. Met.* 139 (2003) 21.

[37] D. Aradilla, F. Estrany, E. Armelin, R. Oliver, J. I. Iribarren, C. Alemán, *Macromol. Chem. Phys.* 211 (2010) 1663.

[38] B. Stuart, *Infrared Spectroscopy: Fundamentals and Applications*, New York, Ed. John Wiley & Sons Ltd., 2004, Chapter 6, pp. 117 and 198.

[39] Y. C. Liu, B. J. Hwang, *Synth. Met.* 113 (2000) 203.

[40] J. Duchet, R. Legras, S. Demoustier-Champagne, *Synth. Met.* 98 (1998) 113.

[41] K. P. R. Nilsson, J. Rydberg, L. Baltzer, O. Inganäs, *Proc. Natl. Acad. Sci.* USA 101 (2004) 11197.

[42] B. Rezaei, S. Damiri, *J. Solid State Electrochem.* 14 (2010) 1079.

[43] T. Kobayashi, H. Yoneyama, H. Tamura, *J. Electroanal. Chem.* 177 (1984) 293.

## 5.2 – Response of poly(3,4-ethylenedioxythiophene) to the interaction with morphine

The interaction between morphine, a very potent analgesic psychoactive drug, and poly(3,4-ethylenedioxythiophene) has been investigated considering different environments for the detection, *i.e.* acid (pH= 2), neutral (pH= 7) and basic (pH= 8.5 and 12) TRIS solutions. For this purpose, conducting polymer samples were incubated in morphine solutions and examined by cyclic voltammetry and electrochemical spectroscopy impedance, results being compared with those obtained using blank samples. The sensing ability of poly(3,4-ethylenedioxythiophene) has been found to be maximum at pH= 2 and 7 for incubation times of 3 h and 12 h, respectively, the anodic current density at 1.40 V being an excellent indicator of the interaction with morphine molecules. Moreover, detection measurements are reproducible after consecutive oxidation-reduction cycles due to the high electrostability of this conducting polymer. Scanning electron microscopy has been used to investigate the remarkable influence of the incubation medium, the oxidation-reduction processes and the absorption of morphine on the morphology of PEDOT. Finally, a simple portable device, which is based on the use of PEDOT electrodes and the optimum sensing conditions (pH= 2 and 3 h incubation), has been proposed for the detection of morphine.*

* - Results reported in this section have been provisionally accepted for publication in *Journal of Applied Polymer Science*.

### 5.2.1 – Introduction

Because their chemical and physical properties may be tailored over a wide range of characteristics, the use of polymers is finding a permanent place in sophisticated electronic measuring devices such as sensors.[1-5] Among this wide family of organic materials, intrinsically conducting polymers (CPs), which are π-conjugated macromolecules that show electrical, electrochemical and optical property changes when they are doped by some chemical agents, have emerged as attractive candidates for sensing elements. Thus, these property changes can be observed at room temperature when they are exposed to lower concentrations of chemical species, making CPs useful as sensors of gases, metallic ions, biomolecules, etc, for environmental and clinical monitoring. [6-17]

Poly(3,4-ethylenedioxythiophene) (Scheme 1), abbreviated PEDOT, and its derivatives were settled among the most successful CPs due to their excellent properties: high electrochemical and environmental stability, high conductivity, high transparency and high electrocompatibility.[18-24] Due to these advantageous properties, PEDOT is a very promising material for biosensor applications, as was recently reviewed.[25] We are currently interested

in the development of CP-based biosensors to detect narcotic drugs able to affect the road safety. Within this specific context, the development of advanced systems to detect morphine (MO), which is the principal active component in opium, is particularly interesting since it is frequently used in medicine to relieve severe pain of patients. The ability to drive is seriously affected by this extremely potent analgesic psychoactive drug, which in addition is toxic in excess or when abused.

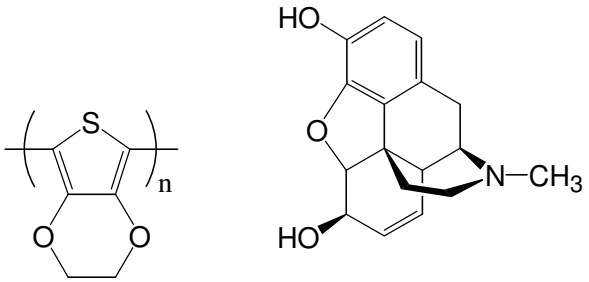


PEDOT MO

**Scheme 1 –** Molecular structure of PEDOT and MO.

Currently, detection of MO in clinical assays is carried out using high-performance liquid chromatography followed by UV spectroscopy and conventional electrochemical methods.[26-28] Recently, the excellent properties of PEDOT were used to propose a more convenient method to detect MO.[29,30] Specifically, a microfluidic system based on immobilized molecularly imprinted polymer (MIP) particles was used for the amperometric detection of the drug, the detection being successful with MO concentrations ranging from 0.01 to 0.2 mM. More recently, Atta and co-workers successfully investigated the electrochemical determination of MO at PEDOT modified platinum electrode in presence of sodium dodecyl sulfate.[31] In spite of the satisfactory results reported in such works, no other attempt to develop MO biosensors using this excellent and popular CP has been reported.[29-31]

In this work we present a comprehensive study about the intrinsic abilities of PEDOT to interact with MO. According to our recent findings on complexes formed by PEDOT and plasmid DNA, this CP is able to form weak specific interactions protecting nucleotide fragment with well-defined sequences from the attack of restriction enzymes.[31,32] This ability to form weak specific interactions is expected to play also an essential role in the detection of MO, which also contain groups able to act as hydrogen bonding donors (Scheme

1). Specifically, this study examines the detection of MO with PEDOT films deposited on platinum (Pt) electrodes using cyclic voltammetry (CV) and electrochemical impedance spectroscopy (EIS), and considering different pHs and incubation times.

### 5.2.2 – Methods

*Materials.* 3,4-ethylenedioxythiophene (EDOT) monomer and acetonitrile, both of analytical reagent grade, were purchased from Aldrich and used as received. Anhydrous $LiClO_4$, analytical reagent grade from Aldrich, was stored in an oven at 80 ˚C before use in the electrochemical trials. MO solution also was purchased from Aldrich, and used as received. TRIS buffer solutions, purchased from Aldrich, were adjusted to different pH values: pH=2 and 7 with HCl (purchased from Panreac), and pH=8.5 and 12 with NaOH (purchased from Panreac).

*Preparation*. PEDOT films were prepared by chronoamperometry (CA) under a constant potential of 1.40 V using polymerization times of $\theta$= 900 s and $\theta$= 300 s for CV and EIS studies, respectively. Anodic electropolymerization and electrochemical experiments were performed on a VersaStat II potenciostat-galvanostat using a three-electrode two-compartment cell under nitrogen atmosphere at 25 ˚C. The anodic compartment was filled with 40 mL of a 10 mM monomer solution in acetonitrile containing 0.1 M $LiClO_4$ as supporting electrolyte, while the cathodic compartment contained 10 mL of the same electrolyte solution. Pt and steel AISI 316 sheets of 1 $cm^2$ area were employed as working electrodes for CV and EIS experiments, respectively, whereas counter electrodes were made of steel AISI 316 in all cases. The reference electrode was an Ag|AgCl electrode containing a KCl saturated aqueous solution.

*Electrochemical behavior*. The ability to store charge (electroactivity) and electrochemical stability upon consecutive oxidation-reduction cycles (electrostability) of the films studied in this work were determined by CV using TRIS buffer solutions adjusted to pH = 2, 7, 8.5 and 12. The initial and final potentials were -0.50 V, while a reversal potential of 1.40 V was considered. The electroactivity increases with the similarity between the anodic and cathodic areas of the first control voltammogram, whereas the electrostability decreases with the oxidation and reduction areas of consecutive control voltammograms.

Accordingly, electroactivity and electrostability were determined through direct measure of the anodic and cathodic areas in the control voltammagrams using the Power Suite Princenton Applied Research software. A scan rate of 100 $mV \cdot s^{-1}$ was used in all cases. Cyclic voltammograms were recorded for PEDOT films deposited on Pt that were previously immersed at room temperature in TRIS buffer solutions at pH= 2, 7, 8.5 and 12 during 3 h, 12 h and 24 h (*blank samples*), and for PEDOT films deposited on Pt that were incubated at room temperature during 3, 12 and 24 h in 3.5 mM MO TRIS buffer solutions at pH= 2, 7, 8.5 and 12 (*incubated samples*).

EIS studies were carried out on an Autolab 302N potenciostat-galvanostat with GPES and FRA software programs (Eco Chimie, Netherlands) using a three-electrode compartment cell. The cell was filled with 45 mL of TRIS buffer solution at the desired pH values (pH= 2, 7, 8.5 and 12). Blank or incubated PEDOT films coating steel AISI 316 sheets were used as working electrodes. EIS measurements were carried out in the frequency range 1-10000 Hz using $\pm$0.05 V amplitude sinusoidal voltage for 70 frequencies at room temperature. The electrochemical cell was represented using a Randles circuit. The data obtained following the EIS experiments have been represented as a Nyquist plot. The expression for impedance (Z) is composed of real ($Z_{re}$) and imaginary ($Z_{im}$) parts. The imaginary part is due to capacitative effects of the alternating current frequency and the real part is due to resistance. The Nyquist graphic, in which $Z_{re}$ is plotted on the X axis and the negative of $Z_{im}$ on the Y-axis, for a bare electrode shows a semicircular region at higher frequencies on the $Z_{re}$ axis followed by a straight line.

*Morphological characterization*. The morphology of the blank and incubated PEDOT samples was examined using scanning electron microscopy (SEM). Images were analyzed using a Focused Ion Beam Zeiss Neon40 scanning electron microscope at 3 kV.

### 5.2.3 – Results and Discussion

The interaction between the CP and MO was examined by CV considering incubation times of 3 h, 12 h and 24 h and pH values of 2, 7, 8.5 and 12. Comparison of the control voltammograms of the blank and incubated PEDOT samples with those of uncoated Pt is provided in Figure 1. It is worth noting that the electrochemical responses of the incubated

samples were different from those obtained for the blank ones in all cases with exception of pH=12, for which the electrochemical response was very weak in all cases. Due to this feature, the latter medium was discarded for subsequent MO detection studies.

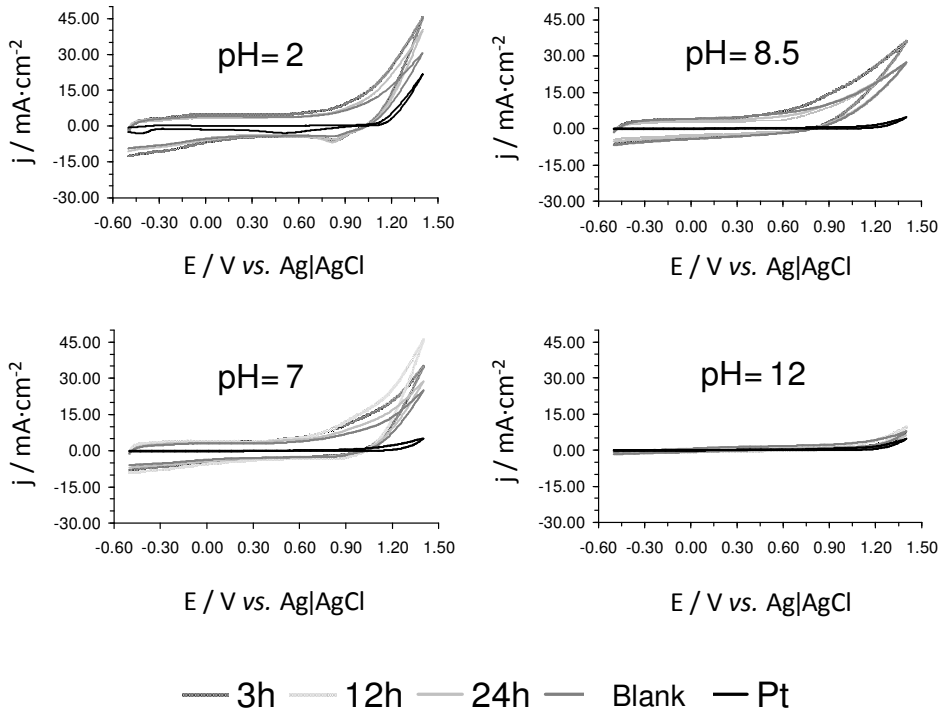


**Figure 1** – Control voltammograms for the oxidation of 3 h, 12 h and 24 h incubated PEDOT samples and the corresponding blank ones. The voltammogram recorded for the uncoated Pt electrode has been included for comparison. Voltammograms were recorded in TRIS solutions at pH= 2, 7, 8.5 and 12. Initial and final potentials: -0.50 V; reversal potential: 1.40 V; scan rate: 100 $mV \cdot s^{-1}$.

Furthermore, the response of PEDOT changes with both the incubation time and the pH. Control voltammograms displayed in Figure 1 indicate that the anodic current density increases from 1.00 V, reaching the maximum value ($j_{max}$) at the reversal potential, 1.40 V, in all cases. The larger $j_{max}$ values were obtained at pH= 2 and 7 for incubation times of 3 h and 12 h, respectively. These $j_{max}$ values are 45.3 $mA \cdot cm^{-2}$ (pH= 2, 3 h) and 45.9 $mA \cdot cm^{-2}$ (pH= 7, 12 h), different incubation times at the same pHs providing significantly lower values (*e.g.* at pH= 7, $j_{max}$=35.0 and 28.7 $mA \cdot cm^{-2}$ for incubation times of 3 h and 24 h, respectively). It should be noted that $j_{max}$ decreases significantly at basic pHs, the largest value at pH= 8.5

being 36.1 $mA \cdot cm^{-2}$ (3 h). On the other hand, it should be remarked that the cyclic voltammogram obtained at pH= 7 for the 12 h incubated sample is the only with an oxidation shoulder, $E_p^a$= 1.02 V, indicating that such conditions considerably favour the interaction of the MO molecules with the PEDOT film.

The electroactivity ($\Delta Q$) consists on the reversible ability to store charge, being directly related with the anodic intensity values obtained for the different anodic scanning potentials. This property has been determined by measuring the area of the voltammograms displayed in Figure 1. Results indicate that the $\Delta Q$ values of samples incubated at pH= 2 and 7 are significantly larger than that of the blank samples, which is fully consistent with the observed $j_{max}$ values. At pH=2, the ability to store charge of the 3 h, 12 h and 24 h incubated samples is 57%, 28% and 22 %, respectively, larger than that of the corresponding blank samples. The increase of $\Delta Q$ detected at pH= 7 is maximum for the 12 h incubated sample (*i.e.* ~87%). Amazingly, the $\Delta Q$ of blank PEDOT is 90% higher at pH= 8.5 than at pH= 2 and 7, whereas in opposition the incubated samples show the lowest $\Delta Q$ at such basic pH. Indeed, the only significant enhancement of $\Delta Q$ at pH= 8.5 occurs for the 3h sample (27%), the difference being lower than 10% for the 12 h and 24 h incubated samples. This fact suggests that the basic pH is not the most appropriated for the MO detection.

The electrochemical stability of CPs, also denoted electrostability, quantifies how the ability to store charge of the material decreases upon consecutive oxidation-reduction cycles. This property, which is essential for technological applications related with electronics, allows to measure how repetitive is the measure of an electrochemical parameter for the detection of MO without detriment in the intensity of the signal. Within this context, it should be mentioned that PEDOT is among the more, if not the most, electrostable polythiophene derivatives.[18-23] Figure 2 shows the control voltammograms recorded after 10 consecutive oxidation-reduction cycles for samples at pH= 2 and pH= 7. Comparison with Figure 1 indicates that the ability to store charge of the incubated and blank samples is considerably preserved, especially in acid conditions, evidencing the usefulness of this CP for the fabrication of efficient MO detectors.

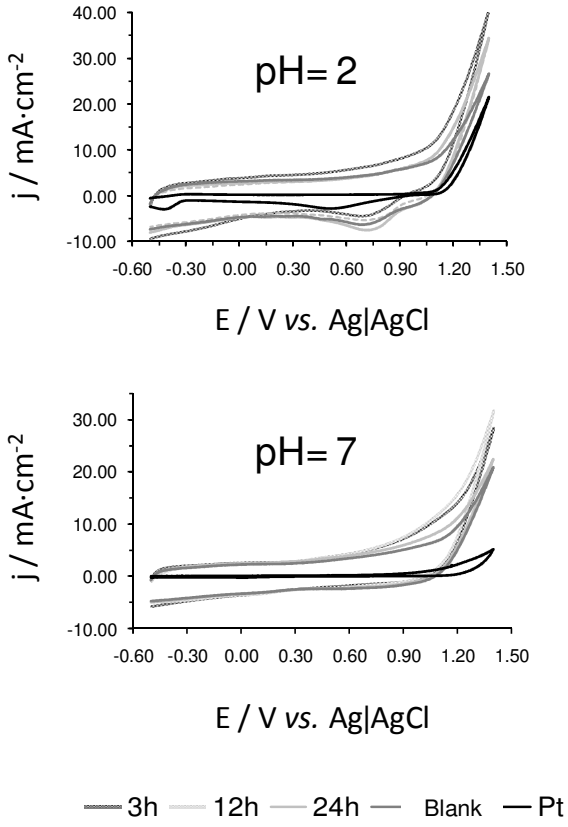


**Figure 2 –** Control voltammograms for the oxidation 3 h, 12 h and 24 h incubated PEDOT samples and the corresponding blank ones after 10 consecutive oxidation-reduction cycles. The voltammogram recorded for the uncoated Pt electrode has been included for comparison. Voltammograms were recorded in TRIS buffer solutions at pH= 2 and 7. Initial and final potentials: -0.50 V; reversal potential: 1.40 V; scan rate: 100 $mV \cdot s^{-1}$.

Figure 3 compares the SEM micrographs of the 24 h incubated samples at pH= 2, 7 and 8.5 with the corresponding blank samples. The globular morphology obtained for the blank sample at pH= 2, which is very similar to that reported for PEDOT produced in other organic media (*e.g.* acetonitrile solution), indicates that the TRIS buffer solution does not affect significantly the surface of the film in such conditions.[33] Thus, the SEM image of the blank film at pH= 2 reflects a porous structure formed by a dense network of thin fiber-like morphologies connecting small clusters of aggregated molecules that are located at very different levels. In spite of this, it should be noted the occasional apparition of small regions covered by a compact coating, which has been attributed to the deposition of small

molecules. In contrast, blank samples at pH= 7 and 8.5 are completely covered by such compact coating, evidencing the significant impact of neutral and basic pHs. Inspection to the morphology of the incubated samples indicates that the MO inhibits considerably the influence of the pH. Thus, incubated films retain the globular and porous morphology typically reported for PEDOT.[33]

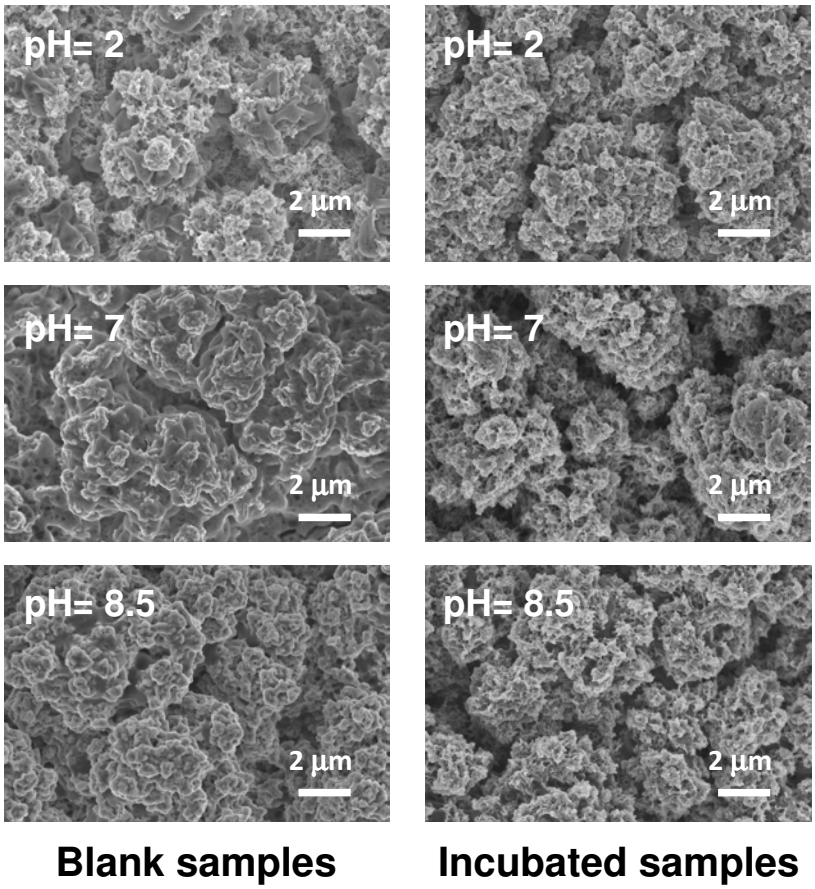


**Figure 3 –** SEM micrographs of the blank and 24 h incubated samples at pH= 2, 7 and 8.5.

Figure 4 shows SEM micrographs of the 24 h incubated and blank samples at pH= 2, 7 and 8.5 after 15 consecutive oxidation-reduction cycles. As it can be seen, the morphology of all samples underwent drastic changes due to the degradation at the surface. The globular and porous morphology transform into a compact and relatively flat surface, the fiber-like structures that connect the molecular aggregates disappearing in all cases. This behaviour is

fully consistent with the reduction of electroactivity upon consecutive oxidation-reduction processes. Furthermore, in this case morphological changes at the surface of PEDOT films are accentuated by presence of MO in the incubation media, especially at pH= 2.

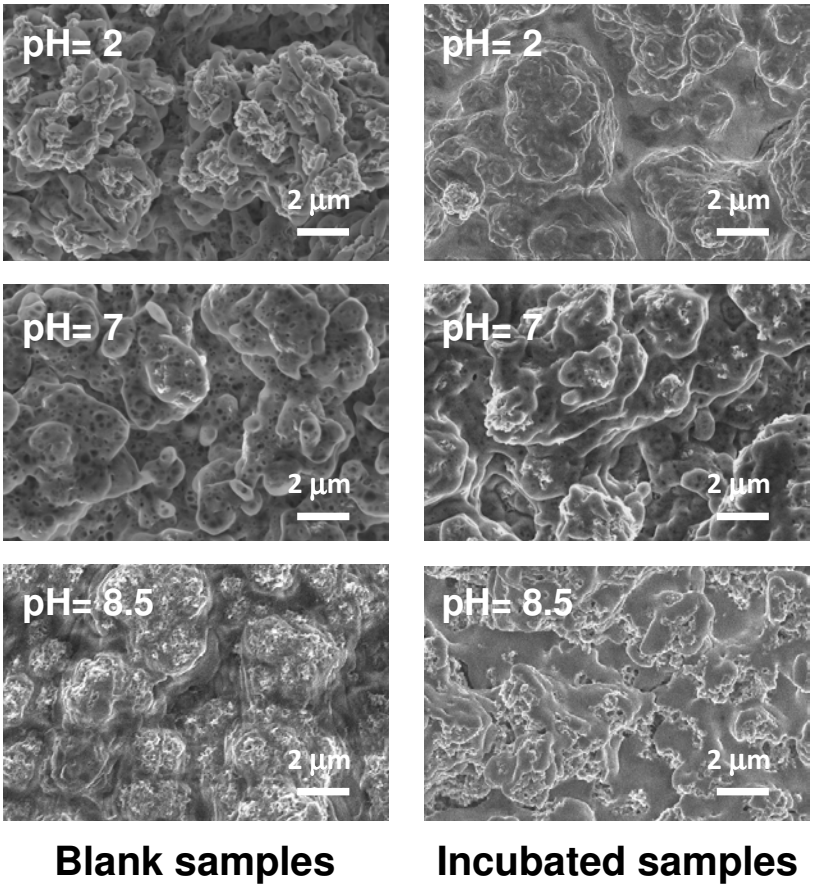


**Figure 4 –** SEM micrographs of the blank and 24 h incubated samples at pH= 2, 7 and 8.5, after 15 consecutive oxidation-reduction cycles.

Electrochemical impedance spectroscopy (EIS) is an effective analytical method for detection since it is very sensible to the interfacial response of surface modified electrodes by applying periodic small amplitude signals. In this case, the adsorption or desorption of insulating MO on the conductive supports can be assayed due to the change of the interfacial electron transfer features at the electrode surface.[34] In the last years, EIS has been used for the determination of DNA, proteins, small drugs, etc. offering important

information about the electrode interfacial properties such as electronic transport resistance and double layer capacitance.[35-37] Figure 5 displays the Nyquist plot recorded for the isolated and incubated PEDOT samples. The polymer resistance ($R_P$) and the double-layer capacitance ($C_{DL}$) obtained by fitting the Nyquist graphic to a Randles circuit are displayed in Table 1.

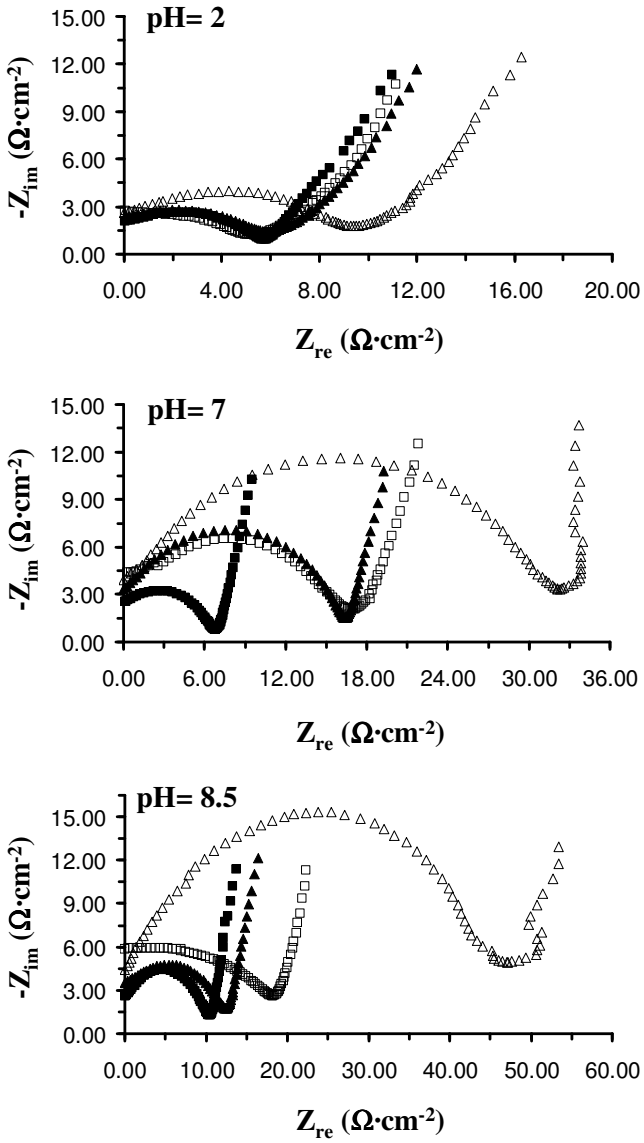


**Figure 5 –** Impedance plots obtained for incubated (3, 12 and 24 h) and blank PEDOT samples at pH= 2, 7 and 8.5.

**Table 1 –** Polymer resistance ($R_P$) and double-layer capacitance ($C_{DL}$) obtained by fitting the Nyquist graphics displayed in Figure 5 to a Randles circuit.

| | Incubation time | $R_p$ ($\Omega/cm^2$) | $C_{dl}$ ($\mu F$) |
|---|---|---|---|
| **pH= 2** | -[(a)] | 7.89 | 72 |
| | 3 h | 8.87 | 104 |
| | 12 h | 13.86 | 47 |
| | 24 h | 10.05 | 139 |
| **pH= 7** | -[(a)] | 8.43 | 41 |
| | 3 h | 17.82 | 32 |
| | 12 h | 34.37 | 62 |
| | 24 h | 18.86 | 66 |
| **pH= 8.5** | -[(a)] | 12.51 | 49 |
| | 3 h | 14.78 | 100 |
| | 12 h | 44.53 | 60 |
| | 24 h | 30.01 | 170 |

EIS spectra of blank PEDOT samples included a semicircle part and a linear part. The semicircle part corresponds to the electron transfer process while the linear part arises from the diffusion process. The semicircular portion of the graphs indicates the impedance due to both the kinetics processes produced by imperfections at the coated electrode surface and the resistance provided by the modified polymer, *i.e.* the semicircular region is expected to be sensible to the presence or absence of adsorbed MO molecules. In the Randles circuit, $R_P$ corresponds to the diameter of the semicircle. The value of $R_P$ of blank samples was found to vary between 7.89 (pH= 2) and 12.51 $\Omega/cm^2$ (pH= 8.5).

MO produces drastic changes in the EIS spectra of the incubated samples, which depend not only on the pH but also on the incubation time. Thus, $R_p$ increases in all cases, the largest $\Delta R_p$ values being measured after 12h of incubation for all the investigated pHs. The % $\Delta R_p$ range of variation for the 3, 12 and 24 h incubated samples ranges from 12% (pH= 2) to 111% (pH= 7), from 76% (pH= 2) to 308% (pH=7) and from 27% (pH= 2) to 140% (pH=8.5), respectively. Although the variation produced by the adsorbed MO in the resistance of the polymer is considerable in all cases, it is particularly remarkable when the incubation time is 12 h.

The dependence of both the CV and EIS results on the incubation time suggests that the interaction between PEDOT and MO is through weak non-covalent interactions. Thus, the electrochemical response of the 24 h incubated samples is, independently of the pH lower, than those obtained using smaller incubation times, which indicates that the adsorbed MO molecules are partially delivered from the PEDOT surface to the incubation medium after 12 h. This feature probes the non-covalent nature of the interactions that immobilize the MO molecules, which are broken because of the degradation of the polymer surface. This is fully consistent with our recent results on complexes formed by CPs and plasmid DNA. Thus, we detect the formation of specific weak interactions with CP bearing groups able to from hydrogen bonds (*e.g.* PEDOT).[32,38,39]

Although both CV and EIS have been found to be very efficient techniques for the detection of MO using PEDOT modified electrodes, the latter presents a practical difficulty since it requires a potentiostat with specific accessories. In contrast, the simplicity of the equipments used for CV measurements combined with the effect of MO on the anodic density at 1.40 V, especially for 3h (pH= 2) and 12h (pH= 7) incubated samples, can be used to propose a simple analytical procedure for the detection of this psychoactive drug in the human body. Within this context, detection at pH=2 is clearly more desirable than at pH=7 since the former acid environment requires the lowest incubation time and minimizes the degradation produced by the TRIS solution on the PEDOT surface. Considering such conditions (*i.e.* pH= 2 and 3 h incubation time), detection of MO could be carried out by individual measurements of the anodic intensity at a potential of 1.40 V, the complete scanning of potentials used in control voltammograms being not necessary. On the basis of these results, we propose a simple detection device, which is schematically displayed in Figure 6, based on a simple portable potentiostat as well as disposable and interchangeable electrodes (*i.e.* two small (1 $cm^2$) electrodes: the working electrode made of a Pt sheet modified with PEDOT and the counter electrode made of uncoated steel).

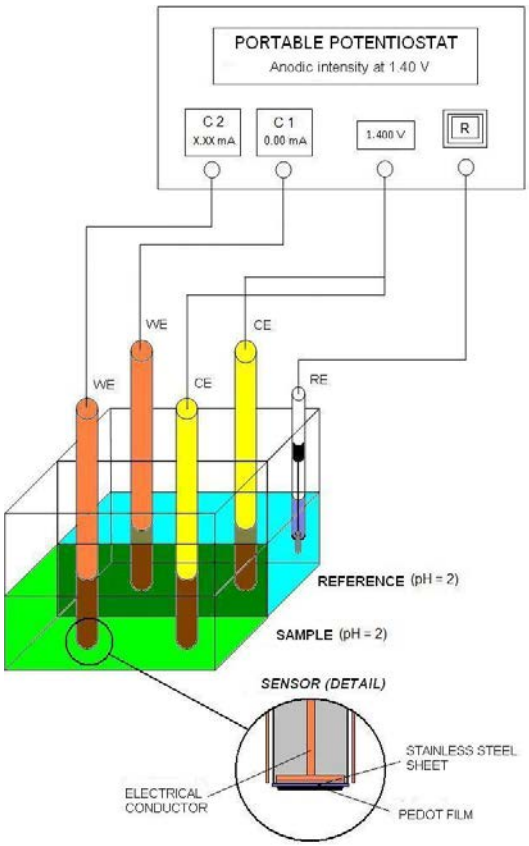


**Figure 6 –** Device proposed for the detection of MO. WE and CE refer to the working and counter electrodes, respectively.

## 5.2.4 – Conclusions

CV assays in TRIS solutions clearly indicate that the electrochemical response of the incubated and blank PEDOT samples is very different at acid and neutral pHs. Cyclic voltammgrams indicate that the interaction between this CP and the MO molecules can be easily identified by comparing the $j_{max}$ values measured at 1.40 V. Although the $j_{max}$ obtained for the incubated sample is significantly larger than that of the blank one in all cases, the maximum difference is observed for incubation times of 3 h (pH= 2) and 12 h (pH= 7). Furthermore, the incorporation of MO to the incubation medium also produces a significant enhancement in the electroactivity of PEDOT, indicating that the ability to store charge of the incubated samples is larger than the blank ones. The maximum increment was detected

for incubation times of 3 h (pH= 2) and 12 h (pH= 7), which is fully consistent with the effect on MO on $j_{max}$. The effect of consecutive oxidation-reduction cycles in $j_{max}$ is relatively small, which should be attributed to the high electrostability of PEDOT. This feature ensures that measures provided by a detection device based on the electrochemical response of incubated PEDOT will be reproducible.

Comparison of the SEM micrographs obtained for blank and incubated samples indicates that the influence of the medium on the morphology of PEDOT, which is very significant at neutral and basic pHs, is inhibited by MO. Thus, independently of both the pH and the incubation time, the morphology of incubated samples is very similar to that typically observed for this conducting polymer. However, this protective role disappears when samples undergo consecutive oxidation-reduction cycles, which produce a considerable degradation of the conducting polymer surface in all cases.

On the other hand, EIS measurements on blank and incubated PEDOT samples evidenced the large effect produced by the adsorbed MO molecules in the resistance of the polymer. This feature was found to be particularly remarkable when the incubation time is 12 h. The fact that the electrochemical response of the 24 h incubated samples is in all cases smaller than that of the 12 h ones indicates that the adsorbed MO are delivered to the incubation medium when the medium degrades the PEDOT surface. This suggests that the MO molecules and the PEDOT surface interact through relatively weak non-covalent forces.

Finally, a simple detection device for the identification of small concentrations of MO has been proposed. This is based on the use of a portable potentiostat, a working Pt electrode coated with PEDOT and an uncoated counter electrode. The proposed device is expected to detect small concentrations of MO by performing reproducible measurements of the anodic intensity at 1.40 V of samples incubated 3 h in acid TRIS solution.

### 5.2.5 – References

[1] S. Cosnier, *Electroanalysis* 17 (2005) 1701.

[2] B. Adhikari, S. Majumdar, *Prog. Polym. Sci.* 29 (2004) 699.

[3] B. D. Malhotra, A. Chaubey, S. P. Singh, *Anal. Chim. Acta* 578 (2006) 59.

[4] L. A. Terry, S. F. White, L. J. Tigwell, *J. Agric. Food Chem.* 53 (2005) 1309.

[5] T. G. Drummond, M. G. Hill, J. K. Barton, *Nat. Biotechnol.* 21 (2003) 1192.

[6] S. J. Marsella, P. J. Carroll, T. M. Swager, *J. Am. Chem. Soc.* 177 (1995) 9832.

[7] L. Torsi, M. Pezzuto, P. Siciliano, R. Rella, L. Sabbatini, L. Valli, P. Zambonin, *Sensors Actuators* 48 (1998) 262.

[8] K. Ogura, T. Saino, M. Nakayama, H. Shiigi, *J. Mat. Chem.* 7 (1997) 2363.

[9] M. J. Marsella, T. M. Swager, *J. Am. Chem. Soc.* 115 (1993) 12214.

[10] P. Bäuerle, S. Scheib, *Adv. Mater.* 5 (1993) 848.

[11] B. Jousselme, P. Blanchard, E. Levillain, J. Delaunay, M. Allain, P. Richomme, D. Rondeau, N. Gallego-Planas, J. Roncali, *J. Am. Chem. Soc.* 125 (2003) 1364.

[12] J. Casanovas, J. Preat, D. Zanuy, C. Alemán, *Chem. Eur. J.* 15 (2009) 4676.

[13] B. S. Gaylord, A. J. Heeger, G. Bazan, *Proc. Natl. Acad. Sci. USA* 99 (2002) 10954.

[14] H.-A. Ho, M. Bossinot, M. G. Bergeron, G. Corbeil, K. Doré, B. Boudreau, M. Leclerc, *Angew. Chem. Int. Ed.* 41 (2002) 1548.

[15] A. Azioune, M. M. Chehimi, B. Miksa, T. Basinska, S. Slonkowski, *Langmouir* 18 (2002) 1150.

[16] G. G. Wallace, L. A. P. Kane-Maguire, *Adv. Mater.* 14 (2002) 953.

[17] M. Martí, G. Fabregat, F. Estrany, C. Alemán, E. Armelin, *J. Mat. Chem.* 20 (2010) 10652.

[18] L. B. Goenendaal, F. Jonas, D. Freitag, H. Pielartzik, J. R. Reynolds, *Adv. Mater.* 12 (2000) 481.

[19] Q. Pei, G. Zuccarello, M. Ahlskog, O. Inganäs, *Polymer* 35 (1994) 1347.

[20] F. Estrany, D. Aradilla, R. Oliver, C. Alemán, *Eur. Polym. J.* 43 (2007) 1876.

[21] D.-H. Han, J.-W. Kim, S.-M. Park, *J. Phys. Chem. B* 110 (2006) 14874.

[22] K. E. Aasmundtveit, E. J. Samuelsen, O. Inganäs, L. A. A. Pettersson, T. Johansson, S. Ferrer, *Synth. Met.* 11 (2000) 393.

[23] L. A. A. Pettersson, F. Carlsson, O. Inganäs, H. Arwin, *Thin Solid Films* 313 (1998) 356.

[24] L. J. del Valle, F. Estrany, E. Armelin, R. Oliver, C. Alemán, *Macromol. Biosci.* 11 (2008) 1144.

[25] N. Rozlosnik, *Anal. Bioanal. Chem.* 395 (2009) 637.

[26] G. Chari, A. Gulati, R. Bhat, I. R. Tebbett, *J. Chromatogr.* 571 (1991) 263.

[27] J. E. Wallace, S. C. Harris, M. W. Peek, *Anal. Chem.* 52 (1980) 1328.

[28] W. J. Liaw, S. T. Ho, J. J. Wang, O. Y. P. Hu, J. H. Li, *J. Chromatogr. B* 714 (1998) 237.

[29] K.-C. Ho, W.-M. Yeh, T.-S. Tung, J.-Y. Liao, *Anal. Chim. Acta* 542 (2005) 90.

[30] C.-H. Weng, W.-M. Yeh, K.-C. Ho, G.-B. Lee, *Sens. Actuators B* 121 (2007) 576.

[31] N. F. Atta, A. Galal, R. A. Ahmed, *Electroanalysis* 23 (2011) 737.

[32] C. Alemán, B. Teixeira-Dias, D. Zanuy, F. Estrany, E. Armelin, L. J. del Valle, *Polymer* 50 (2009) 1965.

[33] D. Aradilla, F. Estrany, C. Alemán, *J. Phys. Chem. C* 115 (2011) 8430.

[34] S.-M. Park, J.-S. Yoo, *Anal. Chem.* 75 (2003) 455A.

[35] L. Alfonta, A. K. Singh, I. Willner, *Anal. Chem.* 73 (2001) 91.

[36] M. J. Wang, L. J. Wang, G. Wang, X. H. Ji, Y. B. Bai, T. J. Li, S. Y. Gong, J. H. Li, *Biosens. Bioelectron.* 19 (2004) 575.

[37] Y. Long, L. Nie, J. Chen, S. Yao, *J. Colloid Interface Sci.* 263 (2003) 106.

[38] B. Teixeira-Dias, D. Zanuy, L. J. del Valle, F. Estrany, E. Armelin, C. Alemán, *Macromol. Chem. Phys.* 211 (2010) 1117.

[39] C. Ocampo, R. Oliver E. Armelin, C. Alemán, F. Estrany, *J. Polym. Res.* 13 (2006) 193.

# Chapter 6

# Conducting Biocomposites

# 6.1 – Conducting polymer-protein composite with antibactericidal and electroactive properties

Lysozyme, an enzyme with bactericidal activity over Gram-positive bacteria cells, has been incorporated in poly(3,4-ethylenedioxythiophene), a conducting polymer with many potential applications in electronics and nanotechnology, for the preparation of films with high bio- and electrochemical activity. For this purpose, two different strategies have been used. In the first one, poly(3,4-ethylenedioxythiophene) films were coated with a layer of enzyme, which was adsorbed on the surface, whereas in the second one the lysozyme was added in the polymerization medium used to prepare the conducting polymer. The enzyme adsorbed in the surface of the polymer produced a biphasic system that retains the electrochemical properties of the conducting polymer but practically unable to protect against bacterial growth. This latter drawback is due to the rapid release of the enzyme to physiological medium. In opposition, the addition of lysozyme to the polymerization medium results in a homogeneous composite in which the enzyme is entrapped within the material matrix. The new composite shows a very high bactericidal activity as well as a relatively high electrochemical activity, even though the latter is smaller than that observed for the unmodified conducting polymer. Moreover, incubation of the new homogeneous material in physiological conditions reflects a progressive, slow and controlled release of the enzyme.*

* - Results reported in this section have been submitted for publication.

## 6.1.1 – Introduction

CPs have electrical and optical properties similar to those of metallic and inorganic semiconductors, and also exhibit some properties typically associated with conventional polymers.[1-3] Among CPs poly(3,4-ethylenedioxythiophene), hereafter abbreviated PEDOT, has emerged as a promising material in different fields, such as electronics and nanotechnology.[4-7] This polythiophene derivative presents high conductivity (up to 500 S/cm), good thermal and chemical stability, fast doping-dedoping processes and excellent electrochemical properties in terms of electroactivity and electrostability.[4-7]

Although the interaction of common CPs (*i.e.* polyaniline and, specially, polypyrrole derivatives) with selected bioentitites, such as amino acids, proteins, DNA and living cells, has been extensively studied, it has been only quite recently that polythiophene derivatives have been explored as materials with promising biotechnological and/or biomedical applications.[8-33] Within these exciting fields, PEDOT has been used to: recognize specific nucleotide sequences; interact with epithelial, fibroblasts and neuronal cells favoring their

adhesion and proliferation; prepare bifunctional films with high bio- and electrochemical activities through the incorporation of collagen, which is one of the known constituents of the extracellular matrix of neurons; construct functionalized devices for protein detection; etc.[12-33]

The quest to interact more efficiently with biosystems, to obtain information related to system performance, to control that performance and to develop new biomedical applications based on CPs remain an essential area of research. In this work we report the interaction of PEDOT with lysozyme (also known as muramidase or N-acetylmuramide glycanhydrolase), an enzyme (EC 3.2.1.17) with bactericidal activity, especially over Gram-positive bacteria cells. This enzyme (129 aminoacids), which is non-specific, produces damage on bacterial cells walls by catalyzing the hydrolysis of the glycosidic bonds between *N*-acetylmuramic acid and *N*-acetylglucosamine residues in peptidoglycan. Its catalytic activity provides some protection against bacterial infections. Thus, the lytic activity on the cell wall of a broad spectrum of Gram-positive micro-organisms led to use lysozyme in alimentary, as a preservative of many food products (*e.g.* wine and cheese), and in pharmaceutical applications related with otorhinolaryngology (*e.g.* treatment of sore throats and of canker sores), and in ophthalmology (*e.g.* eye drop and solutions for the decontamination of contact lenses).[34-36]

In this work we use lysozyme to protect PEDOT films from infection of bacterial micro-organisms. It should be emphasized that PEDOT has been reported to be an efficient electroactive substrate for the adhesion and growing of eukaryotic cells.[26,28] Accordingly, the development of PEDOT films with bactericidal activity is expected to be of great importance in fields like biotechnology and bioengineering, in which PEDOT has many potential applications (*e.g.* tissue regeneration, components of orthopedic devices, and implantable neural and cochlear electrodes). Two different strategies have been used: (i) adsorption of lysozyme on the surface of PEDOT substrates, hereafter denoted PEDOT/LZ; and (ii) anodic electro-copolymerization considering a solution containing both the 3,4-ethylenedioxythiophene (EDOT) monomer and lysozyme, the resulting material being called P(EDOT-LZ). It should be emphasized that P(EDOT-LZ) is a new hybrid material in which the two constituents are homogenously distributed, whereas the binding between the CP and the enzyme is physical in PEDOT/LZ. The morphology, secondary structure and stability of the enzyme, and electroactivity of both PEDOT/LZ and P(EDOT-LZ) have been examined and

compared. Results indicate that P(EDOT-LZ) should be considered as a new bifunctional material with bactericidal and electrochemical activities.

### 6.1.2 – Methods

*Materials.* EDOT monomer was purchased from Aldrich and used as received. Anhydrous $LiClO_4$ from Aldrich, analytical reagent grade, was stored in an oven at 80 ˚C before use in the electrochemical trials. Lysozyme (chicken egg white) was obtained from Sigma and used as received.

*Synthesis of PEDOT.* The CP was prepared by chronoamperometry (CA) under a constant potential of 1.40 V using a polymerization time of 600 s. Both anodic electropolymerization and electrochemical experiments were performed on a VersaStat II potenciostat-galvanostat using a three-electrode two-compartment cell under nitrogen atmosphere (99.995% in purity) at 25 ˚C. The anodic compartment was filled with 40 mL of a 0.01 M monomer solution in acetonitrile containing 0.1 M $LiClO_4$ as supporting electrolyte, while the cathodic compartment contained 10 mL of the same electrolyte solution. Steel AISI 316 sheets of 1 $cm^2$ area were employed as working and counter electrodes. In order to avoid interferences during the electrochemical analyses, the working and counter electrodes were cleaned with acetone before each trial. The reference electrode was an Ag|AgCl electrode containing a KCl saturated aqueous solution ($E^o$ = 0.222 V vs. standard hydrogen electrode at 25 ˚C), which was connected to the working compartment through a salt bridge containing the electrolyte solution.

*Preparation of PEDOT/LZ: Adsorption of lysozyme on PEDOT films.* An aliquot of 40 µL of lysozyme in solution (1.0 µg/µL) was superficially adsorbed on PEDOT substrates. After drying in a vacuum oven, PEDOT/LZ films were stored at 4 ˚C.

*Synthesis of P(EDOT-LZ).* This new hybrid material was generated by CA using a constant potential of 1.40 V and a polymerization time of 600 s. An acetonitrile solution (10 mL) containing 0.01 M of EDOT monomer and 0.1 M of $LiClO_4$ was added to 40 mL of milliQ water solution containing 2 mL of lysozyme (250 mg/mL). The electrochemical process, the

potencisotant-galvanostat and the electrodes used for the preparation of P(EDOT-LZ) were identical to those employed for the synthesis of PEDOT.

*Scanning electron microscopy (SEM) and elemental analyses.* SEM studies were carried out using a Focussed Ion Beam Zeiss Neon 40 scanning electron microscopy equipped with an energy dispersive X-ray (EDX) spectroscopy system, which was used for the elemental analyses of the prepared materials, and operating at 10 kV.

*Electrochemical characterization*. The electrochemical behaviour of PEDOT, PEDOT/LZ and P(EDOT-LZ) films were studied by cyclic voltammetry (CV). Cyclic voltammograms were registered at a scan rate of $100mV{\cdot}s^{-1}$ in the potential range from -0.50 to +1.60 V. For these measurements, films were incubated at 37 ˚C in 10 mL of a sterilized phosphate buffer saline solution (PBS; pH= 7.4 adjusted with NaOH), which was also used as electrolyte in the three-electrode cell. Incubated samples during 28 days were retrieved and dried at intervals of 2 days for electrochemical analysis. PBS was prepared using 137 mM of NaCl (Pharmasal), 2.7 mM of KCl (Merk), 10 mM of $Na_2HPO_4$ (Fluka), 2 mM of $KH_2PO_4$ (Aldrich) and milliQ water.

*Electrophoresis.* The structural stability of the immobilized lysozyme into the surface (PEDOT/LZ samples) or matrix (P(EDOT-LZ) samples) of the CP was examined using dodecyl sulphate polyacrylamide gel electrophoresis, abbreviated SDS-PAGE. Native enzyme (free-state) and molecular weight markers were used as controls. Lysozyme was extracted from films using 0.2 mL Tris-HCl (0.06 mM, pH 6.8), dodecyl sulphate polyacrylamide (1% w/v) and β-mercaptoethanol (0.05% v/v). Samples were kept overnight in a shaker at 200 rpm and constant temperature of 27 ˚C. The resulting suspensions were heated for 10 minutes at 96 ˚C and centrifuged for 10 minutes at 13000 rpm. The supernatants were precipitated using cold acetone (6 vol acetone:1 vol sample) and, subsequently, recovered by centrifugation. After drying in vacuum, they were re-suspended in 50 µL of loading buffer for SDS-PAGE.

The lysozyme content of the extracted solution was determined by a UV-Vis spectrophotometer based on the method of Bradford, in which the concentration was obtained using a standard curve from known concentrations of lysozyme solutions.[37]

*FTIR spectroscopy*. FTIR spectra of lysozyme, PEDOT, PEDOT/LZ and P(EDOT-LZ) were recorded on a FTIR 4100 Jasco spectrophotometer. The samples were placed in an attenuated total reflection accessory with thermal control and a diamond crystal (Specac model MKII Golden Gate Heated Single Reflection Diamond ATR).

FTIR spectroscopy was used to examine the secondary structure of lysozyme. Specifically, the number and position of the peaks in the Amide I region, which were derived from the second derivative and deconvoluted spectra, provided information about the protein conformation. Fourier self-deconvolution was performed with the software PeakFit 4 (Jandel Scientific Software, AISN Software Inc.), the resulting profiles being fitted to Gaussian functions through the OriginPro 7.5 software.[38]

*Bacterial growth and adhesion.* The bacterial strains used in this work were *Escherichia coli* CECT 101 and *Staphylococcus epidermidis* CECT 231 from the Spanish Collection of Type Culture (CECT, Valencia, Spain). Bacteria were grown aerobically to exponential phase in broth culture (5 g/L beef extract, 5 g/L NaCl, 10 g/L peptone, pH 7.2 in distilled water). Bacterial growth was determined by measuring the absorbance at 600 nm with a UV/VIS Cary 100Bio spectrophotometer (Varian, Australia).

Growth experiments were performed in culture tubes of 15 mL. $10^3$ colony forming units (CFU) were seed in 5 mL of broth culture in presence of the materials prepared in this work. Cultures were incubated at 37 ˚C with 100 rpm agitation. After incubation for 24 and 48 h, a 100 µL aliquot was diluted 10 times in distilled water, and the absorbance at 600 nm measured. The bacterial number was counted using a McFarland curve.

Adhesion experiments were carried out using seeds of $10^7$-$10^8$ CFU in 5 mL of broth culture in the presence of investigated materials. Cultures were incubated at 37 ˚C with 100 rpm agitation. After incubation, cultures were aspired and the material washed one time using distilled water. Next, 1 mL of sterile 0.01M sodium thiosulfate was added and vortexes for 2 min. After this, samples were maintained 30 min in repose to remove the bacteria. Finally, 4 mL of broth culture was added and the tubes were incubated for 24 h at 37 ˚C and 100 rpm agitation. The bacterial growth was measured by absorbance at 600 nm allowing count the bacteria adhered on the surface of investigated materials.

All assays were performed in triplicate and results were obtained as the mean ± SD. The t-student test was used as statistical analysis at a confidence level of 95% ($p < 0.05$).

*Enzymatic activity.* The activity of the immobilized lysozyme was determined using a standard procedure.[39] *Micrococcus luteus* CECT 245 was selected as the substrate to determine the catalytic activity of lysozyme by examining the degradation rate of the peptidoglycan at the cells walls. The substrate was introduced and, subsequently, dispersed in a cuvette with TM buffer, *i.e.* 10 mM Tris (pH 6.5) and 5 mM $MgCl_2$. The prepared suspension was monitored by UV-Vis spectroscopy to determine the degradation rate of the *Micrococcus* walls through the variation in the absorbance. The suspension was ready for examination of the enzymatic activity when the absorbance stabilizes at 450 nm. After this, free lysozyme (dissolved in TM buffer), PEDOT/LZ, P(EDOT-LZ) and PEDOT were introduced in the *Micrococcus* suspension and the variation of the absorbance at 450 nm was recorded every 5 minutes.

Experiments were repeated three times for every system, the average curve being used for mathematical analysis. The decay of the enzymatic activity against time was adjusted to a first order model, ANOVA and $\chi^2$ tests being used to evaluate the reliability of such kinetic model.

### 6.1.3 – Results and Discussion

*Identification of the lysozyme and morphology of the PEDOT/LZ and P(EDOT-LZ) samples.*

Table 1 lists the C, O, S, N and Cl elemental composition in the surface of PEDOT, PEDOT/LZ and P(EDOT-LZ) obtained using EDX analysis, the penetration of this technique being limited to ~20 nm. The presence of nitrogen in PEDOT/LZ confirms that the PEDOT film is coated by the adsorbed enzyme. In contrast, the absence of nitrogen and the reduction of sulfur in P(EDOT-LZ) suggest that the enzyme is entrapped within the matrix forming a homogenous composite with the CP.

**Table 1 –** EDX analysis of the PEDOT, PEDOT/LZ and P(EDOT-LZ). The average (five samplings) content of C, O, S, N and Cl (in wt. %) and the corresponding standard deviation is listed for each case.

| | PEDOT | PEDOT/LZ | P(EDOT-LZ) |
|---|---|---|---|
| C | 57.61 ± 0.51 | 51.11 ± 2.72 | 58.66 ± 3.35 |
| O | 30.62 ± 2.46 | 23.23 ± 1.00 | 32.44 ± 3.62 |
| S | 8.99 ± 1.80 | 9.88 ± 1.76 | 4.76 ± 1.04 |
| N | - | 15.76 ± 1.57 | - |
| Cl | 2.78 ± 1.18 | - | 2.84 ± 0.56 |

Figures 1 and 2 show low- and high-resolution SEM images, respectively, comparing the morphologies of PEDOT, PEDOT/LZ and P(EDOT-LZ).

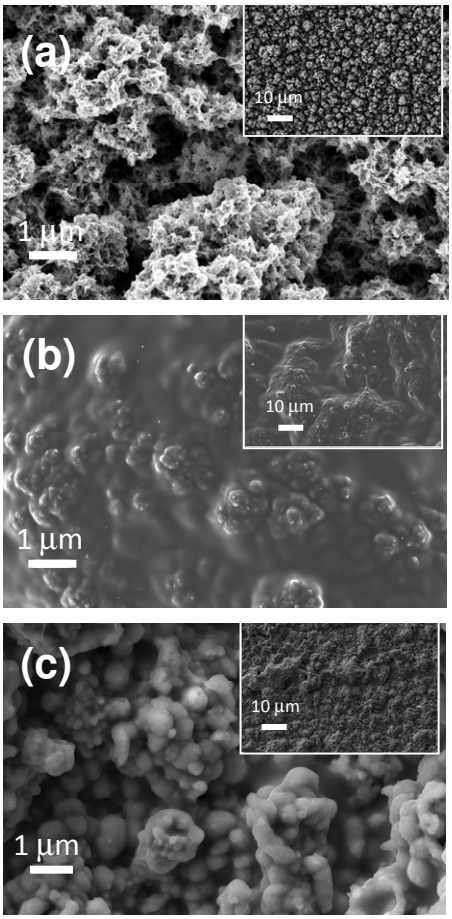


**Figure 1 –** Low resolution SEM images of (a) PEDOT, (b) PEDOT/LZ and (c) P(EDOT-LZ).

PEDOT films show a porous and spongy morphology in which irregular clusters of molecular aggregates connected by thin elements with a fiber-like morphology are uniformly distributed on the surface (Figure 1a and 2a).

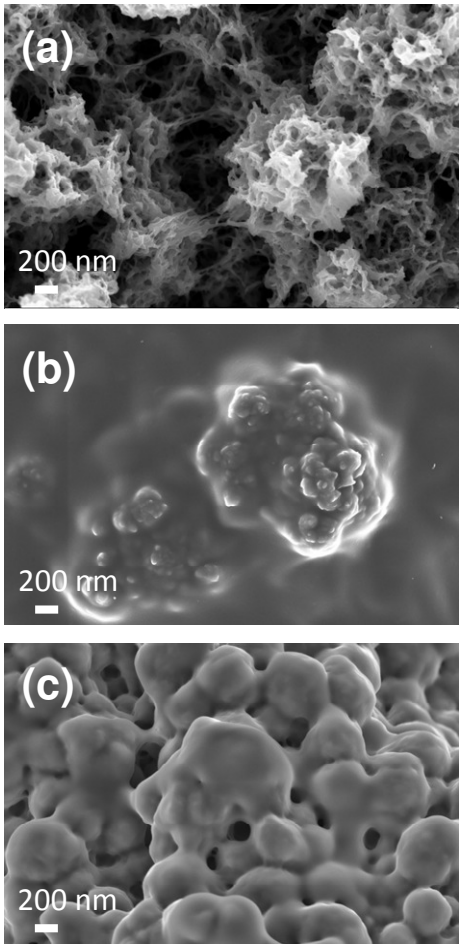


**Figure 2 –** High resolution SEM images of (a) PEDOT, (b) PEDOT/LZ and (c) P(EDOT-LZ).

The adsorption of the enzyme on the surface of PEDOT films results in a ultrathin uniform coating, which is clearly identified in Figures 1b and 2b, without produce significant alterations in the morphology of the CP. Thus, the CP remains below the enzyme coating in a separated phase that can be clearly distinguished, this feature being particularly evident for the protuberances associated to the clusters of PEDOT aggregates. The only relation between the two constituents is the physical contact at the interface between the PEDOT and lysozyme films.

In contrast, inspection to the P(EDOT-LZ) surface (Figures 1c and 2c) reveals significant changes with respect to PEDOT. The participation of the enzyme in the anodic polymerization process produces a material with a compact and irregular surface. Thus, the spongy appearance of PEDOT in the surface transforms into a smooth-like surface with protuberance formed by the dense aggregation of compact elements. This produces a reduction of the porosity found for the CP (Figure 2a). Furthermore, Figure 2c clearly shows that the enzyme and the CP form a single phase suggesting that P(EDOT-LZ) film is formed by a homogeneous composite. In order to ascertain, if this homogeneity is located in the surface only or distributed through the whole sample, the P(EDOT-LZ) film was carefully separated from the electrode to examine the morphology of the internal side. Inspection of low and high resolution micrographs, which are displayed in Figure 3, reveals the same structure for the whole sample. This allows one to conclude that P(EDOT-LZ) is a new material, in which the enzyme is entrapped in the matrix giving place to a uniformly distributed composite.

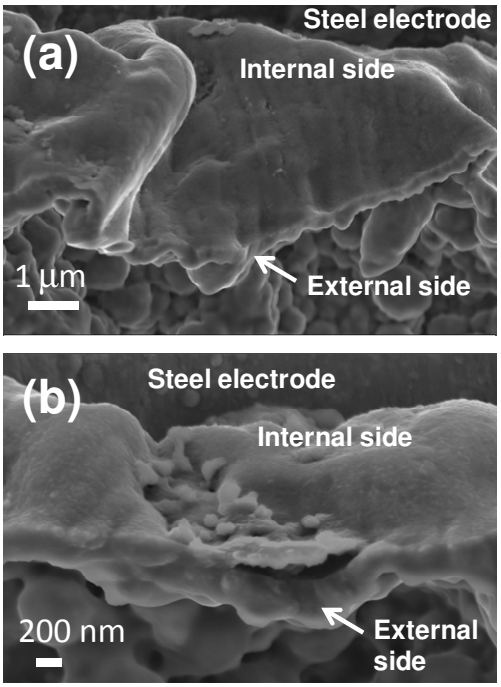


**Figure 3 –** Low resolution (a) and high resolution (b) images of P(EDOT-LZ) showing the morphology of both the internal and external sides of the film.

*Structure of the enzyme.* Figure 4 shows the FTIR spectra of lysozyme (free state), PEDOT, PEDOT/LZ and P(EDOT-LZ) in the 1700-1400 $cm^{-1}$ range. This interval corresponds to the amide I and II bands that has been used to identify the conformational changes of lysozyme in the two latter systems with respect to the free state.

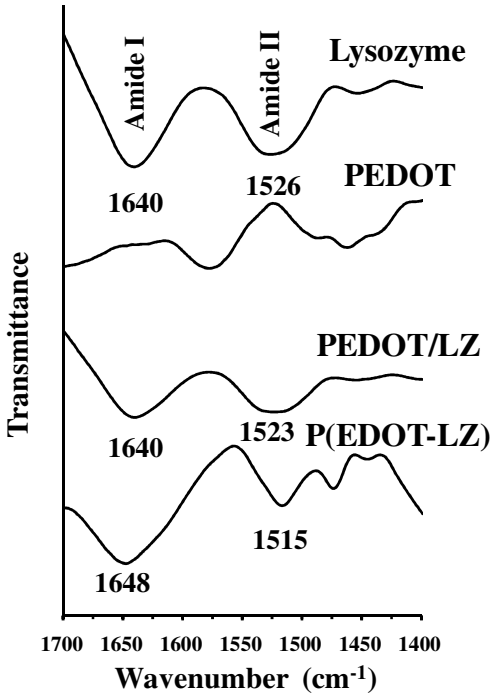


**Figure 4 –** FTIR spectra, in the range 1700-1400 $cm^{-1}$, of lysozyme (free state), PEDOT, PEDOT/LZ and P(EDOT-LZ) at room temperature.

The amide I band (1700-1600 $cm^{-1}$) arises primarily from the C=O stretching vibration of the peptide linkages that constitute the backbone structure of proteins and is well-known to be sensitive to the conformational changes.[40-42] The amide II band (1600-1480 $cm^{-1}$) is assigned to the coupling of the N-H in-plane bending and C-N stretching modes of peptide linkages and is less useful in protein structural analysis.[42] For lysozyme, these vibrations correspond the two strong bands centered near 1640 (amide I) and 1526 $cm^{-1}$ (amide II). These values are slightly lower than those reported in the literature, which are around 1656 and 1540 $cm^{-1}$, respectively.[43,44] The amide I bands around 1650-1656 and 1620-1630 $cm^{-1}$ are assigned to $\alpha$-helix motifs and the intermolecular $\beta$-sheet aggregations, respectively, while the bands

around 1670-1685 $cm^{-1}$ are typically associated to the β-turn structure.[44-46] For PEDOT, the bands in the investigated region are due to the C-C and C=C stretching modes of the thiophene ring, as was previously reported.[47,48]

The FTIR spectrum of PEDTOT/LZ shows the amide I and II bands centred at 1640 and 1523 $cm^{-1}$, respectively, confirming the immobilization of the enzyme on the surface of the PEDOT film. Moreover, these frequencies are very similar to those obtained for the lysozyme in the free-state suggesting that the adsorption process does not induce any conformational change. PEDOT/LZ samples prepared using solutions with different lysozyme concentrations led to very similar results (data not shown). The amide I and II absorption bands of P(EDOT-LZ), which are identified at 1648 and 1515 $cm^{-1}$, respectively, indicate small differences with respect to the spectrum obtained for free lysozyme.

In order to provide a quantitative estimation of the amount of each secondary structural element in the enzyme, the amide I absorption band was fitted to a sum of Gaussian functions. The qualitative assignment of the overlapping Gaussian components to the secondary motifs was performed using the spectra of proteins with known three-dimensional structure for comparison.[49] Thus, after deconvolution, the areas of the different components were associated to the ratios of the different types of secondary structure: α helix, β sheet and turn. Figure 5a represents the fitted Gaussian elements obtained for the amide I absorption band of lysozyme in the free-state. These elements correspond to following populations: 50.1% α helix (1640.2 and 1651.4 $cm^{-1}$), 36.6% β-sheet (1613.6 and 1626.6 $cm^{-1}$), 13.3% turns (1661.8 $cm^{-1}$).

On the other hand, for P(EDOT-LZ) the populations derived from the deconvoluted amide I absorption band (Figure 5b) are: 46.8% α helix (1647.1 $cm^{-1}$), 27.7% β-sheet (1614.1 and 1628.3 $cm^{-1}$), 25.5% turns (1667.8 and 1681.5 $cm^{-1}$). It is worth noting that the conformational differences with respect to the free state are non-negligible (*i.e.* the α helix and β-sheet content decrease 3.3% and 8.9%, respectively, whereas the turn population increases 12.2%). These results indicate that the enzyme undergoes some structural reorganization upon entrapment into the matrix of the new composite. Specifically, the reductions in α helix and β-sheet content suggest a loss of secondary structure and intermolecular aggregation, respectively.[49,50] The increment of the turn population (12.2%) suggests the possible formation of hydrogen bonding interactions between the enzyme and the oxygen atoms of the polymer chains, which is consistent with a decrease of protein

structural integrity. Within this context, it should be mentioned that PEDOT recognizes specific nucleotide sequences in plasmid DNA through the formation of hydrogen bonds, which illustrates the capability of this CP to form weak interactions.[51,52] Results obtained for PEDOT/LZ (data not shown) are practically identical to those displayed in Figure 5a evidencing that, as expected, adsorption does not alter the structure of the enzyme.

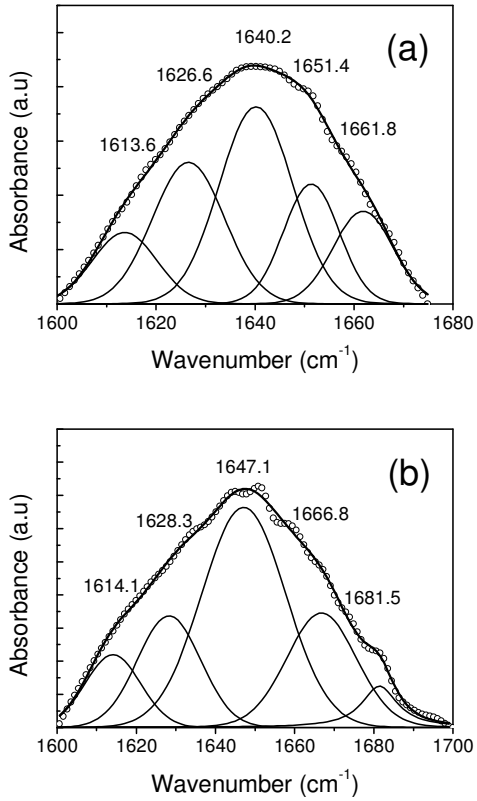


**Figure 5 –** Deconvolution of the amide I absorption band recorded by FTIR spectroscopy for (a) free lysozyme and (b) P(EDOT-LZ) at room temperature.

*Stability of the enzyme in PEDOT films.* The enzyme extracted from PEDOT/LZ and P(EDOT-LZ) films incubated in PBS (see Methods section) was analyzed using SDS-PAGE gels to quantify the stability of the lysozyme immobilized by adsorption and anodic electro-copolymerization, respectively. Within this context, stability refers to the structural integrity of the enzyme retained in substrate, which is inversely proportional to the velocity of the releasing process. Quantitative analysis of the PEDOT/LZ allowed determine the releasing of

38 μg/cm$^2$ after 48 h, which represents a high degree of fast releasing (*i.e*. 95% of the enzyme deposited on the surface of the PEDOT film). Thus, although the lysozyme of PEDOT/LZ is clearly appreciated after a few hours of incubation in PBS, its band becomes undetectable after 48 h (data not shown). In contrast the enzyme incorporated into the P(EDOT-LZ) samples was released progressively, indicating a very high stability. Thus, after 28 days the released lysozyme was in average 28.75 ± 5.52 μg/cm$^2$ from the initial 34.93 ± 3.41 μg/cm$^2$. Thus, approximately 18% of the lysozyme remains immobilized in the P(EDOT-LZ) matrix after almost one month. The progressive release of lysozyme, which is reflected in the electrophoretograms displayed in Figure 6, evidences that P(EDOT-LZ) may be used as a reservoir of such bactericidal enzyme. It should be noted that the release of lysozyme from P(EDOT-LZ) is very slow compared with that of other proteins and drugs encapsulated using core-shell structures or fibres (*e.g.* 45-65% of the protein release was observed after 2 days in fibers with 0.2% of entrapped bovine serum albumin).[53]

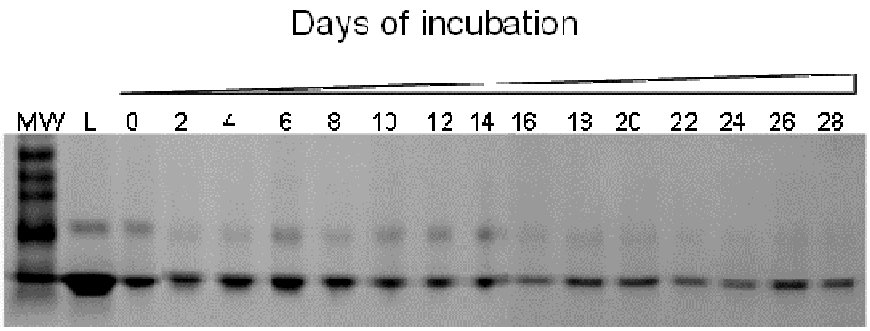


**Figure 6 –** Load and release of lysozyme from P(EDOT-LZ) evaluated using SDS-PAGE gels (see methods). After extract the films, half volume of the extraction was load in the gel (lanes 0-28). From lane 2 to 28, lysozyme was extracted from P(EDOT-LZ) samples incubated in PBS (pH 7.4) during the same number of days that the label of the lane. MW: standard ladder; L: standard lysozyme (40 μg of protein).

*Protection against bacteria and catalytic activity*. The bactericidal activity of PEDOT/LZ and P(EDOT-LZ) has been evaluated using two different but complementary approaches. In the first one the inhibition of bacterial growth was examined, while in the second the catalytic activity of the enzyme was investigated by monitoring the damage on the bacterial wall.

Bacterial strains of *Escherichia coli* (Gram –) and *Staphylococcus epidermidis* (Gram +) were cultured in presence of PEDOT/LZ, P(EDOT-LZ) and PEDOT films, the latter being used as control. After 24 and 48 h, the growth of *E. coli* was not affected by the presence of lysozyme in PEDOT/LZ and P(EDOT-LZ), results being similar to those obtained for PEDOT (Figure 7a).

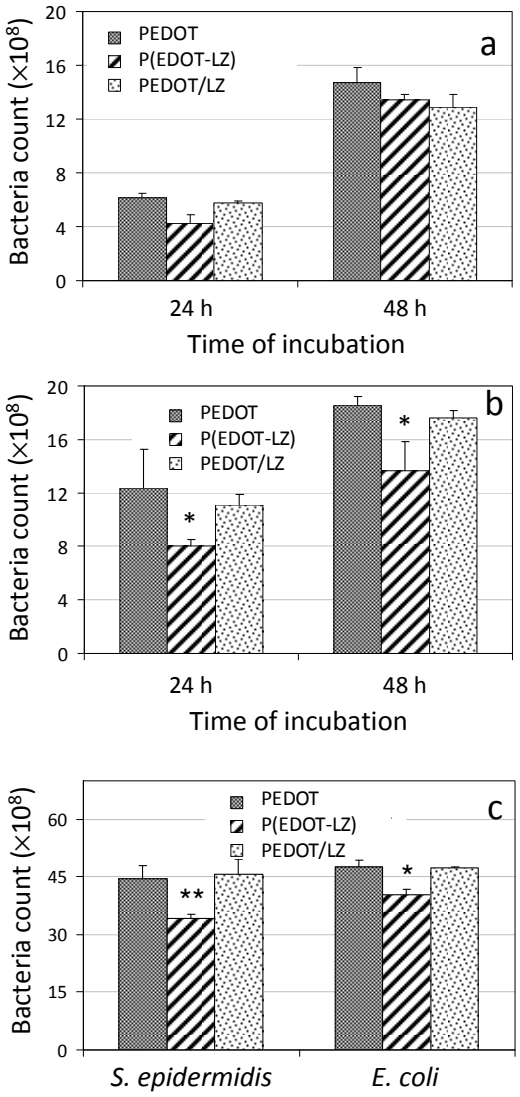


**Figure 7 –** Biological activity of PEDOT (control), PEDOT/LZ and P(EDOT-LZ). The inhibition of bacterial growth was evaluated at 24 and 48 h for (a) *Escherichia coli* and (b) *Staphylococcus epidermidis*. The number of bacteria adhered to the surface of the films (c) was determined after 48 h of culture. All the assays were performed in triplicate. The asterisk indicates $p < 0.05$.

In opposition, the growth of *S. epidermidis* in presence of P(EDOT-LZ) was considerably inhibited with respect to the control (Figure 7b), whereas the enzyme adsorbed in PEDOT/LZ did not affect the bacterial growth. The different effects provided by P(EDOT-LZ) form Gram – and Gram + bacteria are fully consistent with the specificity of the enzyme. On the other hand, adhesion experiments indicated a significant reduction in the number of bacteria, especially of *S. epidermidis*, adhered to the surface of P(EDOT-LZ) with respect to the control (Figure 7c), no effect being detected for PEDOT/LZ. The overall of these results indicate that the antibacterial activity of P(EDOT-LZ) is remarkably better than that of PEDOT/LZ. The poor behaviour of the latter should be attributed to fast releasing of the enzyme, whereas a significant concentration of bactericidal agent remains entrapped in P(EDOT-LZ) films since, as was showed in the previous section, the releasing to the medium is very slow.

The activity of immobilized enzymes has been reported to increase with the surface coverage (*i.e.* the concentration).[54,55] Figure 8 compares the enzymatic activity of free lysozyme (solution), PEDOT/LZ and P(EDOT-LZ), PEDOT being used as control.

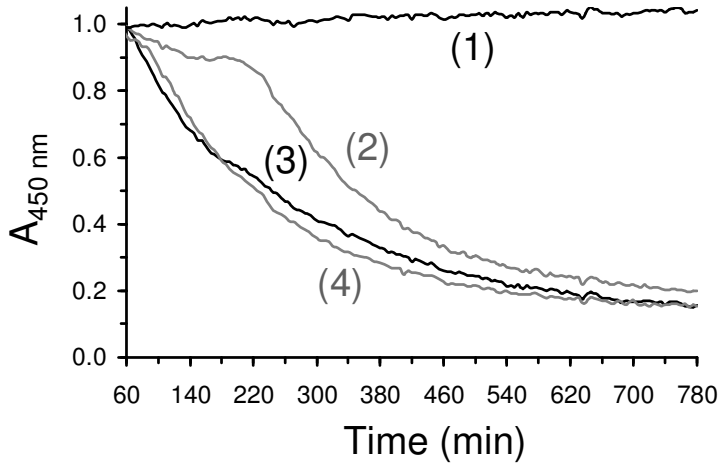


**Figure 8** – Enzymatic activity of lysozyme on the peptidoglycan of *Micrococcus luteus*. Curves refer to: (1) PEDOT (control); (2) PEDOT/LZ; (3) P(EDOT-LZ); and (4) free lysozyme.

The parameters derived from the adjusted kinetic model being displayed in Table 2. The velocity of degradation of the peptidoglycan at the bacterial cell walls was similar for free lysozyme and P(EDOT-LZ), whereas this enzymatic process is slower for PEDOT/LZ. Again, the lower activity of the latter should be mainly attributed to the releasing process, even though

the heterogeneous coverage of the surface and the aggregation of the adsorbed enzyme molecules may also contribute to such effect. However, the latter limitations may be overcome by optimizing the loading amount of enzyme, as was found for lysozyme adsorbed on silica nanotubes.[39]

**Table 2 –** Parameters of the kinetic model used to explain the enzymatic activity of lysozyme in the free state, P(EDOT-LZ) and PEDOT/LZ using *Micrococcus luteus* as substrate. The equation used for the fitting was: $y = y_0 + A_1 e^{-xt_1}$

| Parameter | Lysozyme (free) | P(EDOT-LZ) | PEDOT/LZ |
|---|---|---|---|
| $y_0$ | 0.133 ± 0.002 | 0.127 ± 0.003 | -0.116 ± 0.053 |
| $A_1$ | 1.237 ± 0.008 | 1.098 ± 0.006 | 1.375 ± 0.039 |
| $t_1$ | 181.857 ± 2.085 | 221.078 ± 2.690 | 462.861 ± 40.709 |
| $R^2$ | 0.99727 | 0.99754 | 0.9607 |
| $\chi^2$ /DoF | 1.55E-04 | 1.25E-04 | 0.00317 |
| ANOVA Test[a] | 0.00001 | 0.00006 | |
| Levene's Test[a] | 0.00759 | 0.00034 | |

[a] *p*-value: Lysozyme or P(EDOT-LZ) against PEDOT/LZ

*Electroactivity of PEDOT films covered with lysozyme.* The electroactivity of PEDOT, PEDOT/LZ and P(EDOT-LZ) was determined by CV in a PBS medium. The electroactivity increases with the similarity between the anodic and cathodic areas of the first control voltammogram. Inspection of the recorded voltammograms (Figure 9a) indicates that the electroactivities of PEDOT and PEDOT/LZ films are similar, indicating that the access and escape of dopant anions is not altered by the adsorbed enzyme (*i.e.* the dopant ions cross the lysozyme coating without difficulty). The voltammogram of P(EDOT-LZ) shows a decrease of the cathodic current density, which produces a reduction of the electroactivity with respect to PEDOT and PEDOT/LZ. In spite of such reduction, the electroactivity of P(EDOT-LZ) is still remarkably high in relation with that obtained for other CPs, like for example polypyrrole derivatives.[56] The differences in electrochemical behaviour of P(EDOT-LZ) with respect to PEDOT should be attributed to the changes introduced by the enzyme not only in the porosity of the films (Figures 1c and 2c) but also in the chemical structure of the CP. Thus, the addition of enzyme to the polymerization medium and its entrapment in the composite matrix presumably reduce the π-conjugation of the CP chains.

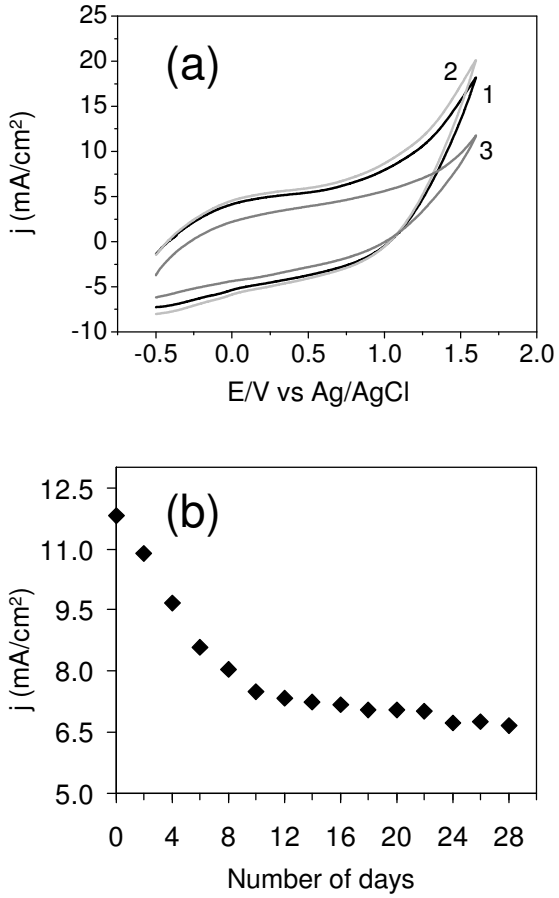


**Figure 9 –** (a) Control voltammograms of PEDOT (curve 1), PEDOT/LZ (curve 2) and P(EDOT-LZ) (curve 3) in PBS. (b) Maximum of current density in control voltammograms against the number of days for P(EDOT-LZ) samples incubated in PBS. Voltammograms were recorded at 100 $mV \cdot s^{-1}$ and 25 ºC. Initial and final potentials: -0.50 V; Reversal potential: 1.60 V.

In order to examine stability of the electrochemical activity of P(EDOT-LZ) in physiological conditions, control voltammograms of samples incubated in PBS at 4 ˚C were recorded at regular intervals. Inspection of Figure 9b, which represents the maximum of current density against the number of days in PBS, indicates that the electroactivity decreases during the first ten days stabilizing at around 7 $mA/cm^2$ after such period of incubation. These results evidence that, although P(EDOT-LZ) samples are affected by the PBS, the electroactivity after 10 days remains relatively high. Thus, the electrochemical

properties of the homogeneous composite made of PEDOT are better than those observed for some conventional CPs.[56]

### 6.1.4 – Conclusions

Lysozyme is an enzyme with bactericidal activity Gram-positive bacteria cell, which have been incorporated into PEDOT via adsorption on the surface of the film and electrochemical polymerization. Adsorption produces films able to retain the electrochemical activity of PEDOT but with relatively low bactericidal activity. In contrast, P(EDOT-LZ) consists on a homogeneous composite, in which the enzyme initially added to the polymerization medium is entrapped in the matrix of the produced material. Results of *Escherichia coli* and *Staphylococcus epidermidis* cultures show that P(EDOT-LZ) allows the growing of the Gram-negative bacteria while it presents remarkably high bactericidal activity against Gram-positive bacteria. Deconvolution of the amide I absorption band indicates that the entrapped lysozyme undergoes some structural changes with respect to the enzyme in the free state. However, such variations do not affect to the catalytic activity of the enzyme, which is similar for both the free lysozyme and P(EDOT-LZ). On the other hand, electrophoretic assays performed on P(EDOT-LZ) samples incubated in PBS indicated a controlled and progressive releasing of the enzyme. Immobilization of lysozyme in PEDOT can serve to improve the potential applicability of this CP in biomedicine, for example in the regeneration of tissues.

### 6.1.5 – References

[1] A. Mishra, C. Q. Ma, P. Baüerle, *Chem. Rev.* 109 (2009) 1141.

[2] J. Roncali, *Chem. Rev.* 97 (1997) 173.

[3] T. A. Skotheim, J. R. Reynolds, In *Handbook of Conducting Polymers,* 3th ed.; CRC Press, Boca Raton, 2007.

[4] M. Dietrich, J. Heinze, G. Heywang, F. Jonas, *J. Electroanal. Chem.* 369 (1994) 87.

[5] C. J. Brabec, N. S. Sariciftci, J. C. Hummelen, *Adv. Funct. Mater.* 11 (2001) 15.

[6] L. Groenendaal, F. Jonas, V. Freitag, H. Pielartzik, J. R. Reynolds, *Adv. Mater.* 12 (2000) 481.

[7] L. Groenendaal, G. Zotti, P.-H. Aubert, S. M. Waybright, J. R. Reynolds, *Adv. Mater.* 15 (2003) 855.

[8] S. I. Jeong, I. D. Jun, M. J. Choi, Y. C. Nho, Y. M. Lee, H. I. Shin, *Macromol. Biosci.* 8 (2008) 627.

[9] H. J. Wang, L. W. Ji, D. F. Li, J. Y. Wang, *J. Phys. Chem. B* 112 (2008) 2671.

[10] D. Sarauli, J. Tanne, G. C. Xu, B. Schultz, L. Trnkova, F. Lisdat, *Phys. Chem. Chem. Phys.* 12 (2010) 14271.

[11] C. C. Chen, J. S. Do, Y. Gu, *Sensors* 9 (2009) 4635.

[12] H. Q. A. Le, S. Chebil, B. Makrouf, H. Sauriat-Dorizon, B. Mandrand, H. Korri-Youssoufi, *Talanta* 81 (2010) 1250.

[13] A. Menaker, V. Syritski, J. Reut, A. Opik, V. Horvath, R. E. Gyurcsanvi, *Adv. Mater.* 21 (2009) 2271.

[14] H. Yoon, S. K. Lee, O. S. Kwon, H. S. Song, E. H. Oh, T. H. Park, J. Jang, *Angew. Chem. Int. Ed.* 48 (2009) 2755.

[15] K. J. Gilmore, M. Kita, Y. Han, A. Gelmi, M. J. Higgins, S. E. Moulton, G. M. Clark, R. Kapsa, G. G. Wallace, *Biomaterials* 30 (2009) 5292.

[16] F. He, S. Wang, *Prog. Chem.* 21 (2009) 2372.

[17] L. B. Liu, M. H. Yu, X. R. Duan, S. Wang, *J. Mat. Chem.* 20 (2010) 6942.

[18] D. F. Li, H. J. Wang, J. X. Fu, W. Wang, X. S. Jia, J. Y. Wang, *J. Phys. Chem. B* 112 (2008) 16290.

[19] N. K. Guimard, N. Gomez, C. E. Schmidt, *Prog. Polym. Sci.* 32 (2007) 876.

[20] C. Ocampo, E. Armelin, F. Estrany, L. J. del Valle, R. Oliver, F. Sepulcre, C. Alemán, *Macromol. Mater. Eng.* 292 (2007) 85.

[21] C. Alemán, B. Teixeira-Dias, D. Zanuy, F. Estrany, E. Armelin, L. J. del Valle, *Polymer* 50 (2009) 1965.

[22] B. Teixeira-Dias, D. Zanuy, L. J. del Valle, F. Estrany, E. Armelin, C. Alemán, *Macromol. Chem. Phys.* 211 (2010) 1117.

[23] R. Blanco-Bazaco, R. Gomez, C. Seoane, P. Bauerle, J. L. Segura, *Tetrahedron Lett.* 50 (2009) 4154.

[24] K. Krishnamoorthy, R. S. Gokhale, A. Q. Contractor, A. Kumar, *Chem. Commun.* 40 (2004) 820.

[25] S. C. Luo, S. S. Liour, H. H. Yu, *Chem. Commun.* 46 (2010) 4731.

[26] L. J. del Valle, D. Aradilla, R. Oliver, F. Sepulcre, A. Gamez, E. Armelin, C. Alemán, F. Estrany, *Eur. Polym. J.* 43 (2007) 2342.

[27] C. Salto, E. Saindon, M. Bolin, A. Kanciurzewska, M. Fahlman, E. W. H. Jager, P. Tengvall, E. Arenas, M. Berggren, *Langmuir* 24 (2008) 14133.

[28] L. J. del Valle, F. Estrany, E. Armelin, R. Oliver, C. Alemán, *Macromol. Biosci.* 8 (2008) 1144.

[29] M. H. Bolin, K. Svennersten, X. J. Wang, I. S. Chronakis, A. Richter-Dahlfors, E. W. H. Jager, M. Berggren, *Sensors and Actuators* 142 (2009) 451.

[30] K. Svennersten, M. H. Bolin, E. W. H. Jager, M. Berggren, A. Richter-Dahfors, *Biomaterials* 30 (2009) 6257.

[31] Y. Xiao, C. M. Li, S. Wang, J. Shi, C. P. Ooi, *J. Biomed. Mater. Res.* 92A (2010) 766.

[32] H. Xie, S.-C. Luo, H.-h. Yu, *Small* 5 (2009) 2611.

[33] B. D. Martin, L. M. Velea, C. M. Soto, C. M. Whitaker, B. P. Gaber, B. Ratna, *Nanotechnology* 18 (2007) 055103.

[34] V. L. Hughey, E. A. Johnson, *Appl. Environ. Microbiol.* 53 (1987) 2165.

[35] L. E. Stenfors, H. M. Bye, S. Räisänen, *J. Laryngol. Otol.* 116 (2002) 264.

[36] Q. Garret, R. W. Garret, B. K. Milthorpe, *Invest. Ophthalmol. Vis. Sci.* 40 (1999) 897.

[37] M. M. Bradford, *Anal. Biochem.* 72 (1976) 248.

[38] H. Susi, D. M. Byler, *Biochem. Biophys. Res. Commun.* 115 (1983) 391.

[39] H. M. Ding, L. Shao, R. J. Liu, Q. G. Xiao, J. F. Chen, *J. Colloid Interf. Sci.* 290 (2005) 102.

[40] H. Susi, D. M. Byler, *Methods Enzymol.* 130 (1986) 290.

[41] A. Dong, W. S. Caughey, *Methods Enzymol.* 232 (1994) 139.

[42] S. Krimm, J. Bendekar, *Adv. Protein Chem.* 38 (1986) 181.

[43] E. Pechkova, P. Innocenzi, L. Malfatti, T. Kidchob, L. Gaspa, C. Nicolini, *Langmuir* 23 (2007) 1147.

[44] A. Dong, T. W. Randolph, J. F. Carpenter, *J. Biol. Chem.* 275 (2000) 27689.

[45] A. Dong, P. Huang, W. S. Caughey, *Biochemistry* 29 (1990) 3303.

[46] G. Thakur, R. M. Leblanc, *Langmuir* 25 (2009) 2842.

[47] K. I. Seo, I. J. Chung, *Polymer* 41 (2000) 4491.

[48] J. Xu, G. Nie, S. Zhang, X. Han, J. Hou, S. Pu, *J. Mat. Sci.* 40 (2005) 2867.

[49] J. M. Hadden, D. Chapman, D. C. Lee, *Biochim. Biophys. Acta* 1248 (1995) 115.

[50] H. L. Casal, U. Koehler, H. H. Mantsch, *Biochim. Biophys. Acta* 957 (1988) 11.

[51] C. Alemán, B. Teixeira-Dias, D. Zanuy, F. Estrany, E. Armelin, L. J. del Valle, *Polymer* 50 (2009) 1965.

[52] B. Teixeira-Dias, D. Zanuy, L. J. del Valle, F. Estrany, E. Armelin, C. Alemán, *Macromol. Chem. Phys.* 211 (2010) 1117.

[53] Y. Z. Zhang, X. Wang, Y. Fena, J. Li, C. T. Lim, *Biomacromolecules* 7 (2006) 1049.

[54] T. Zoungrana, G. Findenegg, W. Norde, *J. Colloid Interf. Sci.* 190 (1997) 437.

[55] T. Zoungrana, W. Norde, *Colloid Surf. B* 9 (1997) 157.

[56] C. Alemán, J. Casanovas, J. Torras, J. Bertran, E. Armelin, R. Oliver, F. Estrany, *Polymer* 49 (2008) 1066.

## 6.2 – Dextrin- and conducting polymer-containing biocomposites: Properties and behaviour as cellular matrix

α-cyclodextrin (cyclohexaamylose) and linear dextrin have been used to prepare biocomposites with poly(3,4-ethylenedioxythiophene). Materials have been prepared electrochemically in aqueous solution. Comparison with the pure conducting polymer indicates that both the electroactivity and electrostability decreases because of the incorporation of the dextrins while the electrical conductivity of the biocomposites and the poly(3,4-ethylenedioxythiophene) are very similar. On the other hand, topographical and morphological images, elemental analyses, and contact angle measures reflect significant differences between the two biocomposites suggesting that the linear dextrin is mainly located at the surface, whereas the cyclodextrin is homogeneously distributed in the polymeric matrix. The concentration of cyclodextrin and linear dextrin in the biocomposites has been found to be 15% and 20% w/w, respectively, the releasing of the former being largely influence by the pH. Cell adhesion and proliferation assays considering two epithelial-like and one fibroblast-like lines indicates that the cellular activity is significantly higher in the dextrins-containing biocomposites than in poly(3,4-ethylenedioxythiophene). Accordingly, the incorporation of dextrins improves the behaviour of the latter conducting polymer as cellular matrix.*

* - Results reported in this section have been accepted for publication in *Macromolecular Materials and Engineering*.

### 6.2.1 – Introduction

Among CPs with π-conjugated bonds, poly(3,4-ethylenedioxythiophene) (PEDOT; Scheme 1), a derivative of polythiophene, has attracted great interest because of its advantageous properties: high electrical conductivity, good electrochemical behaviour, thermal and environmental stability, suitable morphologies, and fast doping/undoping mechanism.[1-4] On the other hand, recent studies indicated that PEDOT shows potential applications related with biotechnology and biomedicine. For example, PEDOT is able to interact with specific DNA nucleotide sequences, act as a bioactive platform for adhesion and proliferation of cells, form biocomposites with collagen, and detect proteins.[5-20]

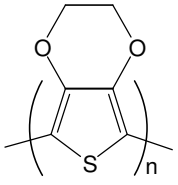


PEDOT

**Scheme 1**

Cyclodextrins (CDs) are toroidally shaped cyclic oligosaccharides with a hydrophobic internal cavity and a hydrophilic outer side. They are soluble in water and form stable inclusion complexes with hydrophobic guests that fit tightly inside the CD cavity. The host-guest interaction leads to encapsulation of small particles into the cavity of oligosaccharides without the formation of chemical bonds (*i.e.* the driving forces for the complexation are non-covalent: van der Waals forces, hydrophobic interactions, etc.) and without changing their chemical structure.[21] Chemical structure, physical properties in solution and solid state, chemical reactivity, electrochemical behaviour, formation and properties of CD-polymeric films and biological effects of CDs have been reviewed.[21-25]

In the last decade, several composites formed by a CPs and CDs have been prepared and characterized.[26-36] Specifically, Lagrost *et al.* prepared composites by electropolymerizing bithiophene and hydroxypropyl-β-cyclodextrin in aqueous media.[26,27] Although the resulting composites showed the usual features of poly(bithiophene), the structure of the films appeared to be considerably modified by the presence of CDs within the material but not grafted onto the polymeric backbone. Shimomura *et al.* and Yoshida *et al.* studied the insulation effect of an inclusion complex formed by polyaniline in the emeraldine base form and β-CD using the oxidation of iodine in solution of N-methyl-2-pyrrolidone.[28,29] Electrochemical methods were also used to prepare composites of polypyrrole and poly(3-methylyrrole) with α- and β-CDs.[30-33] Results evidenced the influence of the CDs on interchain interactions during the electropolymerization process.[31] In addition, composites made with polypyrrole showed different permeabilities towards a variety of metal ions upon appropriated electrochemical stimuli.[30] Hadziioannou and co-workers described the synthesis and visualization of insulated semiconducting polymers based on polythiophene and polyfluorene, with a high coverage of β-CDs as insulating sheath.[34] Regarding to PEDOT, the only reported composites were recently obtained by electropolymerizing 3,4-ethylendioxythiophene monomer and hydroxypropyl-β-CD in aqueous solution.[35,36] The resulting materials effectively catalyzed the oxidation of sulphur oxoanions and nitrite by reducing their overoxidation potential.

On the other hand, systems based on linear dextrins (LDs) have been found to promote the cellular growing.[37-40] This bioreactive response added to the intrinsic characteristics of PEDOT as conducting bioactive platform (*i.e.* substrate electro-compatible with cellular-monolayers that behaves as a cellular matrix) suggest that the combination of

the two materials may result in new composites with important biomedical and biotechnological applications.[14,16] Specifically, composites formed by PEDOT and dextrins are very promising candidates to act as efficient substrates for the adhesion and growing of eukaryotic cells. In spite of this, the many characteristics of these composites, like for example the structure and morphology, remain practically unknown and the investigation their applicability as cell substrate was never explored.

In this work new biocomposites obtained by combining PEDOT with CD and LD, hereafter denoted P(EDOT-CD) and P(EDOT-LD) have been prepared and characterized. The properties of these materials, which were produced by anodic polymerization in aqueous solution, have been characterized in terms of electrochemical and electrical behaviour, morphology and structure, and hydrophobicity of the surface. In order to determine the role played by the dextrins on each of these properties, the two biocomposites have been systematically compared with PEDOT. The concentration of dextrins in the biocomposites has been determined and, in addition, their releasing has been investigated considering different conditions.

### 6.2.2 – Methods

*Materials*. 3,4-ethylendioxythiophene (EDOT), α-CD (cyclohexaamylose), LD [$(C_6H_{12}O_6)_x$ from potato starch] were purchased from Aldrich. Anhydrous $LiClO_4$, analytical reagent grade, from Aldrich was stored in an oven at 80 ˚C before use in the electrochemical trials.

*Synthesis.* PEDOT, P(EDOT-CD) and P(EDOT-LD) were prepared by chronoamperometry (CA) under a constant potential of 1.10 V using a polymerization time θ= 300 s. Both anodic polymerizations and electrochemical experiments were conducted in a three-electrode two-compartment cell under nitrogen atmosphere (99.995% in purity) at 25 ˚C. A VersaStat II (Princenton Applied Research) potenciostat-galvanostat connected to a computer controlled through a Power Suite Princenton Applied Research program was used in all cases. For the preparation of PEDOT, the anodic compartment was filled with 50 mL of a 10 mM EDOT solution in ultrapure MilliQ water containing 0.1 M $LiClO_4$ as supporting electrolyte, while the cathodic compartment was filled with 10 mL of the same electrolyte

solution. For the synthesis of P(EDOT-CD) and P(EDOT-LD) the anodic compartment was filled by adding 10 mL of milliQ water solution containing the corresponding dextrin (50 mg/mL) to 40 mL of the above mentioned EDOT/$LiClO_4$ electrolyte solution. Steel AISI 316 L sheets of 1×1 $cm^2$ were employed as working and counter electrodes. The reference electrode was an Ag|AgCl electrode containing a KCl saturated aqueous solution ($E^o$ = 0.222 V *vs.* standard hydrogen electrode at 25 ˚C), which was connected to the working compartment through a salt bridge containing the electrolyte solution.

*Electrochemical characterization.* The electrochemical properties of PEDOT, P(EDOT-LD) and P(EDOT-CD) films were studied by cyclic voltammetry (CV). The ability to store charge (electroactivity) and electrochemical stability upon consecutive oxidation-reduction cycles (electrostability) were determined using an ultrapure MilliQ water solution with 0.1 M $LiClO_4$. The initial and final potentials were -0.50 V, and the reversal potential was 1.40 V. The electroactivity increases with the similarity between the anodic and cathodic areas of the first control voltammogram, whereas the electrostability decreases with the oxidation and reduction areas of consecutive control voltammograms. Accordingly, electroactivity and electrostability were determined through direct measure of the anodic and cathodic areas in the control voltammagrams using the Power Suite Princenton Applied Research software. A scan rate of 100 $mV \cdot s^{-1}$ was used in all cases.

*Electrical properties.* The electrical conductivity (σ) was measured on films synthesized on steel AISI 316 L sheets of 2×2 $cm^2$ area using the sheet resistance method, as was previously described.[41]

*Electrochemical Impedance Spectroscopy.* Electrochemical impedance spectroscopy (EIS) studies were carried using three-electrode two-compartment cell with an Autolab 302N potenciostat/galvanostat and the FRA software program. The cell was filled with 50 mL of ultrapure MilliQ water solution containing 0.1 M of $LiClO_4$ and all the measurements were performed at room temperature. Coated and uncoated steel AISI 316 L sheets of 1×1 $cm^2$ were employed as working and counter electrodes, respectively. EIS measurements were carried out in the 0.05-20 Hz frequency range and sinusoidal voltage amplitude of ±0.05 V for 70 frequencies. EIS data were plotted in terms of real and imaginary parts of the impedance (Z' and –Z'', respectively).

*Morphology.* Atomic force microscopy (AFM) images were obtained with a Molecular Imaging PicoSPM using a NanoScope IV controller in ambient conditions. The average RMS roughness (*r*) was determined using the statistical application of the Nanoscope software, which calculates the average considering all the values recorded in the topographic image with exception of the maximum and the minimum. Nanometric measurements were conducted under ambient conditions at ~50% relative humidity and 20-22 ˚C. The system was placed on an active vibration isolation table for minimum acoustic disturbance (20 series, TMC, Peabody, MA, USA).

Scanning electron microscopy (SEM) studies were carried out using a Focused Ion Beam Zeiss Neon 40 scanning electron microscope equipped with an energy dispersive X-ray (EDX) spectroscopy system and operating at 3.00 and 10.00 kV (micrographs and EDX analyses, respectively).

*Contact angles measurements.* Contact angles were obtained using the water drop method. Images of water drops (3 µl) in the surface of the films were recorded with a contact angle meter (Dataphysics, Contact Angle System OCA15+) after stabilization (30 s). The images of the drop shapes were analysed and the contact angle measures were carried out with the SCA20 software. Measurements were performed four times for each material.

*Quantification of the concentration of dextrins in composites.* P(EDOT-LD) and P(EDOT-CD) films were removed from the steel working electrodes using a scraper. The resulting material was transformed into a powder using an Agatha mortar prior to the extraction of the dextrins. Powder of each composite (6 mg) was placed in a glass tube, 5 mL of sulphuric acid (12.5 M) being added to extract the dextrins. Centrifugation of the tubes was performed after 24 h to clarify the extracts, and the insoluble material, which forms a pellet, was discarded. The quantification of LD and CD was determined using a phenol-sulfuric acid procedure, which consists on the following three steps:[42] (1) 0.5 mL of extract was mixed with 0.5 mL of phenol (5%); (2) 2 mL of concentrated sulphuric acid (~18 M) was slowly (10 min) added to the tube, the mixture being agitated at the end; and (3) the absorbance at 490 nm ($A_{490}$) was measured after rest 30 min. The control blank was prepared with the solution of extraction. Furthermore, PEDOT was extracted as control

because of the weak colour reaction produced by the aromatic rings. The $A_{490}$ was converted into LD and CD concentration using the respective calibration curves.

The same procedure was used to quantify the concentration of released dextrin in the corresponding release assays (see below). In this case, the concentrations of LD and CD contained in the composites as prepared were used as references.

*Release experiments.* Controlled release experiments were performed using P(EDOT-LD) and P(EDOT-CD) films electrodeposited on AISI 316 L steel electrodes of $1\times0.5$ $cm^2$, which were incubated at 37 ˚C in an orbital shaker at 60 rpm in eppendorf tubes with 1 mL of Phosphate Buffer Saline (PBS, pH 7.2) or Britton-Robinson Buffer (BRB, pH 3.0). The release medium was changed and analyzed every 24 h. For this purpose, the tubes were centrifuged at 13000 rpm during 5 min, and the supernatant was collected and storage at 4 ˚C to determine the concentration of released LD and CD through the phenol-sulphuric acid procedure described above.[42] All the release experiments were repeated three times to control the homogeneity of the results, and the released concentrations were averaged.

*Cell adhesion and proliferation assays.* In vitro adhesion and proliferation assays were performed using three different cellular lines of adherent growth: (i) cells HEp-2 (human line derived from an epidermoid carcinoma of larynx); (ii) cells DU145 (human line derived from a prostate carcinoma); and (iii) cells COS-7 (line derived of *Cercopithecus aethiops* - African green monkey- kidney and immortalized by transformation with SV40). HEp-2 and DU145 have an epithelial morphology while COS-7 is a fibroblast-like cell line.

Cells were plated in 25 $cm^2$ tissue flasks and grown in Dulbecco's Modified Eagle's Medium (DMEM) supplemented with 10% fetal bovine serum (FBS), penicillin G (100 U/ml) and streptomycin (100 mg/mL). The cultures were performed at 37 °C and humid atmosphere with 95% air (5% carbon dioxide). Passage 2 cultures were used for experiments. Cellular confluent cultures were dissociated with 0.05% trypsin and 0.02% EDTA in Hanks' Balanced Salt Solution, harvested by centrifugation, and counted in Neubauer camera using 0.4% trypan blue.

The adhesion and proliferation assays were performed seeding $5\times10^4$ and $2\times10^4$ cells, respectively, from an appropriate cell suspension concentration with viability >95%. PEDOT and composite electrodeposited on 1 $cm^2$ steel sheets were placed in 24-well plates, and

subsequently sterilized by UV-radiation during 15 min in the laminar flow cabinet. Next, cells were seeded by a slowly pipette of the cell suspension onto the top surface of each sample, covering 80-90% of the sample's surface. In order to avoid a reduction of the seeding efficiency, no contact between cell suspensions and the sides of the wells was allowed. The plates were gently place into an incubator, avoid agitating the plate. After 1 h, fresh medium (1 mL) was added into each well and the plate was returned to the incubator. Cultures to evaluate cellular adhesion and proliferation were incubated during 24 h and 7 days, respectively. All experiments were repeated at least three times.

To evaluate the cell number in the samples, the medium of each well was changed by fresh medium supplemented with MTT [3-(4,5-dimethylthiazol-2-yl)-2,5-diphenyltetrazolium; 5 mg/mL] and the plate returned to the incubator for 3 h. After this, the medium of each well was removed and the samples recoveries were placed in wells of a clean plate. The MTT reaction in the viable cells was determined by dissolving the formazan crystals in 1 mL of DMSO/methanol/water (70%/20%/10%, % in vol.).[43] Then, the absorbance at 540 nm was read in a spectrophotometer. The cells number was determined using a standard curve of $A_{540nm}$ *vs*. number of viable cells. Analyses were carried out using the cell adherence density in each sample (number of cells/$cm^2$).

To evaluate the cellular morphology, samples incubated with cells were fixed in 1 mL of 2.5% paraformaldehyde in PBS during 24 h at 4 °C. Then, samples were progressively dehydrated using alcohols of 30°, 40°, 50°, 70°, 90°, 95°, and 100° for 30 min at 4 °C in each one. Finally, samples were coated by carbon sputtering for the observation in the scanning electronic microscope.

### 6.2.3 – Results and Discussion

*Characterization of the biocomposites.* Figure 1a compares the control voltammograms recorded in the potential range from -0.50 to +1.40 V for PEDOT, P(EDOT-LD) and P(EDOT-CD). Results clearly indicate that the dextrins contained in the biocomposites obstruct the formation of polarons and bipolarons in PEDOT chains. The first anodic peak ($O_1$), which is identified as a small shoulder with $E_p^a(O_1)$= 0.74 V for PEDOT, corresponds to the formation of polarons. This process is not detected in P(EDOT-LD) and P(EDOT-CD) due to the blocking effect of the dextrins. The second anodic peak ($O_2$) with

$E_p^a(O_2)$= 1.29 V for PEDOT indicates the presence of bipolarons. These are formed through a process with low reversibility, as evidences the small reduction peak with $E_p^c(R_1)$= -0.16 V detected in the cathodic scanning. For P(EDOT-LD) and P(EDOT-CD) the $O_2$ anodic peak shows $E_p^a(O_2)$= 1.37 and 1.28 V, respectively, suggesting that the behaviour of the former biocomposite looks closer to that of PEDOT. The cathodic scan shows a reduction peak $R_1$ with $E_p^c(R_1)$= -0.25 and -0.23 V for P(EDOT-LD) and P(EDOT-CD), respectively, which corresponds to a reduction of a small concentration of the bipolaron formed in the anodic scan. The variation of the anodic and cathodic peak potentials is fully consistent with the current densities (*j* in Figure 1a), which indicates that the concentration of oxidized molecules is larger for PEDOT than for the biocomposites.

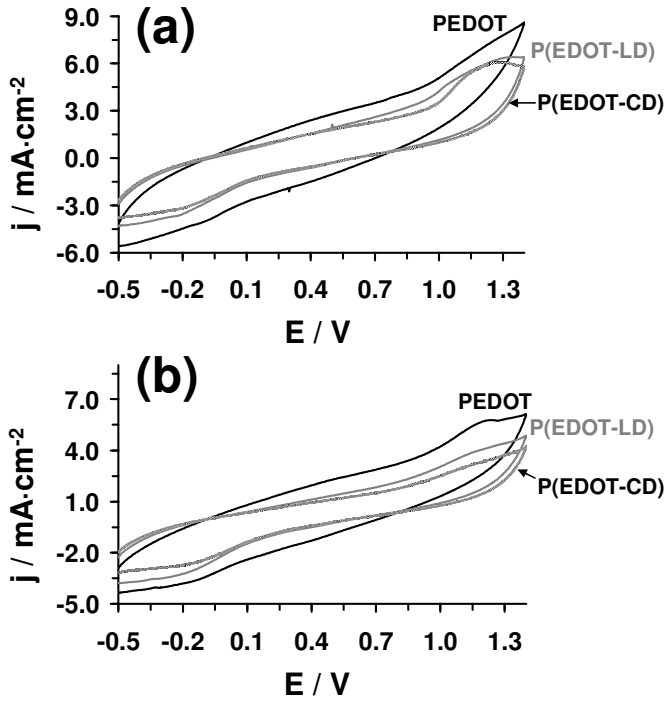


**Figure 1 –** (a) Control voltammograms for the oxidation of PEDOT, P(EDOT-LD) and P(EDOT-CD) films. (b) Control voltammograms for the oxidation of PEDO, P(EDOT-LD) and P(EDOT-CD) films after 30 consecutive cycles of oxidation-reduction.

The voltammograms recorded after 30 consecutive oxidation-reduction cycles ($n_{ox\text{-}red}$= 30), which are displayed in Figure 1b, indicate a drastic reduction of the electroactivity, especially for the biocomposites. Furthermore, the current density decreases drastically for the three materials evidencing that electrochemical degradation produces a significant reduction in the concentration of oxidized CP chains. The electrostability of the three materials is analyzed in Figure 2, which compares the variation of the electroactivity against $n_{ox\text{-}red}$.

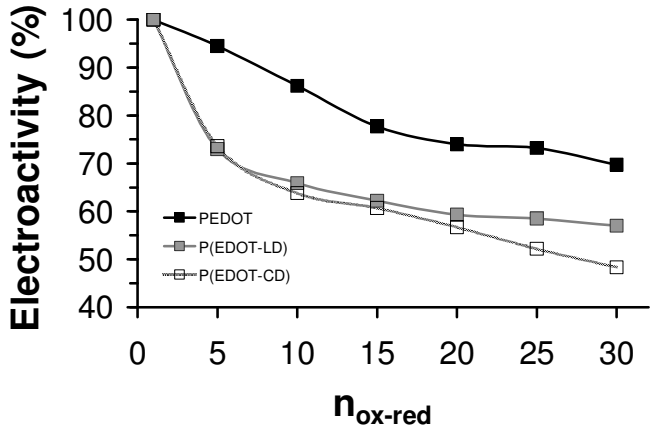


**Figure 2 –** Evolution of the electroactivity (in %) against the number of consecutive oxidation-reduction cycles ($n_{ox\text{-}red}$) for PEDOT, P(EDOT-LD) and P(EDOT-CD).

The electroactivity of PEDOT, which presents the highest electrochemical stability, decreases 30% after 30 consecutive redox cycles, whereas that of P(EDOT-LD) and P(EDOT-CD) reduces by 43% and 52%, respectively. Furthermore, the profiles displayed in Figure 2 reflect that the negative effects of the dextrins in the electrostability of PEDOT occur immediately. Thus, the electroactivity of PEDOT and the two biocomposites decreases by ~5% and ~25%, respectively, after only five consecutive redox cycles.

Nyquist impedance plots of PEDOT and the two biocomposites over a frequency range of 0.05-20 Hz are shown in Figure 3. The impedance spectra show a single semicircle in the high frequency region and a nearly vertical line in the low frequency region, which indicate that the electrode process is controlled by electrochemical reaction at high frequencies and by mass transfer at low frequencies. The incorporation of dextrins produces a significant

enhancement of the capacitance and the resistance. These effects are more important in P(EDOT-LD), which presents the highest resistance, than in P(EDOT-CD).

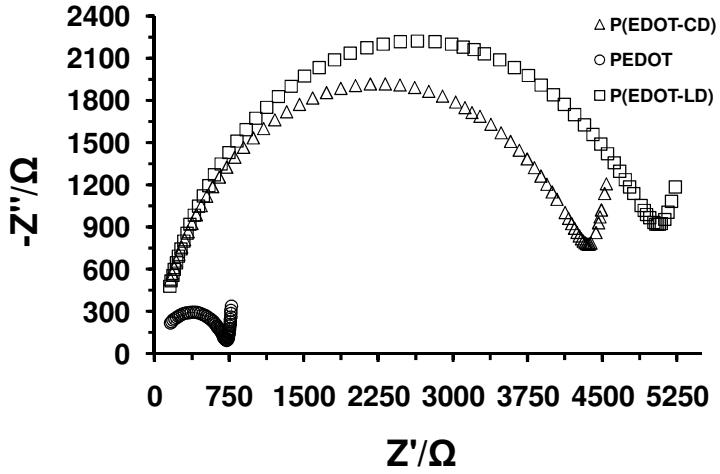


**Figure 3 –** Nyquist impedance plots of PEDOT, P(EDOT-LD) and P(EDOT-CD).

The electrical conductivity of perchlorate-doped PEDOT films generated in aqueous solution at 1.10 V is σ= 5 S/cm, this value being two orders of magnitude smaller than that obtained for perchlorate-doped PEDOT films generated in acetonitrile solution at 1.40 V (σ= 315 S/cm).[44] Interestingly, the incorporation of LD and CD does not alter significantly the electrical conductivity of the CP, the values measured for P(EDOT-CD) and P(EDOT-LD) being σ= 3 and 1 S/cm. This similarity suggests that dextrins do not produce drastic structural changes at the bulk.

Figure 4 compares the 5×5 $\mu m^2$ topographic AFM images of PEDOT, P(EDOT-LD) and P(EDOT-CD). As it can be seen, LD and CD provoke different changes on the topography of the PEDOT surface. Thus, the globular surface of the pure PEDOT films transforms into the powdery and layered topographies of P(EDOT-LD) and P(EDOT-CD), respectively. On the other hand, the average roughness was lower for PEDOT (*r*= 63 nm) than for P(EDOT-LD) (*r*=76 nm) and P(EDOT-CD) (*r*= 105 nm), indicating that the effect of the dextrins in the topological levels of the CP molecules is moderate but non negligible. Similar feature are observed in the high- and low-resolution SEM micrographs displayed in Figure 5. Dextrins affect the morphology of the PEDOT surface, even though the changes induced by LD and CD

are different. Molecular aggregates are significantly smaller in P(EDOT-LD) than in PEDOT, which results in the powdery topography displayed in Figure 4b.

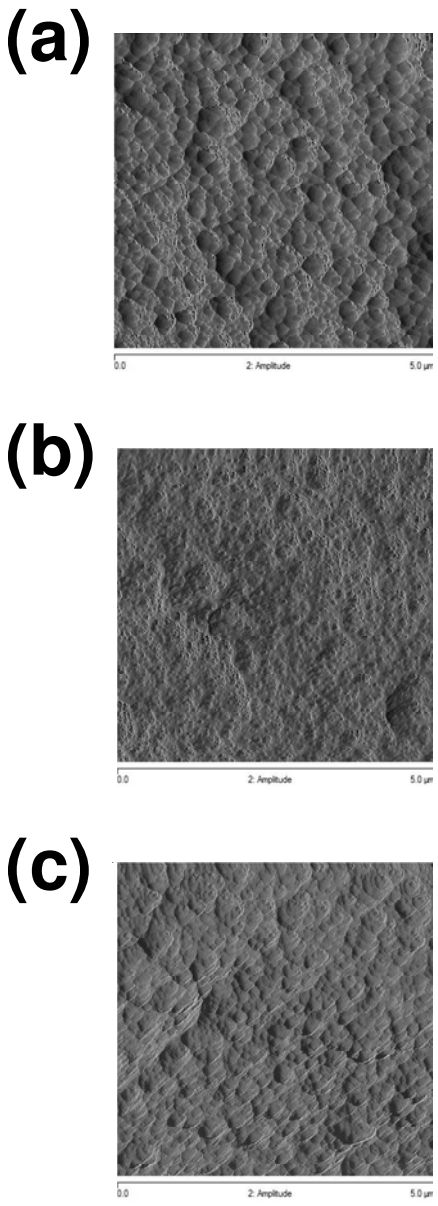


**Figure 4 –** Topographic AFM images of: (a) PEDOT, (b) P(EDOT-LD) and (c) P(EDOT-CD).

In contrast, larger aggregates are identified for P(EDOT-CD) than for PEDOT, explaining the transformation of the globular morphology found for the latter into the layered structure

identified for the former (Figure 5c, inset). However, the relative similitude between PEDOT and P(EDOT-CD) suggests that the cyclic oligosaccharide is homogeneously distributed in the polymeric matrix, producing only small changes in the morphology and topology because of its small size. Moreover, Figure 5 evidences that the porosity of the two biocomposites is lower than that of PEDOT, which is consistent with the lower electroactivity of the biocomposites (Figure 1).

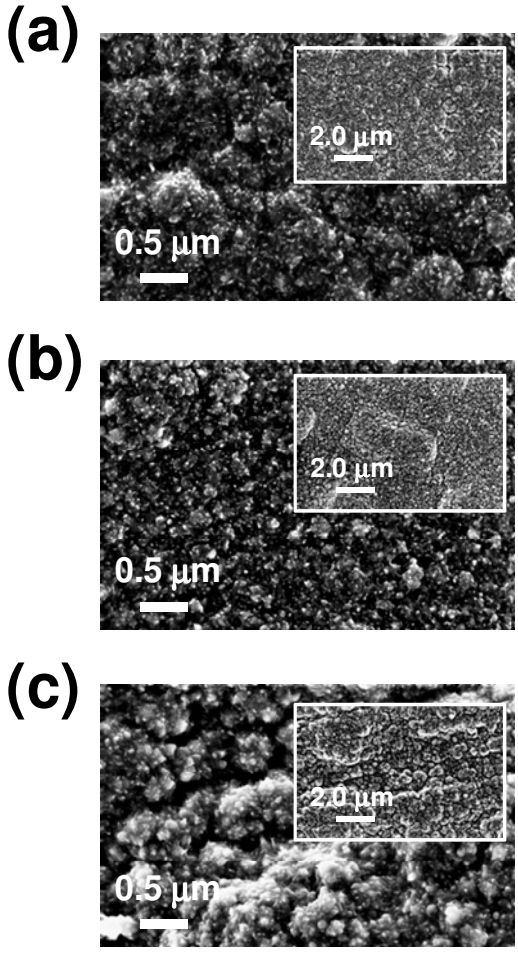


**Figure 5 –** High resolution and low resolution (inset) SEM micrographs of: (a) PEDOT, (b) P(EDOT-LD) and (c) P(EDOT-CD).

Results displayed in Figures 4 and 5 are fully consistent with the energy dispersive EDX spectroscopy analyses performed at the surface of PEDOT, P(EDOT-LD) and P(EDOT-CD) films

(Table 1). Thus, quantitative elemental analyses of C, O, S and Cl (% w/w) evidence different chemical compositions for P(EDOT-LD) and P(EDOT-CD). The concentration of S and C is considerably smaller and larger, respectively, in P(EDOT-LD) than in PEDOT. This feature suggests that the LD is mainly located at the surface, which is consistent with the powdery morphology of the biocomposite. On the other hand, the composition of P(EDOT-CD) and PEDOT are relatively similar.

**Table 1 –** Composition (concentration of C, O, S and Cl) obtained by energy dispersive X-ray spectroscopy analyses at the surface of PEDOT, P(EDOT-LD) and P(EDOT-CD) films.

| | **C** (w/w %) | **O** (w/w %) | **S** (w/w %) | **Cl** (w/w %) |
|---|---|---|---|---|
| PEDOT | 46.0 | 29.5 | 19.7 | 4.8 |
| P(EDOT-LD) | 58.2 | 29.6 | 9.4 | 2.8 |
| P(EDOT-CD) | 43.0 | 30.9 | 17.6 | 8.5 |

Figure 6 shows the contact angle images of PEDOT, P(EDOT-LD) and P(EDOT-CD) films, illustrating the influence of the morphological changes induced by dextrins on the wettability of the films. In general, dextrins are usually considered to be highly hydrophilic since they contain no obvious apolar moieties but a large number of hydroxyl groups. The contact angle of PEDOT at room temperature is $\theta = 54.0° \pm 0.6°$, decreasing to $\theta = 46.9° \pm 0.9°$ and $52.1° \pm 0.7°$ after incorporation of LD and CD, respectively. Thus, the reduction of the hydrophobicity at the surface of the composites with respect to that of PEDOT is significantly higher in P(EDOT-LD) than in P(EDOT-CD). These results are fully consistent with the SEM and AFM images reflecting that the structural changes produced by the CD are relatively small, whereas the LD alters considerably the structure of PEDOT at the surface. Moreover, the concentration of dextrins in the composite was found to be slightly larger for P(EDOT-LD) than for P(EDOT-CD) (see below).

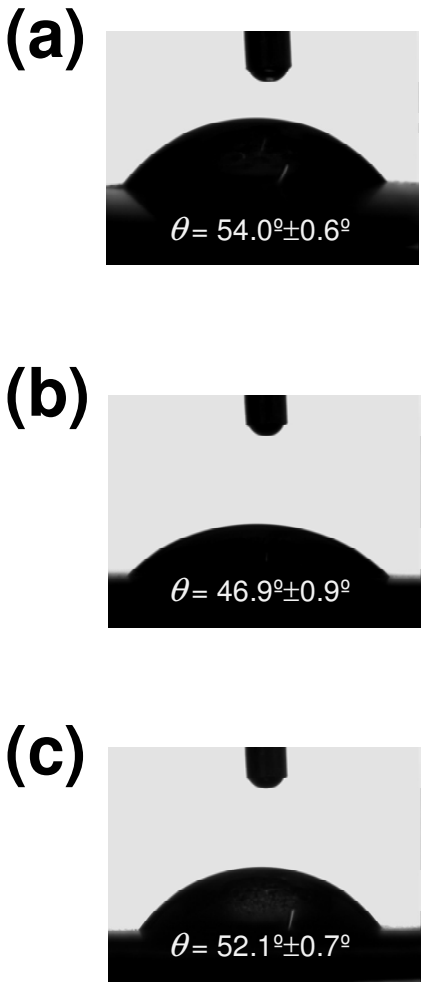


**Figure 6 –** Contact angle measurements of: (a) PEDOT, (b) P(EDOT-LD) and (c) P(EDOT-CD).

*Content and release of dextrins.* The phenol-sulphuric acid method, described in the Methods section, was used to quantify the concentration of dextrins in the P(EDOT-LD) and P(EDOT-CD) composites prepared in this work, which was found to be 20% and 15% w/w, respectively. On the other hand, Figure 7 represents the cumulative dextrins release considering two different media, *i.e.* BRB (pH 3) and PBS (pH 7.2). These releasing curves have been analyzed using four different models: zero order kinetic model, first-order kinetic model, Higuchi model, and Korsmeyer-Peppas model.[45,46] The fitted parameters are listed in Table 2. As it can be seen, the release occurs in the first 4 days of incubation independently

of both the pH and the biocomposite, a plateau being reached in all cases after such incubation period. The release of a molecule entrapped in polymeric matrix is typically controlled by the diffusion through the matrix, the degradation of matrix and the strength of the intermolecular interactions.[47,48]

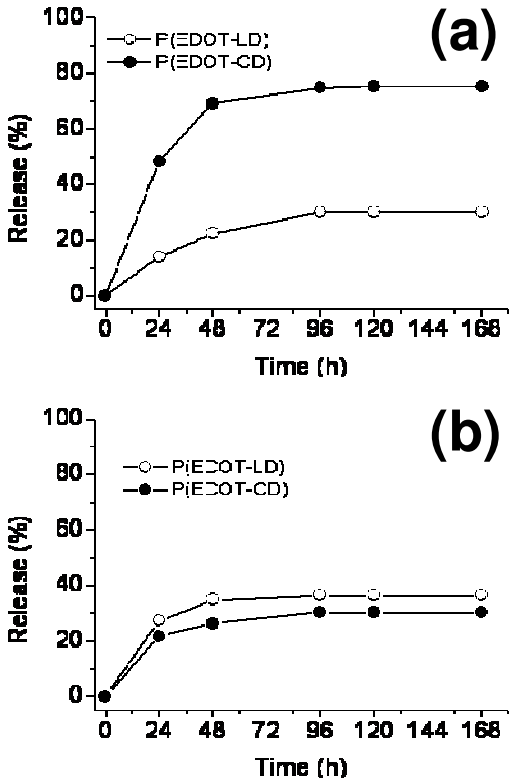


**Figure 7** – Cumulative release of CD and LD from P(EDOT-CD) and P(EDOT-LD) samples, respectively, incubated in (a) BRB (pH= 3.0) and (b) PBS (pH 7.2).

Results evidence the large influence of the pH on the CD releasing process. Thus, in acidic conditions most of the CD (76%) was effectively released from the composite after 96 h, while the releasing of LD reduced to 32%. In contrast, the release of dextrin was similar and relatively low (*i.e.* 32% and36% for CD and LD, respectively) at pH= 7.2. PEDOT chains are expected to form stronger intermolecular interactions with LD than with CD due to the polymeric nature of the former. Accordingly, the release of CD from P(EDOT-CD) is expected to be significantly higher than the release of LD from P(EDOT-LD), as was observed in BRB. However, dextrins tend to self-aggregate at neutral pH, making difficult the diffusion of the

CD molecules for their releasing in PBS.[49] In opposition, the hydroxyl group protonation produced by the strong acidic medium increases the hydrophilic character. This reduces the surface activity and enhances the releasing in BRB, The influence of this pH-effect is relatively low in P(EDOT-LD) since, in this case, the biocomposite is dominated by the interactions between two polymeric systems.

**Table 2 –** Parameters of the release kinetics based on four different models. Releasing assays were carried out in PBS (pH 7.2) and in BRB (pH 3.9). $M_t/M_\infty$ is the cumulative percentage of dextrin release. 100-($M_t/M_\infty$) corresponds to the percentage of dextrin remaining in the matrix.

| Release Medium | Composite | Zero-order | | First-order | | | Higuchi | | Korsmeyer-Peppas | | |
|---|---|---|---|---|---|---|---|---|---|---|---|
| | | $M_t/M_\infty = kt$ | | $100-(M_t/M_\infty) = kt^n$ | | | $M_t/M_\infty = kt^{1/2}$ | | $M_t/M_\infty = kt^n$ | | |
| | | $k_0$ ($h^{-1}$) | $r^2$ | $k_1$ ($h^{-1}$) | n | $r^2$ | $k_H$ ($h^{-1}$) | $r^2$ | $k_{KP}$ ($h^{-1}$) | n | $r^2$ |
| PBS (pH 7.2) | P(EDOT-LD) | 0.4805 | 0.4376 | 1.0016 | 0.1026 | 0.99 | 4.3485 | 0.8871 | 1.1712 | 0.8451 | 0.953 |
| | P(EDOT-CD) | 0.3889 | 0.5252 | 1.0013 | 0.0791 | 0.9996 | 3.4931 | 0.9258 | 1.1471 | 0.7936 | 0.9601 |
| BRB (pH 3.0) | P(EDOT-LD) | 0.3536 | 0.8467 | 1.0188 | 0.0718 | 0.9144 | 3.0725 | 0.9963 | 1.0575 | 0.7682 | 0.9921 |
| | P(EDOT-CD) | 0.9646 | 0.5761 | 1.0619 | 0.2999 | 0.9506 | 8.6291 | 0.9367 | 1.1881 | 1.0109 | 0.9602 |

Table 2 shows the parameters derived from the different kinetic models. As it can be seen, the correlation coefficients ($r^2$) provided by the zero-order model are, in general, very poor. In opposition, the first order-model led to very high $r^2$ values, especially in PBS, indicating a relationship between the releasing rate and the concentration of dextrins. Good correlations were also identified for the Higuchi's model, which reflects the dependence of the release of dextrins with the square root of time (*i.e.* diffusive process).[45] Finally, the Korsmeyer-Peppas model introduces the parameter *n* to describe the morphological characteristics from material (*i.e.* porous materials present $n < 0.5$).[46] In the present study, the coefficient *n* fits to values larger than 0.5 in all cases suggesting a compact morphology.

*Cellular adhesion and proliferation.* The utility of the two dextrin-containing biocomposites in biotechnological applications based on regeneration of tissues has been examined by analyzing cellular adhesion and proliferation on films. Assays were performed considering three different lines of eukaryotic cells: HEp-2, DU145 and COS-7. The former

two are epithelial-like cell lines, while the later is a fibroblast-like cell line. Both PEDOT and tissue culture polystyrene (TCPS) have been used as control substrates.

Quantitative results of cellular adhesion are displayed in Figure 8a. The number of cells by area of material observed on the biocomposites is larger than on the control substrates, independently of the cell line. Thus, incorporation of dextrins to PEDOT promotes cell adhesion, this feature being especially remarkable for the HEp-2 and DU-145 cells (*i.e.* adhesion of these epithelial-like cells on PEDOT is lower than that of COS-7).

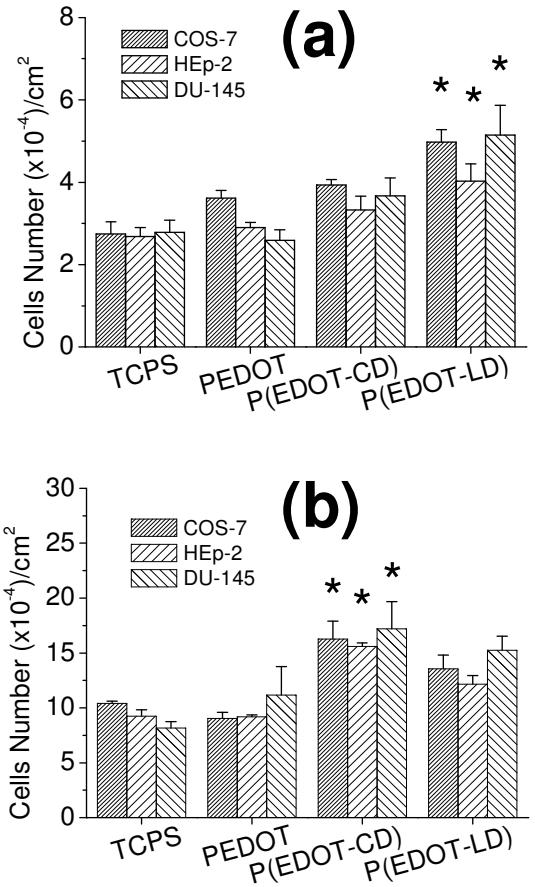


**Figure 8 –** Cellular adhesion (a) and cellular proliferation (b) on the surface of the investigated biocomposites. Values were normalized with respect to the area of material. PEDOT and TCPS were used as control substrates. Bars represent the mean ± standard deviation. The asterisk (*) indicates a significant difference with the control TCPS, Tukey's test ($p<0.05$).

On the other hand, Figure 8a reveals that the adhesion of cells on P(EDOT-LD) films is significantly higher than on P(EDOT-CD). This observation should be attributed to the fact that the cells have a direct contact with the polysaccharide, which has been hypothesized to be mainly located at the surface, whereas the impact of the CD on the cells is lower because of its homogeneous distribution.

The number of viable cells per unit of material after 7 days of culture (*i.e.* proliferation on the material) is displayed in Figure 8b for the four tested susbtrates. In all cases, there is a significant increment in the amount cells with respect to those obtained after 24 h of culture (Figure 8a). Again, the number of cells adhered to the two biocomposites is higher than adhered to control substrates, independently of the cell line, supporting the fact that the dextrins produce a benefit in terms of biocompatibility. However, the number of cells adhered to P(EDOT-CD) is higher than that observed for P(EDOT-LD). This feature suggests that once the cells are adhered to the biocomposite, the activity and proliferation of the cells is promoted by the diffusion of the small CD molecules towards the surface.

SEM micrographs showing details of the adhesion of COS-7 cells to PEDOT, P(EDOT-LD) and P(EDOT-CD) are displayed in Figure 9, the connection sites between the cells and the surface or between two cells being marked with arrows. As it can be seen, in general, there is a significant spreading of cells on the surface of the substrates, which is especially remarkable for the two biocomposites. Details showing the stress fibers formed by the cells to move along the substrates are displayed in Figure 9b (inset). These correspond to the lamellipodia, which are delicate sheet-like extension of cytoplasm that form transient adhesions with the substrate, and the actin filaments known as fillopodia. Interestingly, the formation of fillopodia is detected with much more proliferation and spreading on the P(EDOT-LD) surface (Figures 9f and 9g) than on the P(EDOT-CD) one. Thus, Figure 9d shows a cell without any evident connection to P(EDOT-CD) surface (arrow mark), evidencing that adhesion of the cell with filopodia is much less apparent in the latter biocomposite.

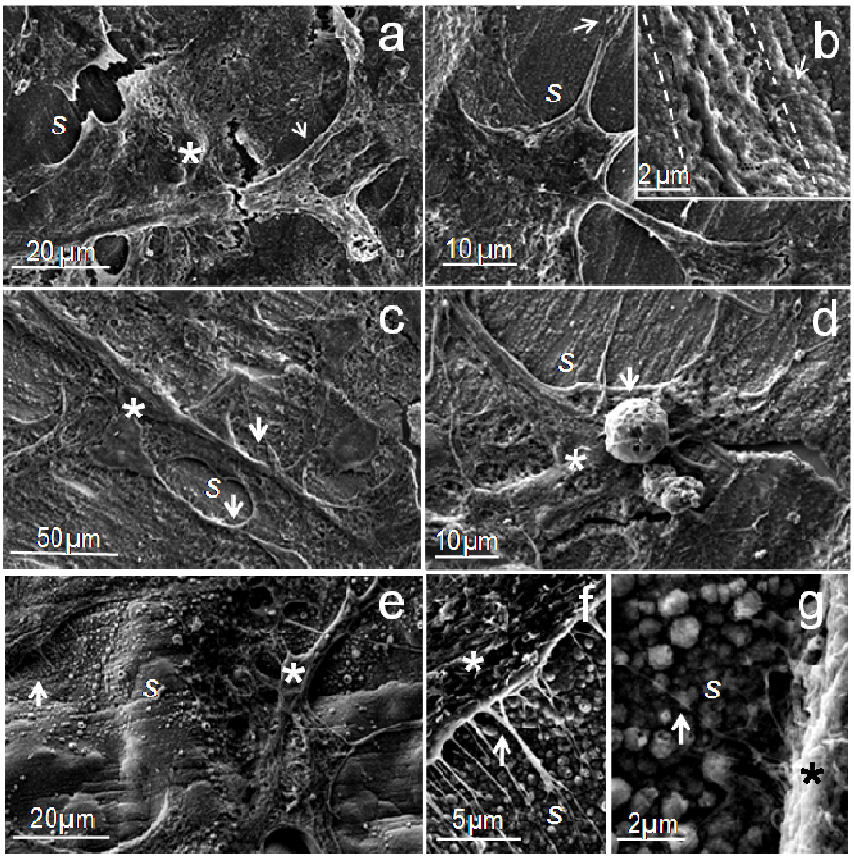


**Figure 9 –** Cellular adhesion of cells COS-7 (fibroblast type) onto PEDOT (a-b), P(EDOT-CD) (c-d), and P(EDOT-LD) (e-g) substrates. The cells adhered on the surface (*s*) are shown with asterisk (✶), while the arrows indicate connections or interactions between the cell and the surface or between two cells.

### 6.2.4 – Conclusions

P(EDOT-LD) and P(EDOT-CD) biocomposites have been prepared electrochemically in water using mixtures of EDOT monomer and the corresponding dextrin. Both the electroactivity and the electrostability of the two biocomposites are considerably lower than those of PEDOT. This is because the incorporation of dextrins promotes the formation of compact structures, reducing the porosity. Consequently, the access and escape of dopant ions upon oxidation and reduction processes, respectively, become more difficult in the biocomposites than in PEDOT films. In contrast, the electrical conductivities of the

biocomposites are similar to that of PEDOT, suggesting that dextrins do not produce significant changes in the bulk. Inspection to the topographies and morphologies indicates that the globular surface of PEDOT transforms into a powdery surface upon the incorporation of LD. The influence of the CD, which changes the aspect of the surface from globular to layered, is less drastic. These observations combined with the EDX elemental analyses suggest that the LD mainly concentrates at the surface of the films, while the CD is homogeneously distributed in the composite.

The concentration of CD and LD in P(EDOT-CD) and P(EDOT-LD) has been found to be 15% and 20%, respectively. The releasing of the CD from the biocomposite depends significantly on the environment, which has been attributed to the aggregation effects at neutral pH and the increase of hydrophilic character at low pH. In contrast, no pH-dependence was found in the releasing of LD from P(EDOT-LD). This is because the latter biocomposite is dominated by strong interactions between the polysaccharide and PEDOT chains. On the other hand, cell adhesion and proliferation assays have been performed considering three different cellular lines: two epithelial-like and one fibroblast-like. Results clearly indicate that the two biocomposites behave as a cellular matrix. Thus, the incorporation of dextrins significantly improves the cellular activity of PEDOT.

### 6.2.5 – References

[1] M. Dietrich, J. Heinze, G. Heywang, F. Jonas, *J. Electroanal. Chem.* 369 (1994) 87.

[2] C. J. Brabec, N. S. Sariciftci, J. C. Hummelen, *Adv. Funct. Mater.* 11 (2001) 15.

[3] L. Groenendaal, F. Jonas, V. Freitag, H. Pielartzik, J. R. Reynolds, *Adv. Mater.* 12 (2000) 481.

[4] L. Groenendaal, G. Zotti, P.-H. Aubert, S. M. Waybright, J. R. Reynolds, *Adv. Mater.* 15 (2003) 855.

[5] A. Menaker, V. Syritski, J. Reut, A. Opik, V. Horvath, R. E. Gyurcsanvi, *Adv. Mater.* 21 (2009) 2271.

[6] H. Yoon, S. K. Lee, O. S. Kwon, H. S. Song, E. H. Oh, T. H. Park, J. Jang, *Angew. Chem. Int. Ed.* 48 (2009) 2755.

[7] K. J. Gilmore, M. Kita, Y. Han, A. Gelmi, M. J. Higgins, S. E. Moulton, G. M. Clark, R. Kapsa, G. G. Wallace, *Biomaterials* 30 (2009) 5292.

[8] L. B. Liu, M. H. Yu, X. R. Duan, S. Wang, *J. Mat. Chem.* 20 (2010) 6942.

[9] C. Ocampo, E. Armelin, F. Estrany, L. J. del Valle, R. Oliver, F. Sepulcre, C. Alemán, *Macromol. Mater. Eng.* 292 (2007) 85.

[10] C. Alemán, B. Teixeira-Dias, D. Zanuy, F. Estrany, E. Armelin, L. J. del Valle, *Polymer* 50 (2009) 1965.

[11] B. Teixeira-Dias, D. Zanuy, L. J. del Valle, F. Estrany, E. Armelin, C. Alemán, *Macromol. Chem. Phys.* 211 (2010) 1117.

[12] K. Krishnamoorthy, R. S. Gokhale, A. Q. Contractor, A. Kumar, *Chem. Commun.* 40 (2004) 820.

[13] S. C. Luo, S. S. Liour, H. H. Yu, *Chem. Commun.* 46 (2010) 4731.

[14] L. J. del Valle, D. Aradilla, R. Oliver, F. Sepulcre, A. Gamez, E. Armelin, C. Alemán, F. Estrany, *Eur. Polym. J.* 43 (2007) 2342.

[15] C. Salto, E. Saindon, M. Bolin, A. Kanciurzewska, M. Fahlman, E. W. H. Jager, P. Tengvall, E. Arenas, M. Berggren, *Langmuir* 24 (2008) 14133.

[16] L. J. del Valle, F. Estrany, E. Armelin, R. Oliver, C. Alemán, *Macromol. Biosci.* 8 (2008) 1144.

[17] K. Svennersten, M. H. Bolin, E. W. H. Jager, M. Berggren, A. Richter-Dahfors, *Biomaterials* 30 (2009) 6257.

[18] Y. Xiao, C. M. Li, S. Wang, J. Shi, C. P. Ooi, *J. Biomed. Mater. Res.* 92A (2010) 766.

[19] H. Xie, S.-C. Luo, H.-h. Yu, *Small* 5 (2009) 2611.

[20] B. D. Martin, L. M. Velea, C. M. Soto, C. M. Whitaker, B. P. Gaber, B. Ratna, *Nanotechnology* 18 (2007) 055103.

[21] P. M. Bersier, J. Bersier, B. Klingert, *Electroanalysis* 3 (1991) 443.

[22] J. Szejtli, T. Osa, In *Comprehensive supramolecular chemistry*, Vol. 3, Cyclodextrins. Elsevier, Oxford (1996).

[23] A. Ferancová, J. Labuda, *J. Anal. Chem.* 370 (2001) 1.

[24] A. Harada, *Acc. Chem. Res.* 34 (2001) 456.

[25] Q. R. Chen, C. Liu, F. Q. Liu, *Progr. Chem.* 22 (2010) 927.

[26] C. Lagrost, K. I. Chane-Ching, J.-C. Lacroix, S. Aeiyach, M. Jouini, P.-C. Lacaze, J. Tanguy, *J. Mat. Chem.* 9 (1999) 2351.

[27] C. Lagrost, M. Jouini, J. Tanguy, S. Aeiyach, J.-C. Lacroix, K. I. Chane-Ching, P. C. Lacaze, *Electrochim. Acta* 46 (2001) 3985.

[28] T. Shimomura, K. I. Yoshida, K. Ito, H. Reinosuke, *Polym. Adv. Technol.* 11 (2000) 837.

[29] K. I. Yoshida, K. Shimomura, K. Ito, R. Hayakawa, *Langmuir* 15 (1999) 910.

[30] D. A. Reece, S. F. Ralph, G. G. Wallace, *J. Membr. Sci.* 249 (2005) 9.

[31] J. Arjomandi, R. Holze, *Cent. Eur. J. Chem.* 8 (2008) 199.

[32] J. Arjomandi, R. Holze, *J. Solid State Electrochem.* 11 (2007) 1093.

[33] K. R. Temsamani, H. B. Jr. Mark, W. Kutner, A. M. Stalcup, *J. Solid State Electrochem.* 6 (2002) 391.

[34] M. Van den Boogaard, G. Bonnet, P. van't Hof, Y. Wang, C. Brochon, P. van Hutten, A. Lapp, G. Hadziioannou, *Chem. Mater.* 16 (2004) 4383.

[35] V. S. Vasantha, K. L. N. Phani, *J. Electroanal. Chem.* 520 (2002) 79.

[36] V. S. Vasantha, R. Thangamuthu, S.-M. Chen, *Electroanalysis* 20 (2008) 1754.

[37] M. Dubs, J. Weisser, R. Linke, A. Pfuch, D. Imhof, M. Schnabelrauch, *Mat.-wiss. u.Werkstofftech* 40 (2009) 853.

[38] J. Carvalho, S. Moreira, J. Maia, F. M. Gama, *J. Biomed. Mat. Res.* 93A (2010) 389.

[39] J. Hardwicke, R. Moseley, P. Stephens, K. Harding, R. Duncan, D. W. Thomas, *Mol. Pharma.* 7 (2010) 699.

[40] S. M. Moreira, F. K. Andrade, L. Domingues, M. Gama, *BMC Biotechnology* 8 (2008) 78.

[41] J. Carrasco, E. Brillas, V. Fernández, P. L. Cabot, J. A. Garrido, F. Centellas, R. M. Rodríguez, *J. Electrochem. Soc.* 148 (2001) E19.

[42] M. Dubois, K. A. Guilles, P. A. Hamilton, P. A. Rebers, F. Smith, *Anal. Chem.* 28 (1956) 350.

[43] T. Mosmann, *J. Immunol. Methods* 65 (1983) 55v.

[44] C. Ocampo, R. Oliver, E. A. Armelin, C. Alemán, F. Estrany, *J. Polym. Res.* 13 (2006) 193.

[45] T. Higuchi, *J. Pharm. Sci.* 52 (1963) 1145.

[46] R. W. Korsmeyer, N. A. Peppas, In "Swelling-controlled delivery systems for pharmaceutical application: macromolecular and modeling consideration. Controlled Release Delivery Systems". Roseman, T. J., Mansdorf, S. Z. (Eds), Marcel Dekker, New York (1983)

[47] B. Amsdem, *Macromolecules* 32 (1999) 874.

[48] W. N. E. Dijk-Wolthuis, J. A. M. Hoogeboom, M. J. van Steenbergen, S. K. Y. Tsang, W. E. Hennink, *Macromolecules* 30 (1997) 4639.

[49] Z. Chen, L. Zhu, T. Song, J. Huang, Y. Han, *Anal. Chim. Acta* 635 (2009) 202.

## 6.3 – Impact of the incorporation of positively charged peptide with advanced properties in the electrochemical and cellular activity of PEDOT

This study reports the synthesis and characterization of poly(3,4-ethylenedioxythiophene) (PEDOT) modified with CREKA, a positively charged pentapeptide that recognizes clotted plasma proteins. Modified PEDOT (PEDOT/CREKA) was prepared by anodic polymerization using as electrolyte solution a mixture of acetonitrile and water with $LiClO_4$. The peptide, which has been identified by high performance liquid chromatography and infrared spectroscopy, has been found to incorporate to the polymer matrix at the first stages of the polymerization process. The concentration of peptide in PEDOT/CREKA films was estimated to be 0.3-0.4% only, which has been attributed to both its small size and its net positive charge. In spite of such small concentration, the peptide imparts a blocking effect against the oxidation of the conducting polymer, improves considerably both the redox capabilities and electrochemical stability of PEDOT, and also enhances the capacitance and resistance. Cellular adhesion and proliferation assays provided similar results for both PEDOT and PEDOT/CREKA.*

* - Results reported in this section have been submitted for publication.

### 6.3.1 – Introduction

Conducting polymer (CP) coatings have been shown to improve the charge transfer characteristics of conventional metal electrodes and biological assays have revealed that cells preferentially adhere to coated electrodes.[1-3] As a consequence, many CPs have been used in tissue engineering applications, even though research efforts have been mainly concentrated on polypyrrole (PPy), poly(3,4-ethylenedioxythiophene) (PEDOT) and their derivatives.[4] Some extracellular matrix biomolecules, specially peptides, are known to support cell attachment and growth when incorporated into CPs or used as a coating.[5-14] The incorporation of these peptides can be carried out using different approaches.

Cell attachment properties improves when the incorporated peptides present an overall anionic behaviour, which has been attributed to role exerted by such anionic biomolecules as dopant agents of the CPs.[4-10] The use anionic peptides as dopants, is achieved through their incorporation into the monomer medium, where the polymerization process occurs. Unfortunately, this particular class of dopants may produce significant undesirable changes in the bulk properties of the CP, reducing the electrical conductivity, the electroactivity, the electrochemical stability, etc. For example, anionically modified laminin

peptides were used to dope PEDOT electrodeposited on platinum electrodes.[8] Comparison of the performance of the peptide doped films with conventional PEDOT films doped with *p*-toluenesulfonate indicated that, in spite of peptide dopant impart better cell attachment properties, the electrochemical stability and electroactivity of PEDOT films were clearly superior.

Besides using anionic peptides as dopants to modify CPs properties, there are other emerging non-covalent approaches to further modify CPs for biomedical applications. For instance, one approach to modify CPs non-covalently was achieved using a peptide selected from phage display libraries, that specifically binds PPy doped with chloride.[11] This study demonstrated that the PPy surface modified with Arg-Gly-Asp (RGD) peptide promotes the PC12 cell adhesion in serum-free media, whereas no adhesion was seen on unmodified surfaces. An advantage of this entrapped approach is that, apparently, it should not modify the intrinsic properties of the CP and could be used with a wide range of different biomolecules that do not need to be negatively charged.

In addition to the dopant and entrapped non-covalent approaches, modification of CPs via covalent bonds has been also explored. Multiple techniques have been used, like for example: the modification of the β-position on PPy to create strong disulfide bonds with the Cys of Arg-Gly-Asp-Cys (RGDS), enhancing osteoblast adhesion; and the modification of the surface to immobilize peptides through covalent bonds, which have been successfully used to immobilize nerve growth factor to the surface of CPs through a photo-crosslinker.[12-14]

Over the last few years, Ruoslahti and coworkers have identified a series of tumor-homing peptides by using *in vivo* screening of peptide libraries.[15,16] Among the homing peptides discovered by this procedure is a linear peptide that contains only five amino acids with sequence Cys-Arg-Glu-Lys-Ala (CREKA).[15,16] This pentapeptide, which recognizes fibrin-fibronectin complexes, was used to design a self-amplifying nanoparticle delivery system.[17] Iron oxide nanoparticles coated with this peptide accumulate in tumor vessels, where they induce additional local clotting and thereby produce new binding sites for more nanoparticles. This amplification system enhanced homing of the nanoparticles in a mouse tumor model without causing clotting or other obvious side effects in the body. Although self-amplified tumor accumulation produced enhancement of tumor imaging, significant inhibition of tumor growth was not obtained. Determination of the bioactive conformation of CREKA through computer aided modelling tools led to engineer a series of analogues by

targeted replacements in Arg and Glu, which were replaced by the corresponding N- and $C^{\alpha}$-methylated amino acids.[18-20] CREKA analogues nanoparticles were combined with nanoparticles coated with another tumor-homing peptide (Cys-Arg-Lys-Asp-Lys-Cys) and nanoparticles with an elongated shape (nanoworms). Treatment of mice with prostate cancer with multiple doses of these nanoworms induced tumor necrosis and highly significant reduction in tumor growth.[20]

Modification of CPs through the incorporation of N- and $C^{\alpha}$-methylated CREKA analogues, which due to their unique properties could extend the biomedical applications of these materials, is highly desirable. Unfortunately, the synthesis of these analogues requires of an expensive and large chemical effort essentially related with the preparation of the modified amino acids. However, as the charge distribution is the same in CREKA that in its N- and $C^{\alpha}$-methylated analogues, the former should be considered a good model in studies devoted to both: (i) select the approach and conditions used for their incorporation into the polymer matrix; and (ii) ascertain the influence of these peptides in the CP properties. Within this context, in this work we have used an entrapping approach to modify PEDOT doped with $LiClO_4$ with CREKA. It should be noted that the cationic nature of CREKA, which involves two positively charged amino acids and only one negatively charged, is expected to difficult its entrapment into the polymer matrix. Furthermore, the impact of the peptide on morphological and electrochemical properties, as well as on the cellular activity, of the CP has been established by comparing PEDOT with modified PEDOT, hereafter referred as PEDOT/CREKA.

### 6.3.2 – Methods

*Materials.* 3,4-ethylenedioxythiophene (EDOT) monomer and acetonitrile (analytical reagent grade) were purchased from Aldrich and used as received without further purification. Anhydrous $LiClO_4$ (analytical reagent grade, Aldrich) was stored in an oven at 80 ºC before use in electrochemical trials. CREKA peptide with > 98% of HPLC purity was purchased from GenScript USA Inc. and prepared by dissolving 4.5 mg of peptide in 5 mL of ultrapure milliQ water.

*Synthesis.* PEDOT was prepared by chronoamperometry (CA) under a constant potential of 1.40 V using a polymerization time of 200 s. Both anodic polymerization and electrochemical assays were performed with a VersaStat II potentiostat-galvanostat (Princeton Applied Research) using a three-electrode compartment cell under nitrogen atmosphere (99.995% pure) at room temperature. The anodic compartment was filled with 5 mL of a 0.01 M EDOT solution in acetonitrile containing 0.1 M $LiClO_4$ as supporting electrolyte and 5 mL of ultrapure milliQ water solution, while the cathodic compartment was filled with 10 mL of the same electrolyte solution. Steel AISI 316 sheets of 1 $cm^2$ in area were used as working and counter electrodes. To prevent interferences during the electrochemical assays, the working and counter electrodes were cleaned with acetone before each trial. The reference electrode was an Ag|AgCl electrode containing a KCl saturated aqueous solution [offset potential versus the standard hydrogen electrode, $E^0$= 0.222 Volts (V) at 25 ˚C], which was connected to the working compartment through a salt bridge containing the electrolyte solution.

The experimental conditions used for the preparation of PEDOT/CREKA were identical to those of PEDOT with the exception of the anodic compartment, which was filled with 5 mL of 0.01 M EDOT solution in acetonitrile containing 0.1 M $LiClO_4$ as supporting electrolyte and 5 mL of CREKA aqueous solution.

*Scanning electron microscopy (SEM) and energy dispersive X-ray (EDX) spectroscopy.* SEM and EDX spectroscopy studies were performed to examine the effect of the peptide on the film surface morphology and composition. Dried samples were placed in a Focussed Ion Bean Zeiss Neon 40 scanning electron microscope at 5 kV, equipped with an EDX spectroscopy system.

*High-performance liquid chromatography (HPLC).* Analyses were carried out using a isocratic gradient of 0.1% trifluoroacetic acid, 10% acetonitrile, and 10% methanol in 100% Water, with 1 mL/h of flux and a sample loop of 20 µL on a Licrospher (Merk) C18 column (4.6 mm x 250 mm) with 5 µm diameter particle. The HPLC system consisted on a LC-410 Perkin Elmer HPLC Pump, a LC-235 Perkin Elmer UV-VIS detector, and a Perkin Elmer (Diode Array Detector) interface. The HPLC analysis was running by 15 minutes and the chromatograms were analyzed using the Grams v.8 software (Galactic Inc.). Samples were detected by two channels of absorbance at 220 nm and 280 nm. The standard curve was

prepared with different concentrations of CREKA, the area of the peaks being represented against the peptide concentration. Models were adjusted through linear regression analyses. The PEDOT/CREKA samples (2 mg of powder) were extracted in the same HPLC buffer (1 mL) overnight. After this, samples were centrifugated and the supernatant isolated for the HPLC analysis. The determination of CREKA in the sample was performed using the method of substance added. Accordingly, samples were injected in the column and the chromatogram recorded. Next, a known amount of CREKA was added to the sample, which was subsequently injected in the HPLC column. This process allowed us to determine the peaks of CREKA in the sample.

*FTIR spectroscopy.* The influence of the polymer matrix on the secondary structure of the entrapped peptide was performed using a FTIR 4100 Jasco spectrophotometer. Spectra of CREKA, PEDOT and PEDOT/CREKA were recorded in the transmittance mode. The samples were placed in an attenuated total reflection accessory with thermal control and a diamond crystal (Specac model MKII Golden Gate Heated Single Reflection Diamond ATR).

*Electroactivity and electrostability.* Electrochemical properties of PEDOT and PEDOT/CREKA were investigated by cyclic voltammetry (CV) using 5 mL of acetonitrile solution containing 0.1 M $LiClO_4$ and 5 mL of ultrapure milliQ water as electrolyte solution. The initial and final potentials were -0.50 V, whereas a reversal potential of 1.60 V was considered. The scan rate was 100 $mV \cdot s^{-1}$ in all cases. The electroactivity increases with the similarity between the anodic and cathodic areas of the first control voltammogram, whereas the electrostability decreases with the oxidation and reduction areas of consecutive control voltammograms.

*Electrochemical impedance spectroscopy (EIS).* EIS studies were carried using three-electrode two-compartment cell with an Autolab 302N potenciostat/galvanostat and the FRA software program. The cell was filled with an electrolyte solution prepared by mixing 5 mL of acetonitrile with 0.1 M $LiClO_4$ and 5 mL of ultrapure MilliQ water. All the measurements were performed at room temperature. Coated and uncoated steel AISI 316 L sheets of $1 \times 1$ $cm^2$ were employed as working and counter electrodes, respectively. EIS measurements were carried out in the 0.05-10000 Hz frequency range and sinusoidal

voltage amplitude of ±10 mV for 70 frequencies. EIS data were plotted in terms of real and imaginary parts of the impedance (Z' and –Z'', respectively).

*Cell adhesion and proliferation test.* In vitro adhesion and proliferation assays were performed using two different cellular lines of adherent growth: (i) cells HEp-2 (human line derived from an epidermoid carcinoma of larynx); and (ii) cells DU145 (human line derived from a prostate carcinoma). HEp-2 and DU145 have an epithelial morphology. Tissue culture polystyrene (TCPS) has been used as control substrate.

Cells were plated in 25 $cm^2$ tissue flasks and grown in Dulbecco's Modified Eagle's Medium (DMEM) supplemented with 10% fetal bovine serum (FBS), penicillin G (100 U/ml) and streptomycin (100 mg/mL). Cultures were performed at 37 °C and humid atmosphere with 95% air (5% carbon dioxide). Passage 2 cultures were used for experiments. Cellular confluent cultures were dissociated with 0.05% trypsin and 0.02% EDTA in Hanks' Balanced Salt Solution, harvested by centrifugation, and counted in Neubauer camera using 0.4% trypan blue.

The adhesion and proliferation assays were performed seeding $2\times10^4$ cells, from an appropriate cell suspension concentration with viability >95%. PEDOT and PEDOT/CREKA electrodeposited on 1 $cm^2$ steel sheets were placed in 24-well plates, and subsequently sterilized by UV-radiation during 15 min in the laminar flow cabinet. Next, cells were seeded by a slowly pipette of the cell suspension onto the top surface of each sample, covering 80-90% of the sample's surface. In order to avoid a reduction of the seeding efficiency, no contact between cell suspensions and the sides of the wells was allowed. The plates were placed with care into an incubator, avoiding agitation. After 1 h, fresh medium (1 mL) was added into each well and the plate was returned to the incubator. Cultures to evaluate cellular adhesion and proliferation were incubated during 24 h and 7 days, respectively. All experiments were repeated at least three times.

To evaluate the cell number in the samples, the medium of each well was changed by fresh medium supplemented with MTT [3-(4,5-dimethylthiazol-2-yl)-2,5-diphenyltetrazolium; 5 mg/mL] and the plate returned to the incubator for 3 h. After this, the medium of each well was removed and the samples recoveries were placed in wells of a clean plate. The MTT reaction in the viable cells was determined by dissolving the formazan crystals in 1 mL of DMSO/methanol/water (70%/20%/10%, % in vol.). Then, the absorbance

at 540 nm was read in a spectrophotometer. The cells number was determined using a standard curve of $A_{540nm}$ *vs*. number of viable cells. Analyses were carried out using the cell adherence density in each sample in comparison to the control (%, relative of control).

To evaluate the cellular morphology, samples incubated with cells were fixed in 1 mL of 2.5% paraformaldehyde in PBS during 24 h at 4 ˚C. Then, samples were progressively dehydrated using alcohols of 30˚, 40˚, 50˚, 70˚, 90˚, 95˚, and 100˚ for 30 min at 4 ˚C in each one. Finally, samples were coated by carbon sputtering for the observation in the scanning electronic microscope.

### 6.3.3 – Results and Discussion

Figure 1a displays low- and high-resolution SEM images representative of the overall PEDOT morphology. This material presents a heterogeneous globular morphology similar to that found when it is generated in pure organic electrolyte solutions.[21] This characteristic morphology has been typically attributed to the linear growing of polymer molecules through α-α linkages (*i.e.* the β-positions of the thiophene are occupied by the dioxane ring).[21,22] In spite of this resemblance, the morphology of PEDOT yielded in acetonitrile is significantly more porous than that obtained with the acetonitrile/water mixture.[21] Differences in porosity are expected to have an impact on the electrochemical properties of CPs (see below). Inspection of the SEM images recorded for PEDOT/CREKA (not shown) does not reflect any significant difference with respect to those displayed in Figure 1a. Similarly, EDX spectroscopy analyses evidenced a very similar elementary composition for PEDOT and PEDOT/CREKA films (data not shown), indicating that the entrapped peptide do not alter the surface of the CP.

In order to ascertain if the peptide affects the surface morphology of the internal side, films were detached from the steel electrodes and coated with an ultrathin layer of carbon. Low- and high-resolution SEM images of the internal side of PEDOT and PEDOT/CREKA are shown in Figures 1b and 1c, respectively. As it can be seen, entrapped CREKA affects both the texture and morphology of PEDOT. The more noticeable results are the homogeneous smooth texture and the practical absence of small nodular outcrops in PEDOT/CREKA films, whereas these are frequently and homogeneously present in PEDOT. These nodules correspond to the typical PEDOT agglomerates previously mentioned, their absence in

PEDOT/CREKA suggesting a more compact internal surface. The similarity between PEDOT and PEDOT/CREKA in the external surface morphology has been attributed to the fact that peptide molecules incorporate to the polymer matrix at the first stages of the polymerization process.

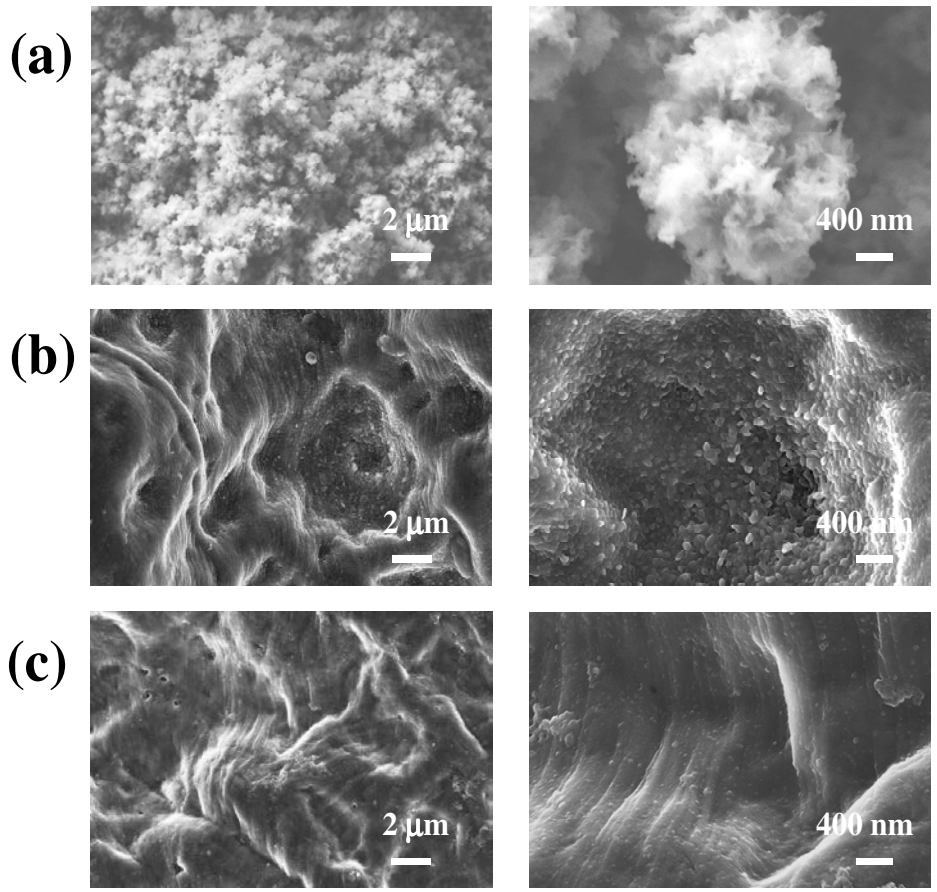


**Figure 1 –** Low- and high-resolution SEM images (left and right, respectively) of (a) the external surface morphology of PEDOT and the internal surface morphology of (b) PEDOT and (c) PEDOT/CREKA. Internal surfaces of PEDOT and PEDOT/CREKA films were coated with an ultrathin layer of carbon.

HPLC analyses were carried to confirm the presence of the peptide in PEDOT/CREKA films as well as to determine the peptide concentration. Results for CREKA, PEDOT and PEDOT/CREKA are displayed in Figure 2. Detection of the eluted at 220 nm produced two peaks with retention times of 3.3 and 4.8 min for CREKA (Figure 2a), whereas a single peak

with a retention time of 4.8-5.0 min was identified when the eluted was detected at 280 nm (data not shown). We assumed that the peak detected at 280 nm corresponds to a honeycomb structure formed by layers of peptides, as was previously found in other polymer-peptide conjugates.[17,18] The response of PEDOT was the same at both 220 and 280 nm, two peaks with different intensities and retention times of 4.8-5.0 min and 9.3 min being detected (Figure 2b).

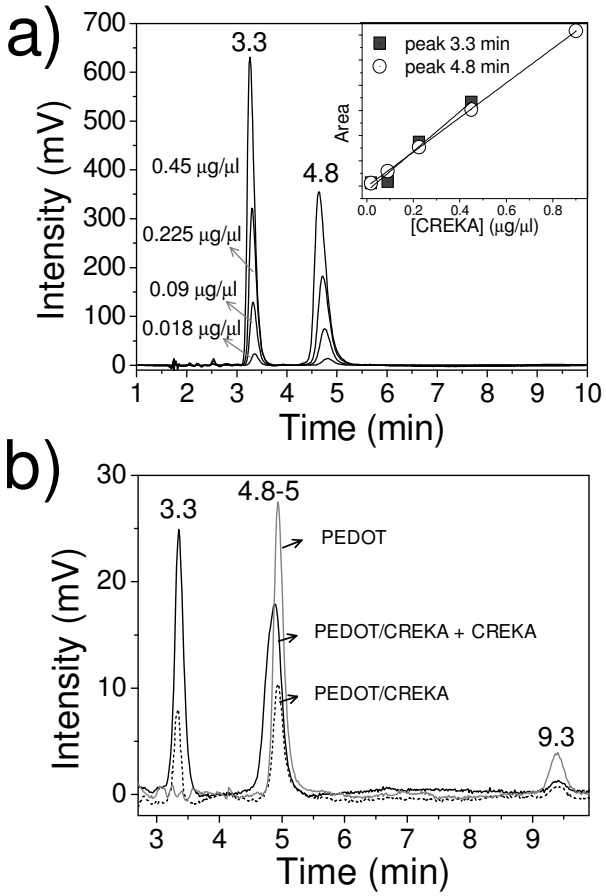


**Figure 2 –** Detection of CREKA in PEDOT/CREKA by HPLC. (a) Chromatograms of CREKA at different concentrations show overlapping. The detection was carried out by absorbance at 220 nm. The retention times are indicated over each peak. The inset shows the linear models obtained using the two peaks of CREKA. (b) Chromatograms used to analyze the peptide extracted from PEDOT/CREKA. The correspondence of peaks was determined by adding a known concentration of CREKA in the extracted sample. A PEDOT extract was used as control to identify the peaks of the conducting polymer.

The chromatograms of CREKA standards have been followed by absorbance at 220 nm, the linear models for the peaks at 3.3 min ($r$= 0.9812) and 4.8 min ($r$= 0.9999) being displayed in the inset of Figure 2a. As a consequence of the excellent correlations between the peak areas and the CREKA concentrations, the two models become indistinguishable.

The concentration of peptide extracted from PEDOT/CREKA was determined using the method of the added concentration (Figure 2b). As can be seen, there is an overlapping between the peaks of CREKA and the peptide extracted from PEDOT/CREKA. The concentration of peptide in the latter was estimated to be 0.3-0.4%, which corresponds to a PEDOT:CREKA mass ratio of 300:1. This ratio is significantly lower than that used for the electropolymerization of the films (3:1). Both the small size of the pentapeptide and its net positive charge made difficult the entrapment of CREKA in the polymer matrix. However, in spite of this small concentration, the peptide produced drastic changes in the electrochemical properties of the CP, as is evidenced below.

Figure 3 displays the FTIR-ATR spectra of CREKA, PEDOT/CREKA and PEDOT. The 1900-1100 $cm^{-1}$ interval shows the amide I, amide II and amide III bands of CREKA, which have been used to examine the influence of the polymer matrix on the structure of the entrapped peptide. The amide I band (1700-1600 $cm^{-1}$) arises primarily from the C=O stretching vibration of the peptide linkages (70-85%) that constitute the backbone structure of peptides and proteins, its sensitivity towards conformational changes being well-known.[23-26] The amide II band (1600-1480 $cm^{-1}$) is assigned to the coupling of the N-H in-plane bending (40-60%) and C-N stretching modes (18-40%) of peptide linkages and C-$C^{\alpha}$ stretching vibrations (~ 10%). This band is conformationally sensitive.[25] Amide III is a very complex band resulting from a mixture of several coordinate displacements. Moreover, this signal depends on the nature of side chain and hydrogen bonding interactions, which limits its use for the extraction of structural information.[23,25]

The amide I of CREKA and PEDOT/CREKA appears centred at 1739 and 1741 $cm^{-1}$, respectively. These wavelengths are slightly larger than those typically identified for the amide I of proteins, which has been attributed to the small size of the pentapeptide. Similarly, the amide III absorptions of CREKA (1368 and 1213 $cm^{-1}$) are not influenced by the polymer matrix in PEDOT/CREKA (1366 and 1210 $cm^{-1}$). In spite of the CP does not alter the amide I and II absorption bands, it induces a small shift in the amide II, which are identified at 1639 and 1618 $cm^{-1}$ for CREKA and PEDOT/CREKA respectively. In addition to confirm the

presence of the entrapped peptide in PEDOT/CREKA, which is consistent with the HPLC analyses, these results indicate that the CP does not produce major alteration in the conformational characteristics of CREKA.

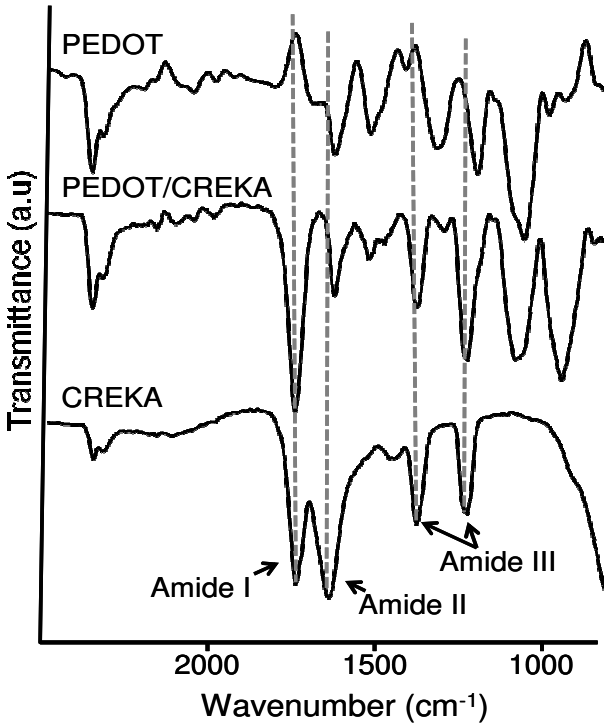


**Figure 3 –** FTIR spectra of CREKA, PEDOT/CREKA and PEDOT at room temperature.

The cyclic voltammograms of PEDOT and PEDOT/CREKA, which were recorded in the potential range from -0.50 to 1.60 V, are compared in Figure 4a. Two consecutive anodic processes, $O_1$ and $O_2$, and one cathodic process, $R_1$, are detected in the voltammograms of both PEDOT and PEDOT/CREKA. Table 1 summarizes the effect of the peptide in the potentials associated to such oxidation and reduction processes. The first oxidation peak of PEDOT, which corresponds to a shoulder with anodic peak potential $E_p^a(O_1)$= +0.713 V, is not detected in the PEDOT/CREKA voltammogram, suggesting that the peptide blocks the formation of polarons at such potential.

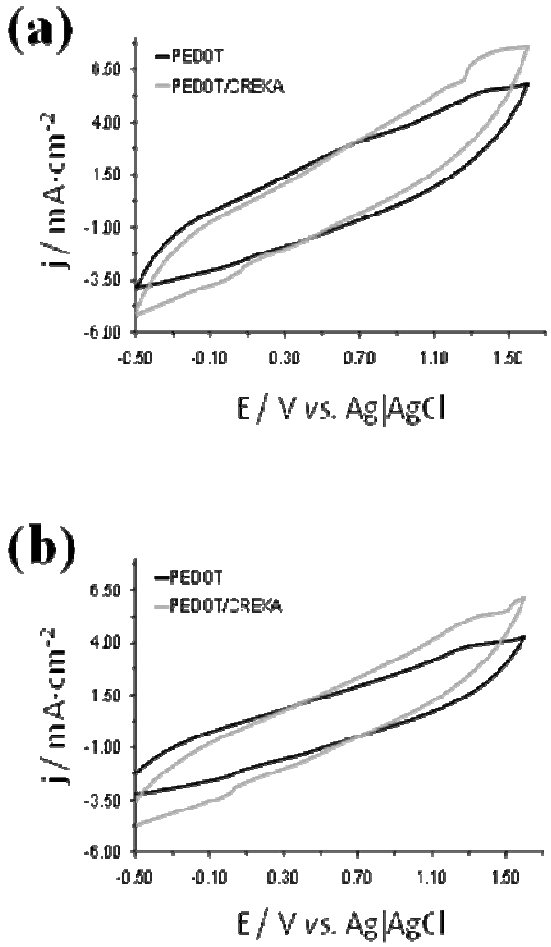


**Figure 4 –** (a) Control voltammograms of PEDOT (black) and PEDOT/CREKA in acetonitrile:water solution recorded using samples (a) as prepared and (b) after 12 consecutive oxidation-reduction cycles.

This is consistent with the fact that the first oxidation shoulder of PEDOT/CREKA appears at a higher potential $E_p^a(O_1)$= +1.183 V. A similar but less pronounced effect is induced by the peptide in the second oxidation shoulder of PEDOT, which has been attributed to the formation of bipolarons. Specifically, the anodic peak potential of PEDOT, $E_p^a(O_2)$= +1.381 V, is shifted to a slightly higher potential, $E_p^a(O_2)$= +1.410 V in PEDOT/CREKA. The fact that the displacement of the anodic potential is smaller for $O_2$ than for $O_1$ is also fully consistent with the previously mentioned blocking effects against oxidation of the CP imparted by CREKA.

Thus, these effects are expected to become more difficult at higher electric potentials. The two voltammograms show a reduction shoulder with very similar cathodic peak potentials: $E_p^c(R_1)$= -0.005 V and $E_p^c(R_1)$= -0.025 V for PEDOT and PEDOT/CREKA, respectively. Redox-pairs associated to the formation of polarons in the CP chains are identified from these reduction peaks. However, as the intensity of the reduction peak is higher in PEDOT/CREKA than in PEDOT, it can be concluded that the peptide promotes the redox capabilities of the CP molecules.

**Table 1 –** Comparison of the oxidation and reduction potentials (in V) for the anodic and cathodic processes detected in the control voltammograms of PEDOT and PEDOT/CREKA using samples as prepared (Figure 4a) and after 12 consecutive oxidation-reduction cycles (Figure 4b).

| | Fresh samples | | After 12 redox cycles | |
|---|---|---|---|---|
| | **PEDOT** | **PEDOT/CREKA** | **PEDOT** | **PEDOT/CREKA** |
| $E_p^a(O_1)$ | +0.713 | +1.183 | - | - |
| $E_p^a(O_2)$ | +1.381 | +1.410 | +1.315 | +1.364 |
| $E_p^c(O_1)$ | -0.005 | -0.025 | -0.046 | -0.029 |

On the other hand, the small concentration of the entrapped peptide does not alter the intrinsically high electroactivity of the CP, as is evidenced by the resemblance between the cathodic and anodic areas of the two voltammograms. In contrast, the peptide enhances considerably the maximum anodic current density ($j_{max}$), which is reached at the reversal potential, 1.60 V, in both cases. Thus, $j_{max}$ increases from 5.84 mA·cm$^{-2}$ (PEDOT) to 7.60 mA·cm$^{-2}$ (PEDOT/CREKA), which represents an increment of 30%.

Figure 5 represents the variation of the relative electroactivity against the number of consecutive oxidation-reduction cycles. The response of the PEDOT and PEDOT/CREKA degraded in the first cycles and tended to plateau after 8 and 12 cycles, respectively. The loss of activity is significantly smaller for PEDOT/CREKA than for PEDOT evidencing that the peptide molecules promote the electrostability of the CP. This result is fully consistent with the fact that CREKA enhances the redox capabilities of the CP molecules, as was discussed above (Figure 4a).

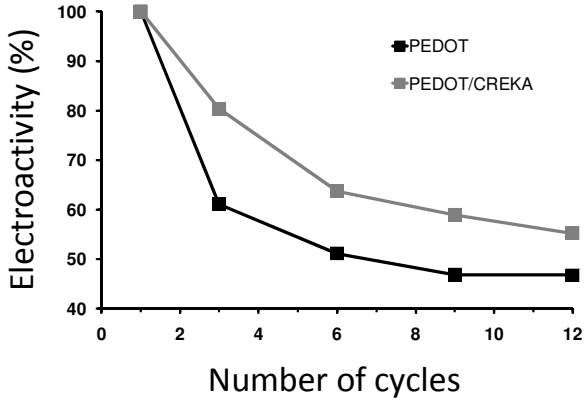


**Figure 5 –** Evolution of the electroactivity over 12 consecutive oxidation-reduction cycles for PEDOT and PEDOT/CREKA. The electroactivity loss is represented as the percentage of the original electrochemical activity measured at cycle 1.

Figure 4b compares the cyclic voltammograms of PEDOT and PEDOT/CREKA after 12 consecutive oxidation-reduction cycles, the anodic and cathodic peak potentials for the detected oxidation and reduction processes being included in Table 1. As it can be seen, in both systems the first oxidation shoulder, which was clearly identified as $O_1$ in the first control voltammogram (Figure 4a), is not detectable. This suggests that the oxidative degradation induces the re-organization of the CP aggregates, blocking the entrance of ions and, consequently, precluding the formation of polarons. The oxidation shoulder identified as $O_2$ in Figure 4a corresponds to the only oxidative process detected in Figure 4b. This anodic peak potential $E_p^a$ ($O_2$) of both PEDOT and PEDOT/CREKA decreases by ~ 0.03-0.05 V due to the oxidative degradation of the CP. A similar effect is observed in the cathodic peak potential $E_p^c$ ($R_1$) of the reduction process, which shifts to more negative potentials.

Figure 6 displays the Nyquist plot recorded for the steel AISI 316 (control), PEDOT and PEDOT/CREKA samples. The impedance plot of PEDOT in the acetonitrile:water mixture shows two semicircles, in the high and low frequency regions, followed by a linear part that arises from the diffusion process. The high frequency semicircle is related with the organic nature of the coating, while the low frequency semicircle is consequence of the pores in the coating.[27] As it can be seen, the incorporation of CREKA produces a significant enhancement of both the capacitance and the resistance. This effect should be attributed to

the structural changes induced by the peptide, which reduces the porosity of the CP. This feature was clearly evidenced in the internal side of PEDOT/CREKA films (Figure 1c).

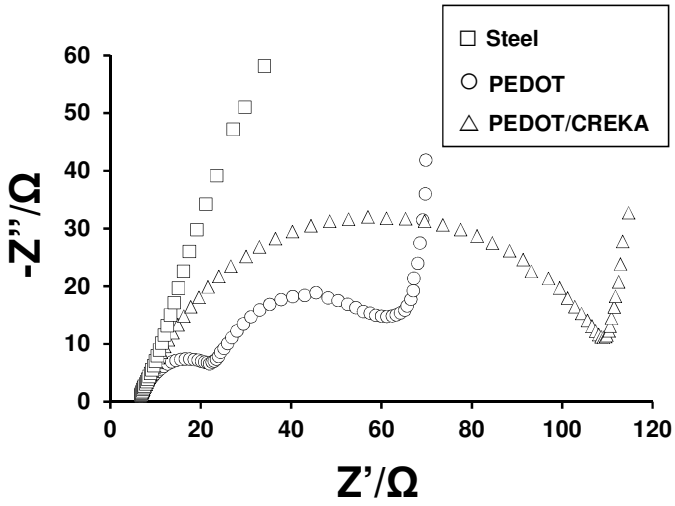


**Figure 6 –** Impedance plots obtained for steel AISI 316 (control sample), PEDOT and PEDOT/CREKA.

The abilities of PEDOT and PEDOT/CREKA to cellular adhesion and proliferation were compared by considering two different cellular lines: HEp-2 and DU-145. These carcinogenic cells were selected due to their fast growth. Quantitative results of cellular adhesion assays are displayed in Figure 7a, TCPS being used as control substrate. As can be seen, the peptide does not affect the adhesion of the cells, which is similar in all cases to that obtained for the control substrate. After 7 days of culture, the cellular activity was re-evaluated. Results, which are displayed in Figure 7b, show a similar number of viable cells per unit of material for the three tested substrates. Although the entrapment of CREKA in the polymer matrix was expected to favour cellular adhesion and/or proliferation through the binding to the fibrin molecules from the serum used as supplement in the culture medium, the peptide concentration is, unfortunately, too low (0.3-0.4%).

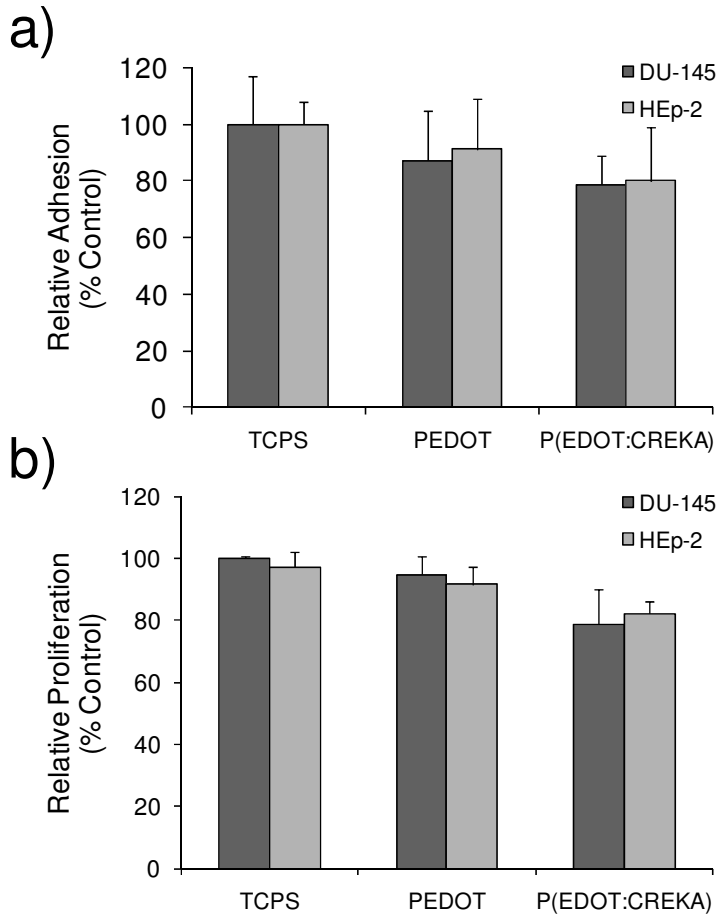


**Figure 7 –** Cellular adhesion (a) and cellular proliferation (b) on the surface of PEDOT and PEDOT/CREKA. TCPS was used as control substrate. DU-145 and HEp-2 cells were cultured during 24 h (adhesion assay) and 7 days (proliferation assay). The experiments were performed using six samples for each substrate.

Figure 8 shows SEM micrographs adhered and subsequently proliferated on the surface of PEDOT and PEDOT/CREKA films. The cellular mechanism for the adhesion of the cells onto the PEDOT/CREKA surface is similar that operating for PEDOT. In both cases the cells connect to the surface with filopodia. The spreading of the cells was achieved through an intimate contact between cells and surface of the films. Thus, abundant cytoplasmatic filopodias were detected forming bridges between the agglomerates of the material at the surface of the PEDOT and PEDOT/CREKA.

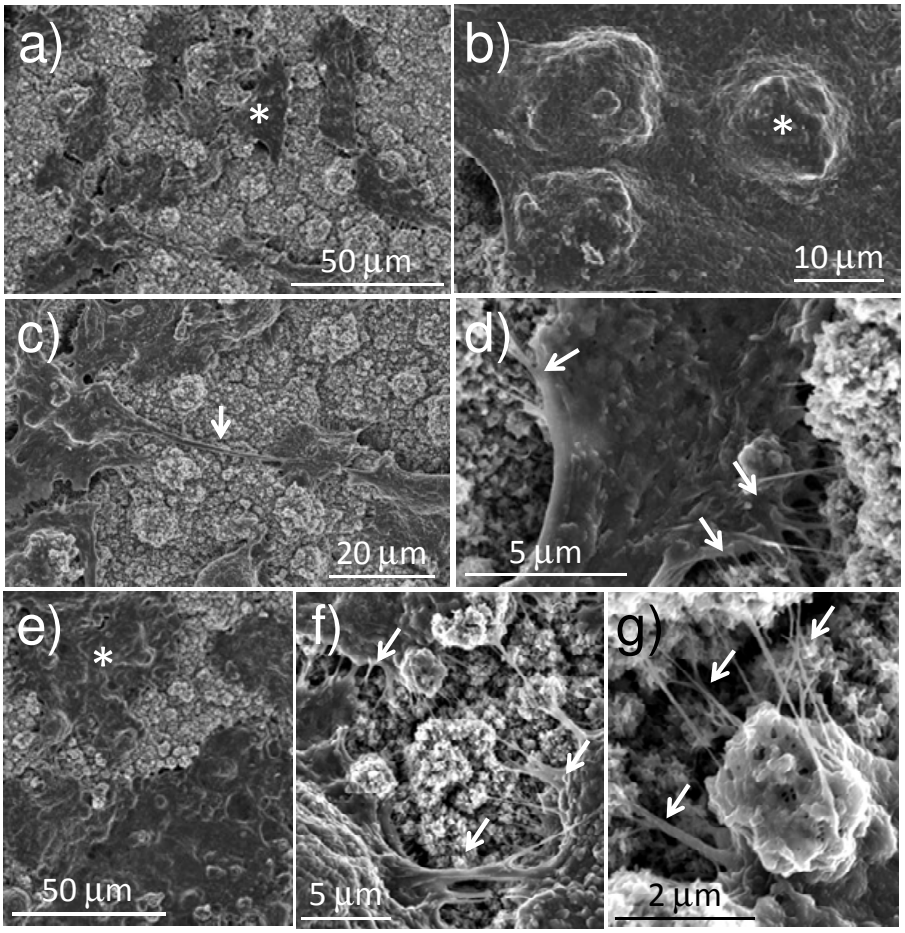


**Figure 8 –** Adhesion and proliferation of DU-145 cells onto PEDOT (a-d) and PEDOT/CREKA) (e-g) surfaces. a) Cells group in cluster (asterisk) to adhere the PEDOT surface. b) The adhesion is tight and recovers diverse irregular elements of the PEDOT surface morphology. c) Clustered cells are connected by bridge cytoplasmatic elements (arrow), which is a prerequisite to colonize the material. d) The cells use filopodias (arrows) to adhere to PEDOT surface. e) Cells grouped in clusters (asterisk) to adhere to PEDOT/CREKA surface. f-g) The filopodias are the cytoplasmatic elements responsible of cellular adhesion to PEDOT/CREKA.

As it was expected, modification of PEDOT with CREKA is not an easy task because of both the small size and, specially, the positive charge of the peptide, the latter precluding its incorporation as a dopant. However, results presented in this work are very promising since, in spite of its small concentration, the peptide promotes and improves the electrochemical properties of the conducting polymer. In order to increase the concentration of CREKA in the polymer, several strategies are currently being tested in our laboratories. The first one refers

to the complete or partial elimination of the positive charges at the peptide through the pH of the generation medium. Unfortunately, preliminary results in this direction evidenced a severe degradation of the electrochemical properties of PEDOT produced in basic environments. Another interesting alternative consists on enhance the incorporation of peptide to the polymer matrix during the whole polymerization process and not only at the first stages, as was observed in this work. Thus, modification of the diffusion coefficient can be reached by introducing the suitable chemical modification at the peptide. Our current research is addressed in this direction.

### 6.3.4 – Conclusions

Comparison of the morphologies of PEDOT and PEDOT/CREKA indicates that the peptide incorporates to the polymer matrix at the first stages of the polymerization process. Interestingly, the entrapment of a very low concentration CREKA (0.3-0.4 % w/w) into PEDOT significantly affects the electrochemical properties of the CP. Specifically the peptide, which has been detected by HPLC and FTIR spectroscopy, not only blocks the oxidation of the CP molecules but also promotes the redox capabilities, electrochemical stability, and impedance characteristics of PEDOT. Unfortunately, the cellular activity of PEDOT was not altered by the incorporation of such low amount of CREKA, even though this peptide is expected to bind the fibrin molecules from the serum used as supplement in the culture medium. Currently, we are examining alternative strategies to incorporate CREKA into the polymer matrix. Elimination of the positive charges of the peptide by varying the pH of the generation medium was found to damage the electrochemical properties of PEDOT. Another possible strategy, which we are developing at present time, consists on the chemical modification of the peptide to promote its incorporation at the last stages of the polymerization process.

### 6.3.5 – References

[1] R. A. Green, C. M. Williams, N. H. Lovell, *J. Mater. Sci. Mater. Med.* 19 (2008) 1625.

[2] X. Cui, V. A. Lee, Y. Raphael, J. A. Wiler, J. F. Hetke, D. J. Anderson, D. C. Martin, *J. Biomed. Mater. Res.* 56 (2001) 261.

[3] X. Cui, D. C. Martin, *Sensors Actuators A* 103 (2003) 384.

[4] N. K. Guimard, N. Gomez, C. E. Schmidt, *Prog. Polym. Sci.* 32 (2007) 876.

[5] Y. Zhong, X. Yu, R. Gilbert, R. V. Bellamkonda, *J. Rehabil. Res. Dev.* 38 (2001) 627.

[6] X. Cui, J. Wiler, M. Dzaman, R. A. Altschuler, D. C. Martin, *Biomaterials* 24 (2003) 777.

[7] B. Garner, A. J. Hodgson, G. G. Wallace, P. A. Underwood, *J. Mat. Sci. Mater. Med.* 10 (1999) 19.

[8] R. A. Green, N. H. Lovell, L. A. Poole-Warren, *Biomaterials* 30 (2009) 3637.

[9] X. Y. Cui, D. C. Martin, *Sensors Actuators B* 89 (2003) 92.

[10] Y. H. Xiao, X. Y. Cui, J. M. Hancock, M. Bouguettaya, J. R. Reynolds, D. C. Martin, *Sensors Actuators B* 99 (2004) 437.

[11] A. B. Sanghvi, K. P.-H. Miller, A. M. Belcher, C. E. Schmidt, *Nat. Mater.* 4 (2005) 496.

[12] E. De Giglio, L. Sabbatini, P. G. Zambonin, *J. Biomater. Sci. Polym. Ed.* 10 (1999) 845.

[13] E. De Giglio, L. Sabbatini, S. Colucci, G. Zambonin, *J. Biomater. Sci. Polym. Ed.* 11 (2000) 1073.

[14] N. Gomez, C. E. Schmidt, *J. Biomed. Mater. Res. A* 81 (2007) 135.

[15] R. Pasqualini, E. Ruoslahti, *Nature* 380 (1996) 364.

[16] J. A. Hoffman, E. Giraudo, M. Singh, L. Zhang, M. Inoue, K. Porkka, D. Hanahan, E. Ruoslahti, *Cancer Cell* 4 (2003) 383.

[17] D. Simberg, T. Duza, J. H. Park, M. Essler, J. Pilch, L. Zhang, A. M. Derfus, M. Yang, R. M. Hoffman, S. Bathia, M. J. Sailor, E. Ruoslahti, *Proc. Natl. Acad. Sci. U S A* 104 (2007) 932.

[18] D. Zanuy, A. Flores-Ortega, J. Casanovas, D. Curcó, R. Nussinov, C. Alemán, *J. Phys. Chem. B* 112 (2008) 8692.

[19] D. Zanuy, D. Curcó, R. Nussinov, C. Alemán, *Biopolymers* 92 (2009) 83.

[20] L. Agemy, K. N. Sugahara, V. R. Kotamraju, K. Gujraty, O. M. Girard, Y. Kono, R. F. Mattrey, J.-H. Park, M. J. Sailor, A. I. Jimenez, C. Cativiela, D. Zanuy, F. J. Sayago, C. Aleman, R. Nussinov, E. Ruoslahti, *Blood* 116 (2010) 2847.

[21] D. Aradilla, F. Estrany, C. Alemán, *J. Phys. Chem. C* 115 (2011) 8430.

[22] D. Aradilla, F. Estrany, E. Armelin, C. Alemán, *Thin Solid Films* 518 (2010) 4203.

[23] H. Susi, D. M. Byler, *Methods Enzymol.* 130 (1986) 290.

[24] A. Dong, W. S. Caughey, *Methods Enzymol.* 232 (1994) 139.

[25] S. Krimm, J. Bendekar, *Adv. Protein Chem.* 38 (1986) 181.

[26] L. Wang, C. T. Middleton, M. T. Zanni, J. L. Skinner, J. *Phys. Chem. B* 115 (2011) 3713.

[27] T. X. H. To, A. T. Trinh, H. N. Truong, K. O. Vu, J. Jean-Baptiste, P. Nadine, *Surface and Coatings Tech.* 201 (2007) 7408.

# Chapter 7

# Discussion of the Results

# Chapter 7

## 7. – Discussion of the Results

Global spending for implantable medical devices was around US$200 billion in 2010. The majority of biomaterials for medical applications are based on metals such as stainless steel and titanium. These materials offer desirable properties, including high tensile strength and stability for medical use; however, their biocompatibility is still a problem that needs to be addressed.[1,2]

Corrosion resistance and superior mechanical properties make stainless steel one of the most potential candidates for manufacturing implantable medical devices. However, it is not fully biocompatible, but poses various biocompatibility problems. The most commonly encountered biocompatibility problems associated with implantation of metallic medical devices include: (i) inflammatory response; (ii) cell migration and proliferation; (iii) coagulation and hemolysis, caused by interaction of the biomaterial with various blood components; and (iv) thrombosis and restenosis as an arterial response to injury. Besides these, protein adsorption on the surface that occurs immediately after implantation is a key determinant of all subsequent unfavorable biological responses, such as platelet activation, adhesion and thrombus formation.[3,4]

Considering these problems, there has been a continuous search for more biocompatible options, which include gold, titanium, cobalt–chromium alloys, tantalum alloys, nitinol and various polymers such as polypropylene, polycarbonates and polyurethanes.[4] Another approach is to modify the steel surface with organic molecules, polymers or inorganic coatings.[5] Improved biocompatibility by surface modification involves: (i) changing the surface properties of the implant, such as surface texture, surface charge, surface energy and surface chemistry, thereby altering the nature of interaction at the material–tissue interface; and (ii) coating the material surface with a polymer or biomolecular layer to prevent its recognition as a foreign body or to create a less reactive layer. This latter approach can be achieved either by: (i) forming a passive surface on the biomaterial which elicits little or no immune response; or (ii) creating an active surface which elicits beneficial responses and suppresses unwanted reaction.[6]

Various coating techniques, such as dip coating, spray coating and electropolymerization, are available for coating the surface of a metal. The use of conducting polymers as coating materials and electropolymerization as a coating method offers several advantages: (i) it is simple and reproducible; (ii) it can form an integrated, uniform and durable film; (iii) the coating composition can be easily controlled; (iv) it can enable copolymerization of different monomers; and (v) grafting functional substituents and entrapment of biomolecules on surface is also possible.[7,8] PTh derivatives are among widely used monomers for the preparation of electroconducting polymeric coatings. In particular, PEDOT offers several advantages, such as easy availability, chemical stability and polymerizability. With the aim of extend the applications of PEDOT to biotechnology and biomedicine, both the lack of toxicity and the remarkable cellular activity of this material was recently proved by our group.[9,10] The ease preparation and manipulation make PEDOT suitable for electrocoating metal surfaces and further provides feasibility of immobilization/coupling of biomolecules.

On the other hand, interaction of CPs with small and large biomolecules, for example drugs and DNA, respectively, is a subject of recent interest. Thus, CPs have emerged as potential candidates for biosensors. Gerard *et al.* have reviewed the literature on applications of CPs to biosensors.[11] Geetha *et al.* have discussed the applications of conducting PPy to drug delivery.[12] Cosnier has discussed the analytical applications of affinity biosensors based on electropolymerized films.[13,14] Ramaniviciene and Ramanavicius have reported an interesting overview on the potential use of CPs as electrochemical based affinity biosensors.[15] Malinauskas *et al.* have reviewed the electrochemical aspects of CP-based nano-structured materials for application to super-capacitors, energy conversion systems, batteries and sensors.[16] Adhikari and Majumdar have discussed the role of non-conducting and intrinsically CPs in sensor devices.[17] Drummond *et al.* have discussed numerous approaches to electrochemical detection based on modified electrodes, electrochemical amplifications with nanoparticles and electrochemical devices using DNA-mediated charge transport chemistry and electrochemistry of DNA-specific redox reporters.[18] Habermuller *et al.* have reported on the various electron-transfer mechanisms operating in amperometric biosensors.[19] Kerman *et al.* have predicted that electrochemical DNA biosensors with suitable microfabrication techniques are likely to be increasingly popular in the near future.[20]

Part of the work presented in this Thesis (Chapters 4 and 5) focuses on the prospective applications of CPs in biosensors. More specifically, Chaper 4 presents different studies devoted to examine the interaction between different PTh derivatives and DNA. These CPs provide a unique surface for DNA binding in that its delocalized electronic structure allows positively charged groups mobility along the chain axis. This surface charge mobility leads us to conclude that DNA as a polyelectrolyte possessing a fixed negative charge distribution would bind very strongly since the surface positive charge could redistribute to maximize a favourable energetic interaction. However, the present Thesis evidences that CPs bearing polar functional groups are also able to act as hydrogen bonding donors and/or acceptors. For example, the side groups of some substituted PTh derivatives are able to form specific interactions with well-defined nucleotide sequences of plasmid DNA. This selectivity reflects that CP···DNA adducts are stabilized not only by electrostatic non-specific interactions but also by additional interactions that depend on the spatial disposition and orientation of the chemical groups.

Amongst specific interactions, hydrogen bonds have been found to be more important than other weak interactions, like π-π stacking and hydrophobic. Electrophoretic and spectroscopic studies on mixtures of plasmid DNA and both oxidized and reduced PEDOT have shown the formation of stable adducts, the formation of interactions with specific nucleotide sequences being evidenced through the protection imparted by this material against restriction enzymes. These investigations allowed us to propose a mechanism for the formation of the adducts with DNA. This consists of an initial stabilization of the complexes through non-specific electrostatic interactions, followed by small structural re-arrangements that allow establishing specific hydrogen bonds between the polar groups of the CP and selected DNA bases. This mechanism requires a structural alteration of the B-DNA double helix, which undergoes a drastic transformation as observed by CD and UV-Vis spectroscopy. Thus, the very high degree of exposition detected for DNA bases was attributed to the effect of the π-conjugated polymer, which promotes the DNA unfolding into two separate strands. Furthermore, results presented in this Thesis reflect that these specific interactions are predominant for the thymine and, especially, the guanine, which is in perfect agreement with previous theoretical observations.

In summary, the studies described in this Thesis were useful to refine the understanding of CP···DNA interactions. PEDOT and other CPs bearing polar groups appear

to be promising substrates for the detection of specific DNA sequences. Their remarkable electronic and optical properties provide intriguing possibilities for use in biosensor and biotechnological device applications. In conjunction with their rational structural modification, incorporation of biological macromolecules such as DNA into novel molecular architectures possessing intelligent properties may be useful for device applications.

Applications of CPs to detection of drugs have recently aroused much interest. This is because these molecular electronic materials offer control of different parameters such as polymer layer thickness, morphology, electrical properties and bio-reagent loading, etc. Moreover, CP based sensors are likely to cater to the pressing requirements such as biocompatibility, possibility of *in vivo* sensing, continuous monitoring of drugs, multi-parametric assays, miniaturization and high information density. Morphine is an opioid analgesic used for the treatment of moderate to severe pain. However, morphine is toxic when used in excess or abused. For safety precautions, sensitive monitoring of morphine in blood or urine is necessary. Several methods have been developed for the detection and determination of morphine, including sequential injection analysis method, cation-selective exhaustive injection and sweeping micellar electrokinetic chromatography, fast Fourier transformation with continuous cyclic voltammetry method, gas chromatography –mass spectrometry, high-performance liquid chromatography – fluorescence method, liquid chromatography – electrospray ionization ion trap mass spectrometry, etc.[21-26] However, these analytical methods are time-consuming and devices are expensive.

Compared with these approaches, electrochemical sensors based on CPs are of particular interest for their practicality, simplicity, low-cost, and suitability for real-time detection. Ho *et al.* reported the amperometric detection of morphine using a Prussian blue-modified indium tin oxide electrode.[27] The selective morphine sensitive devices based on molecularly imprinted polymer have been described.[28,29] Pournaghi-Azar and Saadatirad used Prussian blue film modified-palladized aluminum electrode to monitor morphine by both hydrodynamic amperometry and differential pulse voltammetry.[30] But in most cases, oxidation of morphine at conventional electrodes always requires a high overpotential, or their fabrication process is complex, which usually leads to poor electrochemical performance. As a consequence, CP-modified electrodes turn out to be the candidates because of their stable physicochemical properties and excellent electrocatalytic activity. To

the best of our knowledge, this Thesis presents the first two reports on the electrochemical determination of morphine at CP-modified electrodes.

The results described in this Thesis show the influence of the morphology and the chemical nature of the CP on the detection of morphine. The results show that CPs able to form microstructures with very large accessible surface exhibit improved detection activity. Furthermore, PEDOT-containing electrodes show high sensitivity and fast response towards the electrochemical determination of morphine under well-defined conditions (*i.e.* pH and incubation time). The overall results suggest that CP hold great promising potential applications for narcotic drugs in the voltammetric determination and sensitive detector methods. The main advantages of the electrochemical methods based on the use of CPs are their simplicity and rapidity compared to other determination methods. Moreover, results have provided the basis for designing portable morphine sensors due to its easy and fast preparation, and low cost.

CPs have attracted much interest as suitable matrices of biomolecules, and can be used to enhance stability, speed, sensitivity and hence are finding increasing use in medical diagnostics and nanobiology. A number of techniques such as physical adsorption, electrochemical entrapment and covalent attachment based on coupling chemistry techniques, have been used to improve the stability of the desired biomolecules onto CPs.[31] In this Thesis we have examined the abilities of different electrochemically prepared PEDOT-containing biocomposites as electroactive scaffolds for cell culture. Martin and co-workers modified a neural microelectrode with PEDOT, poly(hydroxymethylated-3,4-ethylenedioxythiophene), or PEDOT/sulfonatoalkoxy EDOT coatings, all of which lowered the impedance of the coated electrode over a wide range, while increasing the charge capacity compared to the bare electrode.[32-34] The same group also reported that the neural probe coated by the order surfactant-templated PEDOT exhibited lower impedance and higher charge capacity than uncoated gold, nodular PEDOT, and nodular PPy-coated electrodes. In addition human neuroblastoma cells can adhere and perform neurite extension on the coated electrode, though the surfactant poly(oxyethylene)$_{10}$-oleyl ether they used is toxic to cells.[35] Development of electrically conducting biomaterials intended for direct, functional contact with electrically active tissue, such as the nervous system, heart and skeletal muscle, signified a new electrode paradigm for creating soft, low impedance implantable electrodes.[36,37] Recently, del Valle *et al.* reported that the steel

electrodes coated by PEDOT films showed good biocompatibility with Hep-2 cells, and revealed that the electroactivity of PEDOT in different biological fluids is significantly enhanced by the attached cellular monolayer.[38] Neuron-to-electrode attachment is vitally important in the performance of deep stimulating electrodes used in the treatment of neural diseases such as Parkinson's and is a concern in the performance of prosthetic devices such as retinal and cochlear implants. This involves electrode materials selection and design, surface chemical modification strategies and optimization of cell culture conditions.[39] Self-assembled method for surface modifications of neural electrodes has proved to be more controllable than with the electrodeposited method.[40]

In the last chapter of results (Chapter 6) much attention has been focused on the combination of PEDOT and biomolecules (lysozyme, dextrins and CREKA) to prepare of electroactive conductive films for cell culture. For this purpose, a simple and straightforward deposition method, which did not require special instrumentation, has been used to produce hybrid biocomposites with reproducible properties. To assess the biocompatibility of the new hybrid material with dextrins and CREKA, the attachment and proliferation of cells were studied. In contrast the bactericide properties of the biocomposite with lysozyme were examined by considering the proliferation of bacteria. From an electrochemical point of view, the properties (*i.e.* electroactivity and electrostability) of the lysozyme- and CREKA-containing hybrid biocomposites are better than those of individual PEDOT. Moreover, all these new materials, without any exception, resulted more compact and less porous than PEDOT controls, suggesting biological entities are evenly distributed in the composites. From a biotechnological point of view, we found that the lysozyme- and dextrins-containing biocomposites are not only biocompatible materials but also display higher cellular activity than PEDOT. However, the incorporation of CREKA into the polymer matrix did not alter the cellular activity of the CP, which has been attributed to the small concentration of peptide.

## 7.1 – References

[1] J. Ouellette, *Ind. Physicist* (2001) 18.

[2] G. Shustak, A. J. Domb, D. Mandler, *Langmuir* 20 (2004) 7499.

[3] Y. Li, K. G. Neoh, E. T. Kang, *J. Colloid Interf. Sci.* 275 (2004) 488.

[4] W. G. Brodbeck, M. S. Shive, E. Colton, Y. Nakayama, T. Matsuda, J. M. Anderson, *J. Biomed. Mater. Res.* 55 (2001) 661.

[5] E. D. Giglio, M. R. Guascito, L. Sabbatini, G. Zambonin, *Biomaterials* 22 (2001) 2609.

[6] C. A. Kavanagh, Y. A. Rochev, W. M. Gallagher, K. A. Dawson, A. K. Keenan, *Pharmacol. Ther.* 102 (2004) 1.

[7] O. Ouerghi, A. Senillou, N. J. Renault, C. Martelet, H. B. Ouada, S. Cosnier, *J. Electroanal. Chem.* 501 (2001) 62.

[8] Z. Weiss, D. Mandler, G. Shustak, A. J. Domb, *J. Polym. Sci., Part A: Polym. Chem.* 42 (2004) 1658.

[9] L. del Valle, D. Aradilla, R. Oliver, F. Sepulcre, A. Gámez, E. Armelin, C. Alemán, F. Estrany, *Eur. Polym. J.* 43 (2007) 2342.

[10] L. del Valle, F. Estrany, E. Armelin, R. Oliver, C. Alemán, *Macromol. Biosci.* 8 (2008) 1144.

[11] M. Gerard, A. Chaubey, B. D. Malhotra, *Biosens. Bioelectron.* 17 (2002) 345.

[12] S. Geetha, C. R. K. Rao, M. Vijyan, D. C. Trivedi, *Anal. Chim. Acta* 568 (2006) 119.

[13] S. Cosnier, *Electroanalysis* 17 (2005) 1701.

[14] S. Cosnier, *Anal. Bioanal. Chem.* 377 (2003) 507.

[15] A. Ramanaviciene, A. Ramanavicius, *Advanced Biomaterials for Medical Applications*, Kluwer Academic Publishers, Netherlands, (2004) 111.

[16] A. Malinauskas, J. Malinauskiene, A. Ramanavicius, *Nanotechnology* 16 (2005) R51.

[17] B. Adhikari, S. Majumdar, *Prog. Polym. Sci.* 29 (2004) 699.

[18] T. G. Drummond, M. G. Hill, J. K. Barton, *Nat. Biotechnol.* 21 (2003) 1192.

[19] K. Habermuller, M. Mosbach, W. Schuhmann, Fresenius, *J. Anal. Chem.* 366 (2000) 560.

[20] K. Kerman, M. Kobayashi, E. Tamiya, *Meas. Sci. Technol.* 15 (2004) R1.

[21] A. M. Idris, A. O. Alnajjar, *Talanta* 77 (2008) 522.

[22] Y. H. Lin, J. H. Li, W. K. Ko, S. M. Wu, *J. Chromatogr. A* 1130 (2006) 281.

[23] P. Norouzi, M. R. Ganjali, A. A. Moosavi-movahedi, B. Larijani, *Talanta* 73 (2007) 54.

[24] M. R. Lee, S. C. Yu, B. H. Hwang, C. Y. Chen, *Anal. Chim. Acta* 559 (2006) 25.

[25] M. Wada, C. Yokota, Y. Ogata, N. Kuroda, H. Yamada, K. Nakashima, *Anal. Bioanal. Chem.* 391 (2008) 1057.

[26] M.-H. Spyridaki, P. Kiousi, A. Vonaparti, P. Valavani, V. Zonaras, M. Zahariou, E. Sianos, G. Tsoupras, C. Georgakopoulos, *Anal. Chim. Acta* 573 (2006) 242.

[27] K. C. Ho, C. Y. Chen, H. C. Hsu, L. C. Chen, S. C. Shiesh, X. Z. Lin, *Biosens. Bioelectron.* 20 (2004) 3.

[28] K. C. Ho, W. M. Yeh, T. Tung, J. Y. Liao, *Anal. Chim. Acta* 542 (2005) 90.

[29] W. M. Yeh, K. C. Ho, *Anal. Chim. Acta* 542 (2005) 76.

[30] M. H. Pournaghi-Azar, A. Saadatirad, *J. Electroanal. Chem.* 624 (2008) 293.

[31] B. D. Malhotra, A. Chaubey, S. P. Singh, *Analyt. Chim. Acta* 578 (2006) 59.

[32] X. Y. Cui, D. C. Martin, *Sens. Actuators B: Chem.* 89 (2002) 92.

[33] Y. H. Xiao, X. Y. Cui, J. M. Hancock, M. Bouguettaya, J. R. Reynolds, D. C. Martin, *Sens. Actuators B: Chem.* 99 (2004) 437.

[34] Y. H. Xiao, X. Y. Cui, D. C. Martin, *J. Eletroanal. Chem.* 573 (2004) 43.

[35] J. H. Yang, D. H. Kim, J. L. Hendricks, M. Leach, R. Northey, D. C. Martin, *Acta Biomater.* 1 (2005) 125.

[36] S. M. Richardson-Burns, J. L. Hendricks, B. Foster, L. K. Povlich, D. H. Kim, D. C. Martin, *Biomaterials* 28 (2007) 1539.

[37] S. M. Richardson-Burns, J. L. Hendricks, D. C. Martin, *J. Neural Eng.* 4 (2007) L6.

[38] L. J. del Valle, D. Aradilla, R. Oliver, F. Sepulcre, A. Gamez, E. Armelin, C. Alemán, F. Estrany, *Eur. Polym. J.* 43 (2007) 2342.

[39] G. E. Slaughter, E. Bieberich, G. E. Wnek, K. J. Wynne, A. Guiseppi-Elie, *Langmuir* 20 (2004) 7189.

[40] A. S. Widge, M. Jeffries-EI, X. Y. Cui, C. F. Lagenaur, Y. Matsuoka, *Biosens. Bioelctron.* 22 (2007) 1723.

# Chapter 8

# Conclusions

# 8. – Conclusions

## 8.1 – Block 1: DNA···Conducting Polymers Interaction

(a) PT3M, PEDOT, PT3AME and PT3MDE form stable adducts with plasmid DNA. However, assays with restriction enzymes show that only the polymers bearing polar groups, especially PEDOT and PT3MDE, are able to interact with specific nucleotide sequences.

(b) The interaction of CPs bearing polar groups with plasmid DNA provokes an alteration in the secondary structure of the latter: the double helix unfolds increasing the exposition of the nitrogen bases. This reorganization allows the formation of specific interactions between the DNA bases and such CPs bearing polar groups.

(c) The formation of specific interactions between the plasmid DNA and the CP depends on the chemical nature of the substituent, even though the presence of polar groups seems to be essential. Thus, the degree of exposition of the DNA bases depends on the concentration of polar groups per repeating unit contained in the CP.

(d) Experiments using PEDOT with different doping levels indicate that neutral PEDOT interacts with DNA only when the concentration of the CP is very high. Thus, non-specific electrostatic interaction between the negatively charged groups of DNA and the oxidized CP are essential to form stable adducts, the stability of the complexes increasing with the doping level of the CP.

(e) Once the CP:DNA adducts are stabilized, weak interactions that depend on the spatial disposition and orientation of the polar groups are formed. These specific interactions, which are possible because of the exposition of the DNA bases, are responsible of the protection imparted by PEDOT, PT3AME and PT3MDE against the attack of the restriction enzymes.

(f) Both UV-Vis and CD spectra indicate that dG6 interact with PEDOT through weak specific interactions, which do not produce major alterations in the secondary structure of the ss-hn. In contrast, dA6:PEDOT and dC6:PEDOT adducts are made of compact structures stabilized by strong electrostatic interactions, giving place to the loss of the ss-hn secondary structure. The characteristics of dT6:PEDOT complexes are half-way between those of dG6:PEDOT and the electrostatic adducts involving dA6 or dC6. Thus, experimental results for dT6:PEDOT complexes suggest that, although electrostatic interaction play an important role in their stabilization, weak specific interactions also participate in their final organization.

(g) Incubation of dG6:PEDOT mixtures with different concentrations of EG and FA, which promote the formation of stacking and hydrogen bonds, respectively, confirmed the presence of the latter interactions in the complexes while the π-π stacking are undetectable. This feature is fully consistent with theoretical results derived from MD simulations on dG6:PEDOT mixtures and quantum mechanical calculations on small model complexes.

(h) The overall of the results obtained in this Thesis suggests that hydrogen bonds are responsible of the interactions with specific nucleotide sequences of DNA. Thus, electrophoretograms and both UV-Vis and CD spectra are fully consistent with this hypothesis, which is also supported by theoretical calculations.

(i) Hydrogen bonded model complexes formed the building blocks of PEDOT and dG6 have been used to reproduce the experimental absorption spectra (both the energy gaps and relative oscillator strength magnitudes). This feature allowed us to conclude the existence of specific N-H···O interactions involving the EDOT oxygen and the N-H moiety of G.

## 8.2 – Block 2: Drug Detection

(a) PNMPy/PSSA hollow microstructures with doughnut-like morphologies, which are adhered to the surface of the PNMPy films, have been prepared by CV followed by CA techniques using gas bubbles as templates. The concentration and dimensions

of the microstructures have been controlled through the distance between the WE and the CE. The high electrochemical stability of PNMPy/PSSA has been attributed to the doughnut shape of these microstructures, which present a high surface area and a good ability to release and catch the ion molecules during the oxidation and reduction processes.

(b) Application of the electrochemical oxidation process in presence of low molecular weight electrolytes, like β-NSA and CSA, produces PNMPy microstructures with a brain-like morphology forming a wrinkle network system. The electrochemical properties of PNMPy/β-NSA and PNMPy/CSA microstructures have been found to be significantly lower than those of the hollow microstructures containing films made of PNMPy/PSSA.

(c) EIS measurements evidenced the interaction between PNMPy/PSSA and morphine molecules. Thus, this prominent material shows a high ability to capture the drug molecules and to retain them for a long period of time. This allows to conclude that PNMPy/PSSA microstructures are potential candidates for the development of new drug detectors. The maximum difference with respect to the blank PEDOT samples was obtained at pH= 2 and 7 for incubations times of 3 and 12 h, respectively.

## 8.3 – Block 3: Conducting Biocomposites

(a) Adsorption of lysozyme in the surface of PEDOT films produces a biphasic composite that retains the electrochemical properties of the CP but with relatively low bactericidal activity. The latter limitation has been attributed to the rapid release of the enzyme to the physiological medium.

(b) The addition of lysozyme to the medium used for the electropolymerization of PEDOT produces a homogeneous composite in which the enzyme is entrapped within the polymer matrix. The electroactivity of this biocomposite is smaller than that observed for the unmodified CP, but relatively high yet. The new biocomposite shows a very high bactericidal activity against Gram-positive

bacteria, which has been attributed to the controlled and progressive release of the enzyme.

(c) P(EDOT-LD) and P(EDOT-CD) biocomposites have been synthesized by anodic polymerization in water. The electroactivity of the two materials is lower than that of pure PEDOT, which has been attributed to the fact that dextrins promote the formation of compact surfaces. In spite of this, the electrical conductivities of PEDOT and the two biocomposites are very similar, suggesting that dextrins do not produce significant changes in the bulk but only in the surface.

(d) The concentration of dextrins in P(EDOT-LD) and P(EDOT-CD) is around 20% and 15% w/w, respectively. Furthermore, the release of dextrins from P(EDOT-CD) depends on the pH, which is due to the existence of aggregation effects at neutral pH and the enhancement of the hydrophilic character at acid pH. In contrast, no pH-dependence is observed in the release of dextrins from P(EDOT-LD). This is because the macromolecular nature of the LD molecules facilitates their interaction with the CP molecules.

(e) Cell adhesion and proliferation assays considering two epithelial-like and one fibroblast-like lines indicates that the cellular activity is significantly higher in the dextrins-containing biocomposites than in pure PEDOT. This allows us to conclude that the incorporation of dextrins improves the behaviour of the latter CP as cellular matrix.

(f) Anodic polymerization of PEDOT in presence of CREKA allows the entrapment of a very low concentration of peptide (0.3-0.4%) into the polymer matrix, which occurs at the first stages of the polymerization process. This low amount of CREKA affects considerably the redox capabilities, electrochemical stability and oxidation characteristics of the CP, even though the intrinsic cellular activity of the latter material remains essentially unaltered.